MODELS FOR STRUCTURE - RHEOLOGY OF HIGHLY CONCENTRATED EMULSIONS

by

REZA FOUDAZI

Thesis submitted in fulfilment of the requirements for the degree

DOCTOR OF TECHNOLOGY : CHEMICAL ENGINEERING

in the Faculty of Engineering

at the Cape Peninsula University of Technology

Supervisor: Prof. Irina Masalova.

Co-Supervisor: Prof. Alexander Ya. Malkin.

MODELS FOR STRUCTURE – RHEOLOGY OF HIGHLY CONCENTRATED EMULSIONS

by

REZA FOUDAZI

Thesis submitted in fulfilment of the requirements for the degree

Doctor of Technology: Chemical Engineering

in the Faculty of Engineering

at the Cape Peninsula University of Technology

Supervisor: Prof. Irina Masalova
Co-supervisor: Prof. Alexander Ya. Malkin

Cape Town Campus
November 2009

Declaration

I, Reza Foudazi, declare that the contents of this thesis represent my own unaided work, and that the thesis has not previously been submitted for academic examination towards any qualification. Furthermore, it represents my own opinions and not necessarily those of the Cape Peninsula University of Technology.

Signed Date

Abstract

Highly concentrated emulsions (HCE) are classified as high internal phase ratio emulsions (or simply HIPRE), and the dispersed phase droplets are ranged in a hexagonal closely packed configuration. This closely packed configuration and the profound hydrodynamic interaction between neighbouring droplets induce mechanical interference between the droplets, thus prohibiting their free movement. Hence, while the highly concentrated emulsions consist of very low viscosity and inelastic components, they show gel-like behaviour with high elasticity and non-Newtonian flow response. It has been suggested in the literature that this behaviour originated from interfacial energy in terms of Laplace pressure. Therefore, the scaling of rheological properties with Laplace pressure is expected, but several publications show a deviation from this scaling behaviour. It seems that the source of deviation from this scaling is interdroplet interaction, which can contribute to the rheological behaviour of highly concentrated emulsions. The shear modulus of highly concentrated emulsions in the presence of interdroplet interaction was developed in this work. The prediction of model was verified by the data presented in the literature. It was shown that a small source of interdroplet interaction can result in deviation from scaling of shear modulus with Laplace pressure. Introducing interdroplet interaction resulted in deviation from the linear dependency of the Princen-Lacasse-Mason models' prediction, $G/\sigma \sim 1/d$, as a result of potential film thickness–droplet size dependency in the interaction term. However, the intercept was still zero (it still satisfies $G \rightarrow 0$, if $d \rightarrow \infty$).

A set of highly concentrated explosive emulsions were prepared in this work to verify and/or develop the models that have been presented both in the literature and in this work. The material used to form emulsions consisted of supersaturated oxidiser solution, hydrocarbon oil and PIBSA-based surfactants. The interfacial characteristics for different surfactant types and variations of droplet size distribution for different droplet sizes, volume fractions, and surfactant types were first examined. Secondly, the proper method for estimating yield stress of prepared emulsions was investigated. Then, the rheology of samples was studied, and different scaling methods and fitting of experimental data were studied. Finally, the physics behind unusual elasticity of emulsion samples were studied by using the model that was developed.

On the basis of flow curve measurements and observed $\tau_y \sim \dot{\gamma}^{1/2}$ scaling, a modified version of Windhab model was suggested which showed excellent fitting of

experimental results. The non-zero intercept of τ_{y0}/σ – $1/d_{32}$ and G'_p/σ – $1/d_{32}$ linear dependences for studied emulsions implied non-linear dependence (resulting from interdroplet interaction) to fulfil the zero intercept requirement. It was established that the zero intercept condition was fulfilled in the $\tau_{y0} \sim \sigma / d_{32}{}^2$ and $G'_p \sim \sigma / d_{32}{}^2$ scalings, although the experimental results for different surfactants were not superimposed. The trend of interfacial dilatational elasticity (dynamic elasticity), as well as of the interfacial tension (static elasticity), was also found to be different from the trend of shear modulus and yield stress of the prepared highly concentrated emulsions. These results could be due to the presence of a significant interdroplet interaction. It was also found that the yield stress determined from the flow curve measurement – which is a threshold between creeping and flowing – is more realistic to report than the frequency dependent yield stress obtained from oscillation measurement. Finally, it was suggested that the unusual elasticity of explosive emulsions originates from electrostatic interdroplet interaction enhanced by reversed micelles.

Dedication

This thesis is dedicated to the following important persons:

First of all, to the God, the creator of thinking, from whom I derived all my strength, perseverance, motivation and health,

Everybody who thought me how to think scientifically and those who helped and supported me to accomplish it,

My mother, Tahereh, the pillar of my strength, encouragement and a beacon of light to me,

My father, Mohammad, for his fatherly advice, motivation and support,

And last but not least, my wife Fahimeh for her lovely inspiration, and support during my PhD.

Acknowledgements

I hereby wish to pass my sincere gratitude to the following people and organisations for their contribution towards completion of this thesis:

Prof. Irina Masalova, my supervisor and the head of Material Science and Technology research unit who gave me the opportunity to pursue my goal, and allowed me to research in her research group, her constant motivational leadership and in-depth knowledge in this field,

Prof. Alexander Ya. Malkin, my co-supervisor, for providing me his invaluable information and useful ideas in all aspect of the project, his insight in the field, encouragement, moral and technical supports,

African Explosive Limited, for the financial support of this research work, as well as the permission to publish the results of this study,

Lake International, the company that provided surfactants for preparing emulsion samples,

My institution Cape Peninsula University of Technology (CPUT), as well as to Engineering Faculty and Chemical Engineering Department,

Nazeem George, Rheology lab manager of CPUT, and Sipho Mudeme for their assistance and help in carrying out the experimental part of this work,

The Material Science and Technology research centre staffs and students, for their assistance and support,

My family and friends (Sipho, Karina, Hamat, Bernard, Steeve, Meraj and Yusef) for their moral support, love and prayers.

Table of Contents

List of Figures

List of Tables

Glossary

Terms/Acronyms/Abbreviations	Definition/Explanation
Capillary number	Ratio between the viscous stress which acts to deform the droplet and stabilising Laplace pressure.
CMC	The critical micelles concentration of surfcatnt above which micelles form.
Explosive emulsion	High internal phase water-in-oil emulsion of a concentrated solution of nitrate salts in water emulsified into an oil base.
Disjoining pressure	The short-range interaction force per area between the oil-water interfaces.
Flow curve	Curve presenting the variation of shear stress against shear rate.
Interfacial tension	Measurement of cohesive (excess) energy present at an interface arising from the imbalance of forces between molecules at an interface (gas / liquid, liquid / liquid, gas / solid, liquid / solid)
Laplace pressure	The pressure difference between fluids separated by an interface resulting from the interfacial tension and the curvature of the interface.
Loss modulus	Its value is a measure of the deformation energy used up in the sample during the shear process and lost to the sample afterwards. This energy is either used up during the process of changing the sample's structure or dissipated into the surrounding environment in the form of heat.
Newtonian fluid	Any fluid that has a direct proportionality between shear stress and shear rate.
Non-Newtonian fluid	A fluid whose flow behaviour does not obey the Newtonian's law, i.e. its viscosity is dependent to the stress or shear rate.
Osmotic pressure	The equilibrium energy density required to confine the dispersed phase droplets to a finite volume fraction of continuous phase.
Plasticity	The state of a solid body that is in the elastic state when the stress is below a critical value, termed the yield stress, and in the plastic state when this value is exceeded. During ideal plastic flow, energy dissipation and stress are independent of the rate of deformation.

Rheological model	An idealised relationship of rheological behaviour expressible in mathematical, mechanical or physical terms.
Rheology	Science of deformation and flow of matter, it deals with the deformation of materials as a result of an applied stress.
Rheometer	An instrument for measuring rheological properties.
Sauter mean diameter	Area-volume mean diameter (d_{32})
Shear rate	Rate of shear deformation, change of deformation per unit time.
Shear stress	Component of stress parallel or tangential to the direction of flow.
Storage modulus	Its value is a measure of the deformation energy stored in the sample during the shear process. After the load is removed, this energy is completely available and acts as the driving force for the reformation which partially or completely compensates the previous deformation.
Viscoelastic material	A time-dependent material exhibiting both viscous and elastic effects under the action of outside stresses in the absence of time dependence.
Viscosity	The property of a material to resist deformation increasingly with increasing shear rate, a measure of this property is defined as the quotient of shear stress divided by shear rate in steady flow.
Viscous	The tendency to resist flow as a result of internal friction. During viscous flow, mechanical energy is dissipated as heat and the stress that develops depends on the rate of deformation.
Yield stress	A critical shear stress value below which an ideal plastic or viscoplastic material behaves like a solid (no flow). Once the yield stress is exceeded, a plastic material yields (deforms plastically) while a viscoelastic material flows like liquid.

Chapter 1 – Introduction

1.1. Background

Most real fluids found nowadays are complex multiphase systems which show predominantly non-Newtonian and viscoelastic behaviour. One of the most important categories of complex fluids is emulsions seen in everyday life. A great deal of effort has over the years been expended on understanding and controlling their structure and rheological properties to ensure acceptable quality, processability and performance of final products.

An emulsion is a mixture of two immiscible (unblendable) substances in which one liquid (the dispersed or internal phase) is dispersed in the other (the continuous or external phase). Emulsions are part of a more general class of two-phase systems of matter called colloids. Although the terms colloid and emulsion are sometimes used interchangeably, emulsion tends to imply that both the dispersed and the continuous phase are liquids. Examples of emulsions include butter and margarine, vinaigrettes, milk and cream, the photo-sensitive side of photographic film, and cutting fluid for metal working. Emulsions are classified according to the distribution of the oil and aqueous phases. A system which consists of water droplets dispersed in an oil phase, is known as a water-in-oil (w/o) emulsion, while the dispersed oil droplets in an aqueous phase is an oil-in-water (o/w) or inverse emulsion. There are also more complicated cases such as oil-in-water-in-oil (o/w/o) and water-in-oil-in-water (w/o/w) emulsions, which are known as multiple emulsions (Figure 1.1).

When deformed, emulsions exhibit a tremendous variety of rheological properties ranging from the viscosity of a liquid to the elasticity of a solid. This variety exists because the droplets can deform if work is done to overcome the interfacial tension, σ, between the oil and water. The interfacial tension creates a substantial pressure difference between the oil and water due to the curvature of droplet interface; this pressure is known as the Laplace pressure. It keeps the droplets spherical when they are not packed together and are sufficiently dilute. However, when work is done against the Laplace pressure, e.g. by sucking out the continuous phase from inter-droplets, they can be packed together so tightly that their interfaces become nearly polyhedral. The viscosity of a dilute emulsion like milk, which can be poured into a glass, is dramatically different from the elasticity of a concentrated emulsion like mayonnaise, which must be spread with a knife.

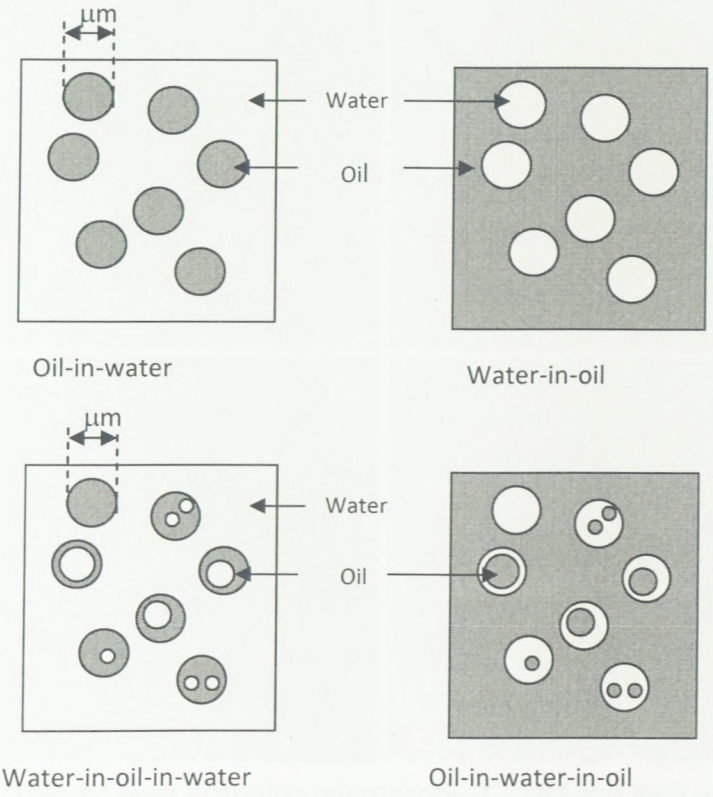

Figure 1.1: Schematic representation of different emulsions

The droplet size distribution of an emulsion is not usually monodisperse. Polydispersity of droplet size introduces a different microscopic length scale, creating differences in the Laplace pressure required to deform the droplets. Furthermore, in polydisperse emulsions, the droplet packing cannot easily be connected to the volume fraction of droplets, because small droplets can fit in the interstices of larger droplets. However, using the area-volume mean diameter (d_{32}) provides an acceptable averaging method for excluding the polydispersity effect on physical properties.

Emulsions share similarities with other kinds of complex fluids. In the dilute limit, the high Laplace pressure acts to keep the droplets spherical, so their behaviour may resemble that of suspensions of non-deformable spheres. However, in the highly compressed limit, emulsions have only thin films of continuous phase between the droplets, similar to that of gas foams, which are also known as biliquid foams (Figure 1.2).

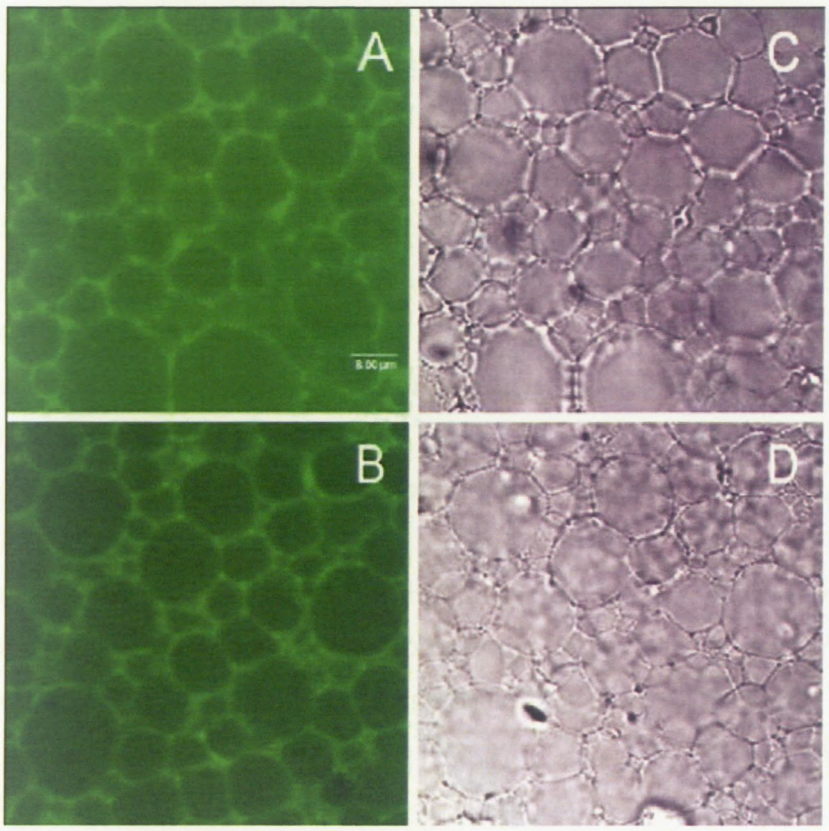

Figure 1.2: Confocal laser scanning microscopy (CLSM) and light microscopy (LM) images for emulsions containing 65% w/w oil and 1% w/w gluten (a, c); 75% w/w oil and 1% w/w gluten (b, d). Images on the left are the confocal (fluorescent) equivalents of the images on the right
(Bengoechea et al., 2006)

Nowadays, there is considerable interest in highly concentrated emulsions (HCE) or gel emulsions, due to their numerous potential industrial applications, e.g. cosmetics, mining, oil recovery, and explosives. The aim of this study was to deliver appropriate models for the rheology of highly concentrated emulsion explosives. These emulsions are dispersions of an aqueous phase (up to 90% by volume) in an oil phase. The dispersed droplets consist of an aqueous solution of nitrate salts which is supersaturated at room temperature, comprising less than 20% water by mass. Compounds of this kind are thermodynamically unstable and their instability is related to the coarsening of the emulsion (droplet coalescence) and phase transition (crystallisation) in the dispersed phase.

1.2. Problem statement

An aqueous dispersed phase with above 80% volume fraction in a continuous oil phase is referred as a highly concentrated w/o emulsion (HCE). All the previously stated models in the literature predict the scaling of rheological properties by Laplace

pressure (the ratio of interfacial tension to droplet size), while several experimental results in the literature show a deviation from those models.

1.3. Objectives

The main objectives of this study were as follows:

- Predicting the geometry of dispersed phase in a static case and using it to model the osmotic pressure
- Modelling the deformation of a compressed droplet under shear in order to predict the shear modulus
- Using the presented model to investigate the physics behind the unusual high elasticity of explosive emulsions
- Presenting appropriate semi-empirical models for the flow curve, yielding behaviour, and linear viscoelastic properties of samples based on systematic experimental work on the highly concentrated explosive emulsions

1.4. Research Design and Methodology

To accomplish these objectives, the research was conducted in the manner outlined below:

- Considering the problem of quasi-static properties of "compressed" emulsions: to investigate – how pressure creates highly concentrated emulsions depending on the parameters of an emulsion: its concentration, surface properties of interfacial layers, size of droplets. This was done in both two-dimensional (as in Princen's approach) and three-dimensional models (using Brakke's surface evolver software) by including the effect of interdroplet interaction.
- Applying deformation on the compressed droplet in the presence of interdroplet interaction, to model the shear modulus based on variation of free energy as a function of strain.
- Calculating different sources of interdroplet interaction and inputting it in the model, in order to investigate the phenomena behind the unusual high elasticity of highly concentrated explosive emulsions.
- Performing systematic experimental work in order to study highly concentrated explosive emulsions including:
    - Preparation of emulsions using a Hobart N50 mixer
    - Quality control of samples by Leica optical microscope
    - Measuring the droplet size distribution with a Malvern Mastersizer instrument

- Measuring the interfacial properties of samples by the Kruss K100
- Characterising the rheological properties of samples in terms of shear modulus, yield point, flow curve, linear viscoelastic behaviour
- Correlating the experimental results in order to present semi-empirical relations for the rheology of highly concentrated explosive emulsions

For the mentioned methodology, the following assumptions were made:

- Due to the tight arrangement of droplets in highly concentrated emulsions, the temperature-dependent kinetic of droplets, $k_B T$, was ignored.
- The interdroplet interaction between droplets was considered to be present dominantly in the flattened area where two droplets touched each other.
- Break-up and coalescence were negligible in the highly concentrated emulsion under study.

1.5. Outline

The thesis is subdivided into seven chapters. The first (current) chapter serves as an introduction to the thesis. The general concepts in emulsion science are briefly presented in Chapter 2. In this chapter, the emulsification process, stability and structure of emulsions after preparation, and microscopic and macroscopic properties of emulsion systems are given. Relevant literature on highly concentrated emulsions is reviewed in Chapter 3. This includes theoretical and semi-empirical models, and experimental studies on common and explosive types of highly concentrated emulsions.

The theoretical models for shear modulus and osmotic pressure that are developed in this work are presented in Chapter 4. The verification of the developed models and some of their typical predictions are included at the end of this chapter. In Chapter 5, the materials, instrument, and prepared matrix of samples are stated. The results which were obtained by these experimental techniques are presented in Chapter 6 and are discussed to deliver semi-empirical models for the rheology of highly concentrated emulsions. The predictions of the model presented in Chapter 4 are compared with the experimental shear modulus results, as well, in order to discuss the unusual elasticity of highly concentrated explosive emulsions. The summary and conclusions from the research findings are reviewed in Chapter 7.

Chapter 2 – General Concepts in Emulsion Science

2.1. Basic Components

The most basic components of any emulsion system are two immiscible fluids. In our case, we considered water-in-oil emulsions in which the oil phase was nonpolar. The third component in emulsion systems is the surfactant. The primary role of a surfactant is to prevent coalescence of the emulsion by providing repulsion between droplet interfaces. Surfactant molecules are amphiphilic; one end of the surfactant molecule is attracted to oil, while the other end of the molecule is attracted to water. Surfactant molecules are soluble in at least one fluid phase, but it is energetically favourable for them to spread over the interfaces between the two phases. At the interface, the surfactant molecules orient so that each end can interact with the fluid phase to which it is most attracted, thereby lowering the surface's free energy.

Whether an emulsion turns into a water-in-oil emulsion or an oil-in-water emulsion depends on the volume fraction of both phases and on the type of emulsifier. Generally, the Bancroft rule applies: surfactants tend to promote dispersion of the phase in which they do not dissolve very well; for example, proteins dissolve better in water than in oil and so tend to form oil-in-water emulsions (Bancroft, 1913).

A more sophisticated criterion was proposed by Griffin (1954), who introduced the concept of hydrophilic-lipophilic balance (HLB). As far as emulsification is concerned, surfactants with an HLB number in the range from 3 to 6 must form water-in-oil (w/o) emulsions, whereas those with HLB numbers from 8 to 18 are expected to form oil-in-water (o/w) emulsions. Different formulae for calculating the HLB numbers are available; for example, the Davies expression (1957), which reads:

$$HLB = 7 + (\text{hydrophilic group number}) - 0.475 n_c \qquad (2\text{-}1)$$

where n_c is the number of $-CH_2-$ groups in the lipophilic part of the molecule. Shinoda and Friberg (1986) proved that the HLB number is not a property of the surfactant molecules only, but also depends strongly on the temperature (for non-ionic surfactants), on the type and concentration of added electrolytes, on the type of oil phase, etc. They proposed using the phase inversion temperature (PIT) instead of HLB for characterisation of emulsion stability.

There are two major classes of surfactants: ionic and non-ionic. Ionic surfactant molecules have a charged head group connected to a neutral tail; the head prefers a polar fluid, like water, while the tail prefers nonpolar fluid, like oil. Most ionic surfactants are salts that dissociate in water; their solubility in the oil is extremely small. Non-ionic surfactants have an uncharged, polar head group connected to a hydrocarbon tail; the head prefers the water, while the tail prefers the oil. Non-ionic surfactants have greater solubility in oil than ionic surfactants.

In nature, as well as in man-made technology, macromolecular emulsifiers and stabilisers play a major role in the preparation and stabilisation of emulsions. By the proper choice of chemical compositions, such materials can be made to absorb strongly at the interface between the continuous and dispersed phases. By their presence, such materials can reduce the energetic driving force to coalescence by lowering the interfacial tension and/or forming a mechanical barrier between droplets. The effectiveness of polymeric materials at lowering interfacial tension is usually quite limited. More important to their function is the fact that polymers can form a substantial mechanical and thermodynamic barrier at the interface that retards the approach and coalescence of individual emulsions droplets. The polymeric nature of materials like proteins has the result that each molecule can be strongly adsorbed at many sides of the interface. Because of this, the chance of adsorption is greatly reduced or effectively eliminated, and the interfacial layer attains a degree of strength and rigidity not easily found in systems of monomeric materials. In addition, the presence of polymeric materials in the system can retard processes such as creaming by increasing the viscosity of the continuous phase in addition to reducing the rate of droplets encounter, which could lead to flocculation or coalescence (Myers, 2006).

The second type of effective emulsifying agents commonly encountered consists of finely divided solid articles. Particles of colloidal dimensions (e.g. less than 1mm in diameter) which are wetted by both aqueous and organic liquids can form stabilising films and produce both o/w and w/o emulsions with significant stability (Pickering, 1907; Schlaerpfer, 1918; Finkle et al., 1923). Emulsion stabilisation by solid particles relies on the specific location of the particles at the interface to produce a strong rigid barrier that prevents or inhibits the coalescence of droplets (Myers, 2006).

The last major type of emulsifiers and stabilisers comprises the monomeric surfactants that adsorb at the interface and produce electrical, mechanical, and steric barriers to

droplet coalescence, in addition to their role of lowering the interfacial free energy between the dispersed and continuous phases (Myers, 2006).

It is generally accepted that the volume fraction of the dispersed phase in a reasonably stable emulsion can be increased relatively easily up to a certain critical value, above which the emulsion tends to break or invert (Becher, 1983). In the case of a monodisperse emulsion, this point is reached at, or is close to $\varphi=0.7405$, i.e., the volume fraction that corresponds to the hexagonal close packing of undistorted spheres. However, emulsions with a dispersed phase volume fraction as high as 0.99 have been reported in the literature from time to time. These systems have been studied in some detail, pioneered particularly by Lissant (1966), Lissant et al. (1974), Nixon and Beerbower (1969), Princen (1979) and Princen et al. (1980). The high values of dispersed phase volume fraction were attained in the absence of a centrifugal force field which can compress emulsion considerably (Mittal, 1975) and forces droplets to deform in a polyhedral shape. In the case of centrifugal emulsions, the imposed deformation will normally relax as soon as the centrifugal force field is removed.

2.2. Emulsification

Emulsions do not form spontaneously when oil and water are placed in contact; mixing is required to disperse the droplets. Emulsification is a rheological process in which vigorous mechanical shearing of the viscous fluids overcomes the restoring force of interfacial tension, creating instabilities that nucleate droplets at the interfaces of the two fluids. An emulsion can be formed by emulsification of pure oil and pure water, but droplets coalesce quickly and form two completely separated phases, because, the total interfacial area of the droplets after emulsification is much greater than the original minimal area between the two bulk fluids. Therefore, emulsions are thermodynamically unstable systems (Israelachvili, 1992) that can be made kinetically stable or metastable (Atkins, 1994) for a reasonable period of time by introducing emulsifier or surfactant before or during the emulsification process.

Immiscible fluids can be emulsified using a vast number of differing compositions and procedures. The literature on emulsions contains many descriptions of emulsification techniques (Becher, 1983). The factors which most critically affect emulsification are the relative volume ratios and viscosities of the two phases, the surface tension, the shear rate $\dot{\gamma}$ produced by the mixer, and the duration of mixing. These factors can vary substantially from one procedure to another. For a continued reduction of droplet size,

the shear stress on existing droplets of radius, R, must exceed the Laplace pressure, σ/R, which prevents them from deforming. Common to all procedures is a dimensionless Capillary number, defined as the ratio of the viscous shear stress to the interfacial pressure $Ca = \eta\dot{\gamma}R/\sigma$.

2.3. Emulsion Stability

There are two principal types of stability for colloidal emulsions. The first type is droplet stability and is common to all emulsions, whether colloidal or not. Without droplet stability, the oil droplet would demix, destroying the emulsion. Droplet stability is dependent on the bulk properties of the fluids and the nature of the surfactant. For colloidal emulsions, the second type of stability is dispersion stability. As in other colloidal suspensions, dispersion stability is stability against aggregation or flocculation.

The two principle mechanisms which destroy the droplet stability are coarsening and coalescence. Coarsening is dependent primarily on the solubility of the dispersed phase in the continuous phase, whereas coalescence is dependent on the degree of repulsion provided by the surfactant at the droplet interfaces. Coarsening involves an increase in the average size of the emulsion droplets due to the solubility of two phases. Transfer of the dispersed phase from smaller to larger droplets is driven by their differences in the Laplace pressure, provided the solubility is significant. The small droplets continue to decrease in size until they disappear, because their interfacial pressure increases as they get smaller. The big droplets around them become even larger as they receive molecules from the smaller droplets. The growth of these larger droplets through coarsening is also known as Ostwald ripening. The rate of molecular diffusion through the interface is also dependent on the interfacial barrier created by the surfactant (Leal-Calderon et al., 2007).

Coalescence is the abrupt rupturing of the film of continuous phase between droplet interfaces. When two droplets of the dispersed phase approach each other, they will coalesce, thereby reducing their total interfacial area, unless repulsion between the duplet interfaces inhibits this process. To prevent coalescence, a surfactant must provide effective repulsion between droplet interfaces. The repulsion is dependent on the surfactant concentration on the interface, and a minimum surfactant concentration, which depends on the chemistry of the surfactant, is usually necessary to prevent coalescence. If the surfactant provides only weak repulsion, the droplets will coalesce and the dispersed phase will demix, destroying the emulsion (Leal-Calderon et al., 2007).

By choosing fluids that are extremely insoluble and using an appropriate surfactant, one can render emulsion droplets stable over many years. For such emulsions, measurements of their properties can be made over time scales which are negligible compared to the time scale of the droplet stability.

Dispersion stability is defined for any particulate suspension of colloidal particles. It refers to the stability of the dispersion against macroscopic phase separation (Russel et al., 1989). Dispersion stability in emulsions means that the droplets do not aggregate or flocculate. Each droplet has an entropic thermal energy of roughly k_BT, where k_B is Boltzmann's constant and T is the absolute temperature. This energy drives Brownian motion of the droplets and keeps them dispersed, provided it is larger than microscopic interdroplet attractive energies.

If the mass density of the dispersed phase is smaller than that of the continuous phase, the droplets may cream due to buoyant forces if the Brownian forces are smaller. The creaming rate is affected by the droplet size and the viscosity of the continuous phase. For micron-sized droplets and most common fluids, creaming is noticeable after many weeks. Figure 2.1 shows schematically different instability in emulsion systems (Tadros, 2005).

As indicated by Myers (2006), the effectiveness of an adsorbed film of surface-active materials in retarding the inevitable movement of emulsified systems toward a minimum in total energy may be considered in at least three contexts. The adsorbed molecules can (1) reduce the potential energy of the dispersed system by lowering the interfacial tension, (2) erect a rigid or highly viscous barrier at the interface capable of preventing or retarding the coalescence of droplets that collide as a result of random Brownian motion, thermal convection, or mechanical agitation, and (3) in cases where the adsorbed molecules carry an electric charge, impart that charge to the surface of droplets, resulting in the formation of an electrical double layer that lessens the frequency and effectiveness of close droplet approach and contact leading to droplet growth.

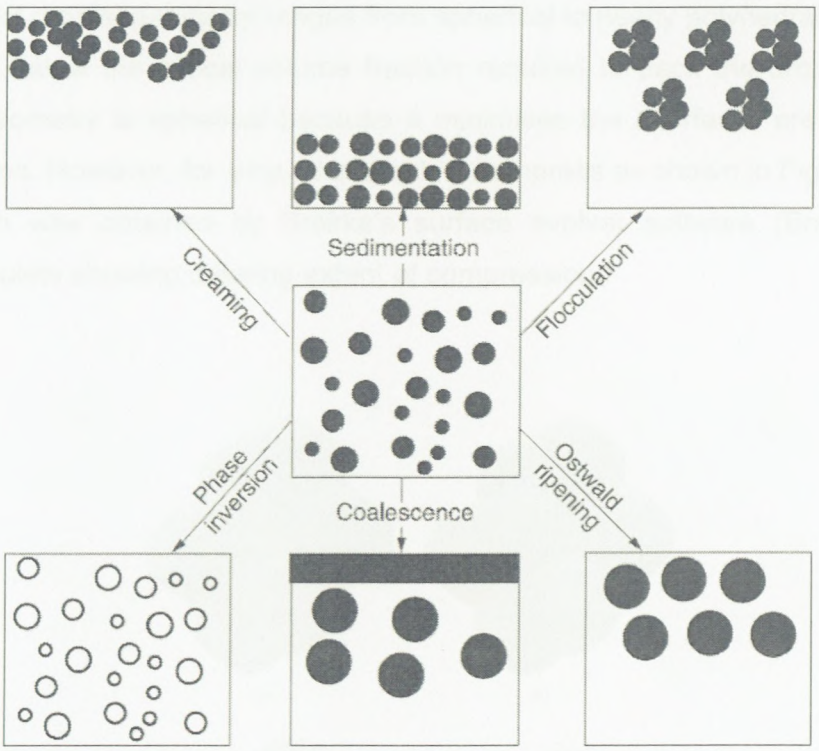

Figure 2.1: Schematic of the emulsion breakdown processes (Tadros, 2005)

While it may be tempting to attribute emulsion stability to the existence of a low interfacial tension, it is generally accepted today (Myers, 2006; McClements, 1999) that the interfacial tension effects are less important to overall long-term emulsion stability than the nature of the interfacial film. The ability of the interfacial film to withstand the pressures of droplet contacts (tenacity), its properties as a barrier to the passage of the dispersed phase into the continuous phase (to limit Ostwald ripening), and its ability to erect a physical or electrical barrier to droplet contact appears to be the major characteristics determining the ultimate stability of an emulsion (Myers, 2006).

2.4. Emulsion Structure

The structure of an emulsion can be divided into two primary types. The first class of structure is related to the interfacial geometry of individual droplets. Emulsions comprise a dispersion of deformable droplets, and this deformability allows droplets to assume different interfacial configurations. The second class of structure is related to the relative positions of a collection of droplets; the different positional configurations of droplets can be classified as ordered and disordered. For both classes of emulsion, the structure is strongly dependent on the volume fraction.

The interfacial droplet geometry ranges from spherical to nearly polyhedral. For volume fractions, φ, below the critical volume fraction required to pack the droplets, φ_c, the interfacial geometry is spherical because it minimises the interfacial area for a fixed droplet volume. However, for $\varphi > \varphi_c$, the droplets compress as shown in Figure 2.2. This figure, which was obtained by Brakke's surface evolver software (Brakke, 1992), presents droplets showing differing extent of compression.

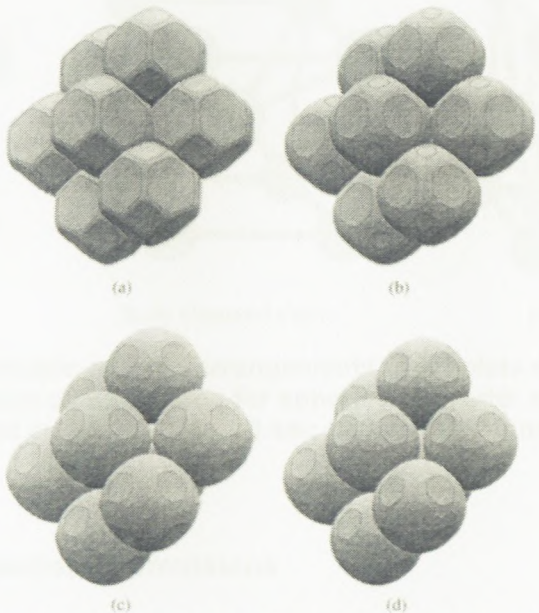

Figure 2.2: Droplets with different extent of compression in ordered emulsion (Durian, 2002)

The unit cell represented in this figure is a tetrakaidecahedron, possessing eight hexagonal and six square faces; the specific details of its geometry do not alter the definitions that follow (Durian, 2002). An array of droplets pressing against each other can be imagined by filling space with many unit cells stacked together. The droplet inside the unit cell has deformed to create flat facets which form one half of a water film between it and a neighbouring droplet. The region of water outside of where two facets meet is called a Plateau border. The number of facets on a particular droplet depends on the positional structure relative to its neighbours, and the figure serves only as an example for a particular structure.

In general, we can classify the ordered droplet arrangement as similar to crystals (Figure 2.3). However, the positional structure of dispersed colloidal droplets can range from that of a disordered gas to that of an ordered crystal. As with the interfacial

tension structure, the positional structure is most significantly affected by the volume fraction. At volume fractions well below φ_c, the droplets are free to execute Brownian motion and have a disordered structure resembling a gas. At volume fractions near and above φ_c, the droplets usually have a disordered, glassy structure (Lacasse et al., 1996b).

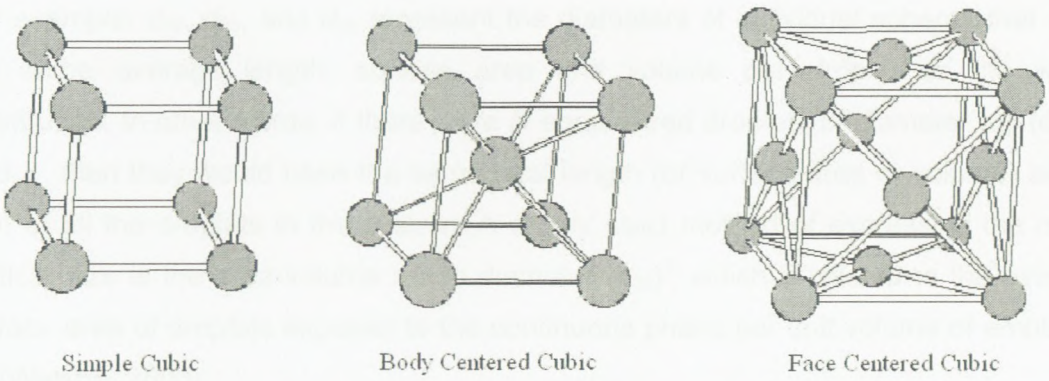

Figure 2.3: Different possible ordered arrangements of droplets which result in different formations of maximum close packing for spherical droplets: simple cubic, SC ($\varphi_m \approx 0.52$); body-centred cubic, BCC ($\varphi_m \approx 0.68$); face-centred cubic, FCC ($\varphi_m \approx 0.74$)

2.5. Microscopic Properties of Emulsions

2.5.1. General Terms

A complete description of an emulsion involves macroscopic and microscopic characteristics. It includes the microscopic properties of the fluids, droplets and interface, and their structure within the bulk emulsion. It also includes macroscopic properties like the osmotic pressure and volume fraction, which govern the equation of state for emulsion. The emulsion's macroscopic properties are determined from the microscopic properties; understanding emulsion properties at the colloidal length scale is necessary for understanding their properties at a macroscopic scale.

The droplet size distribution as one of the most important microscopic properties is characterised by statistics. Let d shows the droplet size (diameter), and $f(d)$ represents its frequency distribution given in number per unit volume per unit of d frequency. The n^{th} moment of the distribution, S_n, is defined as follows (Walstra, 2003):

$$S_n = \int_0^\infty d^n f(d)\mathrm{d}d \approx \sum_{i=1} N_i d^n \qquad (2\text{-}2)$$

where N_i represents particles in size class i; therefore S_0 is the total number of particles. Different average droplet sizes can be defined on the basis of distribution moments:

$$d_{ab} = \left(\frac{S_a}{S_b}\right)^{1/(a-b)} \quad (2\text{-}3)$$

For example, d_{10}, d_{20}, and d_{30} represent the diameters of individual spheres that have the same average length, surface area and volume per droplet as the whole distribution. In other words, if there were N equal-sized droplets of diameter d_{10} (or d_{20} or d_{30}), then they would have the same total length (or surface area or volume) as the sum of all the droplets in the system. A widely used method of expressing the mean particle size is the area-volume mean diameter $(d_{32})^*$, which is related to the average surface area of droplets exposed to the continuous phase per unit volume of emulsion, A_N (Walstra, 2003):

$$A_N = \frac{6\varphi}{d_{32}} \quad (2\text{-}4)$$

where φ is the volume fraction of the dispersed phase. The relative standard deviation or the variation coefficient of the distribution weighted with the n^{th} power of d is as follows (Walstra, 2003):

$$c_n = \left(\frac{S_n S_{n+2}}{S_{n+1}^2} - 1\right)^{1/2} \quad (2\text{-}5)$$

The uniformity ratio is an index of the polydispersity of the different droplet sizes, defined by the following expression:

$$U = \frac{\sum V_i \left| d(v,0,5) - d_i \right|}{d(v,0,5) \sum V_i} \quad (2\text{-}6)$$

where $d(v,0,5)$ is the median for the distribution, and V_i is the volume of droplets with a diameter d_i (Romero et al., 2008).

---

* Sauter mean diameter

The origin of the interfacial properties of emulsions lies in the interactions between the molecular constituents of the fluids and surfactant. These cause the interfacial tension, Laplace pressure, disjoining pressure, film thickness, and contact angle which describe the behaviour of the droplet interfaces at a mesoscopic, colloidal scale. They play an important role in describing the microscopic state of the emulsion, and the explanation of many macroscopic emulsion phenomena are facilitated by them.

The interfacial tension, σ, at the surfactant-coated droplet/matrix interface is determined by differences in intermolecular attraction and the surface density of the surfactant. Because the surface density is related to the bulk density of surfactant, σ depends on the bulk surfactant concentration, C. A finite surfactant concentration lowers the interfacial tension from its maximum at $C=0$, but once the surfactant concentration at the interface reaches the equilibrium with the micelles and free surfactant in the bulk, the interfacial tension becomes relatively insensitive to a larger C. This concentration is known as the critical micelles concentration, or CMC (Figure 2.4). Emulsions typically have relatively high interfacial tension, of the order of $\sigma=10mN/m$. If the interfacial tension were to approach zero, the oil, water and surfactant would spontaneously form a different colloidal system known as a microemulsion (Tadros, 2005).

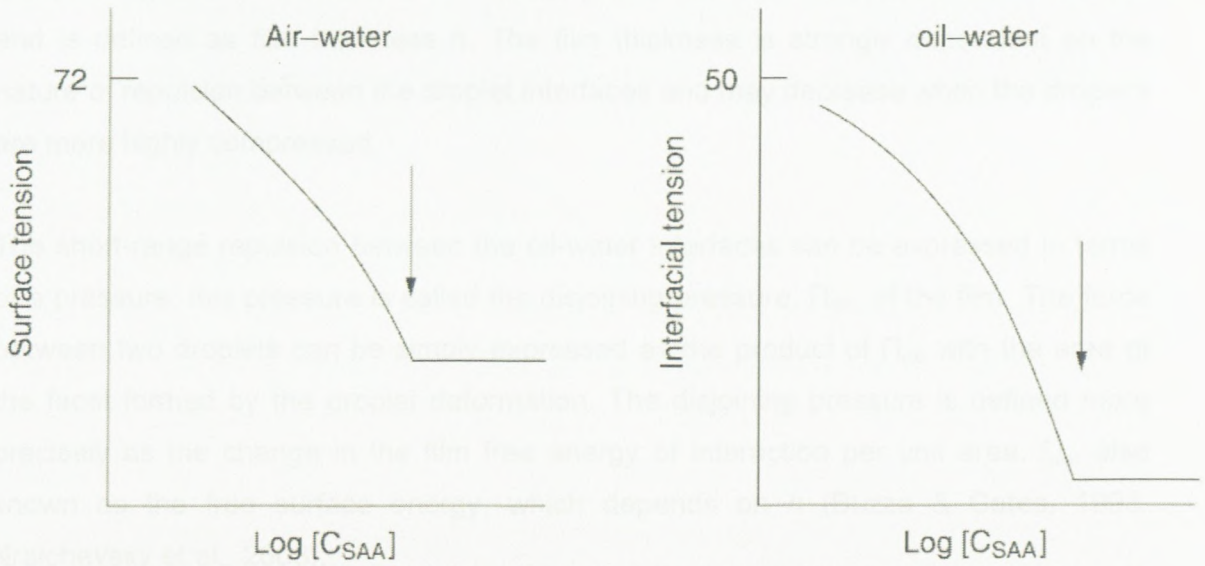

Figure 2.4: Variation of surface and interfacial tension with log[C_{SAA}] at the air-water and at the oil-water interface, where [C_{SAA}] denotes the concentration of surface active agent in bulk solution (Tadros, 2005)

The Laplace pressure, Π_L, is the pressure difference between fluids separated by an interface resulting from the interfacial tension and the curvature of the interface. If the local mean radii of curvature at a particular point on the interface are given by R_1 and R_2, the Laplace pressure would be:

$$\Pi_L = \sigma(\frac{1}{R_1} + \frac{1}{R_2}) \quad (2\text{-}7)$$

For an undeformed droplet, $R_1=R_2=R$, so the formal definition of the Laplace pressure of an undeformed droplet is $\Pi_L=2\sigma/R$. However, for the purpose of discussion, the factor of two is omitted, and σ/R is referred to as the Laplace pressure scale. If a droplet is distorted from its lowest energy spherical shape, then the Laplace pressure between the oil and water is also increased because the term in parentheses must be larger (Tadros, 2005).

2.5.2. Disjoining Pressure

The stabilising repulsion between droplets ensures that their interfaces do not get close enough to cause coalescence. Consequently, a region of continuous phase remains between them. When two droplets are pressed together, their interfaces begin to distort at a separation slightly larger than the undeformed droplet diameter due to the short-range stabilisation repulsion. As the droplet distorts, a thin film of continuous phase is created. Figure 2.5 illustrates a continuous phase film that lies between the interfaces and is defined as film thickness h. The film thickness is strongly dependent on the nature of repulsion between the droplet interfaces and may decrease when the droplets are more highly compressed.

The short-range repulsion between the oil-water interfaces can be expressed in terms of a pressure; this pressure is called the disjoining pressure, Π_{dis}, of the film. The force between two droplets can be simply expressed as the product of Π_{dis} with the area of the facet formed by the droplet deformation. The disjoining pressure is defined more precisely as the change in the film free energy of interaction per unit area, f_{dis}, also known as the free surface energy, which depends on h (Buzza & Cates, 1993, Kralchevsky et al., 2003):

$$\Pi_{dis}(h) = -\frac{\partial f_{dis}(h)}{\partial h}$$
$$f_{dis}(h) = \int_h^\infty \Pi_{dis}(h)dh \qquad (2\text{-}8)$$

For a positive, stable, disjoining pressure, $\partial f_{dis}/\partial h$ must be negative; the behaviour of $f_{dis}(h)$ is determined by the nature of the surfactant and the way in which it creates the repulsion. At the critical film thickness where the film becomes unstable, h^*, there is also a critical disjoining pressure, Π_{dis}^*.

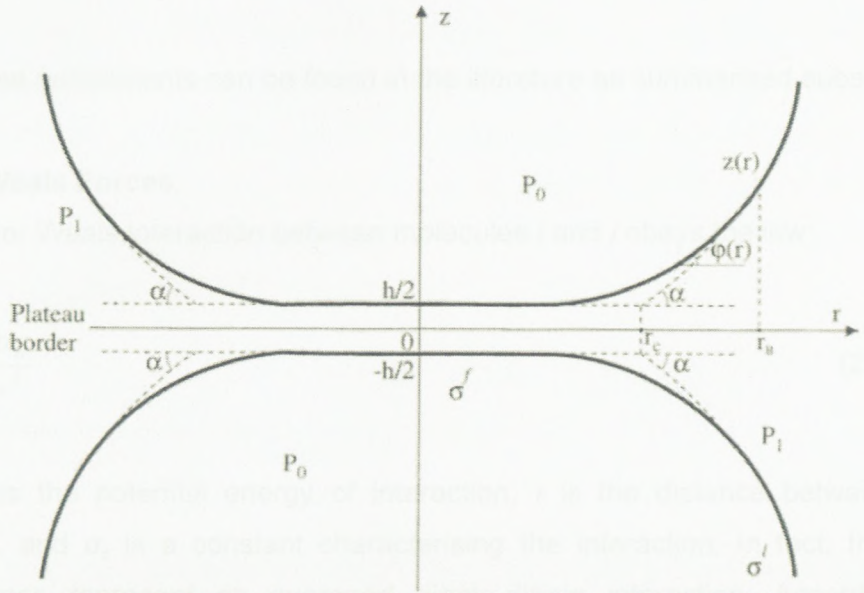

Figure 2.5: Liquid film between two attached fluid particles. The solid lines represent the actual interfaces, whereas the dashed lines show the extrapolated interfaces in the transition zone between the film and the Plateau border. (Kralchevsky et al., 2003)

If there are attractive forces in addition to the short-range repulsion between the droplet interfaces, the droplets can develop a nonzero contact angle, α, which is also illustrated in Figure 2.5. The contact angle is defined as half the total angle subtended by the droplet interfaces at the point where the thin film ceases to have a uniform thickness. In general, it depends on the film thickness and determines the behaviour of the free surface energy, $f_{dis}(h) = -2\sigma[1-\cos\alpha(h)]$, which, when substituted into the previous equation, relates it to the disjoining pressure (Aronson & Princen, 1980). It is a mesoscopic property, defined only at the length scale of a droplet, because there cannot be true discontinuity of the interfacial curvature at a microscopic level. For weak long-ranged attraction between interfaces, the contact angle is nearly zero.

The interaction between the surfaces of droplets that is named disjoining pressure, a concept traditionally used in the field of foams and emulsions (fluid system) in colloid and interface science (Bergeron, 1999), is completely analogous to what is commonly referred to as surface forces when considering interactions in thin films that separate two solid phases.

It is customary to separate the various contributions of the disjoining pressure Π_{dis} into the following components (Bergeron, 1999):

$$\Pi_{dis}(h) = \Pi_{el} + \Pi_{vw} + \Pi_{steric} + \Pi_{supra} + \ldots \quad (2\text{-}9)$$

where these components can be found in the literature as summarised subsequently.

Van der Waals Forces

The Van der Waals interaction between molecules *i* and *j* obeys the law:

$$u_{ij}(r) = -\frac{\alpha_{ij}}{r^6} \quad (2\text{-}10)$$

where u_{ij} is the potential energy of interaction, r is the distance between the two molecules, and α_{ij} is a constant characterising the interaction. In fact, the Van der Waals forces represent an averaged dipole-dipole interaction. According to the microscopic theory by Hamaker (1937), the Van der Waals interaction between two macroscopic bodies can be found by integration of Equation (2-10) over all couples of molecules, followed by subtraction of the interaction energy at infinite separation between the bodies. The result depends on the geometry of the system. For a plane-parallel film from component 3 located between two semi-infinite phases composed from components 1 and 2, the Van der Waals interaction energy per unit area and the respective disjoining pressure, stemming from Equation (1-10), are (Kralchevsky et al., 2003):

$$f_{vw} = -\frac{A_H}{12\pi h^2}; \quad \Pi_{vw} = -\frac{A_H}{6\pi h^3} \quad (2\text{-}11)$$

where, as usual, h is the thickness of the film and A_H is the compound Hamaker constant:

$$A_H = A_{33} + A_{12} - A_{13} - A_{23}; \qquad (A_{ij} = \pi^2 \rho_i \rho_j \alpha_{ij}; \quad i, j = 1,2,3) \tag{2-12}$$

A_{ij} is the Hamaker constant of components i and j; and ρ_i and ρ_j are the molecular number densities of phases i and j built up from components i and j, respectively (Derjaguin, 1989).

Lifshitz (1956) developed an alternative approach to the calculation of the Hamaker constant A_H in condensed phases, named the macroscopic theory. The latter is not limited by the assumption for pairwise additivity of the Van der Waals interaction. The Lifshitz theory treats each phase as a continuous medium characterised by a given uniform dielectric permittivity, which is dependent on the frequency, v, of the propagating electromagnetic waves. For the symmetric configuration of two identical phases "i" interacting across a medium "j", the macroscopic theory provides the expression (Israelachvili, 1992; Kralchevsky et al., 2003):

$$A_H = \frac{3}{4} k_B T \left(\frac{\varepsilon_i - \varepsilon_j}{\varepsilon_i + \varepsilon_j}\right)^2 + \frac{3 h_p \nu_e (n_i^2 - n_j^2)^2}{16\sqrt{2}(n_i^2 + n_j^2)^{3/2}} \tag{2-13}$$

where ε_i and ε_j are the dielectric constants of phases i and j; n_i and n_j are the respective refractive indices for visible light; h_p, as usual, is the Planck constant; ν_e is the main electronic absorption frequency, which is $\approx 3.0 \times 10^{15}$ Hz for water and most organic liquids. The first term on the right-hand side of Equation (2-13), $A_{iji}^{(\nu=0)}$, is the so-called zero-frequency term, expressing the contribution of the orientation and induction interactions. Indeed, these two contributions to the Van der Waals force represent electrostatic effects. Equation (2-13) shows that the zero-frequency term can never exceed ¾kT $\approx 3 \times 10^{-21}$ J (Kralchevsky et al., 2003).

Electrostatic Forces

One of the first and most studied contributions to the disjoining pressure arises from electrostatic interaction. These interactions result from the overlapping of the electric double layer that develops at charged interfaces. In the simplest case, a repulsive force develops between the interfaces due to the entropic confinement of the counter-ions which neutralise a charged interface. When two droplets approach to a distance h that

is smaller than the double layer extension, double layer overlap occurs and this leads to repulsion (the double layers cannot be fully developed). The electrostatic double-layer forces are obtained by solving the Poisson-Boltzmann equation under a variety of different boundary conditions (Bergeron, 1999).

The electrostatic double-layer force for constant surface potential, ψ_0, and constant surface charge, σ_0, respectively are as follows (Bergeron, 1999):

$$\Pi_{el}^{\psi} = \frac{\varepsilon \psi_0^2}{8\pi} \operatorname{sech}^2(\kappa h) \tag{2-14}$$

$$\Pi_{el}^{\sigma} = \frac{2\pi\sigma_0^2}{\varepsilon} \left(\frac{1+\operatorname{sech}(\kappa h/2)}{\tanh(\kappa h/2)}\right)^2 \tag{2-15}$$

where ε is the dielectric constant for medium, and Debye length $\lambda = 1/\kappa$ is defined from the following equation:

$$\lambda = \sqrt{\frac{\varepsilon k_B T}{8\pi n^0 e^2}} \sim C^{-1/2} \tag{2-16}$$

In this equation, n^0 is the number density of ions, e is the elementary charge, and C is the concentration of electrolyte (mole/lit).

Steric Interaction

Steric interaction can be observed in foam or emulsion films stabilised with non-ionic surfactants or with various polymers, including proteins. The usual non-ionic surfactant molecules are anchored (grafted) to the liquid interface by their hydrophobic moieties. When the surface concentration of adsorbed molecules is high enough, the hydrophilic chains form a brush (Figure 2.6b).

The steric interaction between two approaching surfaces appears when the film thickness becomes of the order of, or smaller than, $2L$, where L is the mean-square end-to-end distance of the hydrophilic portion of the chain. If the chain were entirely extended, then L would be equal to Nl with l the length of a segment; however, due to the Brownian motion L is lower than Nl. For an anchored chain, such as that depicted in Figure 2.6a, in a theta solvent, L can be estimated as (Russel et al., 1989):

$$L \approx L_0 = l\sqrt{N} \qquad (2\text{-}17)$$

In a good solvent $L>L_0$, whereas, in a poor solvent, $L<L_0$. In addition, L depends on the surface concentration, Γ, of the adsorbed chains; i.e., L is different for an isolated molecule and for a brush (Figure 2.6).

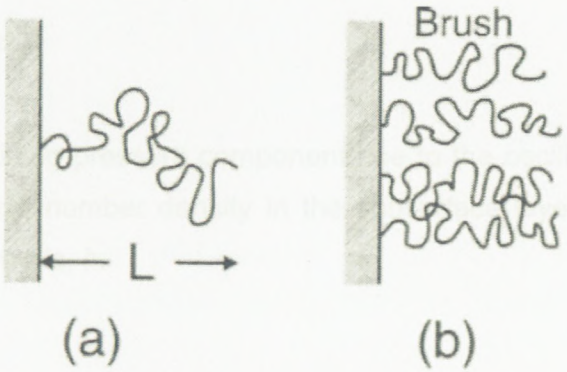

Figure 2.6: Polymeric chains adsorbed at an interface: (a) terminally anchored polymer chain of mean end-to-end distance L; (b) a brush of anchored chains (Kralchevsky et al., 2003)

We now consider the case of terminally anchored chains, like those depicted in Figure 2.6a and b. Dolan and Edwards (1975) calculated the steric interaction free energy per unit area, as a function on the film thickness, h, in a theta solvent:

$$\begin{aligned} f_{steric} &= k_B T\Gamma[\frac{\pi^2}{3}\frac{L_0^{\,2}}{h^2} - \ln(\frac{8\pi}{3}\frac{L_0^{\,2}}{h^2})] \quad \text{for} \quad h < L_0\sqrt{3} \\ f_{steric} &= 4k_B T\Gamma \exp(-\frac{3h^2}{2L_0^{\,2}}) \quad \text{for} \quad h > L_0\sqrt{3} \end{aligned} \qquad (2\text{-}18)$$

In the case of good solvent, the disjoining pressure can be calculated by means of the de Gennes (1987) theory as:

$$\Pi_{steric} = k_B T\Gamma^{3/2}[(2L/h)^{9/4} - (h/2L)^{3/4}]; \quad \text{for} \quad h < 2L_g;\ L_g = N(\Gamma l^5)^{1/3} \qquad (2\text{-}19)$$

where L_g is the thickness of a brush in a good solvent. The positive and the negative terms in the right-hand side of Equation (2-19) correspond to osmotic repulsion and elastic attraction.

Oscillatory Structural Forces

The oscillatory structural forces appear when monodisperse spherical (in some cases ellipsoidal or cylindrical) particles are confined between the two surfaces of a thin film. The oscillatory structural force is a result of overlap of the structured zones at two approaching surfaces. A simple connection between density distribution and structural force is given by the contact value theorem (Israelachvili, 1992):

$$\Pi_{os} = k_B T[n_s(h) - n_s(\infty)] \qquad (2\text{-}20)$$

where Π_{os} is the disjoining pressure component due to the oscillatory structural forces and $n_s(h)$ is the particle number density in the subsurface layer as a function of the distance between the walls, h.

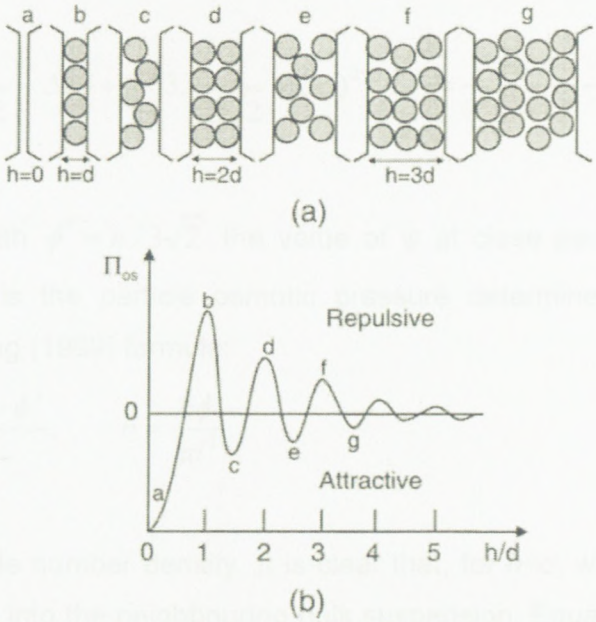

Figure 2.7: (a) Sketch of the consecutive stages of the thinning of a liquid film containing spherical particles; (b) plot of the related oscillatory structural component of disjoining pressure, Π_{os}, versus the film thickness h (Kralchevsky et al., 2003)

Figure 2.7 illustrates the variation of ns with h and the resulting disjoining pressure, Π_{os}. We see that in the limit of very small separations, as the last layer of particles is eventually squeezed out, $n_s \to 0$ and:

$$\Pi_{os} \to -k_B T n_s(\infty); \quad \text{for} \quad h \to 0 \qquad (2\text{-}21)$$

In other words, at small separations Π_{os} is negative (resulting in an attractive force that is known as the depletion force, for which see Section 2.5.3 below) (Kralchevsky et al., 2003).

The following semi-empirical formula for the oscillatory structural component of disjoining pressure has been proposed (Kralchevsky & Denkov, 1995):

$$\Pi_{os} = P_0 \cos(\frac{2\pi h}{d_1}) \exp(\frac{d^3}{d_1^2 d_2} - \frac{h}{d_2}); \text{ for } h > d$$
$$\Pi_{os} = -P_0; \quad \text{for } 0 < h < d \qquad (2\text{-}22)$$

where d is the diameter of the hard spheres, and d_1 and d_2 are the period and the decay length of the oscillations which are related to the particle volume fraction, φ, as follows:

$$\frac{d_1}{d} = \sqrt{\tfrac{2}{3}} + 0.237(\frac{\pi}{3\sqrt{2}} - \Delta\phi) + 0.633(\frac{\pi}{3\sqrt{2}} - \Delta\phi)^2 \; ; \; \frac{d_2}{d} = \frac{0.4866}{\frac{\pi}{3\sqrt{2}} - \Delta\phi} - 0.420 \qquad (2\text{-}23)$$

Here $\Delta\phi = \phi^* - \phi$ with $\phi^* = \pi/3\sqrt{2}$ the value of φ at close packing (Kralchevsky & Denkov, 1995). P_0 is the particle osmotic pressure determined by means of the Carnahan and Starling (1969) formula:

$$P_0 = nk_B T \frac{1 + \phi + \phi^2 - \phi^3}{(1-\phi)^3}, \qquad n = \frac{6\phi}{\pi d^3} \qquad (2\text{-}24)$$

where n is the particle number density. It is clear that, for $h<d$, when the particles are expelled from the slit into the neighbouring bulk suspension, Equation (2-24) describes the depletion attraction. The contribution of the oscillatory structural forces to the interaction free energy per unit area of the film can be obtained by integrating Π_{os} (Kralchevsky et al., 2003):

$$\mathrm{f}_{os} = \frac{P_0 d_1 \exp(d^3/d_1^2 d_2 - h/d_2)}{4\pi^2 + (d_1/d_2)^2} [\frac{d_1}{d_2} \cos(\frac{2\pi h}{d_1}) - 2\pi \sin(\frac{2\pi h}{d_2})]; \text{ for } h \geq d$$
$$\mathrm{f}_{os} = \mathrm{f}_{os}^{\,h \geq d}\Big|_{h=d} - P_0(d-h); \quad \text{for } 0 \leq h \leq d \qquad (2\text{-}25)$$

This semi-empirical model of structural oscillatory forces can be used to predict the micellar forces in colloid systems.

Other Forces

Repulsive hydration forces; hydrophobic attraction; fluctuation wave forces including undulation and peristaltic forces; and protrusion force are in the class of short-range interaction forces.

2.5.3. Depletion Attraction

The depletion attraction between droplets is completely entropic in origin; it is essentially due to the size difference between the droplets and the surfactant micelles. The centres of the smaller particles (micelles), of diameter *d*, cannot approach the surface of a bigger particle (of diameter *D*) at a distance shorter than *d/2*, which is the thickness of the depletion layer. When the two depletion layers overlap (Figure 2.8), some volume between the large particles becomes inaccessible for the smaller particles. This gives rise to an osmotic pressure, which tends to suck out the solvent between the bigger particles, thus forcing them against each other. The total depletion force experienced by one of the bigger particles is (Asakura & Oosawa, 1958):

$$F_{dep} = -nk_B TS(h_0) \tag{2-26}$$

where the effective depletion area is:

$$\begin{aligned} S(h_0) &= \frac{\pi}{4}(2D + d + h_0)(d - h_0); \quad \text{for } 0 \le h_0 \le d \\ S(h_0) &= 0; \quad \text{for } h_0 \ge d \end{aligned} \tag{2-27}$$

Here, h_0 is the shortest distance between the surfaces of the larger particles, and *n* is the number density of the smaller particles. By integrating Equation (2-27) we can derive an expression for the depletion interaction energy between the two larger particles, $U_{dep}(h_0)$ (Kralchevsky et al., 2003).

In the case of plane-parallel films, the depletion component of disjoining pressure is:

$$\begin{aligned} \Pi_{dep} &= -nk_B T; \; h < d \\ \Pi_{dep} &= 0; \qquad h > d \end{aligned} \tag{2-28}$$

which is similar to Equation (2-22). This is not surprising because in both cases we are dealing with the excluded volume effect (Kralchevsky et al., 2003).

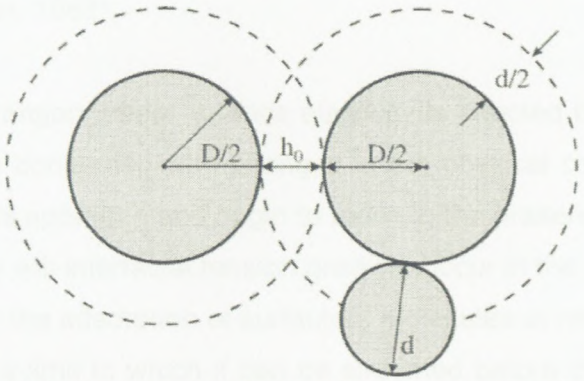

Figure 2.8: Illustration of the excluded volume. When two large spheres of diameter *D* are at a separation $h_0 < D+d$, small spheres of diameter *d* are geometrically excluded from exploring the volume between the large spheres. (Kralchevsky et al., 2003)

2.5.4. Others

At equilibrium, the interfacial tension in a system will be uniform. However, in the dynamic environment of an emulsion system, non-uniformities will arise as a result of droplet deformation in which new surface area will be produced by deviation of the droplet from a perfectly spherical shape. Since the diffusion of new surfactant molecules to the interface to lower the interfacial tension will require a finite amount of time, interfacial tension gradients will develop, leading to the presence of surface elastic response. If sufficient differences in local interfacial tension develop, a rapid spreading of surfactant molecules into regions of higher tension will occur. Concurrent with the movement of surfactant into region of high interfacial tension, underlying layers of liquid associated with the surfactant may be dragged along. This phenomenon and its corresponding stress are known as Marangoni effect and Marangoni stress, respectively (Sherman, 1968).

Surface elasticity in the sense under consideration cannot exist in a system of pure liquid phases. In a system containing surfactant molecules, gradients of interfacial tension can arise as a result of the formation of a new area, as mentioned above, or because of the loss of interfacial area. In the former case, the time lag between the formation of new interface and the diffusion of surfactant to that interface will produce an interfacial tension that is higher than equilibrium. The local value of the surface

concentration will fall and the value of interfacial tension will approach that of the pure system. The net effect will be a tendency for the interface to contract, providing a "healing" effect to reduce the chance of droplet coalescence. In the case of loss of interfacial tension area, there will be a time lag from the point of compression of the interfacial film until the excess surfactant molecules can desorb and diffuse away from the interface (Sherman, 1968).

In addition to the Marangoni effect, surface elasticity is affected by what is termed the Gibbs effect, which is concerned with changes in the physical conditions of the liquid lamella as two droplets approach and begin to touch in the presence of flocculation and coalescence. Not only will interfacial tension gradient occur in the film as a result of the finite time required for the adsorption of surfactant molecules at newly formed interface, but the film will have a limit to which it can be stretched before the lamellar interfacial tension increases to the point where the stabilising effect of the film is lost. The coefficient of elasticity, E, for an interfacial film under such conditions was given by Gibbs (1931) as $E=2Ad\sigma/dA$, where A is the interfacial area occupied by a given quantity of surfactant concentration. As in the case of the Marangoni effect, the Gibbs elasticity will be significantly affected by the surface activity of the adsorbing species (Sherman. 1968).

Beside the possible existence of the interfacial tension gradients, other interfacial rheological stresses of a viscous nature may arise, such as those relating to interfacial shear and dilatational viscosities. Many surfactant and polymer films also exhibit non-Newtonian interfacial rheological behaviour that may be characterised by Bingham plastic models and interfacial viscoelasticity (Tadros, 2005).

2.6. Macroscopic Properties of Emulsions

2.6.1. General Terms

The important macroscopic properties that describe the state of an emulsion are the oil volume fraction, φ, osmotic pressure, Π, rheological properties, and temperature, T. This state is ultimately determined by the microscopic droplet deformation and structure.

The oil volume fraction φ is simply defined as the volume of the oil present in a macroscopic volume of the emulsion divided by that macroscopic volume. Near $\varphi \approx 0$, the emulsion is a dilute dispersion of spherical oil droplets, while near $\varphi \approx 1$, the emulsion is a concentrated dispersion of highly deformed oil droplets.

2.6.2. Osmotic Pressure

The osmotic pressure Π is a general equilibrium property of a heterogeneous system composed of a continuous and a dispersed phase (McGlashan, 1979). An emulsion consisting of dispersed phase in a continuous phase is a heterogeneous system and has osmotic pressure. Consider the emulsion in contact with a reservoir of continuous phase, but separated by a partition made of a semi-permeable membrane, as shown in Figure 2.9. The membrane partition prevents droplet flow, and Π is the difference between the partial continuous phase pressure of the emulsion, P_1, and the reservoir, P_2, at equilibrium temperature $T_1=T_2$ and continuous phase chemical potential $\mu_1=\mu_2$. The osmotic pressure of an emulsion is the equilibrium longitudinal stress required to confine the oil droplets to a finite volume fraction, allowing for the free exchange of the water with the reservoir.

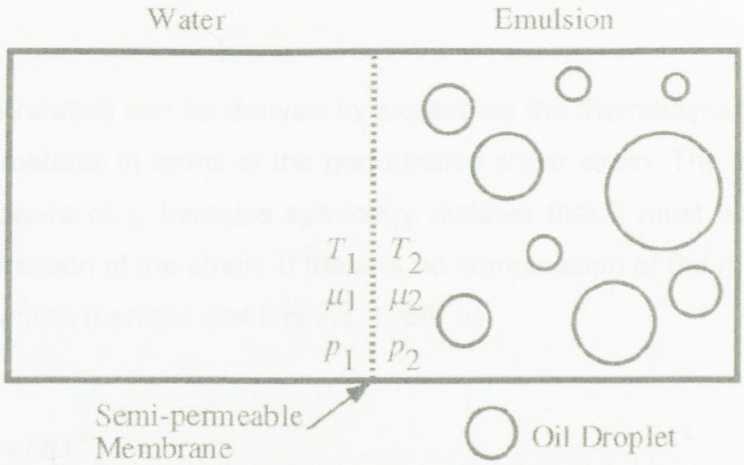

Figure 2.9: Schematic diagram of a polydisperse emulsion separated from a reservoir of water by a semi-permeable membrane (Mason, 1995)

The osmotic pressure of an emulsion is defined more formally in terms of a thermodynamic derivate of the total Helmholtz free energy, F, of the droplets. It is the first derivative of F with respect to total volume, V, at fixed dispersed phase volume, $V_\circ$:

$$\Pi = -\left.\frac{\partial F}{\partial V}\right|_{V_\circ} = \frac{\varphi^2}{V_\circ}\left.\frac{\partial F}{\partial \varphi}\right|_{V_\circ} \qquad (2\text{-}29)$$

It represents the equilibrium energy density required to confine the dispersed phase droplets to a finite volume fraction of continuous phase.

The temperature T is a measure of energy exciting the emulsion system from its lowest energy ground state. It defines the thermal energy per degree of freedom, $k_B T/2$, of the emulsion system above the state, consistent with the equipartition theorem of thermodynamics. It sets the amplitude of the average translational, rotational, and interfacial shape fluctuations of the system of deformable droplets.

2.6.3. Linear Shear Elasticity

When a small shear stress is applied to a material, the material deforms, exerting a restoring stress which exactly opposes the applied shear. The strain deformation and the shear stress are linearly related by a form of Hooke's law, with G, the elastic shear modulus, as the coefficient of linearity:

$$\tau = G\gamma \tag{2-30}$$

This constitutive relation can be derived by expanding the thermodynamic free energy for an isotropic material in terms of the perturbative shear strain. The free energy is a sum of even powers of γ, because symmetry dictates that it must be invariant with respect to the direction of the strain. If there is no compression of the material, the free energy can be written (Landau and Lifshitz, 1986) as:

$$F = F_0 + VG\frac{\gamma^2}{2} + O[\gamma^4] \tag{2-31}$$

where F_0 is a constant energy of the expansion and does not play a role in the shear rheology. Hooke's law, eq. (2-30), can be recovered by differentiating the free energy once with respect to γ:

$$\tau = \frac{1}{V}\frac{\partial F}{\partial \gamma}\bigg|_{\gamma=0} \tag{2-32}$$

where the condition $\gamma=0$ is used to eliminate any nonlinear dependence. The elastic shear modulus can be found by differentiating again with respect to γ (Mason, 1995):

$$G = \frac{1}{V}\frac{\partial^2 F}{\partial \gamma^2}\bigg|_{\gamma=0} = \frac{\varphi}{V_0}\frac{\partial^2 F}{\partial \gamma^2}\bigg|_{\gamma=0} \tag{2-33}$$

2.6.4. Shear Viscoelasticity

In order to model the viscoelastic behaviour, the small changes in stress can be assumed to equal small changes in the modulus times the strain:

$$d\tau = \gamma dG \tag{2-34}$$

The *memory function* can be defined as the time derivative of *G*:

$$M(t) = -\frac{dG(t)}{dt} \tag{2-35}$$

Since the relaxation modulus *G(t)* decreases with time, the derivative will be negative. Thus the minus sign is added to make *M(t)* a positive function. Therefore:

$$d\tau = -M\gamma dt \tag{2-36}$$

If the relaxation modulus (and thus the memory function) depends only on time, we can make up any larger deformation (but deformations still within the linear range of the material) by summing up all the small deformations (Macosko, 1994):

$$\int_0 d\tau = \tau = -\int_{-\infty} M(t-t')\gamma(t')dt' = -\int_0^{\infty} M(s)\gamma(t-s)ds \tag{2-37}$$

We can also write the model directly in terms of the relaxation modulus. Consider a small change in stress due to a change in strain:

$$d\tau = Gd\gamma = G\frac{d\gamma}{dt}dt = G\dot{\gamma}dt \tag{2-38}$$

Integrating this expression gives:

$$\tau = \int_{-\infty} G(t-t')\dot{\gamma}(t')dt' = \int_0^{\infty} G(s)\dot{\gamma}(t-s)ds \tag{2-39}$$

Thus the stress is an integral, over all past time, of the relaxation modulus times the rate of strain. Since the deformation might be changing with time, $\dot{\gamma}$ is a function of time. This is the form that is most frequently used because *G(t)* can be measured directly (Macosko, 1994).

One of most important experiments for examining the linear viscoelasticity of material is the application of sinusoidal deformation. Within a few cycles of start-up and often much less, the stress will also oscillate sinusoidally at the same frequency but in general will be shifted by a phase angle δ with respect to the strain wave. This is illustrated in Figure 2.10 and expressed mathematically as follows:

$$\begin{aligned} \gamma &= \gamma_0 \sin \omega t \\ \dot{\gamma} &= d\gamma / dt = \dot{\gamma}_0 \cos \omega t \\ \tau &= \tau_0 \sin(\omega t + \delta) \end{aligned} \qquad (2\text{-}40)$$

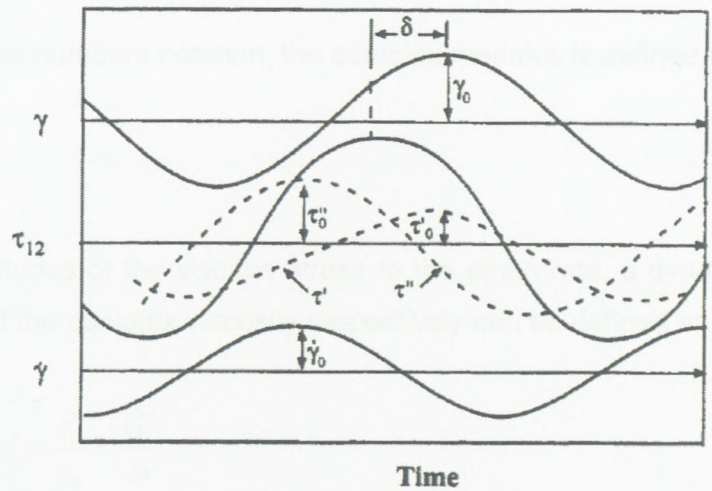

Figure 2.10: Sinusoidally oscillating shear strain produces a sinusoidal stress phase shifted by an amount δ. For analysis, the stress wave is broken down into two waves, τ' in phase with γ and τ'', 90° out of phase. Note that τ'' is in phase with the rate of strain wave $\dot{\gamma} = d\gamma / dt$. (Macosko, 1994)

Such data are analysed by decomposing the stress wave into two waves of the same frequency, one in phase with the strain wave ($\sin \omega t$) and one 90° out of phase with this wave ($\cos \omega t$). Thus (Macosko, 1994):

$$\tau = \tau' + \tau'' = \tau_0' \sin \omega t + \tau_0'' \cos \omega t \qquad (2\text{-}41)$$

Trigonometry shows that:

$$\tan\delta = \frac{\tau_0''}{\tau_0'} \tag{2-42}$$

This decomposition suggests two dynamic moduli:

$$G' = \frac{\tau_0'}{\gamma_0}; \qquad G'' = \frac{\tau_0''}{\gamma_0} \tag{2-43}$$

Where G' is the in-phase or elastic modulus, and G'' is the out-of-phase, viscous, or loss modulus. So, we have:

$$\tan\delta = \frac{G''}{G'} \tag{2-44}$$

By using complex numbers notation, the complex modulus is defined as follows:

$$G^* = G' + iG'' \tag{2-45}$$

From the magnitudes of the viscous stress to the strain rate, a dynamic viscosity and an elastic part of the complex viscosity respectively can be defined as follows:

$$\eta' = \frac{\tau_0''}{\dot{\gamma}_0} = \frac{G''}{\omega}; \quad \eta'' = \frac{\tau_0'}{\dot{\gamma}_0} = \frac{G'}{\omega} \tag{2-46}$$

and:

$$\eta^* = \eta' - i\eta'' \tag{2-47}$$

Mason (1995) and Mason et al. (1996) suggested that the strain at which the behaviour departs from linear viscoelasticity in sinusoidal experiment can be taken as yield stress; because a plastic material behaves as a general linear viscoelastic material at sufficiently small deformations, but it begins to flow at larger deformations. When it begins to flow, the stress resulting from a harmonic strain will not be sinusoidal, but will

exhibit flattened peaks. By plotting the strain and the peak stress amplitude at the top of the flattened peak, a stress-strain diagram like the one in Figure 2.11 is obtained. The yield strain and yield stress can be defined by a knee in the stress amplitude versus strain amplitude diagram. The log-log plot exhibits a slope of one in the linear regime at low τ and γ. However, at high τ and γ, the slope is much less than one, where it was argued to be an indication of a regime of plastic flow offering less resistance to deformation. The definition of yield stress and yield strain based on this method is schematically shown in Figure 2.11. We use the "dynamic yield" term to differentiate it from the yield stress defined from steady shear flow (see next section).

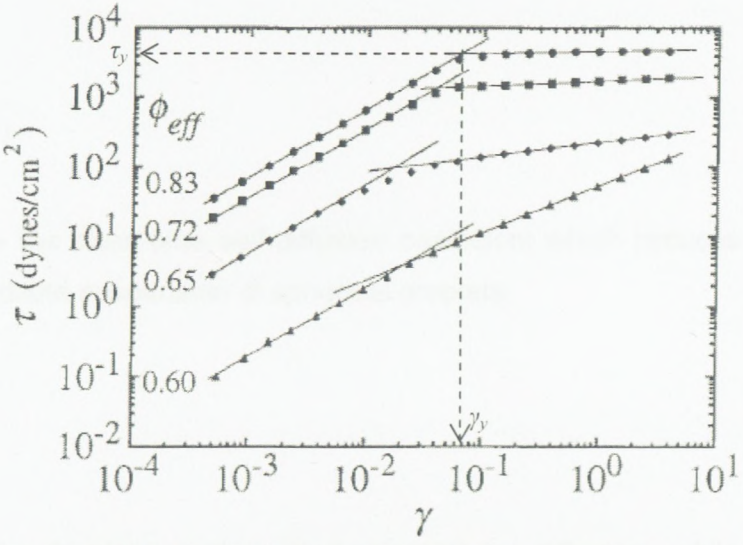

Figure 2.11: The method of determining yield point for concentrated emulsions based on sinusoidally oscillating shear experiments (Mason et al., 1996)

As a consequence of the extrapolation from the linear regime, the yield stress is proportional to the yield strain and the magnitude of the complex modulus, $|G^*|$:

$$\tau_y = |G^*|\gamma_y \tag{2-48}$$

The accuracy of the intersection method drops when the nonlinear flow regime has a slope that approaches one, for weakly yielding materials. Furthermore, since $|G^*|$ can depend on frequency, the yield point definition may depend on measurement frequency, which will be investigated in the results and discussion of this dissertation.

2.6.5. Steady Shear Flow Properties

Steady shear rheology is more complicated, because it can completely change the equilibrium of the microscopic structure. This change in structure, in turn, alters the resistance to flow given by the stress until a self-consistent dynamic equilibrium is reached between the structure and flow.

The steady shear flow of a dilute colloidal emulsion can be characterised by the dimensionless Peclet number which indicates whether droplet motion is dominated by the convective shear flow or by Brownian motion. The Peclet number, *Pe*, is defined as the ratio of the time required for a droplet to diffuse a distance of its radius, R^2/D_s, divided by the time required for it to convect the same distance, $1/\dot{\gamma}$:

$$Pe(\varphi) = \frac{\dot{\gamma} R^2}{D_s(\varphi)} \tag{2-49}$$

where $D_s(\varphi)$ is the short-time self-diffusion coefficient which reduces to the following equation for a dilute suspension of spherical droplets:

$$D_0 = \frac{k_B T}{6\pi\eta R} \tag{2-50}$$

For *Pe<<1*, the droplet's motion is dominated by diffusion, while for *Pe>>1* the convection dominates the droplet motion (Mason, 1995).

The degree of deformation of a droplet in steady shear flow is characterised by the dimensionless capillary number, *Ca*. and is defined by the ratio of the viscous stress, $\eta\dot{\gamma}$, to the Laplace pressure, σ/R:

$$Ca(\varphi) = \frac{R\dot{\gamma}\eta(\varphi)}{\sigma} \tag{2-51}$$

where $\eta(\varphi)$ can be interpreted as an effective viscosity of the continuous phase, which includes the effects of neighbouring droplets at high φ, or in other words, the emulsion viscosity. The capillary number indicates whether the shape of the droplet interface is dominated by the interfacial tension (*Ca<<1*, creeping flow) or convective flow of the

viscous fluid surrounding the droplet ($Ca>>1$, where droplets may break-up) (Mason, 1995).

Moreover, the behaviour of different materials at very low shear stresses has always been a subject of special interest. This interest arises from the idea that applying low stresses allows the properties of the unperturbed structure of a material to be explored.

Generally speaking, there are two limiting situations in low shear stresses. In the first case, a regime of constant viscosity is observed over a relatively wide range of shear rates (or stresses) which is being referred to as the initial Newtonian viscosity. In the second case, an unlimited growth in viscosity occurs at some limiting shear stress, below which flow becomes impossible. This may be viewed as a transition to solid-like behaviour. If the transition takes place sharply, the point of transition is deemed to be the yield stress. The phenomenon of the yield stress was proposed as the first milestone of rheology by Bingham (1922) and continues to be the focus for numerous authors. The concept of yielding at low stresses is commonly accepted for many materials, including various different types of suspension, consistent greases, filled polymer melts, ice suspensions, and concentrated emulsions like mayonnaise.

However, in the determination of either the low-shear-rate Newtonian viscosity or the yield stress, some doubts remain: are the experimental conditions appropriate for speaking about a genuine threshold situation? This problem has been discussed in several publications (Barnes & Walters, 1985; Nguyen & Boger, 1992; Barnes, 1999, 2007). As the yield stress is often found by extrapolation of experimental data, the result may strongly depend on the chosen procedure of experimental data fitting. So the conclusion: "It depends on what you mean ... by the yields stress" (Barnes, 2007) seems to be the most reasonable answer to the problem of measuring "the yield stress" (Figure 2.12).

But in some cases, at least, the existence of yielding and the transition from solid-like to liquid-like behaviour seem evident. This is true for many multi-component systems where a dispersed phase creates some form of rigid structure and the yield stress characterises its strength. Besides the experimental evidences, the existence of the physically-based yielding behaviour of highly concentrated emulsions was proven in several theoretical publications devoted to modelling the properties of these materials (Princen, 1983; Princen & Kiss, 1989; Mason et al., 1996; Mason, 1999).

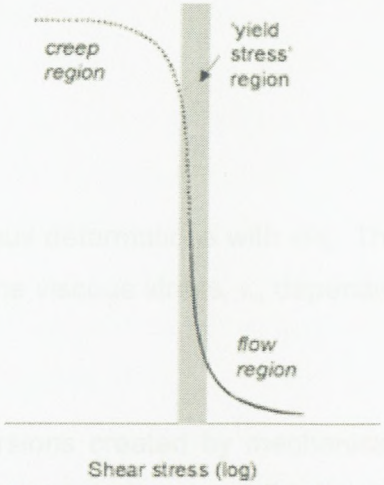

Figure 2.12: The flow curve of typical structured liquids, showing the 'creep' and 'flow' regions. The precise position of the yield stress within the yield stress region often depends on the method used to measure it or the equation used to fit the data. (Barnes, 2007)

Nevertheless, the problem of the experimental determination of yield stress has continued to be debated. As a general rule, the yield stress is assigned to the vertical part of a viscosity against the shear stress curve obtained from different deformation modes, and particularly from the decreasing shear rate mode. In that case, the value of the yield stress is either quite unambiguous or is found by extrapolation of experimental points, using a fitting equation such as the Bingham, Casson, Herschel-Bulkley (Malkin & Isayev, 2006) and Windhab (1993) models respectively, as follows:

$$\tau = \tau_y + \eta_p \dot{\gamma} \tag{2-52}$$

$$\tau^{1/2} = \tau_y^{1/2} + (\eta_p \dot{\gamma})^{1/2} \tag{2-53}$$

$$\tau = \tau_y + K\dot{\gamma}^n \tag{2-54}$$

$$\tau = \tau_{y0} + \eta_\infty \dot{\gamma} + (\tau_{y1} - \tau_{y0})[1 - \exp(-\dot{\gamma}/\dot{\gamma}^*)] \tag{2-55}$$

where τ_y is the yield stress, η_p is the plastic viscosity, and K and n are empirical constants. The Windhab (1993) model includes the directly measured yield stress, τ_{y0}, and the high shear viscosity, η_∞. It also considers the crossover point, τ_{y1}, which is usually observed in the flow curve of highly concentrated emulsions at medium shear rates.

As a concluding remark, the total stress is generally assumed to be the sum of the yield and viscous stresses:

$$\tau(\dot{\gamma}) = \tau_y + \tau_v(\dot{\gamma}) \quad (2\text{-}56)$$

which is valid for homogeneous deformations with $\tau > \tau_y$. The yield stress is independent of strain rate, however, and the viscous stress, τ_v, depends on the strain rate.

2.7. Summary

Emulsions are biliquid dispersions created by mechanical mixing and stabilised by a surfactant. Their primary microscopic feature is the Laplace pressure, which must be overcome to deform the droplets. A second important feature is the existence of a continuous phase film between droplets due to the short-range stabilising repulsion. These films exist even when the droplets are highly deformed and faceted. The most important microscopic parameters are disjoining pressure and depletion attraction, while the osmotic pressure and rheological properties are basic macroscopic properties. The microscopic properties provide the formulation for understanding the macroscopic state and rheological behaviour which will be treated in following chapters.

Chapter 3 – Highly Concentrated Emulsions

3.1. Introduction

Highly concentrated emulsions (HCE) are classified as high internal phase ratio emulsions (or simply HIPRE), and the dispersed phase droplets are ranged in a hexagonal closely packed configuration (i.e. far beyond the close packing limit of spherical droplets of 74%). This closely packed configuration and the profound hydrodynamic interaction between neighbouring droplets induce mechanical interference between the droplets, thus prohibiting their free movement. In such systems, extensive aggregation or flocculation of the dispersed phase droplets occur, which results in a stable, weak, gel-like particulate network (Jager-Lézer et al., 1998; Partal et al., 1997).

3.2. Theoretical Models

Princen and Princen and Kiss, in a series of papers in the 1980s (Princen 1983, 1985, 1986; Princen & Kiss 1986, 1987, 1989) derived rheological models of emulsions by focusing on what happens at the droplet scale when an emulsion is put under stress. They did this in order to get a more profound understanding of emulsion rheology. Although Princen and Kiss originally thought of emulsions as models for foam, which was their primary concern, their droplet scale studies are seminal to present-day understanding of emulsion behaviour. For many purposes, dense emulsions can be thought of as incompressible foams. Princen and Kiss furthermore persuasively argued that droplet/bubble dynamics in emulsions and foams have similar affects on their rheology. They included theoretical and experimental results for real emulsions. They calculated the stress response of the material up to yield point, derived a yield stress and determined a viscosity for the material. Furthermore still, they tried to extend this for a variety of dispersed phase concentrations.

Their earliest work was based on a two-dimensional hexagonal model of highly concentrated emulsion: a honey-comb of bubbles. In two dimensions, the maximum packing density for identical close-packed bubbles is $\pi\sqrt{3}/6 \approx 0.9069$. At this volume fraction, two-dimensional droplets touch at single contact point. As soon as this packing fraction is exceeded, the bubble contacts are replaced by bubble-to-bubble interfaces. These areas between touching bubbles are thin interfacial films of the continuous phase. As the packing density increases towards one, droplet crowding causes further deformation and the interfacial area become larger. When the packing density reaches

its maximum, the circular shape of the droplets changes to hexagonal and the material takes on a honeycomb structure. This honeycomb structure is the most efficient way for filling area with a single shape, in terms of minimising interfacial length (Hales, 2001; Princen, 1983). Further, a necessary condition for mechanical equilibrium is that the intersection of interfacial films always involves three films, meeting at 120° (Lamarle, 1885, as cited in Princen, 1983).

In their model, Princen and Kiss and Princen explicitly showed that the bubbles rearrange under shear. At first, shear causes stretching (or shortening, depending on their orientation to the shear direction) of droplet interfaces. Because of the ideal packing of these identical droplets, each droplet in the model responds exactly like every other droplet in the model. The strain-induced distortion of the hexagonal shape continues until the interfaces that shorten disappear. As soon as one interface disappears, another forms. The new interface has a new orientation, and connects two droplets that have not previously been in contact. Due to the symmetry of this ideal system, droplets rearrange in rows. A rearrangement is the shifting of an entire row of bubbles past another entire row of bubbles by one droplet diameter. Along with this rearrangement there is a sudden, finite release of stress. Focusing on just four bubbles, a rearrangement involves an exchange of nearest neighbours: two touching bubbles moving away from each other, while two other bubbles come into contact for the first time (Figure 3.1). This neighbour exchange is commonly called a T1 event.

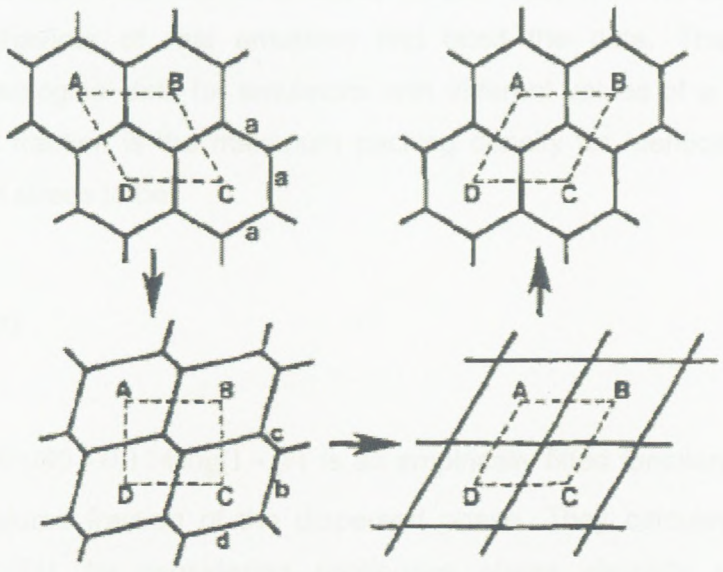

Figure 3.1: The proposed T1 events in foams

Rearrangements lead to sudden drops in stress, but are not the exclusive mechanism for stress release in emulsions. Two other widely considered mechanisms include viscous flow within the liquid interfaces and along the plateau borders and viscous dissipation within the surfactant layer (Buzza et al., 1995). In the modelling work by Princen and Princen and Kiss, they did consider viscous dissipation within the interstices, but ignored any flow that may occur in the thin film of the system.

After developing the two-dimensional model, Princen and Kiss generalised their results to three dimensions. In three dimensions, the criteria for mechanical equilibrium inside a foam (or an emulsion with a high volume fraction) are known as Plateau's rule (Plateau, 1873):

- Liquid films in a foam always meet in groups of three, known as Plateau borders;
- At the plateau borders, the film always forms angles of 120°;
- The Plateau borders meet in groups of four in the tetrahedral angle of 109.5°.

Later, Taylor mathematically proved the validity of three laws for dry foam, $\varphi=1$ (Almagren & Taylor, 1976; Taylor, 1976). In reality, though, no emulsion or foam is absolutely dry.

In their work, Princen & Kiss assumed that the three-dimensional equations predicting yield stress, stress of systems under flow, and viscosity are functionally similar to the equation derived from their two-dimensional model. They then measured stress and yield stress behaviour of real emulsion and fitted the data. They did this with experimental rheological data for emulsions with different values of φ, from 0.74 up to 1.0. The lowest fraction is the maximum packing density for identical spheres. They determined yield stress to be:

$$\tau_y = \frac{\sigma}{R_{32}} \varphi^{1/3} Y(\varphi) \qquad (3\text{-}1)$$

where $Y(\varphi) = -0.080 - 0.114 \log(1-\varphi)$ is an empirically fitted function (Princen, 1983) and φ is the volume fraction of the dispersed phase. They calculated the capillary number, eq. (2-51), by considering continuous phase viscosity as the effective viscosity. The functional dependence of *Ca* deviated from the two-dimensional model

(where $\tau_y \sim Ca^{2/3}$), and was determined experimentally. After the onset of flow, they got the flow curve prediction as shear stress and emulsion viscosity:

$$\tau = \tau_y + 32(\varphi - 0.73)\frac{\sigma}{R_{32}}Ca^{1/2} \quad (3\text{-}2)$$

$$\eta_{emulsion} = \frac{\tau_y}{\dot{\gamma}} + 32(\varphi - 0.73)\eta_{cont\ phase}Ca^{-1/2} \quad (3\text{-}3)$$

To generate data in order to determine the fitting parameters, Princen and Kiss took rheological measurements. Probably one of the most important issues to address when making rheological measurements on emulsion has to do with wall slip. Emulsions tend to form a slip plane, often at or near one of the walls of the container in which the sample is held. When wall slip occurs, the emulsion effectively separates into a highly sheared band and a relatively unsheared region (or regions). The bulk of the shear applied to the system is felt by the material in the shear band.

Rheologically, the shear band (and wall slip) introduces several problems. Firstly, the stress response measured by the rheometer is not a bulk property of the emulsion. The response of the system is dominated by the material involved in the slip plane. Second, since the width of the slip region cannot be measured, it is not clear how much strain the material in the slip region actually feels. Finally, if the slip plane is at the wall, the stress response is not a material property of the emulsion, but is a wall-emulsion property.

There are several ways to eliminate wall slip. Most commonly, this involves roughening the sample chamber. This can be done by deliberately scratching the wall by sand blasting – or other means – with particles about the same size as the emulsion droplets. Alternatively, small particles, about the same size as the emulsion droplets, can be glued to the sample chamber.

When Princen and Kiss ran their experiments, they chose not to eliminate slip at all. Instead they ran their experiments knowing that slip existed in their system and then explicitly subtracted it from their experimental data sets. They ran experiments specifically designed to measure wall slip. Princen and Kiss did not examine the effects of polydispersity. In fact, it is never mentioned as a relevant parameter. They presented a size-distribution histogram of droplet diameter for their emulsion samples, although

they did not characterise their emulsion with a quantitative measure of the distribution. They argued that the major effect of polydispersity on their system was that it reduced the maximum packing density from 0.74 to about 0.72.

In a series of papers, Khan and Armstrong (Khan & Armstrong 1986, 1987, 1989; Khan 1988) reported starting with the two-dimensional model of Princen and Kiss. They expanded on the earlier work by allowing flow within the film between bubbles. However, their model was more limited because they were restricted to φ's much closer to one. For instance, they showed that the flow of the continuous phase within the bubble interfaces is negligible. They also established that the yield stress is proportional to the Laplace pressure – something Princen had demonstrated in 1983. Later, there were attempts to confirm this through experimental work on several relatively monodisperese, dense emulsion systems (Mason & Bibette, 1996). Khan and Armstrong (1987) investigated the effect of polydispersity and showed that the yield stress, yield strain and the relationship between stress and strain were independent of the size distribution of the foam – they tested a bimodal versus a monomodal one.

Kraynik et al. (1991) derived a constitutive equation for two-dimensional foams that describes their elastic behaviour in the linear regime. They explicitly took into account polydispersity. They created bubbles as irregular hexagons that varied widely in shape and size, and showed that this did not affect the isotropic elastic response of the system. This is true as long as the interfaces between the droplets are straight; intersections of three interfaces retain their three-fold symmetry (a condition necessary for mechanical equilibrium); and the total amount of interface remains constant. Corroborating the earlier work of Weaire et al. (1986), they concluded that a material becomes softer as disorder is introduced – disorder being measured in terms of the second moment of the distribution of the length of bubble sides.

Buzza and Cates (1993) extended Princen's two-dimensional model by considering double-layer forces originated from ionic surfactant. They (Buzza & Cates, 1994) also studied the uniaxial modulus of a concentrated emulsion by modelling the compressed droplet with a truncated sphere in three-dimensional space. Buzza et al. (1995) also discussed various mechanisms for viscous dissipation in the oscillatory shear of incompressible foams. They predicted that the zero shear viscosity is usually dominated by the intrinsic dilatational viscosity of the surfactant monolayers.

A rheological model for highly concentrated emulsions containing 77 to 98% of the dispersed phase was proposed by Babak et al. (2001). The model relates the macroscopic functional properties of these systems (elastic modulus, yield stress and yield strain) to the microscopic physicochemical parameters (droplet size, interfacial tension, surface forces acting in thin liquid films, specific surfaces of these films, adhesion force between the droplets, their deformability, etc.). Whereas Princen's model describes the effect of the capillary pressure and the volume fraction of the internal phase on the elasticity modulus of such emulsions, the model by Babak et al. (2001) also predicts the effect of the adhesion-free energy between the droplets (or the contact angle between the droplets) on the elasticity modulus and the yield stress and strain of these emulsions. This model predicts that properties are scaled with the Laplace pressure.

The bubble model developed by Durian et al. (1995, 1997) can be applied to wet, disordered foams which are very similar to highly concentrated emulsions. The model connects neighbouring bubbles with harmonic spring, mimicking an inter-particle potential. At high packing fractions these bubbles overlap. The degree of overlap is proportional to how much potential energy is stored in the 'springs' – how much the springs are compressed. The potential therefore is zero until the bubbles touch. A viscous drag term is added, which is proportional to the velocity difference between two bubbles and effectively over-damps the system. This model can be used in 2-D and 3-D, for almost any relevant area fraction, and there is quite a bit of flexibility in terms of varying the viscous dissipation and the harmonic repulsion terms.

Durian et al. measured the elastic energy stored in compressions and measured energy drops which occur when bubbles precipitously rearrange. While correlated, energy drops within the system are not a direct measure of the extent of a rearrangement. Most of the bubble motions that lead to average-sized energy drops are rather subtle shifts; there are often no topological rearrangements that can be defined as traditional T1 events. Instead, they loosen the definition T1. Traditional T1 events involve a neighbour exchange in which an interface is replaced. Because of the subtleties of movements in this model, a working definition of a T1 event is that two bubbles approach each other as two others are forced away from each other. There does not need to be a concomitant exchange in interfaces (Tewari et al., 1999). Typically, larger energy drops involve larger number of bubbles. There is more variability for midsize and small events – a large range of energy drops correspond to

the same small number of rearranging bubbles, suggesting that typical rearrangement involve only a few bubbles (Durian, 1995; Tewari et al., 1999).

Gardiner et al. (2000) extended the bubble model into three dimensions. They looked at three-dimensional, polydisperse, wet foams. They examined the effects of volume fraction, shear rate and bubble size distribution. They found that all foams behaved as Bingham plastics at volume fractions above random close packing. They also found that the bubbles' size distribution does not have much of an impact on the rheology, except at the onset of applying shear.

Mason (1995) proposed three different analytical models for osmotic pressure and shear modulus of highly concentrated emulsions: the single droplet model; the contact disorder model; and the free volume model. The basic coefficients of increased droplet area were obtained by fitting in these models. In the single droplet model, the primary assumption was a uniform deformation of all droplets at zero temperature. This led to different scaling between the osmotic pressure and shear modulus with normalised volume fractions. In the contact disorder model, the primary assumption was the existence of localised regions of higher droplet compression at zero temperature, creating stress-supporting networks of droplets and less compressed regions that do not contribute significantly to stress transmission. Assuming that the number of droplets and the area per droplet in the stress-transmitting networks grow simultaneously above a critical volume fraction, this model predicted a quadratic scaling of the osmotic pressure and a linear scaling of the shear modulus with a normalised volume fraction. Finally, in the free volume model, the effects of temperature were included, and the droplet deformation not only facilitated the packing of the droplets to high volume fraction, but it also maximised the available free volume for translational droplet motion. This model predicted the osmotic pressure and the shear modulus to scale linearly above the critical volume fraction at which perfectly hard droplets would pack. Furthermore, unlike the other two models, there is a prediction for their behaviour below the critical volume fraction which is entropic in origin.

Lacasse et al. (1996a; 1996b) modelled the elastic properties of compressed (dense) emulsions. This model has several similarities to the bubble model, not the least of which is that it investigates how entire bubbles interact with each other. Instead of using a harmonic spring potential for the repulsive term, an anharmonic potential was used. This potential was derived by measuring the change in the surface energy of a droplet under different conformations typical of a droplet inside the emulsion, using

Brakke's surface evolver software (Brakke, 1992). They found that the elastic response of a compressed droplet is softer than harmonic, therefore they used an anharmonic interdroplet potential in a 3-D model of droplets. They used this model to determine the elastic response of a monodisperse collection of disordered droplets as a function of volume fraction. They compared their result with measured osmotic pressure and the shear modulus (normalised by the Laplace pressure). The experimental and modelling results were in good agreement. In this model, emulsion droplets respond to shear with both an affine and a non-affine deformation. Compared to a system constrained to undergo strictly affine motion (which is either one in which there is no time for the emulsion to relax or one in which the emulsion is incapable of relaxing), the shear modulus is about three times smaller – much more in line with shear moduli measured in real systems. Interestingly, this non-affine motion of droplets makes larger-scale rearrangements very unlikely. Only a very small fraction of droplets truly change neighbours during shear.

Seth et al. (2006), by using Hertzian pairwise elastic energy associated with two droplets in contact, modelled the elastic properties of emulsions as a three-dimensional system of randomly packed elastic spheres in which the packing is subject to isochoric uniaxial extension. First, they generated a three-dimensional, periodically replicated, random close-packed configuration of hard spheres by the Lubachevsky and Stillinger (1990) algorithm, and after that they treated the spheres as soft with a finite modulus. They obtained osmotic pressure and shear modulus scales with Laplace pressure, which is not surprising as they assumed a linear relation between Hertzian contact energy and Laplace pressure.

This overview of contemporary attempts at modelling emulsion rheology is by no means complete. However, it does touch on most of the main ideas and the most important/common models. It seems clear that rearrangements are central to understanding how emulsions respond to applied shear. However, the precise connection between the internal structure of an emulsion and its rheology will only be definitively established by experimental means. While most of the models can mimic the rheological response of a foam/emulsion to applied shear, the models come to widely different conclusions about rearrangements.

Besides the similarity of emulsion and foam, granular packings also have many similarities to emulsions, particularly when both systems have volume fractions around random close packing, which is to be discussed in the following paragraphs.

The idea of soft glassy materials, as discussed by Sollich et al. (1997), has already been introduced. With this model, Sollich et al. connected foams, dense emulsions, onion phases, colloidal glasses, clay, and pastes, because all of these, to some extent, act like Herschel-Bulkley fluid. Furthermore, they all have nearly flat viscoelastic spectra for $G'(\omega)$ and $G''(\omega)$ at low frequencies. All these materials have common underlying features of disordered packing and metastable states.

Sollich et al. studied these systems using mode coupling theory. They divided the system into mesoscopic elements, not as droplets or bubbles or grains, but as something on about the same scale. At all times, these mesoscopic elements each feel a uniquely defined local strain which slowly grows over time. They also have a uniquely assigned local yield threshold, which is randomly distributed according to a decaying exponential. When the local strain energy gets close to the yield energy, the mesoscopic element yields (Sollich et al., 1997). Yielding rests the local strain to zero and assigns a new yield energy to the element, which is strikingly similar to a rearrangement. When a macroscopic strain (stress) is applied to the material, the strain energy builds at a much greater rate than it would if simply left to 'age'. Most of the work in this area has used scalar fields, but the model can be refined by using vector fields and tensor mathematics (Cates & Sollich, 2004).

Sollich's model (Sollich et al., 1997; Sollich, 1998) predicts four different states for the material based on an effective noise temperature, x. Based on the modelling performed for the different x, the following scalings of shear moduli were found:

$$\begin{aligned} &G' \sim \omega^2, G'' \sim \omega && 3 < x \\ &G' \sim \omega^{x-1}, G'' \sim \omega && 2 < x < 3 \\ &G' \sim \omega^{x-1}, G'' \sim \omega^{x-1} && 1 < x < 2 \\ &G' \sim const., G'' \sim \omega^{x-1} && x < 1 \end{aligned} \qquad (3\text{-}4)$$

For $x>3$ the system is Maxwell-like at low frequencies, whereas for $2<x<3$ there is an anomalous power law in the elastic modulus. Most interesting is the regime $1<x<2$, where G' and G'' have constant ratio; both vary as ω^{x-1}. The frequency exponent approaches zero as $x \rightarrow 1$, resulting in essentially constant values of G' and G''. Below glass transition, $x<1$, if a cut-off on the yield energies is introduced an equilibrium state

exists, in which the storage modulus is constant and the loss modulus decreases at low frequencies.

Sollich's model describes soft, glassy materials in terms of the competition between energy barriers to rearrangements and shearing forces which remove these barriers. Other models along this line replace the physics in the competition with stress and shear-induced changes in stress (Hébraud & Lequeux, 1998), fluidity and shear-induced changes in fluidity (Lemaître, 2002), free volume and shear induced changes in free volume (Bonn et al., 2002; Coussot et al., 2002) or degree of jamming and shear-induced changes in jamming (Berthier et al., 2000). Fuchs and Cates (2002) focused on suspensions. They looked at how shear can induce density fluctuations that allow a given particle to move freely, suppressing the caging of the particle by its neighbours. In general, the rheological behaviour of soft, glassy materials results from the interplay between the slow (locally defined) dynamics of the system and shear acceleration of these dynamics. Details about droplets (or bubbles, or grains) and their physics are not considered. In models like Sollich et al.'s soft, glassy rheology that use mode-coupling theory (MCT), it is possible to make claims of being generally applicable to several materials because they do not appeal directly to the structural basis of a specific material.

Liu et al. (1996) proposed a model for concentrated emulsions based on non-affine deformation speculation under macroscopic shear strain in the randomly close-packed droplet structure. have reported high levels of viscous dissipation in dense emulsions under high-frequency oscillatory shearing deformations. Their data for the complex modulus G^* can be represented by following expression:

$$G^* = G' + iG'' = G'_p + A(\varphi)(i\omega)^{1/2} + \eta_\infty i\omega \qquad (3\text{-}5)$$

where i is the imaginary unit. This expression contains a low-frequency plateau modulus, G'_p, a high-frequency viscosity η_∞ due to the continuous phase in the films, and an anomalous power-law contribution $G^*(i\omega) \sim (i\omega)^{1/2}$ at intermediate frequencies. According to the theory of Liu et al. (1996), the anomalous power-law contribution is caused by slippage of layers of bubbles against each other along randomly oriented "weak planes" where the modulus at that orientation is locally minimum.

Petsev and his co-workers presented different research studies concerning the interaction energy between droplets in emulsion systems (Danov et al., 1993; Denkov et al., 1993; Petsev & Linse, 1997; Petsev & Bibette, 1995; Denkov et al., 1995; and Petsev et al., 1995). Danov et al. (1993) modelled the interaction energy between deformable droplets by using the microscopic approach of Hamaker for Van der Waals interaction. Explicit expressions for the electrostatic, steric and other types of interaction were also derived on the basis of Derjaguin's approximation. This work was later extended to the deformable Brownian droplets (Denkov et al., 1993). Although Petsev and Linse (1997) also tried to model the properties of dense emulsions and microemulsions, their model only considers the deformation energy as dominant pair interaction energy and is limited to low concentrations.

3.4. Semi-empirical Models

After developing the two-dimensional models, Princen and Kiss generalised their results to three dimensions. They assumed that the three-dimensional equations predicting yield stress, stress of the system under flow, and viscosity are functionally similar to the equations derived from their two-dimensional models. They then measured stress and yield behaviour of real emulsions and fitted the data. Their results provide the dependence of elastic modulus to the reciprocal size of droplets.

Princen and Kiss (1986, 1989) proposed the following relations for the yield stress and the static shear modulus:

$$\tau_y/(\sigma/R) = \varphi^{1/3}[-0.08 - 0.114\log_{10}(1-\varphi)] \quad (3\text{-}6)$$

$$G/(\sigma/R) = 1.769\varphi^{1/3}(\varphi - 0.712) \quad (3\text{-}7)$$

Pal (2006) also presented an empirical model for highly concentrated emulsions, as follows:

$$\begin{aligned} G/(\sigma/R) &= 1.769\varphi^{1/3}(\varphi - 0.712) \quad when\ \varphi_{eff} \le 0.93 \\ G/(\sigma/R) &= [1.769 + 8.33(\varphi_{ff} - 0.93)]\varphi^{1/3}(\varphi - 0.712) \quad when\ \varphi_{eff} \ge 0.93 \end{aligned} \quad (3\text{-}8)$$

This model is identical to Princen's model when $\varphi_{eff} \le 0.93$, while the equation for $\varphi_{eff} \ge 0.93$ was obtained by fitting experimental results.

Mougel et al. (2006) suggested exploring the possibility that the dominant interaction energy is due to Van der Waals forces in the case of non-ionic surfactants, because they observed that the shear modulus scale with the reciprocal of squared diameter rather than reciprocal of diameter. Their empirical relation in comparison with experiments is:

$$G = 3.66 \frac{2\pi\sigma D_{\circ}\varphi}{R^2(\varphi^* - \varphi)} \qquad (3\text{-}9)$$

Masalova and Malkin (2007a) proposed a model for shear modulus for highly concentrated emulsions and confirmed it through both geometrical-energetic arguments and dimensional analysis. The idea for the model originated from rheological results which deviated from Princen's model and it includes the width of an elastic layer as an additional geometrical factor:

$$G = k \frac{\delta}{D^2} \gamma(\varphi - \varphi^*) \qquad (3\text{-}10)$$

As expected, when the droplet size tends to infinity, the shear modulus limits to zero. They showed, by performing experimental studies on highly concentrated explosive emulsions, that their new model satisfies this supposition, while the models predicting the scaling of shear modulus with Laplace pressure (like Princen's model) are unable to do this, as shown in Figure 3.2.

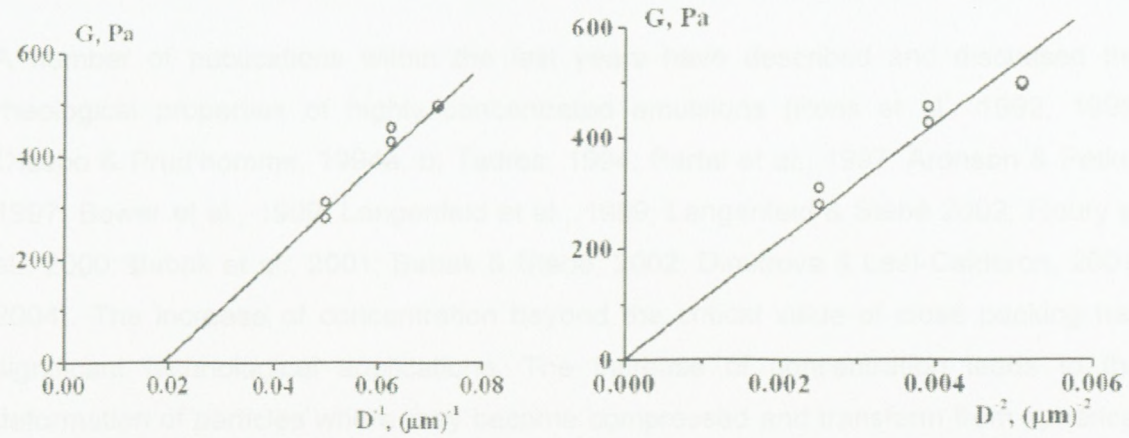

Figure 3.2: Different fitting of shear modulus dependency on the droplet size

3.5. Experimental Studies

3.5.1. Common Highly Concentrated Emulsions

Models are only as good as their ability to reproduce experimental results. Unfortunately, there is not a single model that can truly reproduce experimental results and, conversely, it is hard to design an experiment that can be easily modelled. For instance, experiments are inherently 3-D, while the vast majority of modelling data is in two dimensions. It is possible to visualise a 2-D plane in a 3-D experiment, but the plane that is easiest to access may not be the plane that is most easily modelled. This said, experimental results on real materials are true accounts of the material. Models are predictions of what the important parameters are.

High internal phase ratio emulsion systems exhibit a plastic-like response to shear deformations (shear elasticity); for small deformations, they resist the deformation, with the stress being linearly proportional to the strain; however, for large enough deformations, they flow, offering comparatively much less additional resistance (Webber, 1999; Malkin et al., 2004a). Grassi et al. (1996) mentioned that the plastic behaviour is generally ascribed to the existence of a three-dimensional network under limiting shear conditions (i.e. $\dot{\gamma} \to 0$). The described shear-dependent behaviour is typical for weak gel systems (many polymer solutions and dispersed systems) in which the application of large or continuously increasing deformations results in progressive breakdown of their networks into smaller clusters (Grassi et al., 1996), leading to a strong decrease in viscosity and permitting the flow of the system (Manca et al., 2001). Since practical applications of emulsions require their transport, it is important to understand how their flow behaviour is influenced by the properties of the constituent droplets, such as packing, degree of deformation, droplet size and volume fraction.

A number of publications within the last years have described and discussed the rheological properties of highly concentrated emulsions (Pons et al., 1992, 1995; Otsubo & Prud'homme, 1994a, b; Tadros, 1994; Partal et al., 1997; Aronson & Petko, 1997; Bower et al., 1999; Langenfeld et al., 1999; Langenfeld & Stébé 2002; Floury et al., 2000; Babak et al., 2001; Babak & Stébé, 2002; Dimitrova & Leal-Calderon, 2001, 2004). The increase of concentration beyond the critical value of close packing has significant technological applications. The increase of concentration leads to the deformation of particles where they become compressed and transform from spherical to polyhedral type shapes. Direct measurements of their size distribution (Malkin et al., 2004a) and microscopic evidences confirm this phenomenon (Jager-Lézer et al., 1998; Rocca & Stébé, 2000; Babak et al., 2001; Masalova et al., 2005).

It is important to emphasise that the increase of concentrations of the emulsion beyond some critical value could trigger the transformation of its rheological properties. In particular, the structural transformation appears as the effect of yielding (Mason et al., 1995, 1996; Mason, 1999). The Bingham model and the Herschel-Bulkley model provide the simplest description of emulsions and the other materials that yield (Malkin & Isayev, 2006). These macroscopic descriptions do not examine the structural dynamics of the emulsions, and are only mathematical relationships between stress and strain of yield stress fluids. No real material behaves exactly as these models describe. In particular, the idea of a well-defined yield stress is the subject of much debate. Many believe it is impossible to unambiguously define a yield stress (Barnes, 1999, 2007; Barnes & Walters, 1985). For materials that 'yield', there does exist a small range of applied stress (an 'apparent yield') over which the mechanical properties of a material changes dramatically (Barnes, 1999, 2007). However, the actual value of the 'apparent yield stress' is experiment-specific. In contrast, many believe that yield stress fluids do exist. Fluids with an internal structure, such as concentrated emulsions, and suspensions, in particular, require an applied stress to flow (Kraynik, 1988). The idea behind this is the necessity to supply energy to the system in order to put the jammed, structural elements into motion. The system cannot flow macroscopically before enough energy is put into it (Bolton & Weaire, 1992; Durian, 1997; Hutzler et al., 1995; Reinlet & Kraynik, 1996; Sollich et al., 1997).

The influence of electrolytes on the properties and stability of highly concentrated water-in-oil emulsions was studied by Aronson and Petko (1993). In this research, the electrolytes appeared to enhance the stability of water-in-oil emulsions by increasing the resistance of the water droplets to coalescence. It is proposed that this was achieved by a higher adsorption density of emulsifier at room temperature storage, and in the frozen state by the fractionation of a concentrated electrolyte solution that wetted the ice crystals and prevented their fusion.

Pal (1996) limited the experiments to two types of emulsions characterised as "fine" and "coarse". The difference in the rheological behaviour of these emulsions was quite evident qualitatively. Otsubo and Prud'homme (1994b) in their study showed that, for concentrated emulsions, the viscosity is inversely proportional not only to the area-volume mean diameter, but the flow behaviour also depends on the width of the droplet size distribution.

In oscillatory shear, the evolution of linear viscoelastic functions in frequency range between 10^{-2} and 10^{2}rad/s; for highly concentrated emulsions, is characterised by the appearance of a minimum in the loss modulus at intermediate frequencies and a "plateau region" in the storage modulus. In addition, the frequency dependence of both moduli is clearly dependent on the emulsion concentration, processing conditions and nature of the emulsifier used (Franco et al., 1995, 1997; Tadros, 1994).

The linear viscoelastic properties can be matched, for example, to a generalised Maxwell model, with discrete or continuous spectrum (Guerrero et al., 1996). Madiedo and Gallegos (1997) used a different empirical model that described those regions in the relaxation spectra of oil-in-water emulsions stabilised by a mixture of two low molecular weight surfactants with different hydrophilic-lipophilic balances.

It was demonstrated (Pons et al., 1995) that viscoelastic properties of emulsions of concentrations up to 0.96 are well described by the simplest Maxwell model with a single relaxation time where it is possible to treat the plateau value of elastic modules as the static modules, G_0. Viscoelastic properties of highly concentrated reverse water-in-oil emulsions with a concentration of 0.94 were studied by Langenfeld et al. (1999) and also described by the single-relaxation time Maxwell model. However, Babak et al. (2001) found that the rheological behaviour of the same highly concentrated emulsions is more complicated and requires an advanced model, which should also predict the existence of the yielding effect.

As was mentioned by Guerrero et al. (1998), the plateau region of G' may be related to the formation of an elastic structural network due to interactions among the emulsifier molecules located at the oil-water interface of adjacent droplets (Dickinson, 1989; Franco et al., 1995). A zone of constant response (plateau region) indicates an unaltered structure, not disturbed by shear. It is related only to the equilibrium microscopic structure, forces, and inherent dissipation of fluctuations (Bird et al., 1987).

The rheological study of w/o emulsions (exemplified by mayonnaise samples) covering both linear and non-linear domains of viscoelastic behaviour was carried out by Bower et al. (1999). These authors observed several phenomena typical of such systems: non-Newtonian flow curves, strong amplitude dependence of dynamic modulus, possibility of slip on solid surfaces, and structure rearrangement induced by shearing.

The concentration dependence of viscoelastic properties of highly concentrated emulsions were discussed on the basis of Princen's theory (Ponton et al., 2001; Jager-Lézer et al., 1998; Pons et al., 1995). The comparison of experimental data with Princen's theoretical model in such work showed good agreement.

Mason et al. (Mason, 1995; Mason et al., 1995; 1996; 1997) conducted a systematic study of dense emulsions. One reason this work is so pivotal is that they worked with a monodisperse emulsion. With all of the droplets about the same size, they were able to make broad generalisations about several physical properties of the droplets. In addition, they could assume that the Laplace pressure was the same for each of the droplets, which set the scale for all the stresses in the emulsions. Some of their most important results include:

- The shear modulus, when scaled by the Laplace pressure, follows a universal dependence on the volume fraction of dispersed phase: $\varphi(\varphi - \varphi_c)$, where φ_c has a value of 0.635 – basically random close packing.
- The osmotic pressure used to compress the emulsions was almost the same as the shear modulus, at least for a range of volume fraction above φ_c.
- When dynamic yield is defined as the onset of a non-linear stress response to an applied strain, the φ dependence of γ_y is independent of radius and exhibits a minimum near the critical volume fraction φ_c.
- The dynamic yield stress τ_y increases dramatically as the volume fraction increases above φ_c and scales with Laplace pressure.
- The dynamic yield strain γ_y and the dynamic yield stress τ_y when scaled as proposed, are independent of droplet radius – for a given frequency.

Although the proposed models (Princen, Princen & Kiss, Lacasse et al.) predict that shear modulus and osmotic pressure scale with Laplace pressure, reported experimental results often show deviation from this scaling (Malkin et al., 2004a; Perrin, 2000; Pons et al., 1992, 1995; Otsubo and Prud'homme, 1994a, b; Dimitrova & Leal-Calderon, 2001, 2004; Bengoechea et al., 2006; Romero et al., 2008; Mougel et al., 2006; Masalova & Malkin, 2007a, b; Alvarez-Solano, 2006). This deviation is attributed to different parameters, e.g. neglecting continuous phase viscosity and film thickness (Pons et al., 1992); sticky surface aggregates of protein surfactant (Dimitrova & Leal-Calderon, 2001, 2004); Van der Waals interaction (Mougel et al., 2006); and ignoring the film thickness (Masalova & Malkin, 2007a), which will be discussed in more detail in section 3.5.3.

3.5.2. Highly Concentrated Explosive Emulsions

The highly concentrated emulsions have various important applications in the food and cosmetic industries, but one of the more interesting applications is their use as "liquid explosives" (Bampfield & Cooper, 1985; Webber, 1999).

The referred explosive emulsion in this text is the base emulsion which is sensitised by mixing with sodium nitrite solution in the later stages. This mixing process involves formation of N_2 gas in the system, which results in a foam structure (da Silva et al., 2006). The base emulsion is pumped into a mine using pipelines before it is sensitised, so its rheological properties is of special interest for industry, as well as academy (Masalova et al., 2003). The base explosive emulsion is a water-in-oil emulsion composed of an oxidiser solution, organic fuel and an emulsifying system. The oxidiser solution forms the discontinuous phase of the explosive with a volume fraction about 80~90% and generally comprises inorganic oxidiser salt, in an amount from 45% to about 95% by weight of the total composition. The oxidiser salt is primarily ammonium nitrate (AN), and sodium nitrate (SN) and calcium nitrate may be used in amounts up to 50% (Hales et al., 2004). The oxidiser solution is a supersaturated over-cooled solution at room temperature, which is in the state of hydrous melt where ions can move about easily (Bengtsson et al., 1994). The supersaturated overcooled state of oxidiser solution means that it has the potential to crystallise instantly, however explosive emulsions are stable against crystallisation for months. The organic fuel should be immiscible with oxidiser solution. It can be aliphatic, alicyclic, and/or aromatic and can be saturated and/or unsaturated, as long as it is liquid at the formulation temperature (Hales et al., 2004). The characteristics of a proper emulsifying system for explosive emulsions are as follows:

- Since the aqueous phase is dispersed in the oil phase, the surfactant should have low HLB.
- It aids the process of droplet subdivision and dispersion in the continuous phase by reducing the interfacial tension and energy required to create new interfaces.
- It reduces the rate of coalescence by covering the surface of droplets.
- It acts as a crystal habit modifier to control and limit crystallisation.
- It may enhance absorption of the hydrocarbon fuel on the small salt crystals that may form.
- It should be able to cover the new interfaces that may be created under high shear during pumping

It is recommended in patents discussing the emulsion explosives that an emulsifying system comprises a mixture of at least one amphiphatic synthetic polymer emulsifier (such as those based on various adducts of polyisobutylene succinic anhydride, PIBSA), and one conventional water-in-oil emulsifier, such as sorbitan monooleate, SMO (e.g. Boer, 2003).

The polymeric surfactants are known to give excellent shelf life to emulsion explosives; however, attempts to homogenise (under high shear) polymeric emulsifier-based emulsions generally cause significant crystallisation to occur (e.g. Hales et al., 2004). The polymeric surfactants seem to be capable to salt formation when used to form explosive emulsions at low pH (Venter & Kruger, 1996), or formation of a hydrogen bond with oxidiser ions (Ganguly et al., 1992), which could be the reason for stability against crystallisation. The conventional emulsifiers are more mobile than the more bulky polymeric emulsifiers. Thus, when new interfaces are created by the high shearing action of homogenisation, they quickly migrate to cover the interface and stabilise it (Chattopadhyay, 1990). However, they negatively affect the shelf life or long-term stability of the emulsion phase, both before and after homogenisation (Hales et al., 2004).

For high internal phase systems such as emulsion explosives, there are no published data on the behaviour of the surfactant film. It may be speculated that, for the system to flow, both distortion of droplet shape and shearing of the interdroplet layer must be involved. Indeed, in a quantitative way, this can be observed, e.g. oxazoline and amine surfactants tend to give lower viscosity emulsions than do sorbitain derivatives, but little systematic work has been done (Becher, 1983).

There is a further mechanism by which a surfactant in this system can affect the rheology. Bampfield and Cooper (1985) showed that certain polymeric surfactants dramatically increase the viscosity of emulsion explosives, while at the same time making them rubbery. It is possible that such materials operate by bridging the area between the droplets, giving some structure to the emulsion.

Reynolds et al. studied the microstructure of highly concentrated explosive emulsions by small-angle neutron scattering (2000, 2001) as well as X-ray reflectometry (2003). The employed surfactant was in form of the adduction of monoethanolamine with PIBSA, which is known as PIBSA-MEA. They found that micelles exist in this system

and that their diameter does not change with increasing surfactant concentration, but the volume fraction of micelles in the oil phase increases. They also showed that the surfactant adsorption at the interface increases on increasing the surfactant concentration, and that the organic salt which dissolved in the dispersed water phase has a significant influence on the surfactant absorption at the interface, generating a smooth interface, while its effect on the micelles' diameter is not pronounced.

Masalova et al. (2003, 2005, 2006a, b), Malkin et al. (2004a, b), Malkin and Masalova (2005, 2007), and Masalova and Malkin (2007a, b, c) systematically studied the rheological properties and crystallisation behaviour of explosive emulsions stabilised by two undisclosed surfactants based on mixtures of PIBSA derivatives. Malkin et al. (2004a), by measuring the linear viscoelastic properties, showed that explosive emulsions have gel-like behaviour that is a frequency independent storage modulus in a wide range of frequencies and amplitudes (Figure 3.3). This frequency independent storage modulus is regarded as the shear modulus of the emulsion (Mason, 1995; Mason et al., 1997). However, while Princen-Lacasse models predict the scaling of shear modulus with reciprocal of droplet size, d_{32}^{-1}, it was found (Malkin et al., 2004a; Masalova & Malkin, 2007a) that the shear modulus scales with d_{32}^{-2}.

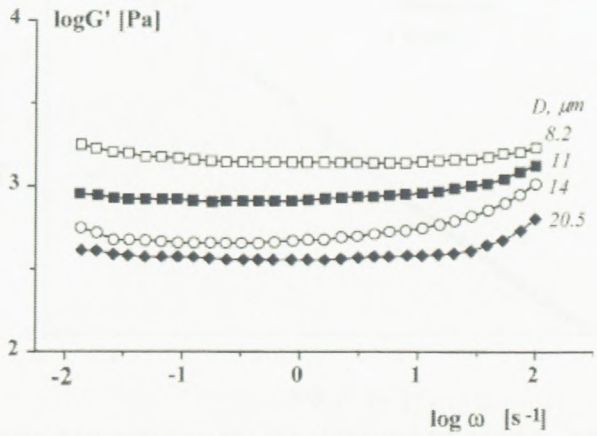

Figure 3.3: Frequency independencies of dynamic modules for emulsions with different droplet sizes (Malkin et al., 2004a)

The flow curve measurement of explosive emulsions showed the existence of a low shear rate Newtonian plateau by measuring viscosity from low to high stress (Figure 3.4), but its absence when measurements were made at decreasing stress levels (Masalova et al., 2005; Masalova & Malkin, 2007b). The downward curve shows the

existence of a yield stress. However, measuring the viscosity by time sweep tests at different shear rates and creep experiments demonstrated that the downward branch of the flow curve is physically meaningful, and identifies rheological properties of the emulsion in which shear-induced structure has been created by loading (Figure 3.5). Hence, the presence of yield stress for this type of emulsion is apparent.

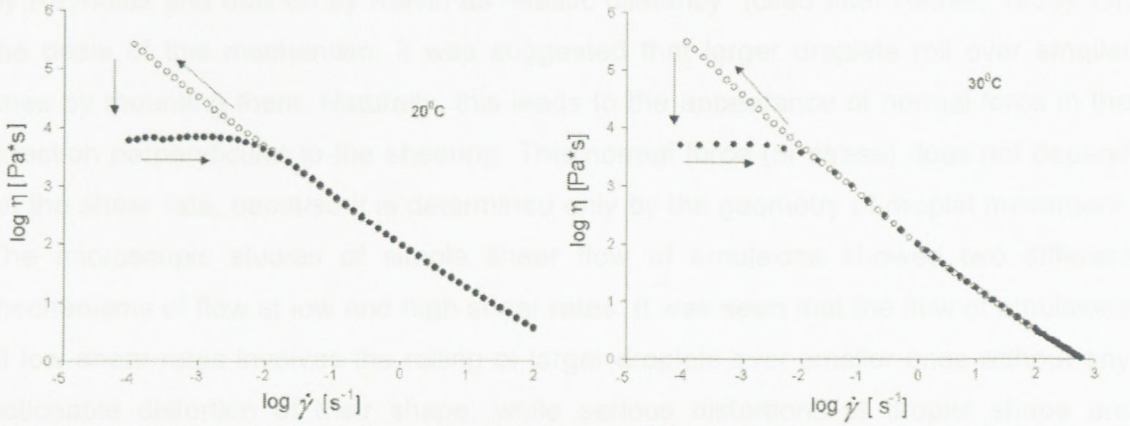

Figure 3.4: Rheopectic behaviour of emulsions at different temperatures as a function of shear rate (Masalova et al., 2005)

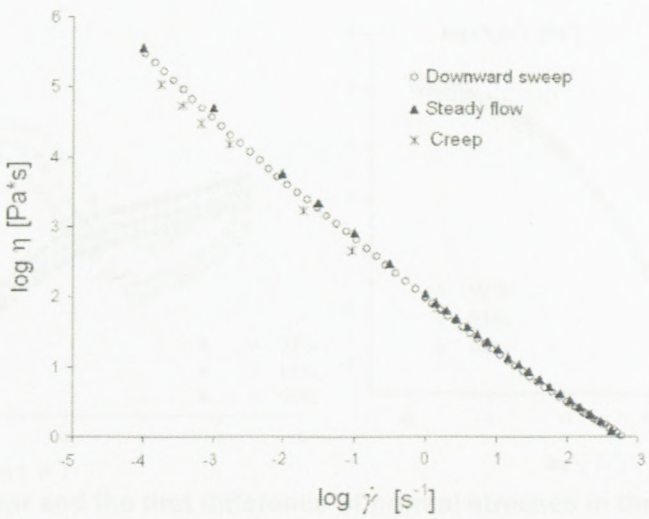

Figure 3.5: Shear rate dependence of viscosity as obtained in different deformation modes (Masalova et al., 2005)

The normal stress measurement during the downward flow curve measurement (Malkin & Masalova, 2007; Masalova & Malkin, 2007b) showed that the character of the variations of normal stresses with shear rate is quite unusual and unexpected (Figure 3.6). It turned out that normal stresses are almost constant within a wide range of shear

rates, contrary to their expected growth. Moreover, they abruptly change by several orders of magnitude within a rather narrow range of shear rates. By plotting N_1/σ^2 versus shear rate (coordinate of Lodge equation), it was found that the elastic modulus ($G=2\sigma^2/N_1$) is not constant, contrary to the result found in oscillation experiments. Therefore, it was concluded that the appearance of normal stresses in the range of low shear rates does not originate from the Weissenberg-Lodge mechanism of elasticity. The observed phenomenon much more resembles the dilatancy in the sense described by Reynolds and defined by Kelvin as "elastic dilatancy" (cited after Reiner, 1958). On the basis of this mechanism, it was suggested that larger droplets roll over smaller ones by mounting them. Naturally, this leads to the appearance of normal force in the direction perpendicular to the shearing. This normal force (or stress) does not depend on the shear rate, because it is determined only by the geometry of droplet movement. The microscopic studies of simple shear flow of emulsions showed two different mechanisms of flow at low and high shear rates. It was seen that the flow of emulsions at low shear rates involves the rolling of larger droplets over smaller ones without any noticeable distortion of their shape, while serious distortions of droplet shape are observed at high shear rates.

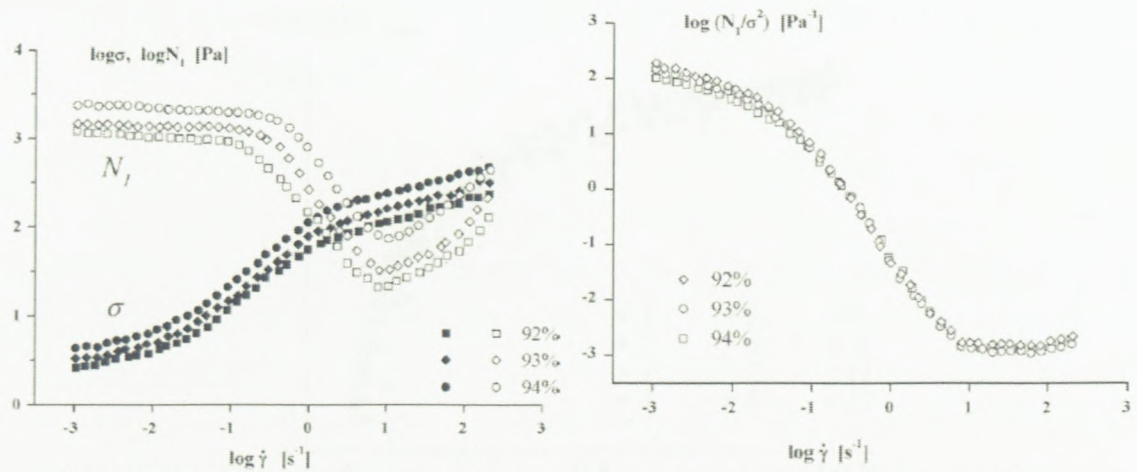

Figure 3.6: Shear and the first difference of normal stresses in the steady flow of emulsions with different concentrations of a disperse phase. In the right-hand graph the data are presented in the Lodge coordinate. (Malkin & Masalova, 2007)

Masalova et al. (2006a), Masalova and Malkin (2007c) and Kharatiyan (2005) studied the variation of rheological properties and crystallisation behaviour of explosive emulsions as they age. They found that both shear modulus and yield stress increase as the crystallisation process starts (Figure 3.7). They showed that the kinetic of

crystallization follows the Johnson-Mehl-Avrami-Kolmogorov (JMAK) equation, $X = 1 - e^{-(t/\theta)^n}$ in which X and t are the degree of crystallinity and ageing time, respectively, and θ, the characteristic time, and n, the power, are fitting parameters. Finally, they showed the relative change of yield stress versus degree of crystallinity superimpose on a single master curve (Figure 3.8).

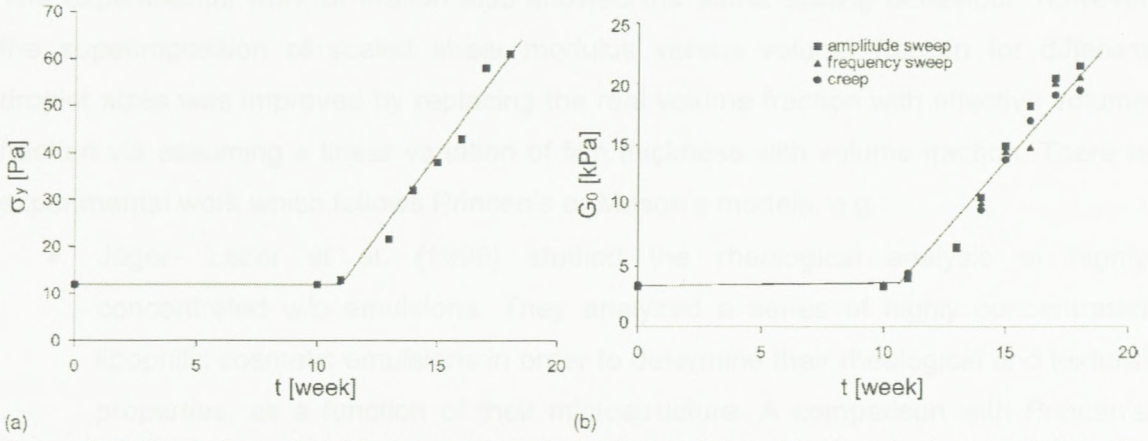

Figure 3.7: Evolution of yield stress (a) and elastic modules (b) of explosive emulsions in aging (Masalova et al., 2006a)

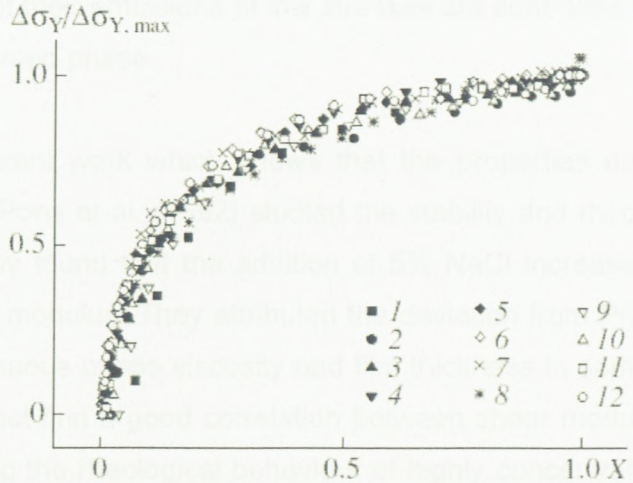

Figure 3.8: Correlation between the relative change of yield stress and the degree of crystallinity for 12 different samples (Masalova & Malkin, 2007c)

3.5.3. Properties Scaling with the Laplace Pressure?

Viscoelastic properties of highly concentrated emulsions have already been studied widely, both experimentally and theoretically. It has been shown that the viscoelastic properties depend on the mean diameter of dispersed particles, polydispersity, interfacial tension, and particularly on the dispersed volume fraction, although it is

accepted that, in considering the area-volume mean droplet size, the polydispersity does not have a pronounced effect. Some studies showed that the osmotic pressure, shear modulus and yield stress scale with the Laplace pressure (Barry, 1975; Princen 1979, 1983, 1985, 1988; Princen et al., 1980; Princen and Kiss, 1986, 1989; Bibette, 1992; Aronson & Petko, 1993; Benali, 1993; Reinelt & Kraynik, 1990, 1993; Otsubo & Prud'homme, 1994b; Babak et al., 2001).

The experimental work of Mason also showed the same scaling behaviour, however the superimposition of scaled shear modulus versus volume fraction for different droplet sizes was improved by replacing the real volume fraction with effective volume fraction via assuming a linear variation of film thickness with volume fraction. There is experimental work which follows Princen's or Mason's models, e.g.:

- Jager- Lézer et al. (1998) studied the rheological analysis of highly concentrated w/o emulsions. They analyzed a series of highly concentrated lipophilic cosmetic emulsions in order to determine their rheological and textural properties, as a function of their microstructure. A comparison with Princen's theoretical models showed good agreement.
- Hemar and Horne (2000) measured the dynamic rheological properties of highly concentrated protein stabilised emulsions and found out that the elastic properties of their emulsions at low stresses are controlled by Laplace pressure of the dispersed phase.

There also is different work which shows that the properties do not scale with the Laplace pressure. Pons et al. (1992) studied the stability and rheological properties of gel emulsions. They found that the addition of 5% NaCl increased the stability, yield stress and storage modulus. They attributed the deviation from Princen's theory to the neglecting of continuous phase viscosity and film thickness in some cases. Pons et al. (1995) also could not find a good correlation between shear modulus and the Laplace pressure in studying the rheological behaviour of highly concentrated oil-in-water (o/w) emulsions.

Otsubo and Prud'homme (1994a, b) showed that the viscosity of their highly concentrated oil-in water emulsion did not scale with the capillary number, which means that their results deviate from Princen's model.

Perrin (2000) studied the rheological properties of concentrated emulsions which were stabilised by a hydrophobically modified poly(sodium acrylate). The fine tuning of the

hydrophile-lipophile (HL) properties of the system achieved by changing ionic strength allowed the formation of both oil and water continuous emulsions over a wide range of dispersed phase volume fraction (up to 0.9). In other words, the macro-surfactant used was able to stabilise the interfaces of both concentrated direct and inverse emulsions. The water-in-oil emulsion showed higher shear modulus and its shear modulus did not follow Princen's theory, which was attributed to droplet-droplet interaction. The higher shear modulus of w/o emulsions was also evident (Figure 3.9). The interactions in direct emulsions were well-described by the Princen's model since they arose solely from the compression of the droplets above the close packing concentration.

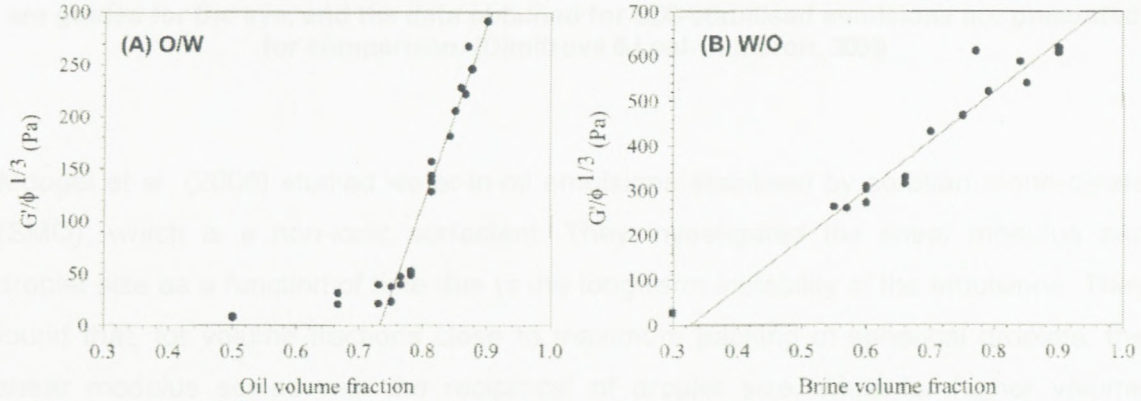

Figure 3.9: $G'/\varphi^{1/3}$ versus φ plots in the case of direct (A) and inverse (B) emulsions (Perrin, 2000)

Dimitrova and Leal-Calderon (2001, 2004) demonstrated that protein-stabilised emulsions have higher elasticity than that which is predicted by Princen's theory (Figure 3.10). The unusual high elasticity was not attributed to a specificity of the continuous phase, because the osmotic equation of the state of their emulsions was found to be identical to the one obtained for samples stabilised by classical (SDS) surfactants studied by Mason et al. (1996; 1997). The thin film experiments showed that the protein adsorption layers contained a substantial number of sticky surface aggregates, which suggested severely obstructed local rearrangements of individual drops with respect to their neighbours.

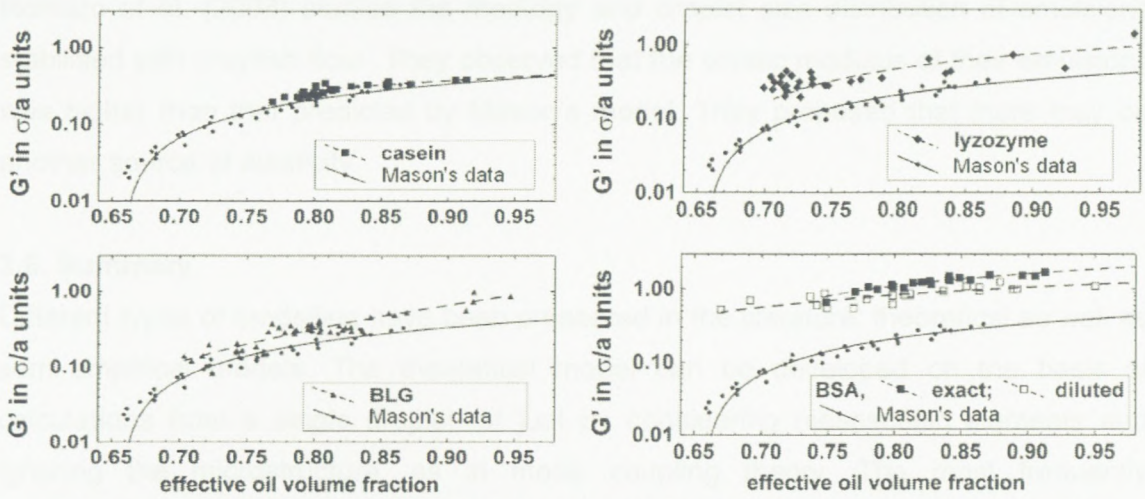

Figure 3.10: Storage modulus (*G'*) of hexadecane-in-water emulsions stabilised by different proteins, as a function of the effective oil volume fraction. In all plots, the lines are guides for the eye, and the data obtained for SDS-stabilised emulsions are presented for comparison. (Dimitrova & Leal-Calderon, 2004)

Mougel et al. (2006) studied water-in-oil emulsions stabilised by sorbitan mono-oleate (SMO), which is a non-ionic surfactant. They investigated the shear modulus and droplet size as a function of time due to the long-term instability of the emulsions. They found that, for volume fractions close to maximum packing of spherical droplets, the shear modulus scaled with the reciprocal of droplet size, while for higher volume fractions, a scaling with squared reciprocal droplet size was evident. This scaling was attributed to dominant Van der Waals interaction at high volume fraction.

Malkin et al. (2004a) and Masalova and Malkin (2007a) found that the shear modulus scales with squared reciprocal diameter in the highly concentrated explosive emulsion studied by them. They explained, by both geometric and dimensionless modelling (Masalova & Malkin, 2007a), that this is due to the ignoring of a finite film thickness between emulsion droplets.

Bengoechea et al. (2006) used Mason's model of the elasticity of compressed emulsions and found that it resulted in adequate fitting but underestimated the elastic properties of the highest concentration of gluten in gluten-stabilised oil-in-water emulsions. They suggested that these deviations may be explained in terms of an enhancement of the elastic network formed in the aqueous phase in which the glutenin fraction has to play an important role.

Romero et al. (2008) studied the rheology and droplet size distribution of emulsions stabilised with crayfish flour. They observed that the elastic modulus of their emulsions was higher than that predicted by Mason's model. They proposed that there may be another source of elasticity.

3.6. Summary

Different types of modelling have been presented in the literature: theoretical as well as semi-empirical models. The theoretical model can be developed on the basis of calculations from a single droplet, or just by considering mesoscopic elements and ignoring the microstructure, as in mode coupling theory. The most frequently encountered results of modelling in the literature involve the shear modulus (which is equivalent to frequency independent of storage modulus) and the yield stress of highly concentrated emulsions, while flow curve and non-linear viscoelastic behaviour are rarely modelled as based on the microstructure evolution.

Different experimental research studies were undertaken in the area of highly concentrated emulsions with different applications, namely cosmetic and food emulsion, and explosive emulsions. While the basic theories, such as those of Princen, Babak and Lacasse, and some experimental work, especially that of Mason, suggest the scaling of properties with Laplace pressure, great doubt is involved concerning it, because all of these investigations tried to ignore the effect of the finite film thickness, introducing an arbitrary, suggested to be effective, dispersed phase volume fraction. Besides this, much experimental work showed that the properties did not scale with Laplace pressure, and suggested an additional source of elasticity.

Chapter 4 – Theoretical Modelling

4.1. Introduction

The starting point for the calculation of elastic properties of highly concentrated emulsions is the formulation of free energy F of compressed liquid droplets comprising a dispersed phase. We claim that the free energy has two dominant sources: interfacial energy and interdroplet interaction. The interfacial energy scales with the interfacial area of one droplet, while the interdroplet interaction is significant in the flattened (contact) area of neighbouring droplets (see Figure 4.1). Therefore, the factor determining the free energy of the system is the droplet shape as a function of volume fraction.

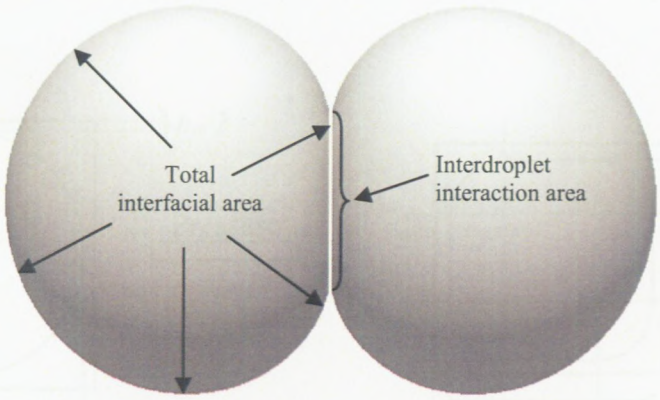

Figure 4.1: Typical deformation of two droplets pushed together

The basic physical assumption for the deformed droplet shape is the requirement of the minimal surface area. This can be done though two-dimensional or three-dimensional modelling.

4.2. Two-dimensional model

4.2.1. Geometrical Model

To develop a complete two-dimensional model, some earlier ideas proposed in the basic publications were used, therefore it is instructive to refer briefly to the main concepts of earlier work for a two-dimensional case.

According to the scheme in Figure 4.2, for a compressed droplet in a cubic arrangement of droplets we have:

$$a = d_2 - 2r \tag{4-1}$$

where *r* is the radius of curvature in the angles and *a* is the length of the plateau region. It is clear that the limiting concentration φ_c for maximum close-packing of spherical droplets is:

$$\varphi_c = \frac{\pi d^2}{4(d + h_\circ)^2} \Rightarrow \varphi_c(h_\circ = 0) = \varphi^* = \frac{\pi d^2}{4d^2} = \frac{\pi}{4} \tag{4-2}$$

where the film thickness at the critical volume fraction φ_c is not zero, but the φ^*, which is the effective volume fraction of close-packed spherical droplets with zero film thickness, was introduced for further calculation.

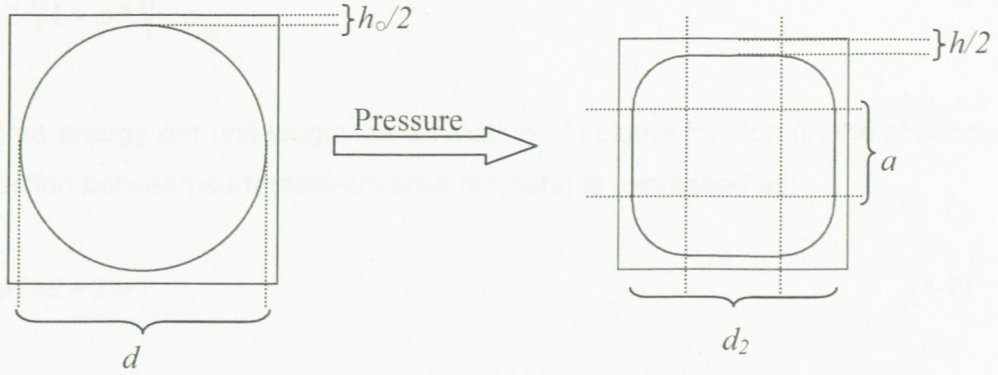

Figure 4.2: Schematic representation of droplet compression

The concentration, φ, of compressed droplets can be expressed as:

$$\varphi = \frac{S}{(d_2 + h)^2} \tag{4-3}$$

where *S* is the area of a compressed droplet. By the droplet incompressibility (the volume of droplet is conserved) assumption, $S = \frac{\pi d^2}{4}$.

It is convenient to introduce an "effective volume fraction" φ_{eff} of a dispersed phase with zero film thickness defined as $\varphi_{eff} = \pi d^2 / 4 d_2^{\,2}$. Then, the following relationship is valid:

$$\varphi_{eff} = \frac{\pi d^2}{4 d_2^{\,2}} \Rightarrow \frac{d_2}{d} = \sqrt{\frac{\varphi^*}{\varphi_{eff}}} \tag{4-4}$$

and the real volume fraction can be written as:

$$\varphi = \frac{\pi d^2}{4(d_2 + h)^2} \Rightarrow \frac{1}{\varphi} = \left(\frac{1}{\sqrt{\varphi_{eff}}} + \frac{h/d}{\sqrt{\varphi^*}}\right)^2 \tag{4-5}$$

After some geometrical calculations, we come to the following relationship:

$$\frac{r}{d} = \frac{1}{2}\sqrt{\frac{\varphi^*}{1-\varphi^*}}\sqrt{\frac{1-\varphi_{eff}}{\varphi_{eff}}} \tag{4-6}$$

The free energy per unit length* as a function of volume fraction (in the absence of any interaction between surfactant-covered droplets) is expressed as:

$$F = \sigma(4a + 2\pi r) \tag{4-7}$$

or,

$$F = \pi d \sigma \left(\frac{1}{\sqrt{\varphi^* \varphi_{eff}}} - \sqrt{\frac{1-\varphi^*}{\varphi^*}}\sqrt{\frac{1-\varphi_{eff}}{\varphi_{eff}}}\right) \tag{4-8}$$

where σ is the interfacial tension. Based on the above-mentioned equations, the osmotic pressure is:

$$\Pi = \frac{\varphi^2}{V_\circ}\frac{\partial F}{\partial \varphi}\bigg|_{V_\circ} = \frac{\varphi^2}{V_\circ}\frac{\partial F}{\partial \varphi_{eff}}\frac{\partial \varphi_{eff}}{\partial \varphi}\bigg|_{V_\circ} \tag{4-9}$$

* The *F* in the section of the two-dimensional model is free energy per unit length and its dimension is J/m.

where $V_\circ$ is the volume of incompressible droplet, and:

$$\left.\frac{\partial F}{\partial \varphi_{eff}}\right|_{V_\circ} = \pi d\sigma\left(-\frac{1}{2\sqrt{\varphi^* {\varphi_{eff}}^3}} + \sqrt{\frac{1-\varphi^*}{\varphi^*}} \times \frac{1}{2{\varphi_{eff}}^2}\sqrt{\frac{\varphi_{eff}}{1-\varphi_{eff}}}\right) \qquad (4\text{-}10)$$

And according to eq. (4-5), we can write:

$$\frac{\partial \varphi_{eff}}{\partial \varphi} = \left(\frac{\varphi_{eff}}{\varphi}\right)^{\frac{3}{2}} \qquad (4\text{-}11)$$

Therefore, the scaled osmotic pressure by the Laplace pressure – σ/R^* – is:

$$\frac{\Pi}{\sigma/R} = \sqrt{\frac{\varphi}{\varphi^*}} \times \left(\sqrt{\frac{1-\varphi^*}{1-\varphi_{eff}}} - 1\right) \qquad (4\text{-}12)$$

It can easily be shown that the osmotic pressure of a hexagonal arrangement of droplets follows the same function. This equation is valid only if the droplets do not interact with each other, as was assumed by different researchers (Princen, 1979, 1986, 1985, 1983; Princen & Kiss, 1986, 1987; Morse & Witten, 1993; Buzza & Cates, 1994; Buzza et al., 1995; Lacasse et al., 1996a, b; Mason et al., 1995).

It should be noted that, in this case, if it is assumed that the interdroplet film thickness has a constant value in all volume fractions, the osmotic pressure calculated from eq. (4-12) is slightly dependent on the droplet size and thus does not scale with the reciprocal droplet size.

For modelling the shear modulus, the strain derivation of free energy, eq. (4-8), can be used. By assuming droplet incompressibility, the free energy of a deformed droplet in the cubic (equations signed with "a") and hexagonal (equations signed with "b") lattices under a small γ shear deformation corresponding to the θ angle ($\tan\theta = \gamma << 1$), with a primary orientation angle α as shown in the Figure 4.3 ($0 \le \alpha \le \pi/4$ for cubic arrangement and $0 \le \alpha \le \pi/6$ for hexagonal arrangement), can be written as follows:

* For the sake of simplicity, it is assumed to be half of the actual Laplace pressure

$$F = \sigma(4a + 2\pi r)(\frac{x+y}{2}) = \sigma A_{\gamma=0}(\frac{x+y}{2}) \quad (4\text{-}13a)$$

$$F = \sigma(6a + 2\pi r)(\frac{x+y+z}{3}) = \sigma A_{\gamma=0}(\frac{x+y+z}{3}) \quad (4\text{-}13b)$$

where x, y and z are the change ratios of length sides of the deformed unit cell under strain. By introducing the geometrical sizes, we come to:

$$F = \frac{\sigma A_{\gamma=0}}{2}(\sqrt{1+\sin^2(\frac{\pi}{4}+\alpha)\gamma^2 - \sin(\frac{\pi}{2}+2\alpha)\gamma} + \sqrt{1+\sin^2(\frac{\pi}{4}-\alpha)\gamma^2 + \sin(\frac{\pi}{2}-2\alpha)\gamma}) \quad (4\text{-}14a)$$

$$F = \frac{\sigma A_{\gamma=0}}{3}(\sqrt{1+\sin^2(\frac{\pi}{6}+\alpha)\gamma^2 - \sin(\frac{\pi}{3}+2\alpha)\gamma} + \sqrt{1+\gamma^2} + \sqrt{1+\sin^2(\frac{\pi}{6}-\alpha)\gamma^2 + \sin(\frac{\pi}{3}-2\alpha)\gamma}) \quad (4\text{-}14b)$$

and calculation of $\frac{\partial^2 F}{\partial \gamma^2}$ leads to:

$$\left.\frac{\partial^2 F}{\partial \gamma^2}\right|_{\gamma=0} = \frac{\sigma A_{\gamma=0}}{2}(\sin^2(\frac{\pi}{4}+\alpha) - \frac{1}{4}\sin^2(\frac{\pi}{2}+2\alpha) + \sin^2(\frac{\pi}{4}-\alpha) - \frac{1}{4}\sin^2(\frac{\pi}{2}-2\alpha))$$
$$= \frac{\sigma A_{\gamma=0}}{2}(1 - \frac{1}{2}\cos^2(2\alpha)) \quad \Rightarrow \quad \left.\frac{\sigma A_{\gamma=0}}{4}\right|_{\alpha=0} \le \left.\frac{\partial^2 F}{\partial \gamma^2}\right|_{\gamma=0} \le \left.\frac{\sigma A_{\gamma=0}}{2}\right|_{\alpha=\pi/4} \quad (4\text{-}15a)$$

$$\left.\frac{\partial^2 F}{\partial \gamma^2}\right|_{\gamma=0} = \frac{\sigma A_{\gamma=0}}{3}(1 + \sin^2(\frac{\pi}{6}+\alpha) - \frac{1}{4}\sin^2(\frac{\pi}{3}+2\alpha) + \sin^2(\frac{\pi}{6}-\alpha) - \frac{1}{4}\sin^2(\frac{\pi}{3}-2\alpha))$$
$$= \frac{\sigma A_{\gamma=0}}{3}(\frac{11}{8} + \sin^2\alpha - \frac{1}{4}\cos^2(2\alpha)) \quad \Rightarrow \quad \left.\frac{9\sigma A_{\gamma=0}}{24}\right|_{\alpha=0} \le \left.\frac{\partial^2 F}{\partial \gamma^2}\right|_{\gamma=0} \le \left.\frac{25\sigma A_{\gamma=0}}{48}\right|_{\alpha=\pi/6} \quad (4\text{-}15b)$$

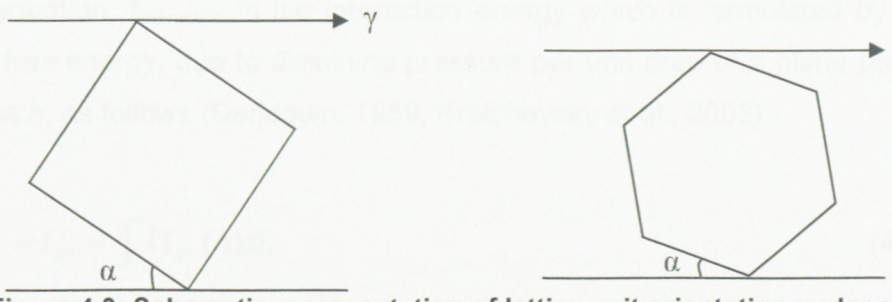

Figure 4.3: Schematic representation of lattice unit orientation under shear

Therefore, it can be concluded that the second partial derivative of free energy with respect to the strain for any type of orientation in a two-dimensional model is proportional to $\sigma A_{\gamma=0}$ by factor varying as $1/4 \le k_\alpha \le 25/48$. Finally, the shear modulus can be expressed as:

$$G = \frac{\varphi}{V_\circ}\frac{\partial^2 F}{\partial \gamma^2}\bigg|_{\gamma=0} = k_\alpha \frac{2\sigma}{d}\varphi\left(\frac{1}{\sqrt{\varphi^* \varphi_{eff}}} - \sqrt{\frac{1-\varphi^*}{\varphi^*}}\sqrt{\frac{1-\varphi_{eff}}{\varphi_{eff}}}\right) \tag{4-16}$$

$$\Rightarrow \frac{G}{\sigma/R} = k_\alpha \varphi\left(\frac{1}{\sqrt{\varphi^* \varphi_{eff}}} - \sqrt{\frac{1-\varphi^*}{\varphi^*}}\sqrt{\frac{1-\varphi_{eff}}{\varphi_{eff}}}\right) \tag{4-17}$$

It is clear from the above equation that, for a constant film thickness, the shear modulus normalised by the Laplace pressure should be slightly dependent on the droplet size and film thickness similar to the osmotic pressure case. This is a more general result than obtained in earlier publications where $\frac{G}{\sigma/R}$ was invariant to the droplet size, though the difference is not big.

4.2.2. Modified 2-D Model: Introducing disjoining pressure and optimised film thickness

By including the interaction between surfactant-covered droplets, the free energy per unit length of a compressed emulsion in a two-dimensional model can be modified as:

$$F = \pi d\sigma\left(\frac{1}{\sqrt{\varphi^* \varphi_{eff}}} - \sqrt{\frac{1-\varphi^*}{\varphi^*}}\sqrt{\frac{1-\varphi_{eff}}{\varphi_{eff}}}\right) + f_{\text{interaction}} \tag{4-18}$$

In this equation, $f_{\text{interaction}}$ is the interaction energy which is formulated by the excess surface free energy, due to disjoining pressure per unit area of a plane-parallel film of thickness h, as follows (Derjaguin, 1989; Kralchevsky et al., 2003):

$$\frac{f_{\text{interaction}}}{\mathrm{S}_{\text{cont}}} = \mathrm{f}_{dis} = \int_h^\infty \Pi_{dis}(h)dh \tag{4-19}$$

where S_{cont} is the area of contact between two neighbouring droplets. By neglecting the interaction in the plateau border region, the free energy per unit length is:

$$F = \pi d\sigma\left(\frac{1}{\sqrt{\varphi^* \varphi_{eff}}} - \sqrt{\frac{1-\varphi^*}{\varphi^*}}\sqrt{\frac{1-\varphi_{eff}}{\varphi_{eff}}}\right) + na\,\mathrm{f}_{dis}(h) \qquad (4\text{-}20)$$

where n is the number of neighbouring droplets, being 4 for cubic and 6 for hexagonal arrangements. By replacing a with its volume fraction function, we will have:

$$F = \pi d\sigma\left[\left(\frac{1}{\sqrt{\varphi^* \varphi_{eff}}} - \sqrt{\frac{1-\varphi^*}{\varphi^*}}\sqrt{\frac{1-\varphi_{eff}}{\varphi_{eff}}}\right) + \frac{\mathrm{f}_{dis}(h)}{\sigma}\left(\frac{1}{\sqrt{\varphi^* \varphi_{eff}}} - \frac{1}{\sqrt{\varphi^*(1-\varphi^*)}}\sqrt{\frac{1-\varphi_{eff}}{\varphi_{eff}}}\right)\right] \qquad (4\text{-}21)$$

In order to determine the osmotic pressure of a highly concentrated emulsion, the optimum film thickness corresponding to the minimum free energy should be obtained, and then the osmotic pressure can be calculated by using eq. (2-29). The algorithm is as follows:

1- Definition of the h domain: The maximum film thickness in a fixed volume fraction can be obtained when the droplet is fully compressed to a cube or hexagon respectively, in cubic or hexagonal lattices ($a=d_2$):

$$\varphi = \frac{{d_2}^2}{(d_2 + h_{\max})^2} \Rightarrow h_{\max} = d_2\left(\frac{1}{\sqrt{\varphi}} - 1\right) \qquad (4\text{-}22)$$

And according to incompressibility assumption for this fully compressed case, we have:

$$h_{\max} = d\sqrt{\varphi^*}\left(\frac{1}{\sqrt{\varphi}} - 1\right) \qquad (4\text{-}23)$$

This equation is also valid for the hexagonal arrangement of droplets. Therefore the film thickness, h, can vary between zero and h_{max} ($0 \le h \le h_{\max}$).

2- At each volume fraction of emulsion, φ, by changing h, the variation of free energy is calculated, and by using eq. (4-5) and (4-21) and the optimised film thickness, h_{opt}, corresponding to the minimum energy, will be obtained. The interdroplet interaction energy per unit area in eq. (4-21) can be obtained experimentally by disjoining pressure measurement, or predicted from DLVO theory or any other discussed disjoining pressure contributions.

3- The osmotic pressure will be obtained through numerical derivation of free energy with respect to the volume fraction, eq. (2-29).

4- The shear modulus can be obtained through a similar approach to the constant film thickness case. If it is assumed that the film thickness does not change under shearing, the free energy per unit length will be:

$$F = [\sigma A_{\gamma=0} + 4a\Pi_{dis}(h_{opt})](\frac{x+y}{2}) \tag{4-24a}$$

$$F = [\sigma A_{\gamma=0} + 6a\Pi_{dis}(h_{opt})](\frac{x+y+z}{3}) \tag{4-24b}$$

It can be seen that the interfacial interaction force depending on the flattened area increases in shearing. The shear modulus is obtained as follows:

$$G = \frac{\varphi}{V_\circ}\frac{\partial^2 F}{\partial \gamma^2}\bigg|_{\gamma=0} = k_\alpha \frac{2\sigma}{d}\varphi[(\frac{1}{\sqrt{\varphi^* \varphi_{eff}}} - \sqrt{\frac{1-\varphi^*}{\varphi^*}}\sqrt{\frac{1-\varphi_{eff}}{\varphi_{eff}}}) + \frac{f_{dis}(h_{opt})}{\sigma}(\frac{1}{\sqrt{\varphi^* \varphi_{eff}}} - \frac{1}{\sqrt{\varphi^*(1-\varphi^*)}}\sqrt{\frac{1-\varphi_{eff}}{\varphi_{eff}}})] \tag{4-25}$$

And modulus scaled by the Laplace pressure is calculated as:

$$\Rightarrow \frac{G}{\sigma/R} = k_\alpha \varphi[(\frac{1}{\sqrt{\varphi^* \varphi_{eff}}} - \sqrt{\frac{1-\varphi^*}{\varphi^*}}\sqrt{\frac{1-\varphi_{eff}}{\varphi_{eff}}}) + \frac{f_{dis}(h_{opt})}{\sigma}(\frac{1}{\sqrt{\varphi^* \varphi_{eff}}} - \frac{1}{\sqrt{\varphi^*(1-\varphi^*)}}\sqrt{\frac{1-\varphi_{eff}}{\varphi_{eff}}})] \tag{4-26}$$

where k_α changes between 1/4 and 1/2 for the cubic arrangement, and between 9/24 and 25/48 for the hexagonal arrangement of droplets. As the shear modulus is dominated by the weakest arrangement in the sample, we assumed the minimum k_α in this study.

4.2.3. Modified 2-D Model: Introducing disjoining pressure and approximate film thickness

It is clear that the above-mentioned theory is extensively computer-based, and according to the example modelling result – instead of finding an optimised film thickness – it is suggested that a linear dependency of film thickness on volume fraction be assumed. In this case, the critical volume fraction φ_c – see eq. (4-2) – should be obtained experimentally, and it represents the volume fraction in which the trend of osmotic pressure and shear modulus change. Therefore the film thickness dependency will be as follows:

$$h(\varphi) = h_\circ \frac{1-\varphi}{1-\varphi_c} \Rightarrow h(\varphi) = d\frac{\sqrt{\varphi^*/\varphi_c}-1}{1-\varphi_c}(1-\varphi) \tag{4-27}$$

which can be put in eq. (4-21) and eq. (4-26) to obtain the osmotic pressure and shear modulus analytically:

$$\begin{aligned}\frac{\Pi}{\sigma/R} = &\left(\sqrt{\frac{1-\varphi^*}{\varphi^*}}\sqrt{\frac{\varphi}{1-\varphi_{eff}}} - \sqrt{\frac{\varphi}{\varphi^*}}\right) \\ &+ \frac{d\,\mathrm{f}_{dis}(h)}{dh}\frac{2h_\circ\varphi^2}{\sigma(1-\varphi_c)}\left(\frac{1}{\sqrt{\varphi^*(1-\varphi^*)}}\sqrt{\frac{1-\varphi_{eff}}{\varphi_{eff}}} - \frac{1}{\sqrt{\varphi^*\varphi_{eff}}}\right) \\ &+ \frac{\mathrm{f}_{dis}(h)}{\sigma}\left(\frac{1}{\sqrt{\varphi^*(1-\varphi^*)}}\sqrt{\frac{\varphi}{1-\varphi_{eff}}} - \sqrt{\frac{\varphi}{\varphi^*}}\right)\end{aligned} \tag{4-28}$$

$$\begin{aligned}\frac{G}{\sigma/R} = k_\alpha\varphi\Bigg[&\left(\frac{1}{\sqrt{\varphi^*\varphi_{eff}}} - \sqrt{\frac{1-\varphi^*}{\varphi^*}}\sqrt{\frac{1-\varphi_{eff}}{\varphi_{eff}}}\right) \\ &+ \frac{\mathrm{f}_{dis}(h)}{\sigma}\left(\frac{1}{\sqrt{\varphi^*\varphi_{eff}}} - \frac{1}{\sqrt{\varphi^*(1-\varphi^*)}}\sqrt{\frac{1-\varphi_{eff}}{\varphi_{eff}}}\right)\Bigg]\end{aligned} \tag{4-29}$$

4.3. Three-dimensional Model

4.3.1. Geometrical Model

In a three-dimensional model, the number of neighbouring droplets affects the maximum close-packing of spherical droplets, while its structural and rheological properties also depend on the type of packing. In the numerical and analytical modelling performed by Lacasse et al. (1996a), the effect of a variable film thickness which can affect the properties was neglected; see eq. (4-9) and $\frac{\partial \varphi_{eff}}{\partial \varphi}$ term in it.

In order to calculate the osmotic pressure and shear modulus of highly concentrated emulsions, the free energy, F, of a compressed droplet should be formulated. The starting point is the consideration of variations of droplet shape as a function of volume fraction.

The total surface area of a deformed droplet in a concentration higher than the maximum close packing of spherical droplets, φ^*, can only be determined numerically. The basic physical assumption for the deformed droplet shape is the requirement of the minimal surface area. By using Brakke's surface evolver software (Brakke, 1992), the shape of a single droplet with a minimum surface area under the constraint of fixed droplet volume, and as a function of confinement, was calculated. In this study, the droplet was meshed with 196,610 vertices which were confined inside a polyhedral cell, particularly the rhombic dodecahedron (face-centred cubic), truncated octahedron (body-centred cubic), and simple cube, all of which are space-filling polyhedrals. The total area and the flattened area (parts of droplet surface touching the polyhedral confinement) of the droplet with a unit radius were recorded as the results of this simulation.

While Lacasse et al. (1996a) suggested fitting the excess surface area with a power-law relationship $K(\varphi_{eff} - \varphi^*)^{\alpha}$, an improved fitting with $K\varphi_{eff}{}^{\alpha}(\varphi_{eff} - \varphi^*)^{\beta}$ is observed in this work (Figure 4.4). Here φ^* and φ_{eff} respectively are the volume fractions of closest packing and the compressed droplet. So, the total surface area, $A(\varphi)$, and the flattened part of the surface area, $A_F(\varphi)$, of a droplet in different three-dimensional lattices were fitted respectively by the following equations (Table 4.1):

$$\frac{A(\varphi)}{\pi d^2} = 1 + K\varphi_{eff}{}^{\alpha}\left(\frac{\varphi_{eff} - \varphi^*}{1 - \varphi^*}\right)^{\beta} \qquad (4\text{-}30)$$

$$\frac{A_F(\varphi)}{\pi d^2} = K'\varphi_{eff}{}^{\alpha'}\left(\frac{\varphi_{eff}-\varphi^*}{1-\varphi^*}\right)^{\beta'} \qquad (4\text{-}31)$$

Table 4.1: The coefficients of fittings and validity range

Type of Lattice		K	A	β	Validity (2% error)	Closest packing, φ*
FCC	Total area	6.3E-2	4.52	2	96%	$\pi\sqrt{2}/6$
	Flattened area	7.5E-1	4.41	1.1	96%	
BCC	Total area	4.85E-2	2.43	2	94%	$\pi\sqrt{3}/8$
	Flattened area	4.35E-1	2.24	1.1	90%	
SC	Total area	1.36E-1	1.41	2	90%	$\pi/6$
	Flattened area	8.3E-1	1.79	1.1	92%	

An attempt was made to fit the results with fixed exponents in both cases: $(A-A_\circ)/A_\circ = K\varphi_{eff}\left(\frac{\varphi_{eff}-\varphi^*}{1-\varphi^*}\right)^{2.2}$ and $A_F/A_\circ = K'\varphi_{eff}\left(\frac{\varphi_{eff}-\varphi^*}{1-\varphi^*}\right)^{1.3}$ equations were obtained with K_{SC}=*1.41E-1*, K_{BCC}=*4.41E-2*, K_{FCC}=*4.28E-2*; K'_{SC}=*7.71E-1*, K'_{BCC}=*4. 1E-1*, K'_{FCC}=*5.12E-1*. It should be noted that the validity of these fittings with fixed exponents is up to 90 volume percent and with less than 5% error in this approximate method.

The complete expression for the free energy is formulated as follows:

$$F = \sigma A(\varphi) + f_{dis}A_F(\varphi) \qquad (4\text{-}32)$$

Where σ is the interfacial tension, and $A(\varphi)$ and $A_F(\varphi)$ respectively are total and flattened surface areas obtained from eq. (4-30), (4-31). The f_{dis} term with energy per area dimension in the right-hand side of this equation allows us to include the effect of interdroplet interactions, which is not considered in the basic Princen-Lacasse-Mason models of elasticity of highly concentrated emulsions. This interaction energy per unit area is obtained by integrating disjoining pressure of a plane-parallel film between two neighbouring droplets with respect to film thickness *h* as eq. (4-19).

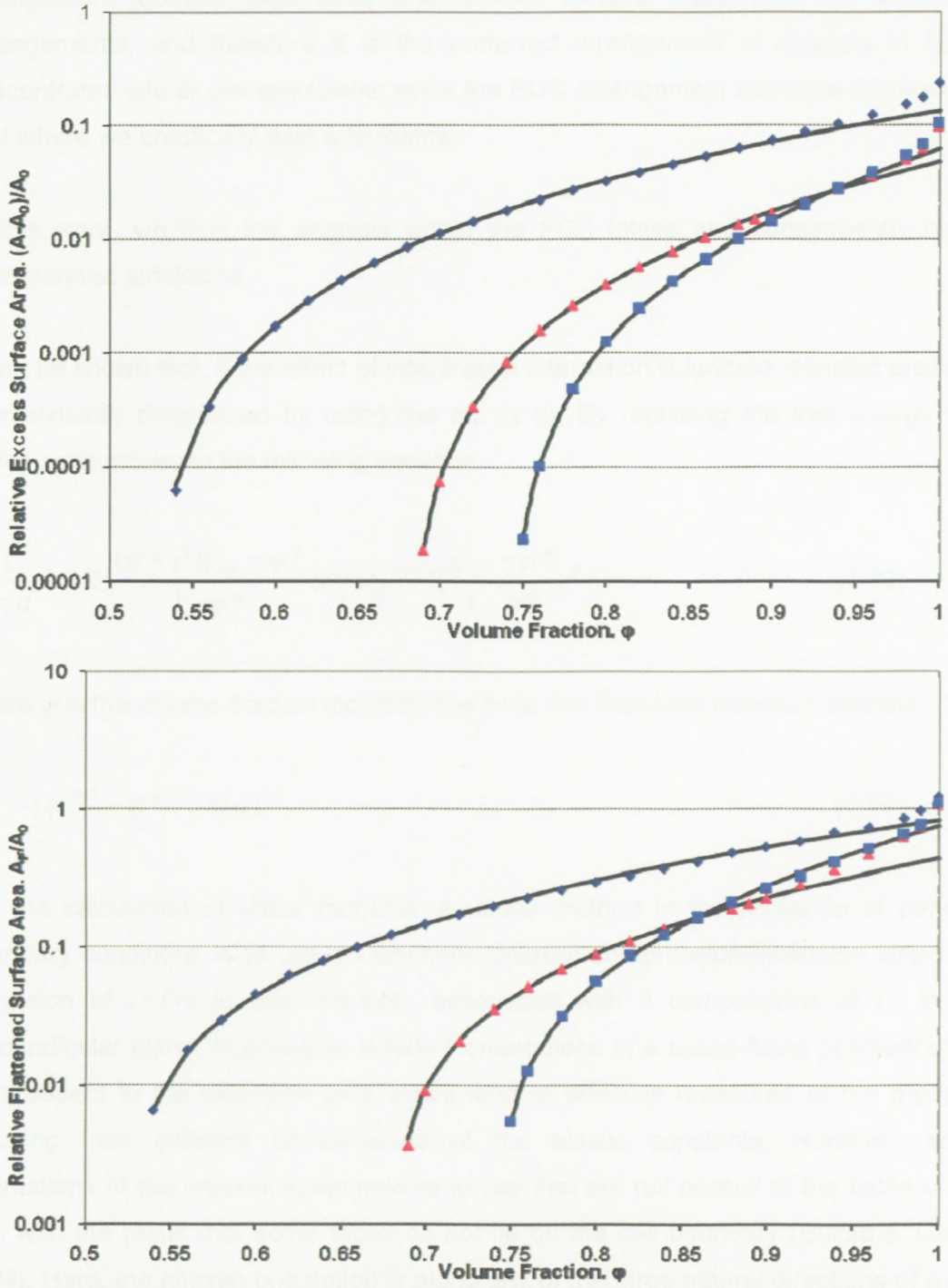

Figure 4.4: The results of simulated total and flattened surface areas for three different lattices: SC (◆) BCC (▲), FCC (■) fitted by eq. (4-30) and (4-31) presented as a continuous line

The disjoining pressure formulations for different types of interactions, for example electrostatic, Van der Waals, steric and micellar forces, are extensively presented in the literature (Israelachvili, 1992; Kralchevsky et al., 2003).

The results of calculations presented in Figure 4.4 show that, up to φ~*0.9*, the FCC arrangement induces lower total and contact surface areas than SC and BCC arrangements, and therefore it is the preferred arrangement of droplets in highly concentrated w/o or o/w emulsions; while the BCC arrangement becomes dominant at φ~*1* where we practically deal with foams.

In this work, we limit the analysis within the FCC lattice and consequently highly concentrated emulsions.

It can be shown that, if the effect of interdroplet interaction is ignored, osmotic pressure is analytically determined by using the eq. (4-9). By replacing the free energy with $\sigma A(\varphi)^*$, one comes to the following equation:

$$\frac{\Pi}{2\sigma/d} = 3K.\frac{(\alpha+\beta)\varphi_{eff}-\varphi^*}{1-\varphi^*}\varphi^{2/3}\varphi_{eff}{}^{\alpha+1/3}\left(\frac{\varphi_{eff}-\varphi^*}{1-\varphi^*}\right)^{\beta-1} \qquad (4\text{-}33)$$

where φ is the volume fraction including the finite film thickness between droplets:

$$\varphi_{eff} = (\varphi^{-1/3} - \varphi^{*-1/3}\, h/d)^{-3} \qquad (4\text{-}34)$$

For the calculation of shear modulus, a useful method in the presence of periodic boundary conditions is to use an isochoric uniaxial compression-extension strain: an extension of $\lambda=1+\varepsilon$ in one direction, associated with a compression of $\lambda^{-1/2}$ in the perpendicular plane. In principle, different orientations of a space-filling polyhedral cell with respect to the extension axis would lead to effective measures of the modulus resulting from different combinations of the elastic constants. However, some orientations of the uniaxial strain involve forces that are not normal to the faces of the cell, with the result that some faces do not lie on the cell boundary (Buzza & Cates, 1994). Here, the chosen orientation is along any of the three natural directions of a unit cell. The effective shear modulus G for small ε is (Seth et al., 2006):

$$u(\varepsilon,\varphi) - u(0,\varphi) = 2G(\lambda^2 - \lambda - \lambda^{0.5} + \lambda^{-0.5}) \qquad (4\text{-}35)$$

---

* In this case, the free energy expression, eq. (4-33), is limited to interfacial energy.

where $u = (F - F_0)/V$ is the excess energy density. The shear modulus can then be obtained by fitting the variation of excess energy density versus $2(\lambda^2-\lambda-\lambda^{0.5}+\lambda^{-0.5}) \approx 3\varepsilon^2/4$.

In the absence of interdroplet interaction, the excess energy density (for $\sigma=1$ and $R=1$) as a function of applied strain in different volume fractions above φ^* was simulated by surface evolver. The results were plotted as shown in Figure 4.5. Therefore, the shear modulus variation versus volume fraction was obtained, and fitted successfully by using the following equation (Figure 4.6) in the range of highly concentrated emulsions ($\varphi \leq 0.95$):

$$\frac{G}{\sigma/R} = 0.6\varphi_{eff}^{-2}(\varphi_{eff} - \varphi^*)^{0.5} + 0.051 \qquad (4\text{-}36)$$

One can see that the scaling of shear modulus with Laplace pressure is exactly valid in the absence of interdroplet interaction. Another important prediction of eq. (4-36) and also of the Princen-Lacasse-Mason models is the linear dependency of shear modulus on reciprocal droplet size at a fixed volume fraction, $G/\sigma \sim 1/d$. It is also clear from eq. (4-36) that, if the droplet size tends to infinity, the shear modulus limits to zero.

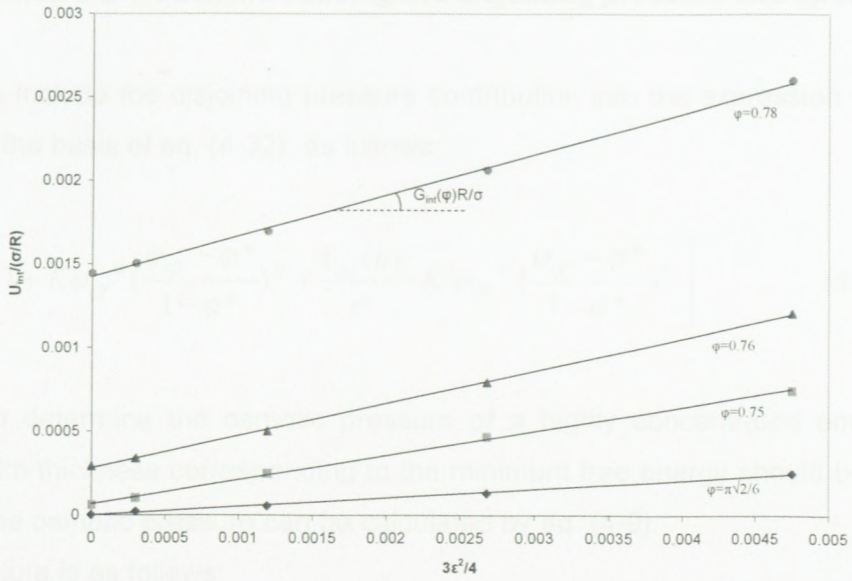

Figure 4.5: Fitting the variation of excess energy density against $3\varepsilon^2/4$ for calculating shear modulus

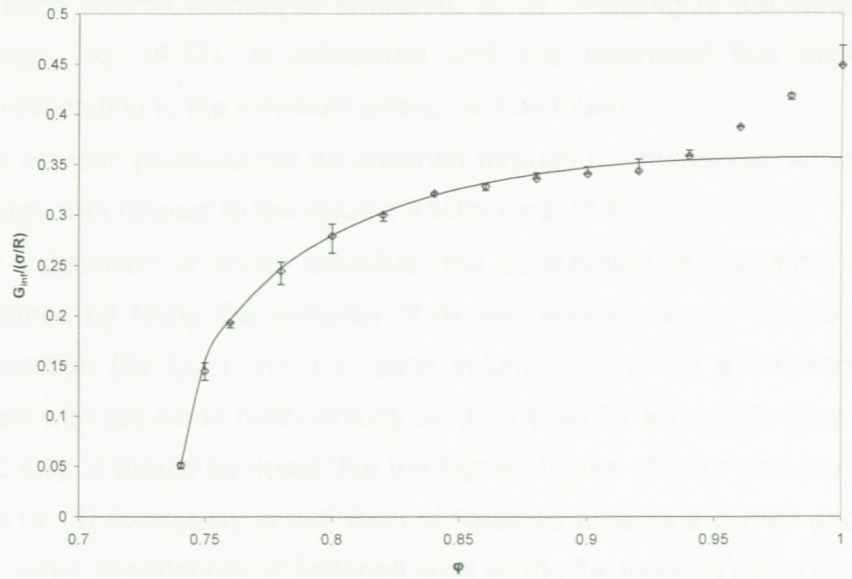

Figure 4.6: The variation of $G_{int}/(\sigma/R)$ versus volume fraction, (◇): results obtained by surface evolver, (–): prediction of fitted eq. (4-36)

It is seen in Figures 4.5 and 4.6 that, at volume fraction equal to φ^*, the shear modulus is not zero that is caused by deformation of constrained spherical droplets; non-zero shear modulus at maximum closest packing of spherical droplets can also be found in experimental results reported by Mason et al. (1997).

4.3.2. Modified 3-D Model: Introducing the disjoining pressure and optimised film thickness

Now let us include the disjoining pressure contribution into the expression for the free energy on the basis of eq. (4-32), as follows:

$$F = \sigma\pi d^2\left[1 + K{\varphi_{eff}}^{\alpha}\left(\frac{\varphi_{eff}-\varphi^*}{1-\varphi^*}\right)^{\beta} + \frac{f_{dis}(h)}{\sigma}\cdot K'{\varphi_{eff}}^{\alpha'}\left(\frac{\varphi_{eff}-\varphi^*}{1-\varphi^*}\right)^{\beta'}\right] \qquad (4\text{-}37)$$

In order to determine the osmotic pressure of a highly concentrated emulsion, the optimum film thickness corresponding to the minimum free energy should be obtained, and then the osmotic pressure can be calculated by eq. (4-9).

The procedure is as follows:

- Definition of the h domain: The maximum film thickness in a fixed volume fraction can be obtained when a droplet is fully compressed:
- $h_{\max} = d\varphi^{*1/3}(\varphi^{-1/3} - 1)$ (4-38)
- Therefore the film thickness, h, can vary between zero and h_{max} $(0 \le h \le h_{\max})$.

- At each volume fraction of emulsion, φ, by changing h, the variation of free energy, eq. (4-37), is calculated and the optimised film thickness, h_{opt}, corresponding to the minimum energy will be found.
- The osmotic pressure will be obtained through the numerical derivative of free energy with respect to the volume fraction, eq. (4-9).
- For calculation of shear modulus, the contribution of disjoining pressure is obtained by fitting the variation of excess energy density due to interdroplet interaction (for $f_{dis}=1$, $R=1$) in each volume fraction as a function of applied strain with the same methodology as discussed for eq. (4-36) (see Figures 4.7 and 4.8). It should be noted that the higher degree of error bars in Figure 4.8 is due to: (1) complexity in definition of flattened area* in a curved geometry, and (2) higher dependency of flattened area on the fluctuations about the converged value of solution.
- Therefore, the shear modulus including both interfacial energy and interdroplet interaction is obtained as follows:

$$G = \frac{\sigma}{R} \times [0.6\varphi_{eff}^{-2}(\varphi_{eff} - \varphi^*)^{0.5} + 0.051] + \frac{f_{dis}(h)}{R} \times [0.8\varphi_{eff}^{-16}(\varphi_{eff} - \varphi^*)^{0.6} + 5.3] \quad (4\text{-}39)$$

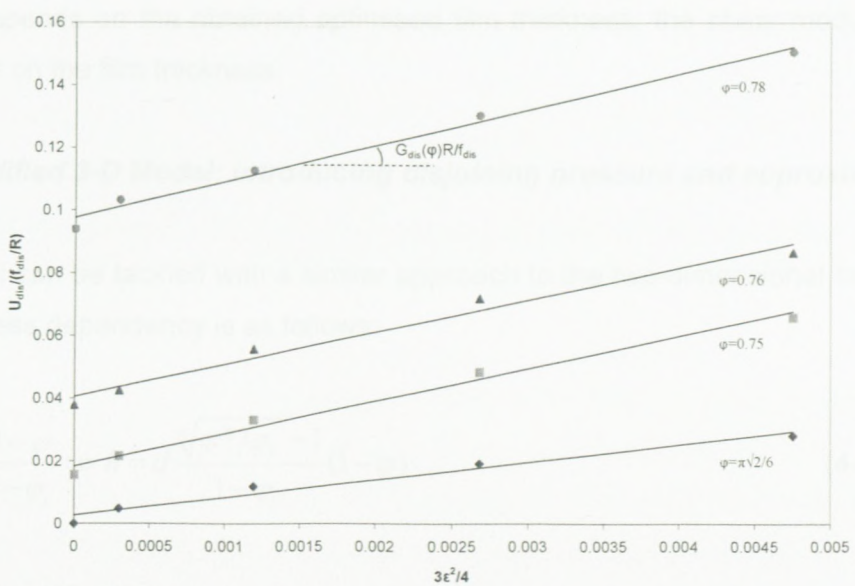

Figure 4.7: Fitting the variation of excess energy density due to the interaction against $3\varepsilon^2/4$ for calculating shear modulus

* As mentioned before, the interdroplet interaction is mainly present in the flattened area between two neighbouring droplets, and $f_{dis}A_F(\varphi)$ shows the free energy of interaction.

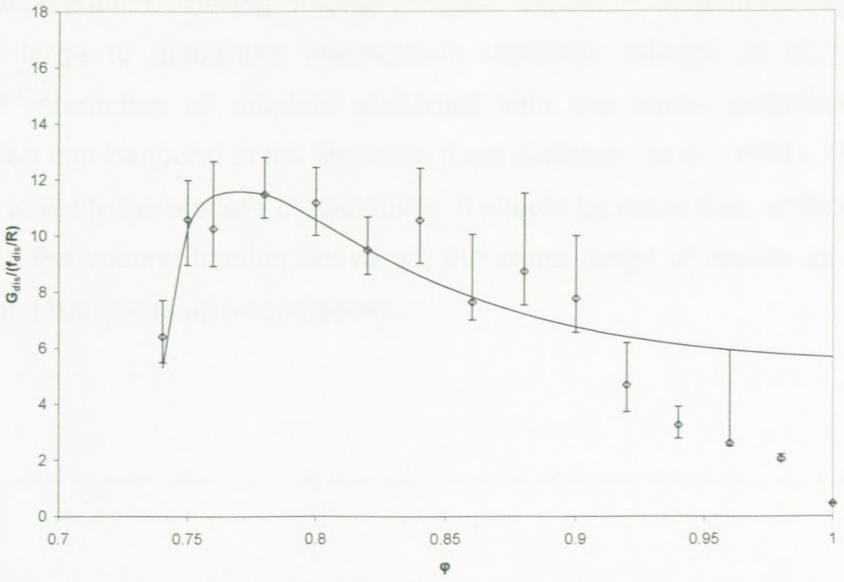

Figure 4.8: The variation of $G_{dis}/(\sigma/R)$ versus volume fraction, (◊): results obtained by surface evolver, (–): prediction of fitted equation

It is immediately clear that the elasticity calculated in the frames of the present model is not scaled with Laplace pressure due to the presence of the interaction term. The linear relationship of shear modulus and reciprocal droplet size also does not exist due to the possibility of film thickness-droplet size dependency in $f_{dis}(h)$ term; but still $G \rightarrow 0$, if $R \rightarrow \infty$. It should be noted that, while the effective volume fraction for each real volume fraction depends on the obtained optimised film thickness, the shear modulus is also dependent on the film thickness.

4.3.3. Modified 3-D Model: Introducing disjoining pressure and approximate film thickness

This model can be tackled with a similar approach to the two-dimensional one, and the film thickness dependency is as follows:

$$h(\varphi) = h_{\circ}\frac{1-\varphi}{1-\varphi_c} \Rightarrow h = d\frac{\sqrt[3]{\varphi^*/\varphi_c}-1}{1-\varphi_c}(1-\varphi) \qquad (4\text{-}40)$$

4.4. Model verification

The rheological properties of mono-dispersed highly concentrated emulsions stabilised by 10mM sodium dodecyl sulphate (SDS) were published by Mason et al. (1997). The studied highly concentrated emulsions were prepared with different droplet sizes and volume fractions. The surfactant concentration was only slightly above the critical

micelle concentration, making micelle-induced depletion attractions negligible, yet sufficiently large to guarantee electrostatic repulsion (Mason et al., 1997). The interdroplet interaction of droplets stabilised with the same surfactant type and concentration can be found in the literature (Leal-Calderon et al., 1994). These results were used to verify the model's predictability. It should be noted that, while our model is restricted to the volume fraction above φ^*, the same range of results as reported by Mason et al. (1997) was also considered.

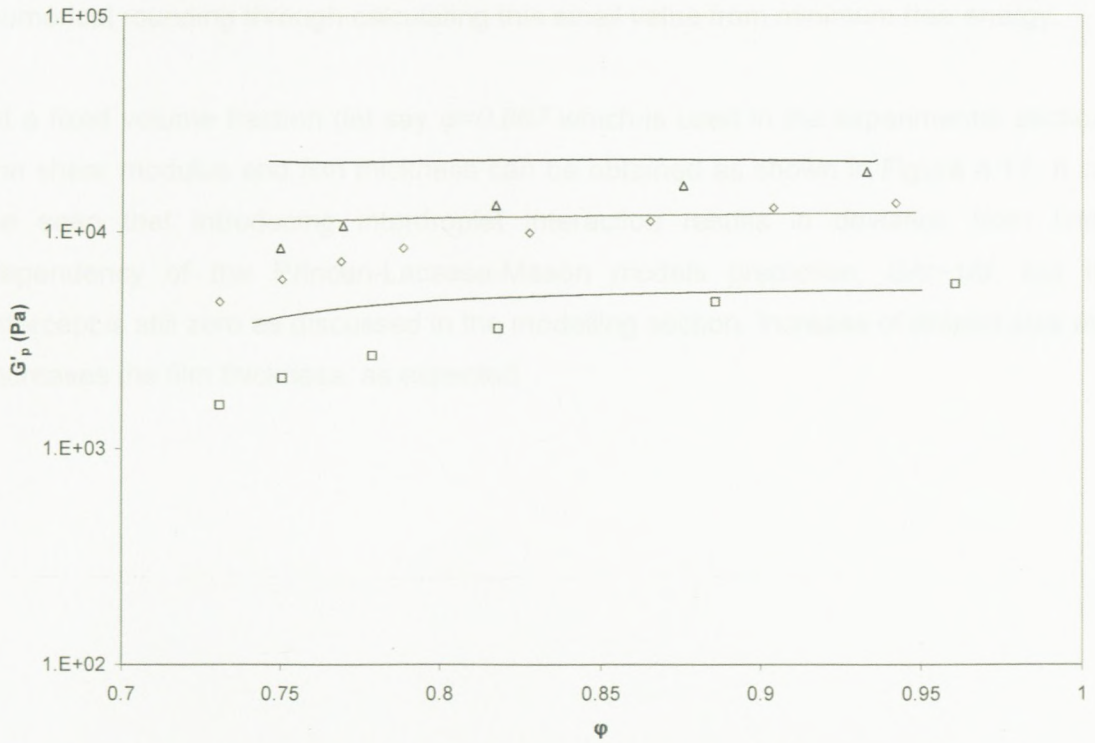

Figure 4.9: The comparison of model prediction with experimental results for different droplet sizes: *R =0.25μm* (△), *R = 0.37μm* (◊) and *R = 0.74μm* (□)

As shown in Figure 4.9, the model prediction indicates good agreement with experimental results for different droplet sizes. The observed deviation at volume fractions close to φ^* may be due to the imperfect FCC arrangement of droplets, which is improved by increasing the volume fraction (Mason et al., 1997).

4.5. Typical predictions of the model

To demonstrate the effect of interdroplet interaction on the osmotic pressure and shear modulus, a power law interaction between flattened parts of two droplets surfaces (soft repulsion) was chosen for a visual example:

$$f_{dis}(h) = A / h^2 \qquad (4\text{-}41)$$

The results of calculations are presented in Figure 4.10. One can clearly see significant deviations from the predictions of the classical model of elasticity considering the surface energy as the sole source of elasticity at even very small values of the coefficient *A* (eq. 4-41). Besides, it is evident that neither osmotic pressure nor shear modulus scales with interfacial tension if the effect of inter-droplet interaction has been taken into account. The fluctuations observed in film thickness variation are due to numerical rounding through calculating this small value from minimum free energy.

At a fixed volume fraction (let say $\varphi=0.867$ which is used in the experimental section), the shear modulus and film thickness can be obtained as shown in Figure 4.11. It can be seen that introducing interdroplet interaction results in deviation from linear dependency of the Princen-Lacasse-Mason models prediction, $G/\sigma \sim 1/d$, but the intercept is still zero as discussed in the modelling section. Increase of droplet size also increases the film thickness, as expected.

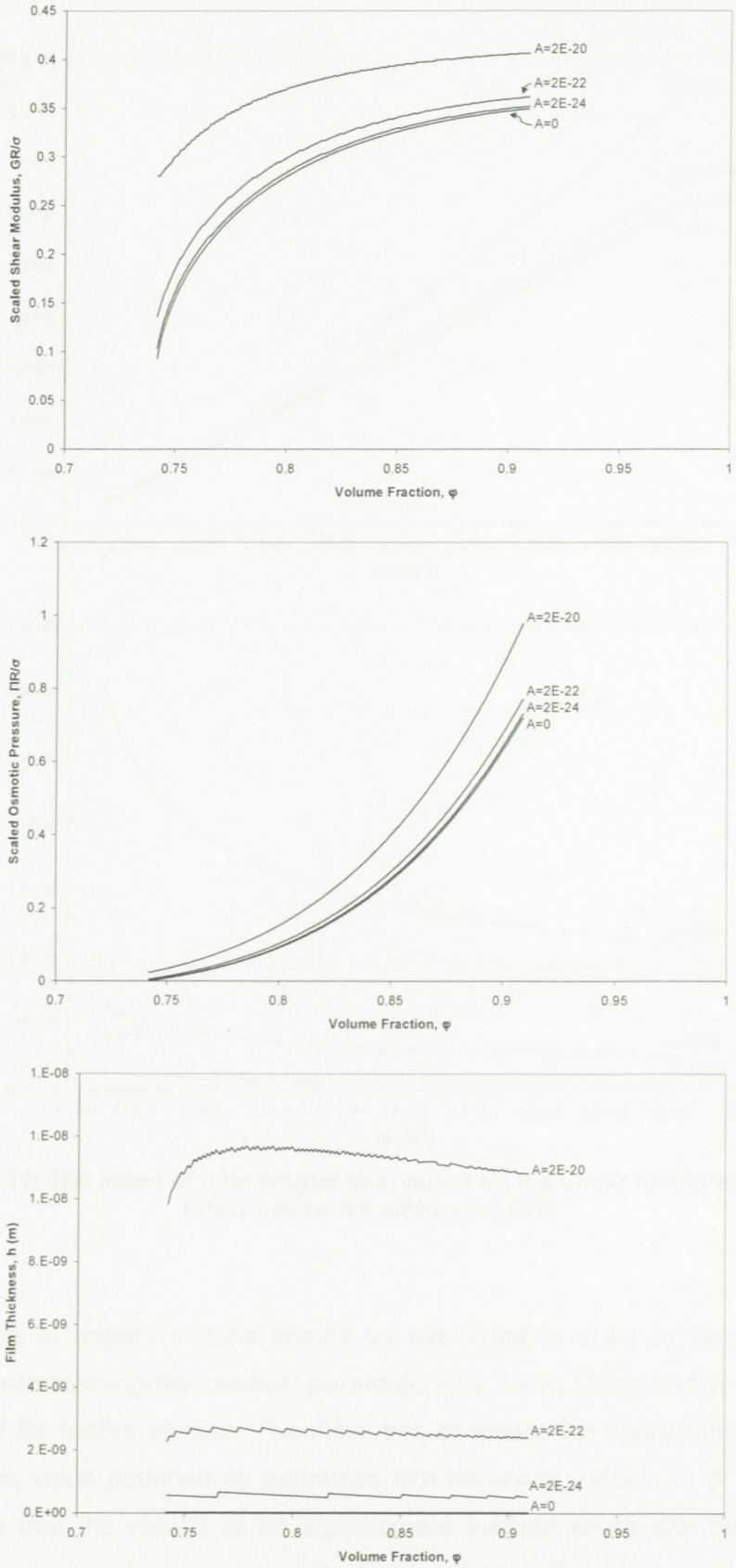

Figure 4.10: The effect of interdroplet interaction on the osmotic pressure and shear modulus (σ=10mN/m, R=1μm)

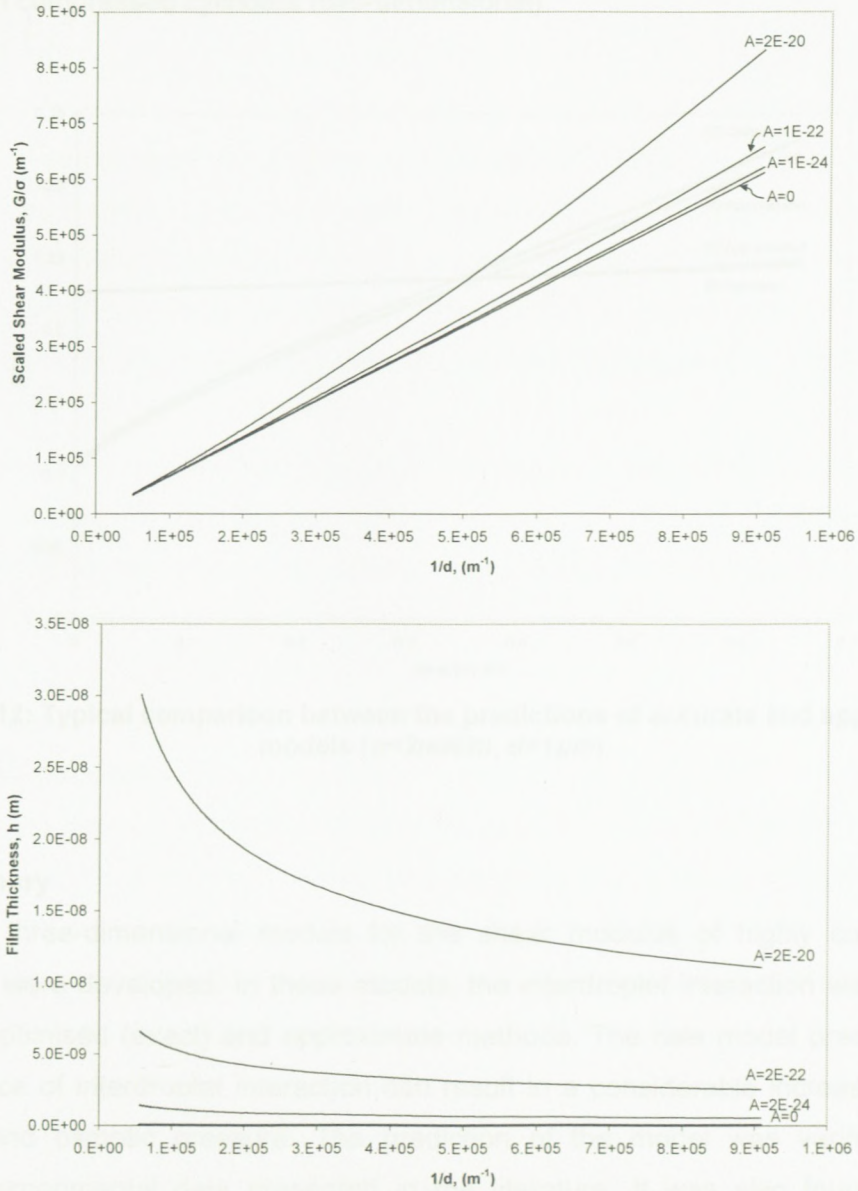

Figure 4.11: The effect of interdroplet interaction on the shear modulus and film thickness (*σ=10mN/m, φ=0.867*)

The difference of approximations should be evaluated in order to be aware of the dependency of obtaining the models' parameters by curve fitting and/or choosing the proper model for further studies. The initial film thickness for approximate cases was chosen as the value obtained by optimised film thickness models at φ^*. Figure 4.12 demonstrates that the results of an approximate method which can be approached analytically are in good agreement with the accurate optimisation method (*A=2E-22* and $f_{dis}(h) = A/h^2$). The difference between two-dimensional and three-dimensional modelling predictions recommends using the three-dimensional case, because highly

concentrated emulsions in reality consist of compressed spheres (three-dimensional) rather than compressed cylinders (two-dimensional).

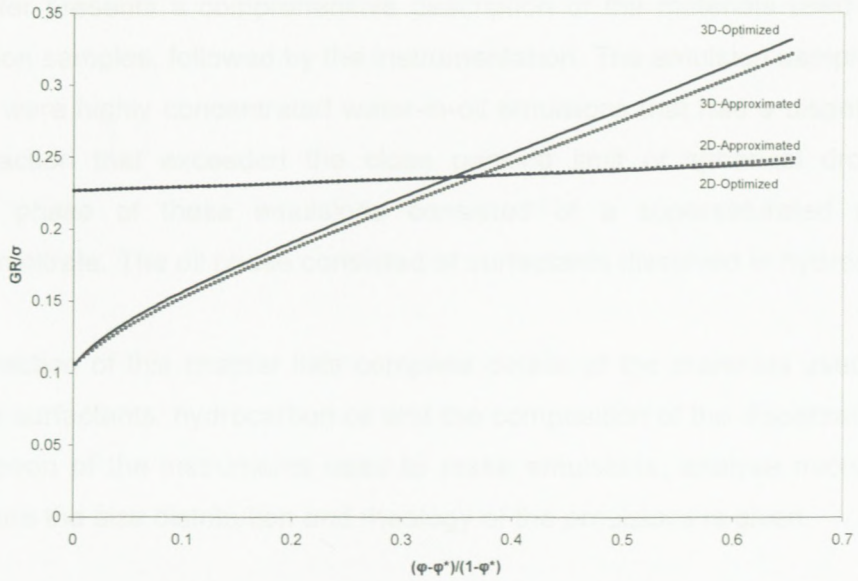

Figure 4.12: Typical comparison between the predictions of accurate and approximate models (σ=2mN/m, d=1μm)

4.6. Summary

Two- and three-dimensional models for the shear modulus of highly concentrated emulsions were developed. In these models, the interdroplet interaction was included by using optimised (exact) and approximate methods. The new model predicts that a slight source of interdroplet interaction can result in a considerable increase in shear modulus and osmotic pressure. The prediction of the model was verified by the standard experimental data presented in the literature. It was also found that the elasticity calculated in the frames of the present model is not scaled with Laplace pressure, due to the presence of the interaction term. The linear relationship of shear modulus and reciprocal droplet size – which is present in the geometrical model – also does not exist due to the possibility of film thickness-droplet size dependency in $f_{dis}(h)$ term. This non-linear dependence still satisfies $G \rightarrow 0$, if $R \rightarrow \infty$ extrapolation.

Chapter 5 – Experimental Details

5.1. Introduction

This chapter presents a comprehensive description of the materials used to prepare the emulsion samples, followed by the instrumentation. The emulsion samples used for this study were highly concentrated water-in-oil emulsions that had a dispersed phase volume fraction that exceeded the close packing limit of spherical droplets. The dispersed phase of these emulsions consisted of a supersaturated solution of ammonium nitrate. The oil phase consisted of surfactants dissolved in hydrocarbon oil.

The first section of this chapter lists complete details of the materials used, including the type of surfactants, hydrocarbon oil and the composition of the dispersed phase. A full description of the instruments used to make emulsions, analyse microscopically, and measure the size distribution and rheology of the emulsions is given.

5.2. Materials

5.2.1. Dispersed Phase

The dispersed phase of the emulsion samples used in this study consisted of a solution of inorganic salt of ammonium nitrate. The water content of the dispersed phase was less than 20% by mass. In order to stabilise the pH of the emulsion, the dispersed phase contained acetic acid and sodium acetate as buffer. These additives that work as a buffer system comprised less than 0.5wt.% of the formulation.

The equilibrium temperature for dissolving 80 wt.% ammonium nitrate (abbreviated as AN) concentration is approximately 65°C and such a solution has a "Fudge Point" or crystallisation point of approximately 58°C. For the preparation of highly concentrated emulsions, super-cooled solutions are prepared by dissolving the granulated AN in the distilled water at temperature 80°C, and are emulsified in the surfactant containing the oil phase before cooling it down to room temperature. As experiments were performed at room temperature, it meant that an aqueous phase was a super-cooled (super-saturated) solution. These solutions are thermodynamically unstable but kinetically, in the emulsion form, do not change for several weeks, which provides the possibility of performing the complex rheological measurements. The internal phase eventually begins to crystallise, as described earlier (Masalova & Malkin, 2007c).

5.2.2. Surfactants

The surfactants used to stabilise the emulsion samples for this work were manufactured and provided by Lake International Technologies, South Africa. Three of surfactants, PIBSA-MEA, PIBSA-Imide and PIBSA-Urea, are based on organic derivatives of poly(isobutylene) succinic anhydride (PIBSA).

Different surfactants were used: PIBSA-MEA, PIBSA-Imide, PIBSA-Urea, and sorbitan monooleate (SMO or Span®80), which is a conventional water-in-oil surfactant. The hydrophobic moiety for the three PIBSA derivatives (PIBSA-MEA, PIBSA-IMIDE and PIBSA-UREA) is the polyisobutylene chain, with an approximate relative molecular weight of 1050. The hydrophilic moiety is the modified succinic anhydride group, with an approximate relative molecular weight of 150. Thus the hydrophilic-lipophilic balance (HLB) leaned heavily towards lipophilicity (i.e. hydrophobicity) at less than 4, and the surfactants were soluble in hydrocarbon oils, but insoluble in water. It can be estimated from the structure presented in Figure 5.1 and eq. (2-1) that, the HLB of PIBSA-MEA is slightly lower than -Urea and somewhat higher than –Imide, however the differences are too low to affect the emulsification process. For the SMO, the hydrophobic moiety is an oleic group, with an approximate relative molecular weight of 280, while the hydrophilic moiety is the sorbitan group with a relative molecular weight of 160. Therefore the balance is towards lipophilicity with the HLB about 4.3. Some characteristics of employed surfactants are summarised below.

PIBSA-MEA: It is the product of poly(isobutylene succinic) anhydride reaction with monoethanolamine in approximately 1:1 ratio to an uncondensed amide/acid head group (Figure 5.1). The *R* indicates a polyisobutylene chain, the repeat unit of which is $-(C\text{-}(CH_3)_2\text{-}CH_2)-$, with 17 repeat units in the chain and a molecular weight of 1048. The overall molecular weight is about 1109.

PIBSA-Imide: This was described as Pibsa-MEA condensed to an N-substituted pyrrolidinedione (succinimide) structure. The molecular weight is about 1091.

PIBSA-Urea: The structure of PIBSA-Urea is shown in Figure 5.1. It is the adduct of PIBSA and urea (Boer, 2003). The molecular weight of this surfactant is about 1047.

SMO: This low molecular weight surfactant is an ester formed between sorbitan and oleic acid (oleic acid is a C18 fatty acid with a single *cis* double bond, written as C18:1). Its molecular weight is 428, and its structure is shown in Figure 5.1.

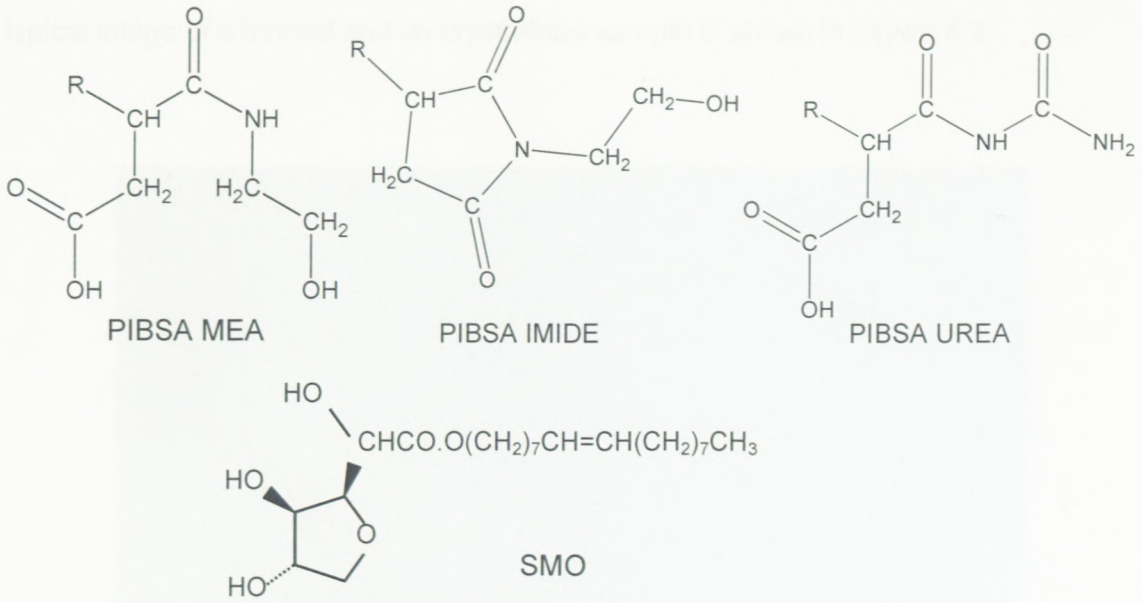

Figure 5.1: The chemical structure of employed surfactants

5.2.3. Hydrocarbon Oil

When originally synthesised, the surfactants were dissolved or dispersed in *Parprol 32*, a paraffinic petroleum oil with no additives. Further dilution with Mosspar-H hydrocarbon-based oil (Lake International, South Africa) was performed to achieve the desired concentration.

5.3. Instrumentation

5.3.1. Sample Preparation

The Hobart N50 mixer was used to manufacture all the samples under study. The mixer consists of an agitator unit and a bowl that was heated to 85°C. The emulsification process included the gentle pouring of pre-dissolved ammonium nitrate solution into the surfactant in the continuous phase solution contained in the bowl. The mixing performance of Hobart is facilitated by intensive shearing of the sample between the agitator and the bowl. The prepared emulsions were cooled to room temperature prior to doing any rheological or droplet size measurements.

5.3.2. Microscopy Observation

For qualitative analysis of the samples, it was checked to ensure that the emulsion was properly formed and the crystallisation of ammonium nitrate had not been started; if these criteria were not met, samples were excluded from the measurements. This

analysis was achieved by using a Leica optical microscope with 500x magnification. A typical image of a formed and un-crystallised sample is shown in Figure 5.2.

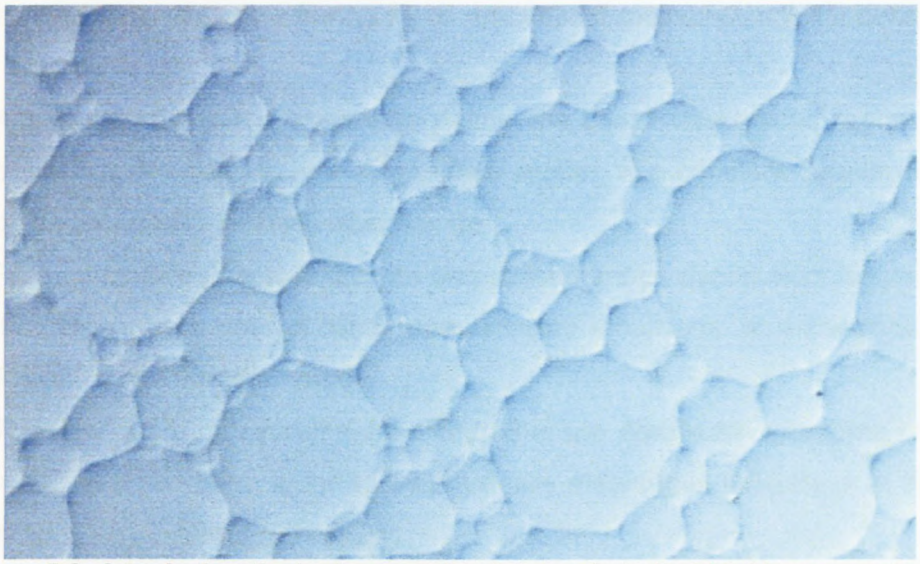

Figure 5.2: A typical optical microscopic picture of studied highly concentrated emulsions (with PIBSA-MEA surfactant and d_{32}=15μm)

5.3.3. Droplet Size Analysis

The droplet size distribution was measured using the Malvern Mastersizer 2000 instrument. The procedure is based on sample dispersion under software control and the measurement of angle dependence of the intensity of scattering of a collimated He-Ne laser beam. The angle at which the light is scattered is inversely proportional to the size of the particles. Particle size in the range from 0.5 to 2000 μm can be measured, which is much wider than the droplet size distribution of the real samples used in this work. The particle size distribution calculations were based on the rigorous Mie theory and the use of the standard software applied to the instrument. The samples were diluted in the same oil as the continuous phase, just before the measurements were taken. All measurements were performed at 20°C.

5.3.4. Rheological Measurements

Rheometry was conducted using the MCR 300 Paar Physica rheometer. The MCR 300 rheometer is a research grade, rotational drag flow instrument designed according to Searle's measuring principle, and is equipped with a permanent magnet synchronous drive that allows both stress-controlled and strain-controlled rheological tests to be done by means of the same instrument. The rheological measurements were performed by using "plate-and-plate" geometry with a plate diameter of 50mm and

sandblasted surface to eliminate any possibility of slip (Masalova et al., 2006a). The measuring gap between the two plates was 1mm. All rheological measurements except the temperature sweep measurement were conducted at 30°C.

The following points describe the types of rheological measurement conducted in this work:

- Amplitude sweep experiment to define the linear viscoelastic region and the behaviour of emulsion in the non-linear region, at a constant angular frequency of 10rad/s and 0.1~200% strain range.
- Frequency sweep test in the pre-determined linear viscoelastic region to study the gel-like behaviour of highly concentrated emulsions, at a constant strain of 1% and 0.1~100rad/s range.
- The flow curve measurement performed in the downward sweeping shear rate mode as it has been found to be physically meaningful (Masalova et al., 2005), in 10^{2}~10^{-5} s^{-1} shear rate range.
- Temperature sweep test in the range of 20~100°C at 1% strain and 1rad/s which was found to be the in the plateau region of storage modulus in the frequency sweep and amplitude sweep experiments.

5.3.5. Interfacial Tension

The Kruss K100 tensiometer was used to measure the interfacial tension, CMC and surfactant concentration at interface. Static measurements with the Wilhelmy plate were used to determine the characteristics of the interfacial area between the oil (Mosspar-H) and the dispersed phase (ammonium nitrate solution).

A vertical thin plate is used in the Wilhelmy plate technique. Plates are often constructed of materials that give a contact angle close to zero, such as roughened platinum or platinum/iridium, as this facilitates the analysis ($\cos\theta = 1$). The force acting vertically on the plate by the liquid meniscus is measured by using a microbalance and converted to the surface or interfacial tension data.

5.4. Matrix of Samples

The proper method of measuring the yield stress, and the correlation between yield stresses measured from flow curve and strain sweep experiments, were examined firstly. In this case, two typical explosive emulsions, two kaolin suspensions of kaolin-in-water and mayonnaise as an oil-in-water emulsion were used.

In the second part, five different concentrations of the dispersed phase were employed in the formulation: 85, 88, 90, 92 and 93.5wt.%. These weight fractions correspond to following volume fractions of the dispersed phase in emulsion: 0.764, 0.807, 0.837, 0.868, and 0.892. In this set of samples, surfactant concentration was kept as 14wt.% and a range of droplet sizes was studied: 7.5~16μm. The frequency sweep, strain sweep, flow curve and temperature sweep measurements were performed on these samples. This set of samples was studied to find semi-empirical relations for their rheological behaviour in different modes of deformations.

On the basis of the theoretical model presented in Chapter 4, the final part of the investigation discussed in this chapter was devoted to the preparation of emulsions with 92wt.% dispersed phase concentration (corresponding to 0.868 volume fraction) with two different surfactant concentrations, namely 8wt.% and 14wt.% in order to investigate an explanation for the unusual elasticity of explosive emulsions. The shear modulus (taken as frequency and strain-independent storage modulus – see section 3.5.2) of these emulsions was studied as a function of droplet size.

5.5. Experimental errors

All measurements are subject to errors which may affect the final conclusion and must therefore be quantified. A primary goal is to identify the reliability of the measurements, and a secondary objective is to identify limitations in the physical property measurements. Experimental errors are grouped into three categories: gross, systematic and random errors.

Gross errors are errors due to blunders, equipment failure and power failures, and these present an immediate cause for the rejection of measurements. Systematic errors are due to improperly calibrated devices or a systematic effect on the measurement. With a systematic error, one can repeat the experiment many times and always get the same results. Systematic errors are often identified by independent calibration of measurements. Random errors are due to experimental instrumental imprecision and imperfectly performed experiments. Instrumental imprecision affects the precision of a measurement. Precision is sometimes called "repeatability" or "reproducibility", and is a measure of the variation between repeated measurements. In most cases, precision is improved by increasing the sample size (i.e. the number of repeated measurements). Often, under certain conditions, fluctuations due to this error obey the Gaussian distribution and this is referred to as statistical errors. Thus, averaging repeated measurements would often improve the precision of the

measurements. The precision of the measurement is indicated by the least significant figures reported as associated with the error of the measurement, e.g. 2.461±0.008Kg.

The statistics used to evaluate the accuracy, as well as the comparative performance, of various models make use of error equations. These errors equations, to name a few, include: mean relative squared error, the log square error, standard error, absolute error and relative error. For this study, only the mean relative squared error was used as a measure of accuracy, and for comparing the performance of the models. All the fittings that were performed in this work did not have any error worth more than 5%.

5.6. Summary

This chapter has presented the description of the substances that constituted the highly concentrated emulsion in which the dispersed phase concentration (consisting of supersaturated, supercooled droplets of ammonium nitrate solution) dispersed in an oil phase (consisting of a surfactant based on organic derivatives of PIBSA) dissolved in Mosspar-H hydrocarbon oil.

This was followed by the description of the instrumentation and the experimental procedure used to achieve the objectives of the research. It included the emulsification process enabled by the agitation process of a Hobart N50 mixer. Following this, two optical analyses were described. One was a qualitative microscopic analysis that was achieved by using a Leica optical microscope; the other determined the particle size distribution within the emulsion material and this was done through laser diffraction using a Malvern Mastersizer instrument. Finally, the rheological measurements, which were performed with the use of a rotational dynamic rheometer MCR 300 were described. These involved amplitude sweep, frequency sweep, flow curve and temperature sweep experiments.

Chapter 6 – Experimental Results and Discussion

6.1. Interfacial Properties

The interfacial characteristics of different employed surfactants were measured to study their effect on the rheological behaviour of highly concentrated emulsions. Firstly, the variation of the interfacial tension of ammonium nitrate solution and oil phase was measured as a function of surfactant concentration in oil phase (see Figure 6.1). The critical micelle concentration (CMC), the interfacial tension above CMC, and the concentration of surfactant at the interface obtained from the Gibbs equation are summarised in Table 6.1. The surfactant concentration at the interface was used to calculate the area occupied by a single surfactant molecule at the interface. The obtained CMC values show that the surfactant concentration is much higher than CMC in all prepared explosive emulsions, and therefore micelles are present in the continuous phase. This is in agreement with small angle neutron scattering (SANS) measurements of Reynolds et al. (2000, 2001), in which the existence of micelles in the continuous phase of explosive emulsions was established.

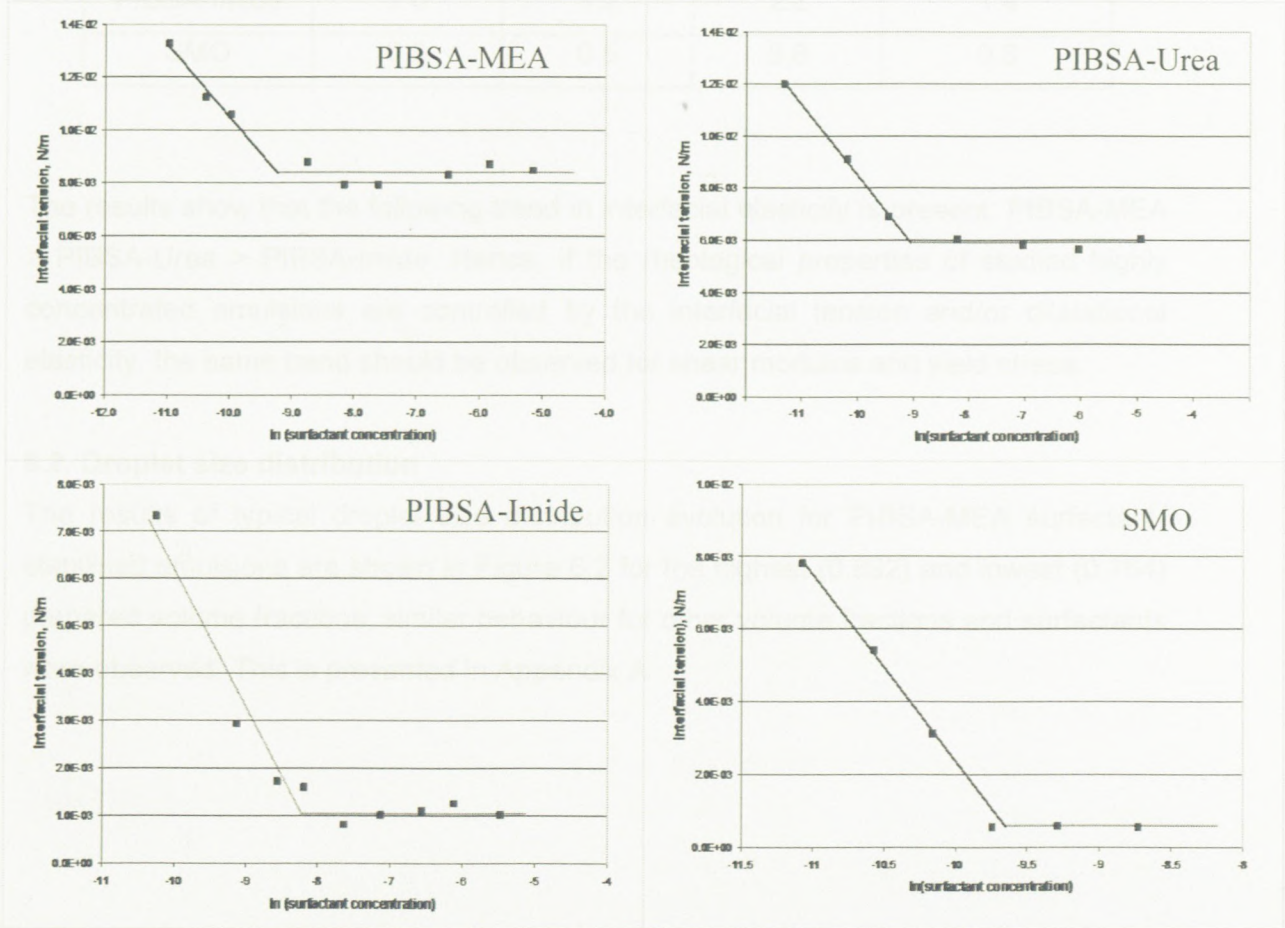

Figure 6.1: Determination of CMC of surfactants

Besides this, the interfacial dilatational elasticities in the presence of different surfactants measured by Sinterface are also presented in Table 6.1 (Costello, 2008). The interfacial dilatational elasticity (dynamic elasticity) shows the same trend as the interfacial tension (static elasticity), something that is not unexpected. While the employed PIBSA-based surfactants occupy almost the same area at the interface, they show significantly different interfacial tensions and dilatational elasticities. This suggests that surfactant concentration at the interface for PIBSA- based surfactants may be controlled by a polymeric tail (which is the same for employed PIBSA-based surfactants), while the interfacial elasticity may originate from the interaction of a dispersed phase and surfactant headgroup.

Table 6.1: Interfacial properties of different surfactants used in this work

Type of surfactant	σ (mN/m)	E' (mN/m) at 0.1Hz	CMC*10^4 (mole/lit)	Area per molecule (nm^2)
PIBSA-MEA	8.4	4.3	0.9	1.5
PIBSA-Urea	5.9	3.2	1.2	1.5
PIBSA-Imide	1.0	1.2	2.2	1.4
SMO	0.6	0.5	0.6	0.8

The results show that the following trend in interfacial elasticity is present: PIBSA-MEA > PIBSA-Urea > PIBSA-Imide. Hence, if the rheological properties of studied highly concentrated emulsions are controlled by the interfacial tension and/or dilatational elasticity, the same trend should be observed for shear modulus and yield stress.

6.2. Droplet size distribution

The results of typical droplet size distribution evolution for PIBSA-MEA surfactant-stabilised emulsions are shown in Figure 6.2 for the highest (0.892) and lowest (0.764) prepared volume fractions; similar behaviour for other volume fractions and surfactants were observed. This is presented in Appendix A.

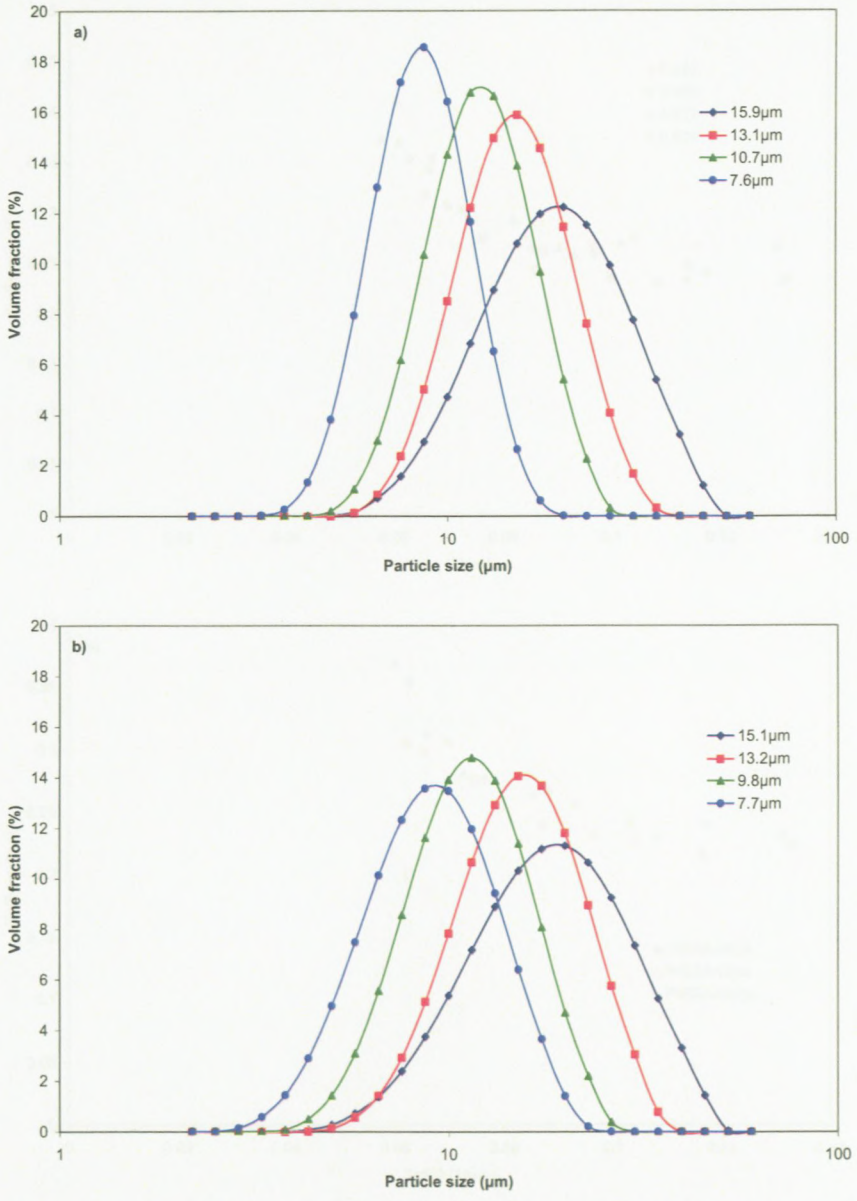

Figure 6.2: The variation of droplet size distribution for PIBSA-MEA stabilised explosive emulsions with (a) 0.892, and (b) 0.764, volume fractions

It is seen that the droplet size distribution becomes narrower by decreasing d_{32}, or increasing $1/d_{32}$. To have a quantitative feeling, the variation of uniformity, eq. (2-6), as a function of reciprocal droplet size, $1/d_{32}$, can be plotted as shown in Figure 6.3. It is seen that the uniformity reaches a plateau after a certain droplet size. Since the process variable to control droplet size is mixing time, it can be said that the uniformity reaches a plateau with increasing mixing time (corresponding to decreasing droplet size). Similar behaviour was observed for different volume fractions and different surfactant types, as presented in Figure 6.3a and Figure 6.3b, respectively.

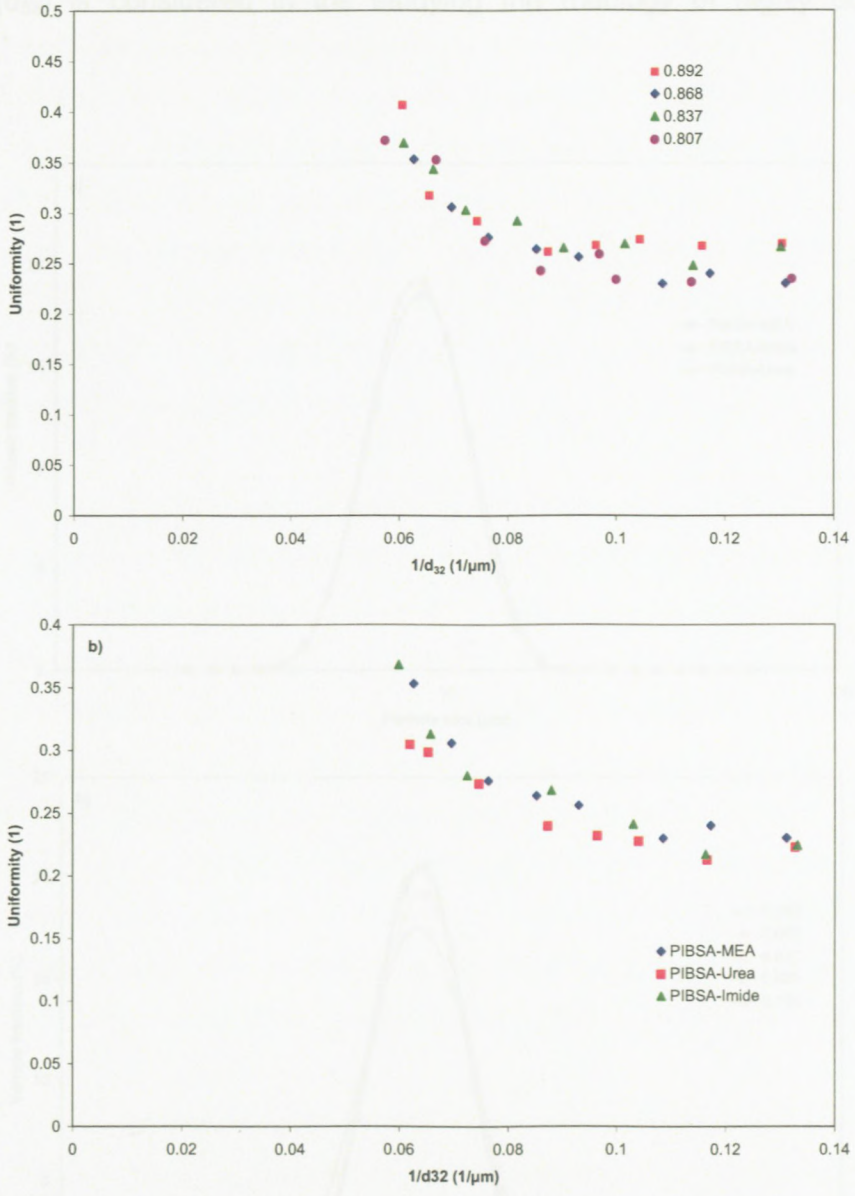

Figure 6.3: Variation of uniformity versus reciprocal droplet size for (a) PIBSA-MEA stabilised emulsions with different volume fractions, and (b) emulsions stabilised with different surfactant types but same φ=0.868

It can be shown qualitatively that the droplet size distribution for emulsions of the same droplet size (d_{32}=7.5±0.1μm) stabilised with different surfactant types (Figure 6.4a) and different volume fractions (Figure 6.4b) is very close. However, some deviation is observed for the lowest volume fraction where we are close to the closest packing of spherical droplets. The results shown in Figures 6.3 and 6.4 suggest that the effect of droplet size distribution on the rheological behaviour of studied emulsions can be ignored;* this effect is somehow excluded, however, when the area-volume mean

* At least in a range of droplet sizes and volume fractions

diameter (d_{32}) is considered in the studying the rheology of highly concentrated emulsions.*

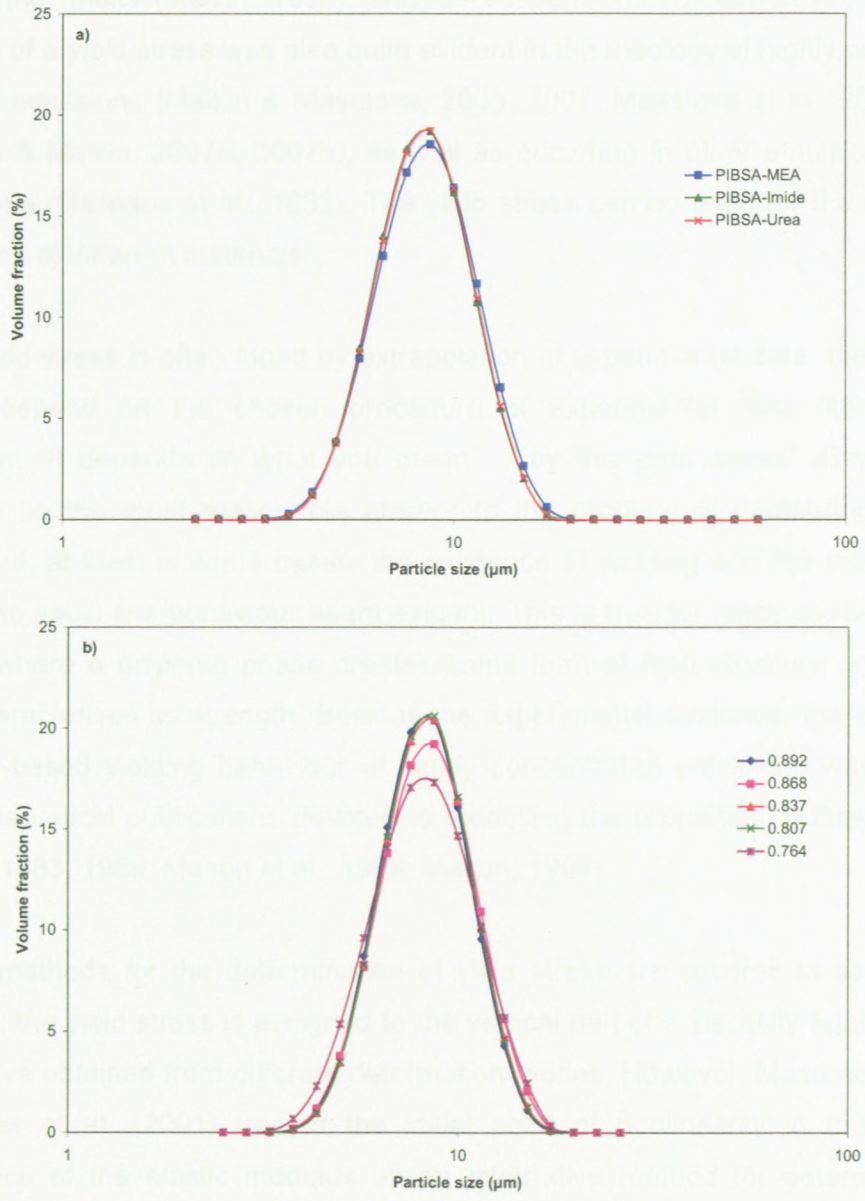

Figure 6.4: Droplet size distribution of explosive emulsions stabilised (a) with different surfactant types but same φ=0.868; and (b) with different volume fractions but same surfactant PIBSA-Urea

6.3. How to estimate yield stress

The phenomenon of yield stress was proposed as the first milestone of rheology (Bingham, 1922) and continues to form the focus of numerous authors. The concept of

* This is because the rheological behaviour of highly concentrated emulsions is controlled by the interfacial area (total area and flattened area) of droplets.

yielding at low stresses is commonly accepted for many materials, for example: various different types of suspension (Abduraghimova et al., 1955; Bird et al., 1983; Heymann et al., 2002; Moan et al., 2003); consistent greases (Vinogradow & Pawlow, 1961); filled polymer melts (Malkin, 1990); and ice suspensions (Stokes et al., 2005). The existence of a yield stress was also quite evident in the rheology of highly concentrated explosive emulsions (Malkin & Masalova, 2005; 2007; Masalova et al., 2005; 2006a; Masalova & Malkin, 2007a; 2007b), as well as occurring in other emulsions such as mayonnaise (Gallegos et al., 1992). The yield stress can be used for the quantitative comparison of different materials.

As the yield stress is often found by extrapolation of experimental data, the result may strongly depend on the chosen procedure of experimental data fitting. So the conclusion: "It depends on what you mean ... by the yield stress" (Barnes, 2007) seems to be the most reasonable answer to the problem of measuring "the yield stress". But, at least in some cases, the existence of yielding and the transition from solid-like to liquid-like behaviour seem evident. This is true for many multi-component systems where a disperse phase creates some form of rigid structure and the yield stress characterises its strength. Besides the experimental evidence, the existence of physically-based yielding behaviour of highly concentrated emulsions was proven in several theoretical publications devoted to modelling the properties of these materials (Princen, 1983; 1989; Mason et al., 1996; Mason, 1999).

Different methods for the determination of yield stress are covered in section 2.6.5. Generally, the yield stress is assigned to the vertical part of a viscosity against a shear stress curve obtained from different deformation modes. However, Mason et al. (1996) and Babak et al. (2001) treated the initial point of nonlinearity in the amplitude dependence of the elastic modulus as an alternative method for determining yield stress.

The goal of this section is to compare the results of two different methods of estimating the yield stress – in steady shearing and in periodic oscillation. Though the main subject of our work is highly concentrated emulsions, the problem was studied using a wider range of materials: kaolin at two concentrations in water as a typical suspension, and mayonnaise as a typical oil-in-water emulsion different from liquid explosives. This was done to make the conclusions of comparison of the two methods under discussion more reliable.

In this study, two typical examples of explosive emulsions were used. These samples, designated as D-13 and D-14, were similar in their chemical composition. They contained 6wt% oil as the continuous phase. The average droplet sizes were 13 and 14μm, respectively. The yielding behaviour of these systems is dependent on the structure formed by surface inter-droplet layers of surfactant and, possibly, on the direct contact of droplets. The latter supposition is based on the observation that the inner structure of droplets (which changes as the ammonium nitrate crystallises) directly influences the yield stress (Masalova et al., 2006a). The mechanisms which control the rheology of explosive emulsions are discussed more specifically in the following sections.

The characteristics of the kaolin powder used for experiments are listed in Table 6.2. Two water dispersions with different concentrations of kaolin - 10 and 14 % (designated below as Kaolin-10 and Kaolin-14, respectively) were prepared by a 30-minute agitation of the water and kaolin mixtures. The yielding behaviour of these suspensions is dependent on the mechanical contacts of solid particles creating a structure with its own strength.

Table 6.2: kaolin characteristics

Mineralogical composition	Kaolinite (race mica & quartz)
Abrasiveness	25g/m^2
Particle size distribution	< 20μm, 98% < 10μm, 90% < 2μm, 48%
Mean particle size	2.1μm
BET surface area	18.73m^2/g
pH value	4.0~5.0
Specific gravity	2.60
Mohs hardness	2.0~2.5

The mayonnaise sample that was used is manufactured by Kraft Foods South Africa Ltd., and marketed under the trade name "REAL". The ingredients are listed as: 52% sunflower oil, water, modified starch, vinegar, pasteurized egg, sugar, salt, preservatives, lemon juice, thickener, garlic and onion powder and spices. The yielding behaviour of this emulsion is assumed to result from the formation of a network structure by lipoproteins (Gallegos et al., 1992).

In discussing the rheological properties of multi-component systems (suspensions and emulsions), it is necessary to pay special attention to the wall slip phenomenon and to exclude this effect before discussing the true bulk properties of a material and the yield stress in particular. Slip occurs in the flow of multi-phase systems because of the displacement of the disperse phase away from solid boundaries. This arises from steric, hydrodynamic, viscoelastic and chemical forces and the constraints acting on the disperse phase immediately adjacent to the walls. The slip effect was reported to exist in suspension and emulsion systems by Barnes (1995), and specifically in kaolin suspensions (Meeten, 2004; Meeker et al., 2004) and mayonnaise (Franco et al., 1998; Plucinski et al., 1998). Before discussing the experimental results related to the bulk flow properties of the materials under study, including the problem of the correct determination of the yield stress, it is necessary to eliminate the possible influence of the wall slip phenomenon.

The slip phenomenon was specially studied for explosive emulsions (Masalova et al., 2005; 2006a; Masalova & Malkin, 2007a) using two types of experiments: flow through tubes (including industrial pipe-lines) of different diameter, and rotational flow using devices with different gaps between stationary smooth, and rotating sandblasted surfaces. In all cases, no influence of wall slip on the results of rheological measurements and output calculations for a pipeline was established. The results therefore were invariant with respect to the wall/volume ratio. It means that we can neglect this possible phenomenon and treat the results of rheological measurements for these systems as the true bulk properties of the materials.

For kaolin suspensions, two types of experiment were also carried out. The first one was the flow through tubes of different diameter. In an earlier publication (Masalova et al., 2006b), the pipe flow of the kaolin suspensions through tubes of 13, 28, and 80mm diameter was experimented, and the technological data were compared with predictions based on laboratory viscometric measurements of these suspensions carried out using a rotational rheometer with sandblasted surfaces. Those results showed no evidence for the existence of any slip effect. Furthermore, experiments with different gap sizes were performed in the present work to investigate the possibility of slip in the rheological results of Kaolin-10, Kaolin-14 and mayonnaise samples. This was carried out using the parallel-plate geometry with sandblasted surfaces in different measuring gaps. The results of measurements clearly show (Figure 6.5) that the experimental technique used allows us to assume that the slip can be neglected.

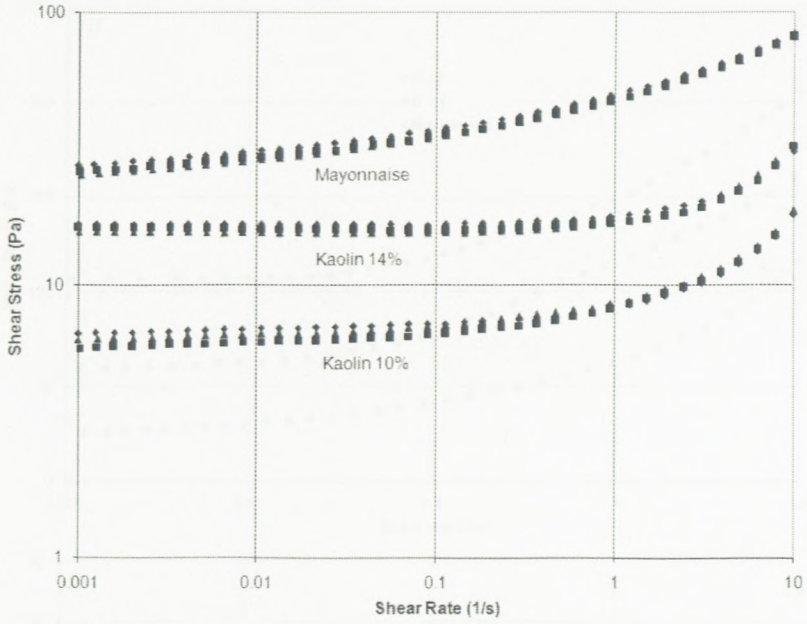

Figure 6.5: The flow curve of Kaolin-10, Kaolin-14 and the mayonnaise sample obtained by parallel-plate geometry with different gaps: (◊) 0.8mm, (□) 1mm, (Δ) 1.2mm

The lower parts (related to the low shear rate domain) of flow curves for the five materials under study are presented in Figure 6.6a-b. These data were obtained in the downward sweeping shear rate experiments, because it has been shown (Masalova et al., 2005; Masalova and Malkin, 2007b) that the real flow curve can be best obtained in this mode of deformations. It should be noted that two different time scales, 5s and 10s, were used for each experimental point of the flow curves for all samples. It is worth noting that the flow curves of all samples were independent of the shearing ramp chosen.

The data are presented on semi-log scales in order to demonstrate that the stress level really remains constant over a rather wide range of shear rates. The yield stress was obtained by fitting the Herschel-Bulkley model, eq. (2-54), to the low shear rate region of flow curve (Table 6.2), where the yield stress is denoted by τ_y^*. In all cases a good fit was achieved. Thus, the yield stress is a real physical characteristic of a material and the values will be used as the benchmark for comparison with other values of characteristic parameters obtained in different experiments. The error in the estimation of τ_y^* is not more than 10% and in most cases is less than 5%.

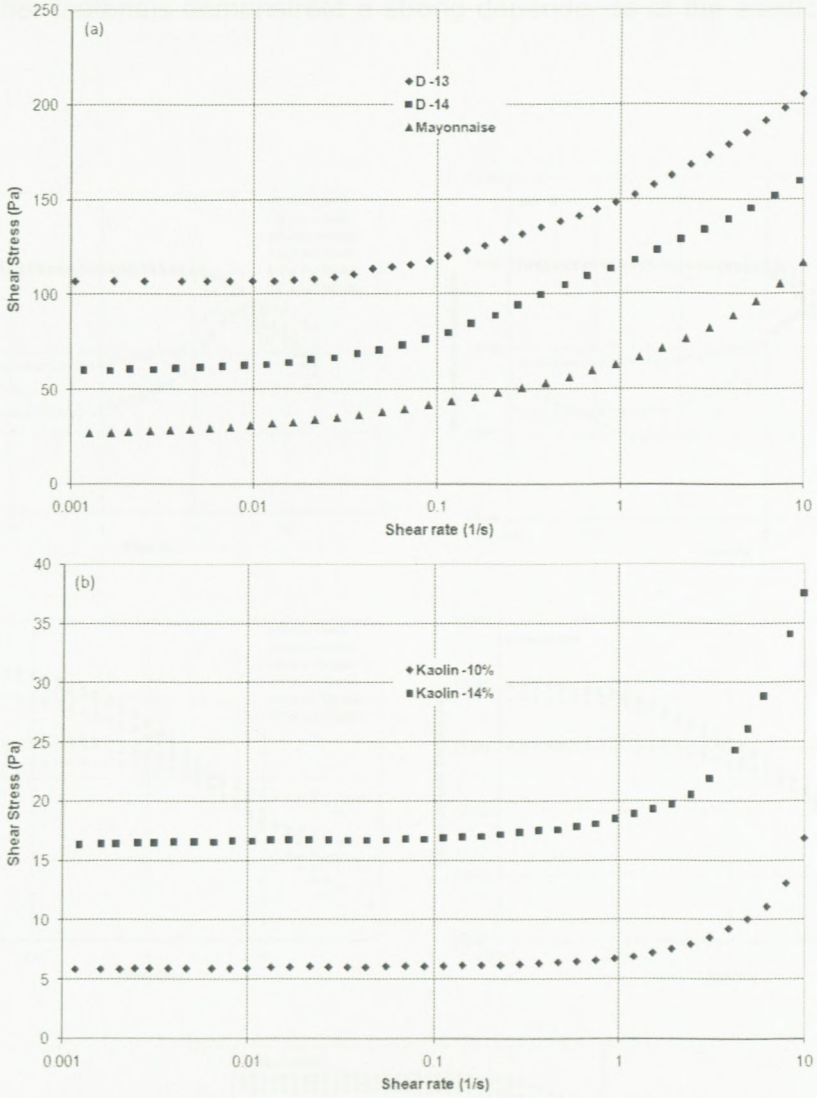

Figure 6.6: The flow curves of (a) three different emulsions (two explosives and a mayonnaise) and (b) two different suspensions.

Table 6.2: Values of Herschel-Bulkley model fitted on different samples

Sample	Fitting Range	τ_Y^*	K	n
D -13	0.001~0.02 s^{-1}	107.21	12158.65	2.66
D -14	0.001~0.02 s^{-1}	59.36	130.82	0.80
Mayonnaise	0.001~1 s^{-1}	21.56	42.87	0.32
Kaolin 10%	0.001~5 s^{-1}	6.02	0.81	1.01
Kaolin 14%	0.001~3 s^{-1}	16.51	2.08	0.74

The amplitude dependencies of the dynamic moduli were measured at three different frequencies 1, 10 and 100rad/s, and are presented in Figure 6.7a-e. One can clearly see the difference in the properties of highly concentrated emulsions, suspensions and a regular emulsion (mayonnaise). While highly concentrated emulsions resemble quasi-solid materials as shown by the absence of any frequency dependence on elastic

modulus, other materials demonstrate a strong dependence of the elastic modulus on frequency.

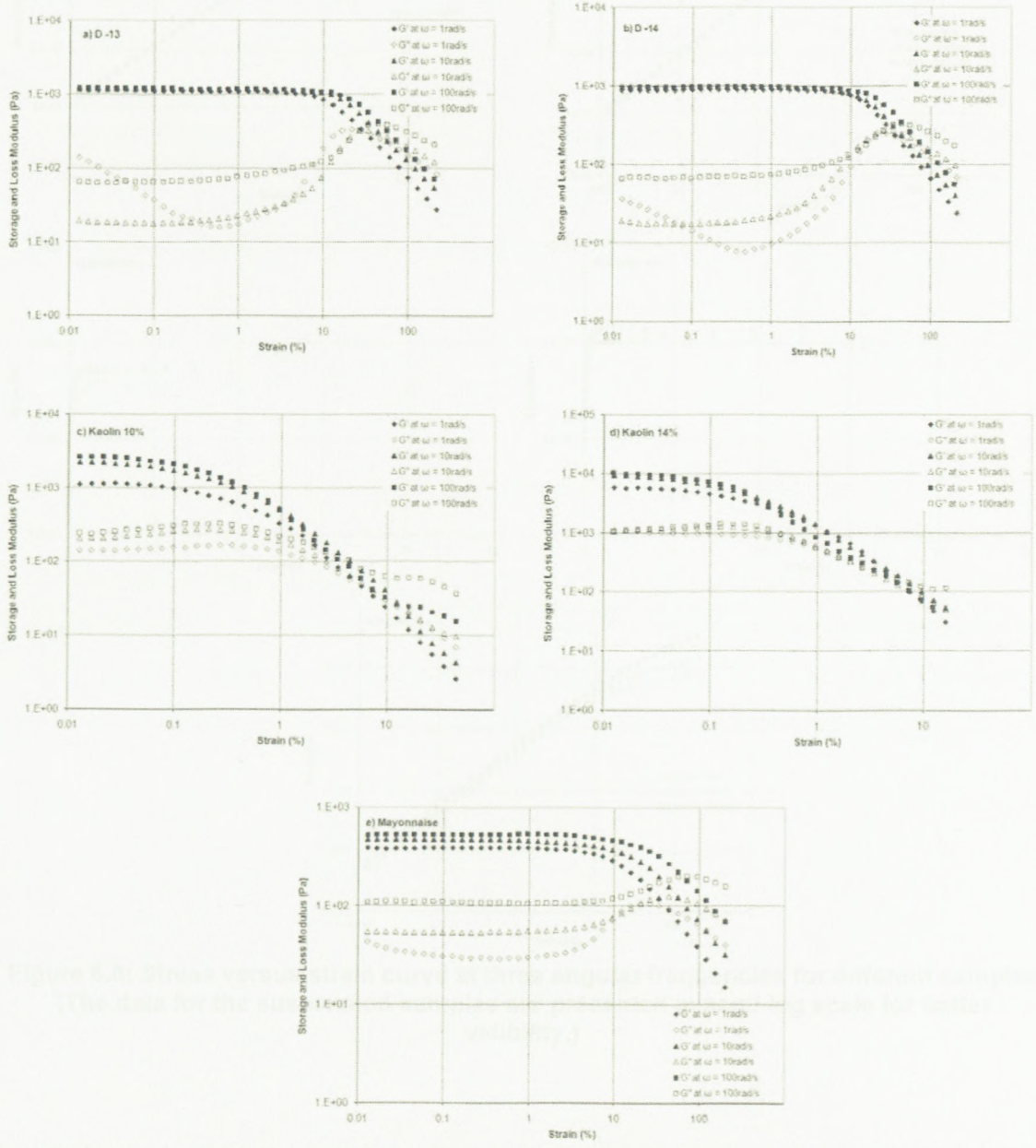

Figure 6.7: Results of amplitude sweep experiments at three angular frequencies for different samples

In accordance with the aim of this study, we will estimate the point of deviation of the mechanical properties in the samples under study from the linear regime of viscoelastic behaviour. Several examples of the amplitude of strain sweep are presented in Figure 6.8 for three types of materials: highly concentrated emulsions, suspensions and the regular emulsion.

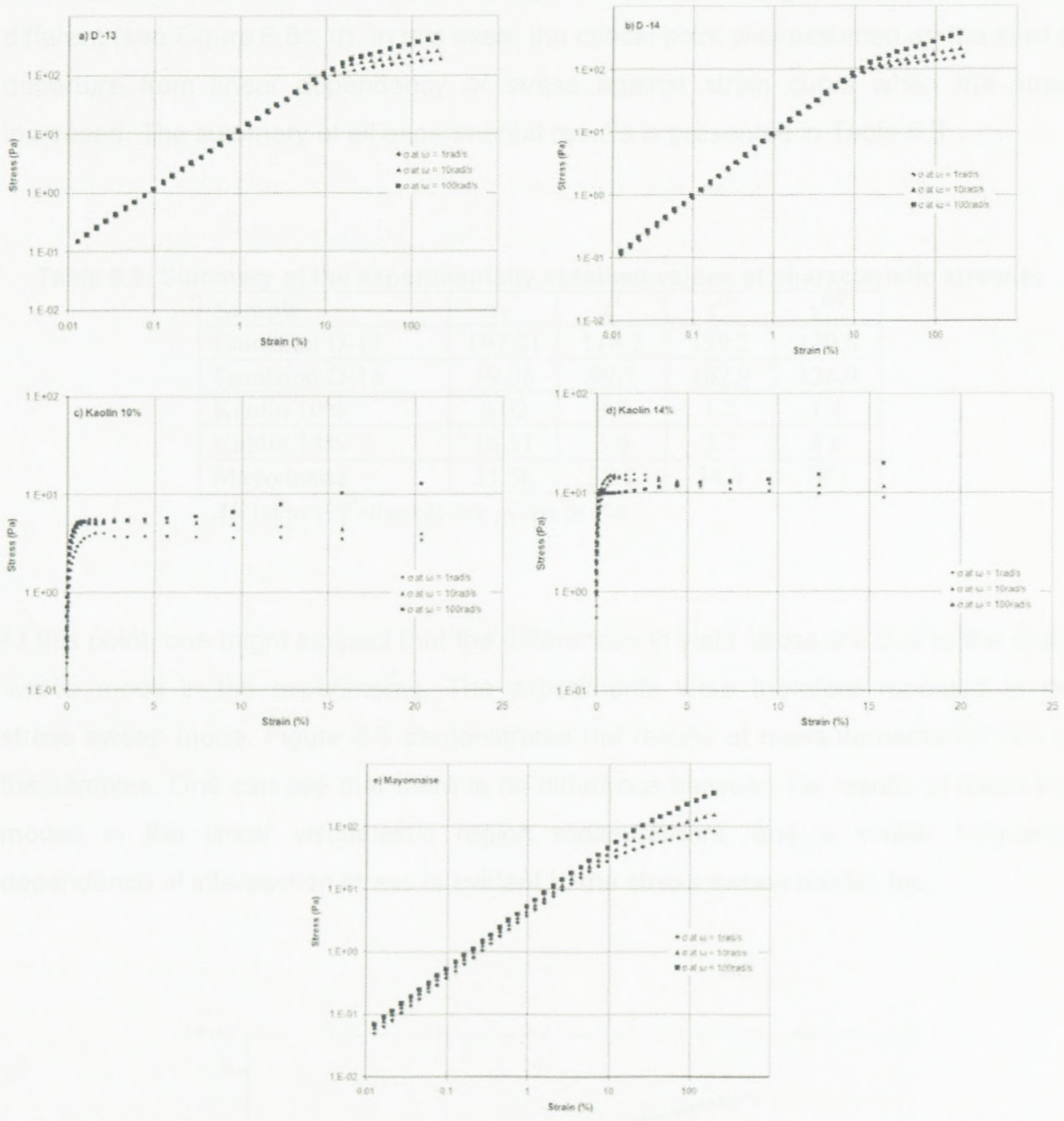

Figure 6.8: Stress versus strain curve at three angular frequencies for different samples (The data for the suspension samples are presented in semi-log scale for better visibility.)

It can be seen that the non-linearity is much more strongly expressed in the loss modulus than in storage modulus. This is quite typical for many materials. We have chosen the following procedure for estimating the "critical" point – the limit of linear behaviour – for highly concentrated emulsions. Following the method proposed by Mason et al. (1996), we plotted the stress amplitude against the strain amplitude and found the critical point from the intersection of straight lines, as shown in Figure 2.11. This method was used for several frequencies and the intersections were designated as τ^{1}, τ^{10}, and τ^{100}, with the superscript showing the frequency at which the intersection stress was measured. The same method was also used for mayonnaise. This method,

however, does not work for suspensions because their stress against strain curves look different (see Figure 6.8c, d). In this case, the critical point was assumed as the start of departure from linear dependency of stress against strain curve when the strain increased. The summary of all experimental results is presented in Table 6.3.

Table 6.3: Summary of the experimentally obtained values of characteristic stresses

Sample	τ_Y^*	τ^1	τ^{10}	τ^{100}
Emulsion D-13	107.21	118.2	139.2	170.8
Emulsion D-14	59.36	99.7	102.9	136.9
Kaolin 10%	6.02	0.8	1.2	1.4
Kaolin 14%	16.51	3.0	3.7	4.0
Mayonnaise	21.56	38.2	54.4	78.1

All values of stresses are given in Pa.

At this point, one might suspect that the differences in yield stress are due to the strain sweep mode in the experiments. The experiments were therefore repeated in the stress sweep mode. Figure 6.9 demonstrates the results of measurements for one of the samples. One can see that there is no difference between the results of these two modes in the linear viscoelastic region measurement, and a similar frequency dependence of intersection stress is evident in the stress sweep model, too.

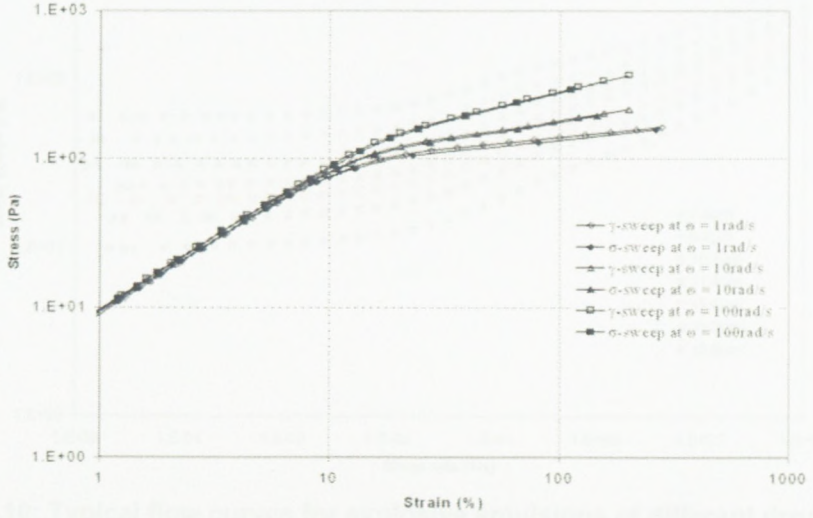

Figure 6.9: The stress versus strain curve of the D-14 sample at different angular frequencies and two different sweeping, stress and strain modes (lines are just for directing eye)

Two things now become rather clear. Firstly, the critical stress found in the oscillating tests (sometimes referred to as the "dynamic yield stress") is not constant but strongly depends on frequency. Secondly, the values of the critical stress found in the oscillating experiment do not coincide with real ("physical") yield stress estimated from flow curves. This means that the "dynamic yield stress" is in no event a physical parameter of a material, and cannot be used for comparison with any theoretical conclusion concerning rheological properties of visco-plastic materials. It is possible to try to extrapolate experimental data for "dynamic yield stress" to "zero" frequency. However, even by this approach, we did not reach a reasonable correlation between τ_Y* and the "zero-frequency dynamic yield stress".

6.4. Rheology of Explosive Emulsions

6.4.1. Flow Curve Results

The flow curves of explosive emulsions stabilised by PIBSA-MEA at a typical volume fraction (*φ=0.868*) and for different droplet sizes are shown in Figure 6.10. It is clear that the emulsions show a pronounced yield stress, but a hump in the flow curve at moderate shear rates ($\dot{\gamma} \approx 0.1 - 1s^{-1}$) is seen*.

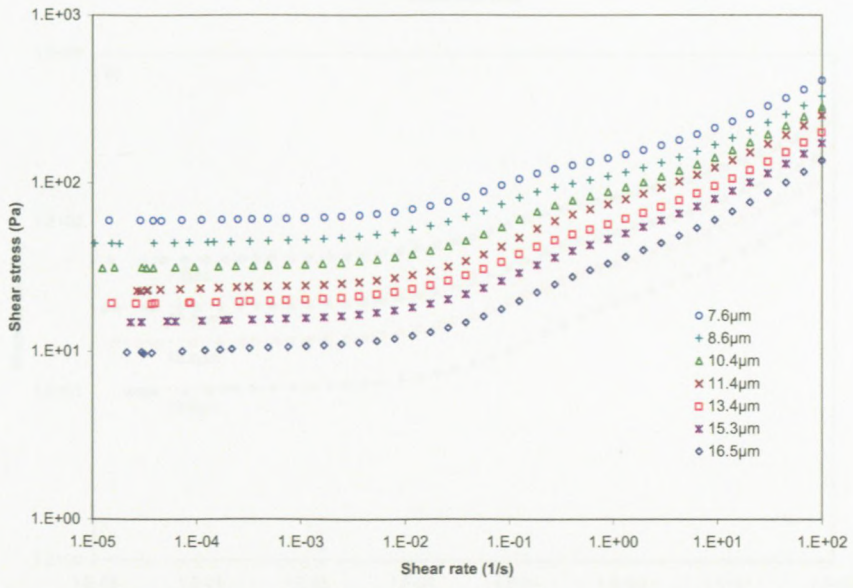

Figure 6.10: Typical flow curves for explosive emulsions of different droplet sizes (*φ=0.868*) stabilised with PIBSA-MEA

* Similar behaviour was observed for different volume fractions and surfactant types, as shown in Appendix B.

This behaviour can be explained by Windhab's model (1993) as a secondary yield stress. Malkin and Masalova (2007) found that, at shear rates above the hump, the droplets are deformed during flow, while the rolling of droplets over each other is the dominant mechanism of flow at shear rates below the hump. It was suggested that this transition is controlled by the Capillary number of systems under flow (Malkin & Masalova, 2007).

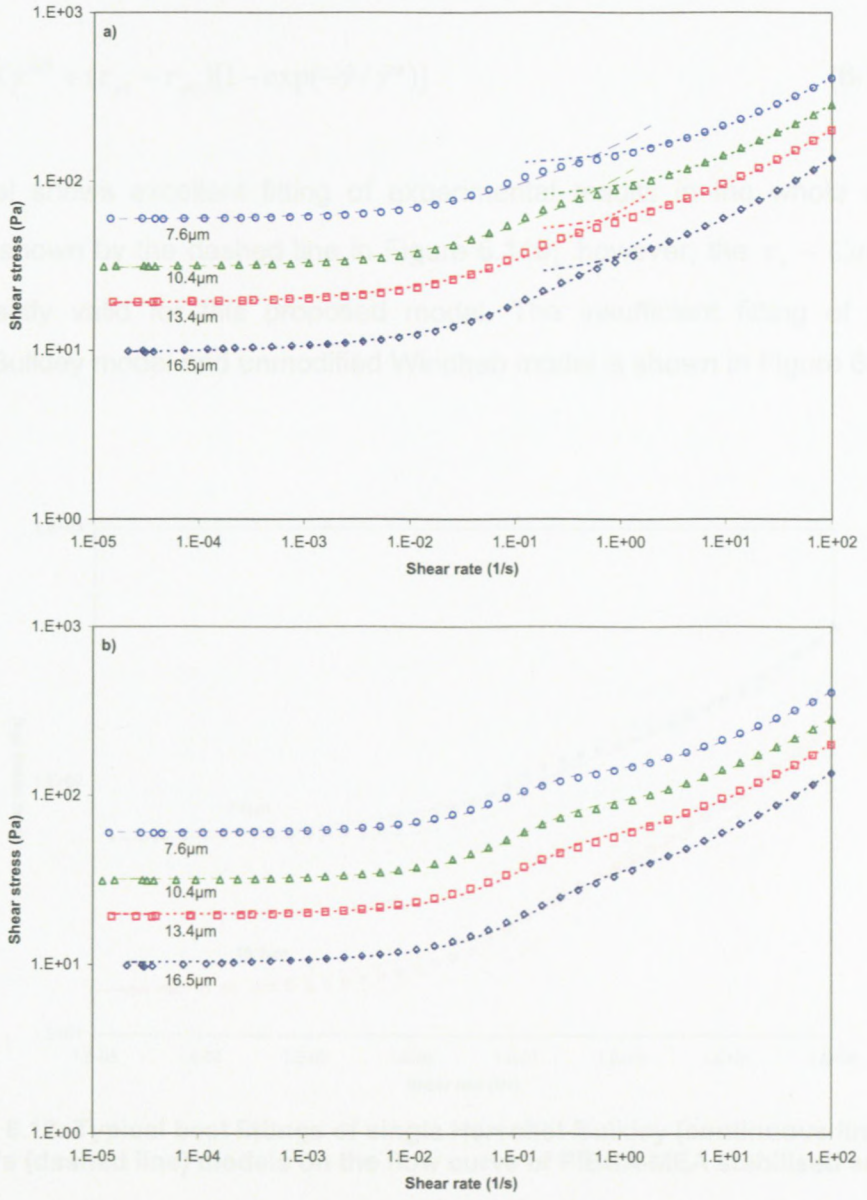

Figure 6.11: Typical fittings of, (a) Herschel-Bulkley model with two different sets of τ_y and *K* coefficients but the same *n=0.5* and, (b) the proposed model, eq. 6-1, on the flow curve of PIBSA-MEA stabilised emulsions

A useful method for modelling the flow curve is fitting Herschel-Bulkley model, eq. (2-54), with two different sets of coefficients below and above the hump (Malkin & Masalova, 2007). This fitting method was used for the flow curves of all explosive emulsions prepared by different PIBSA-based surfactants, various droplet sizes and volume fractions and it was found that, in both regions, *n=0.5* results in a good fitting of flow curves. This is shown by dashed lines in Figure 6.11a, and is in agreement with experimental relation $\tau_y \sim Ca^{1/2}$ suggested by Princen and Kiss (1989). Therefore in this work, it is suggested that Windhab's model should be modified as follows:

$$\tau = \tau_{y0} + K\dot{\gamma}^{0.5} + (\tau_{y1} - \tau_{y0})[1 - \exp(-\dot{\gamma}/\dot{\gamma}^*)] \qquad (6\text{-}1)$$

This model shows excellent fitting of experimental results in the whole shear rate range, as shown by the dashed line in Figure 6.11b;* however, the $\tau_y \sim Ca^{1/2}$ scaling is not exactly valid for this proposed model. The insufficient fitting of the single Herschel-Bulkley model and unmodified Windhab model is shown in Figure 6.12.

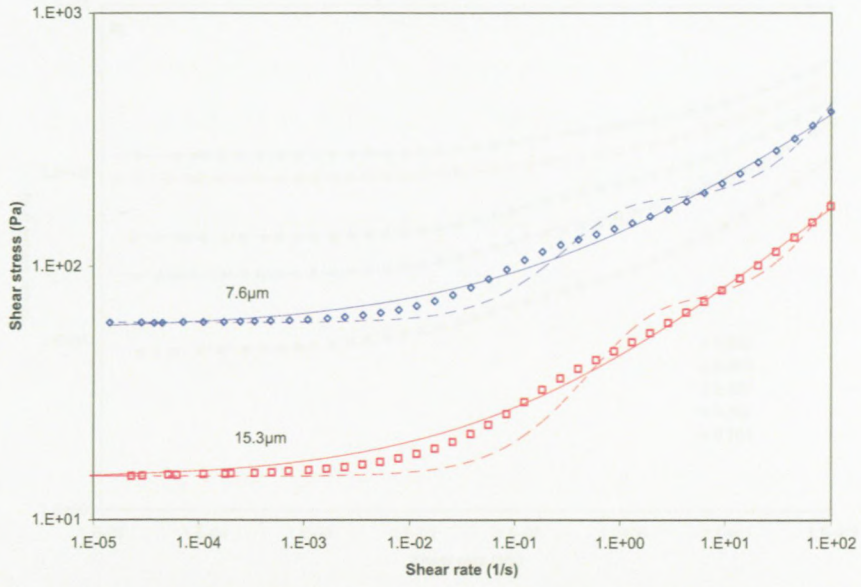

Figure 6.12: Typical best fittings of single Herschel-Bulkley (continuous line) and Windhab's (dashed line) models on the flow curve of PIBSA-MEA stabilised emulsions

* The results shown in Figure 6.11 are typical. Excellent fittings of eq. (6-1) were observed for all samples with different droplet sizes, volume fractions, and surfactant types (Figure 6.13).

It is clear that the Herschel-Bulkley model does not predict the hump at moderate shear rates, and Windhab's model also fails to fit the measured flow behaviour. The flow behaviour of explosive emulsions stabilised with PIBSA-Imide and -Urea surfactants was similar to the PIBSA-MEA stabilised emulsions, as shown in Figure 6.13.

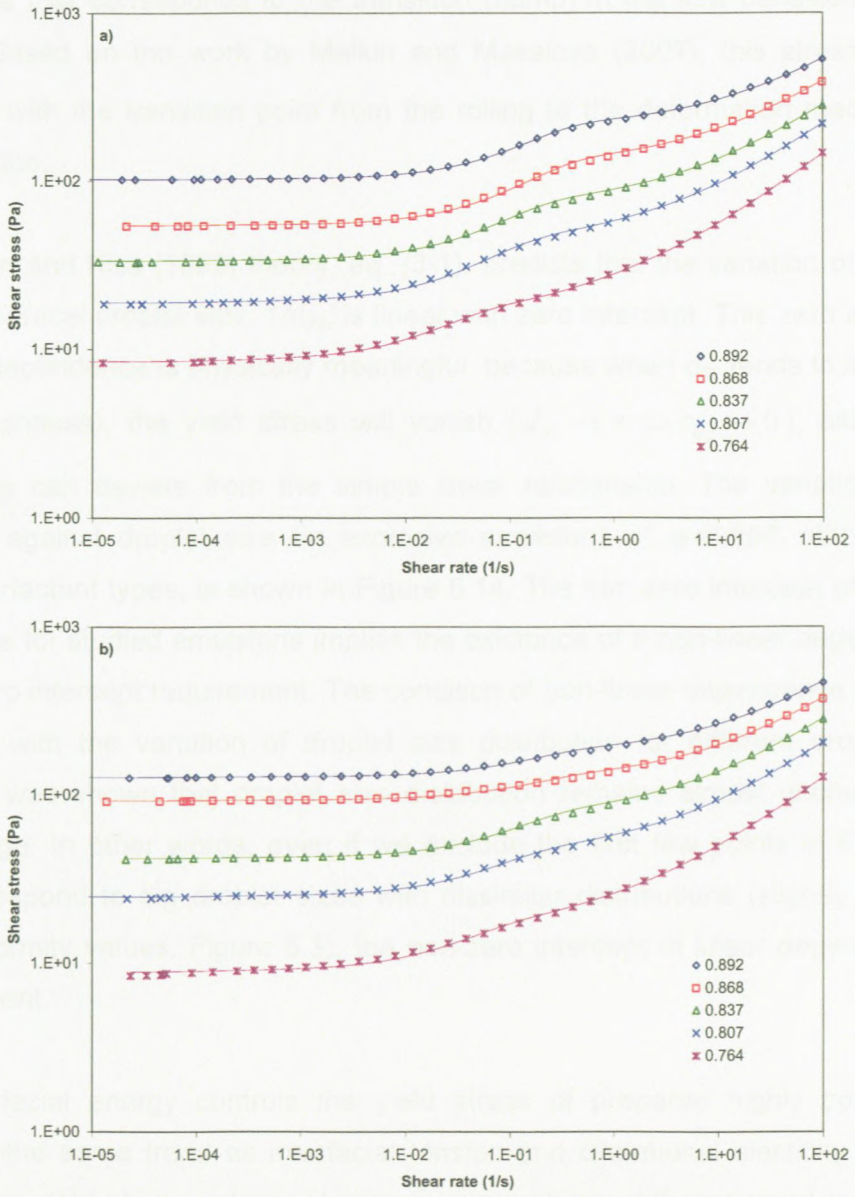

Figure 6.13: Typical flow curves of explosive emulsions of different volume fractions but similar droplet sizes (d_{32}=7.5±0.1μm) stabilised with (a) PIBSA-Urea, and (b) PIBSA-Imide

The viscosity of the surfactant-in-oil solution averaged over the range 6.49s^{-1} to 25.8s^{-1} for all surfactant type was found to be 6.1±0.1mPa.s. Therefore, the differences in flow behaviour of emulsion samples stabilised with different surfactant types can not be attributed to the viscosity of continuous phase, but may be attributed to the micellar

structure of surfactant in the thin film layer of oil phase between aqueous droplets and/or interdroplet interaction* of disperse phase.

It was shown in section 6.3 that the shear stress in simple shear flow below which the material does not flow (which corresponds to τ_{y0} in the proposed model) has some physical meaning and technological benefits. However, τ_{yl} is only an asymptotic yield stress value that corresponds to the transition (hump) in the flow behaviour at shear rate $\dot{\gamma}^*$. Based on the work by Malkin and Masalova (2007), this stress could be associated with the transition point from the rolling to the deformation mechanism of droplet motion.

The Princen and Kiss (1989) theory, eq. (3-1), predicts that the variation of τ_{y0} or τ_{y0}/σ against reciprocal droplet size, $1/d_{32}$, is linear with zero intercept. This zero intercept of τ_{y0} – $1/d_{32}$ dependence is physically meaningful, because when d_{32} tends to infinity (two separated phases), the yield stress will vanish ($d_{32} \to \infty \Rightarrow \tau_{0y} \to 0$), although this dependence can deviate from the simple linear relationship. The variation of yield stress, τ_{y0}, against droplet size for explosive emulsions of $\varphi=0.868$, stabilised with different surfactant types, is shown in Figure 6.14. The non-zero intercept of τ_{y0} – $1/d_{32}$ dependence for studied emulsions implies the existence of a non-linear dependence to fulfil the zero intercept requirement. The condition of non-linear dependence can not be associated with the variation of droplet size distribution for different droplet sizes, because it was shown that droplet size distribution remains almost unchanged in a certain range. In other words, even if we exclude the first few points in Figure 6.14 which correspond to big droplet sizes with dissimilar distributions (slightly broader – higher uniformity values, Figure 6.3), the non-zero intercept of linear dependence will be still present.

If the interfacial energy controls the yield stress of prepared highly concentrated emulsions, the same trend as interfacial tension and dilatational elasticity should be observed for yield stress values. However, a completely different trend is observed: PIBSA-Imide > PIBSA-Urea ≈ PIBSA-MEA. Moreover, the Princen and Kiss (1989) theory, eq. (3-1), predicts τ_{y0}/σ – $1/d_{32}$ linear dependence should be superimposed for

* As it will be discussed in section 6.5, the interdroplet interaction seems to be controlled with electrostatic repulsion enabled by reversed micelles. Thus, different surfactants form different micelles which could result in different interdroplet interaction.

different surfactant types, but depends on the volume fractions.* The non-superimposition of this dependence for different surfactants is shown in Figure 6.15.

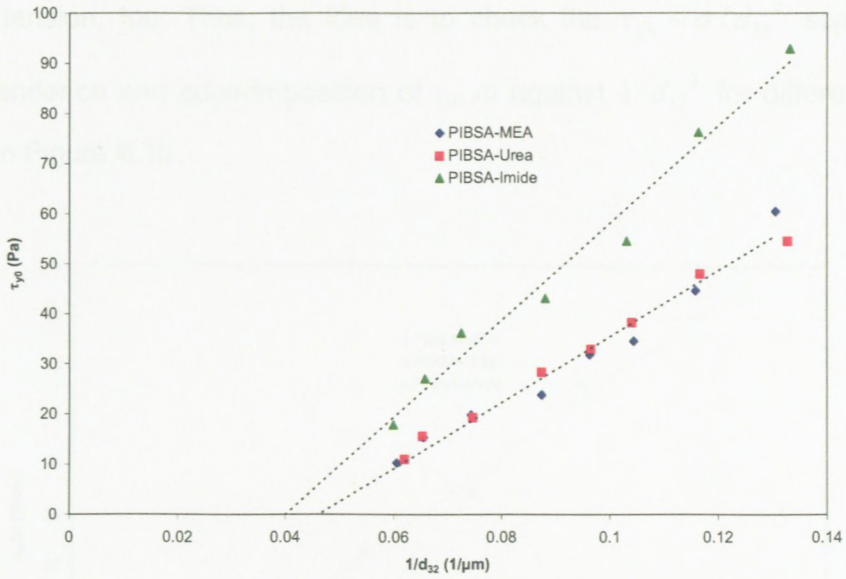

Figure 6.14: Variation of yield stress against reciprocal droplet size for explosive emulsions with different surfactant types (φ=0.868)

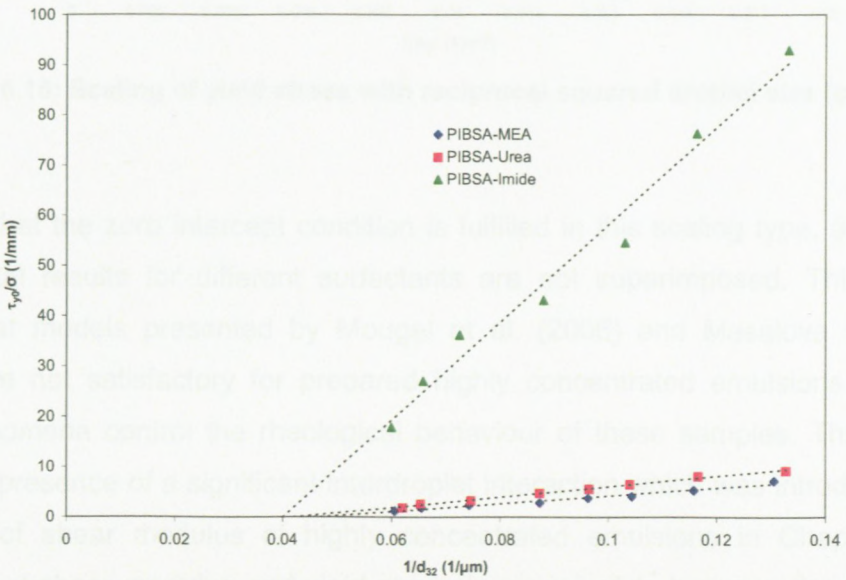

Figure 6.15: Variation of yield stress scaled with interfacial tension against reciprocal droplet size for explosive emulsions with different surfactant types (φ=0.868)

* The scaling of yield stress with Laplace pressure is also proposed in other works, e.g. Mason (1999).

The scaling of rheological properties with reciprocal squared droplet size has been suggested by Masalova and Malkin (2007a), due to the non-zero film thickness between droplets, and attributed to Van der Waals forces between droplets by Mougel et al. (2006). However, both of them predict the scaling of rheological properties with interfacial tension, too. Thus, the idea is to check the $\tau_{y0} \sim \sigma / d_{32}^{\ 2}$ scaling, or the linear dependence and superimposition of τ_{y0} / σ against $1/d_{32}^{\ 2}$ for different samples, as shown in Figure 6.16.

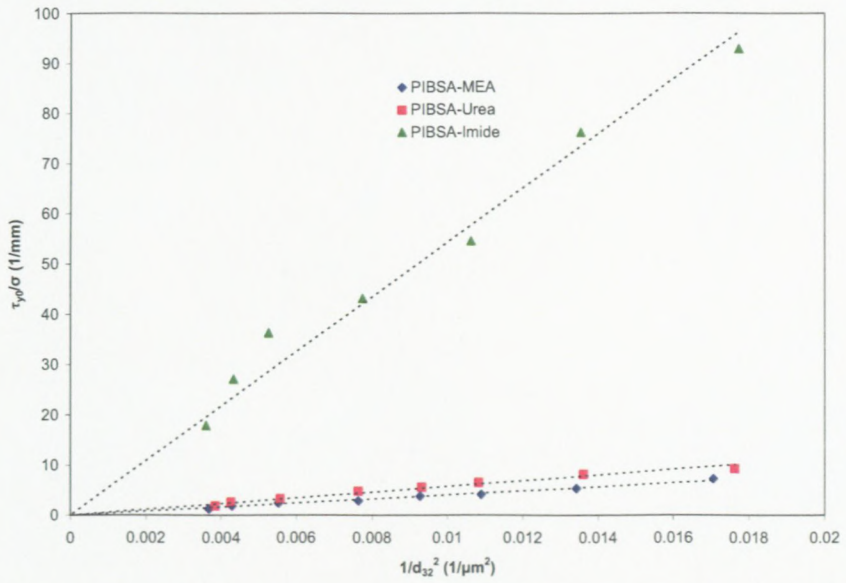

Figure 6.16: Scaling of yield stress with reciprocal squared droplet size (*φ=0.868*)

It is seen that the zero intercept condition is fulfilled in this scaling type, although the experimental results for different surfactants are not superimposed. This deviation reveals that models presented by Mougel et al. (2006) and Masalova and Malkin (2007a) are not satisfactory for prepared highly concentrated emulsions and some other phenomena control the rheological behaviour of these samples. This could be due to the presence of a significant interdroplet interaction which was introduced in the modelling of shear modulus of highly concentrated emulsions in Chapter 4. The correlation of shear modulus and yield stress is meaningful,* because the yield stress and shear modulus show similar trends. While shear modulus is obtained from the gel-like state and yield stress is acquired from the fluid-like state, both of them are controlled by droplet deformation and related to solid-like behaviour. The interfacial

* This correlation is present, see section 6.4.3.

dilatational elasticity cannot be the controlling mechanism of observed behaviour, because it has the same trend as interfacial tension.

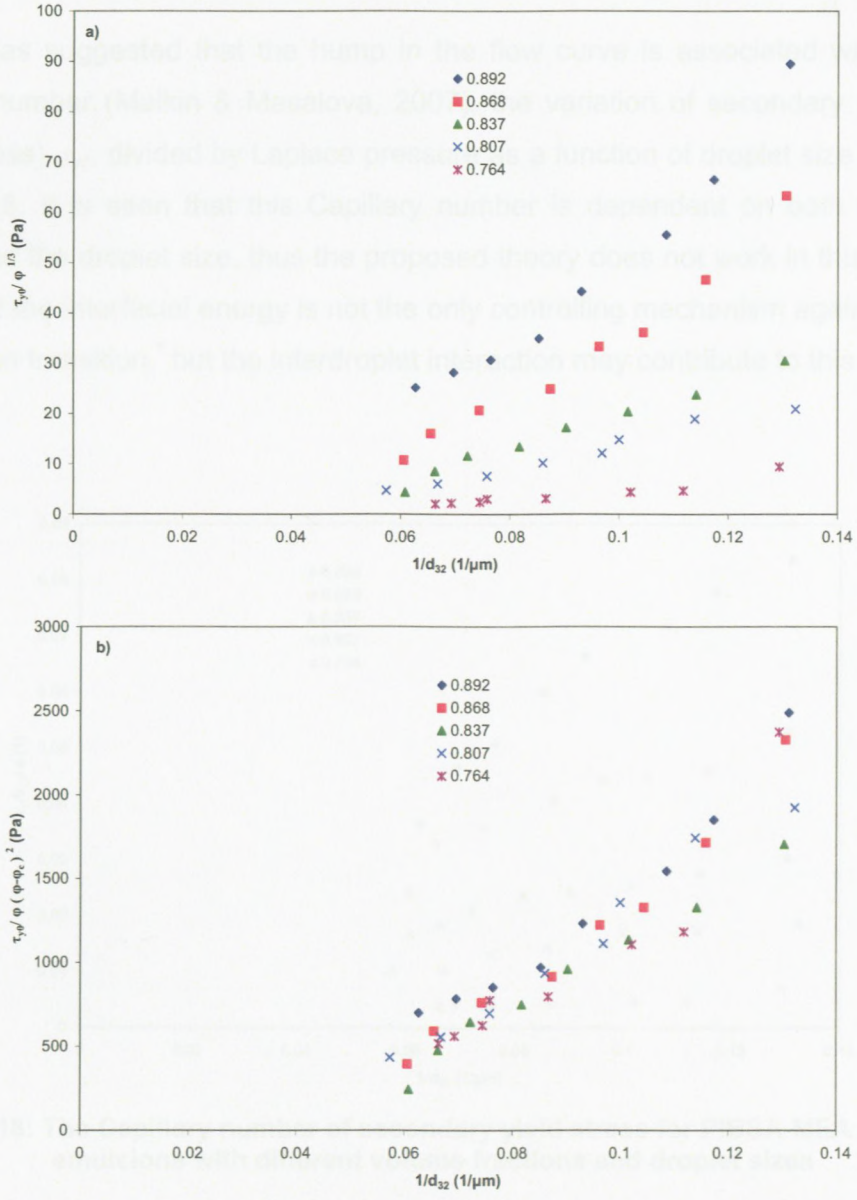

Figure 6.17: Scaling of yield stress with (a) $\varphi^{1/3}$, and (b) $\varphi(\varphi-\varphi_c)^2$

In Figure 6.17, the yield stress for different volume fractions is shown. The scaling of $\tau_y \sim \varphi^{1/3}$ resulting from the Princen and Kiss theory is studied in Figure 6.17a. It is seen that this scaling is not valid for prepared emulsions. The other scaling relationship, $\tau_y \sim \varphi(\varphi-\varphi_c)^2$, which was suggested by Mason (1999), is considered in Figure 6.17b. For big droplet sizes – where the contribution of interdroplet interaction is

less significant – a sufficient superimposition is observed with φ_c=*0.695*. In other words, when the interdroplet interaction becomes significant, deviation from this scaling behaviour is observed. This is reasonable, because Mason's scaling relationship was proposed for the case where the interfacial energy is the sole source of elasticity.

Since it was suggested that the hump in the flow curve is associated with a critical Capillary number (Malkin & Masalova, 2007), the variation of secondary yield stress (hump stress), τ_{y1}, divided by Laplace pressure as a function of droplet size is shown in Figure 6.18. It is seen that this Capillary number is dependent on both the volume fraction and the droplet size, thus the proposed theory does not work in this case. This shows that the interfacial energy is not the only controlling mechanism against rolling to deformation transition,* but the interdroplet interaction may contribute to this transition.

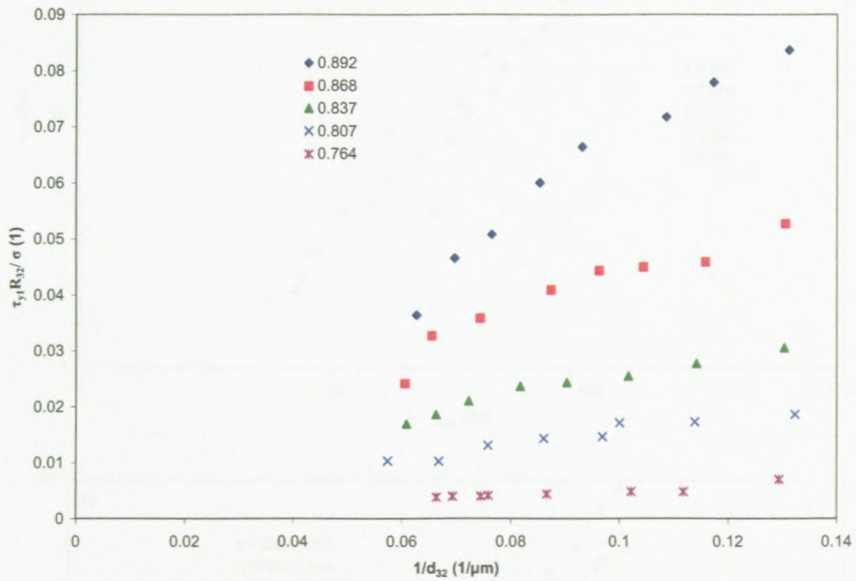

Figure 6.18: The Capillary number of secondary yield stress for PIBSA-MEA stabilised emulsions with different volume fractions and droplet sizes

6.4.2. Strain Sweep Results

The stress against strain results obtained from the amplitude sweep experiment is shown in Appendix C. The method suggested by Mason et al. (1996) was used to estimate the dynamic yield stress, $\tau_{y,d}$, at measurement frequency of ω=*10rad/s*. It has been mentioned that this yield stress is frequency dependent; however, the results are

* As discussed earlier, Malkin and Masalova (2007) suggested that the rolling-deformation transition takes place at secondary yield stress (hump).

presented for comparison with the yield stress values obtained from flow curves. The yield stresses of prepared emulsion obtained from the strain sweep experiment are always higher than those obtained from flow curve results, as can be seen in Figure 6.19. The difference between points with same marker in this figure is droplet size. Finding an experimental correlation between two differently obtained yield stresses is not successful, because it depends on the type of surfactant (Figure 6.19b). This result again confirms that the yield stress determined from the flow curve measurement – which is a threshold between creeping and flowing – is more realistic to be reported than the frequency-dependent yield stress obtained from oscillation measurement.

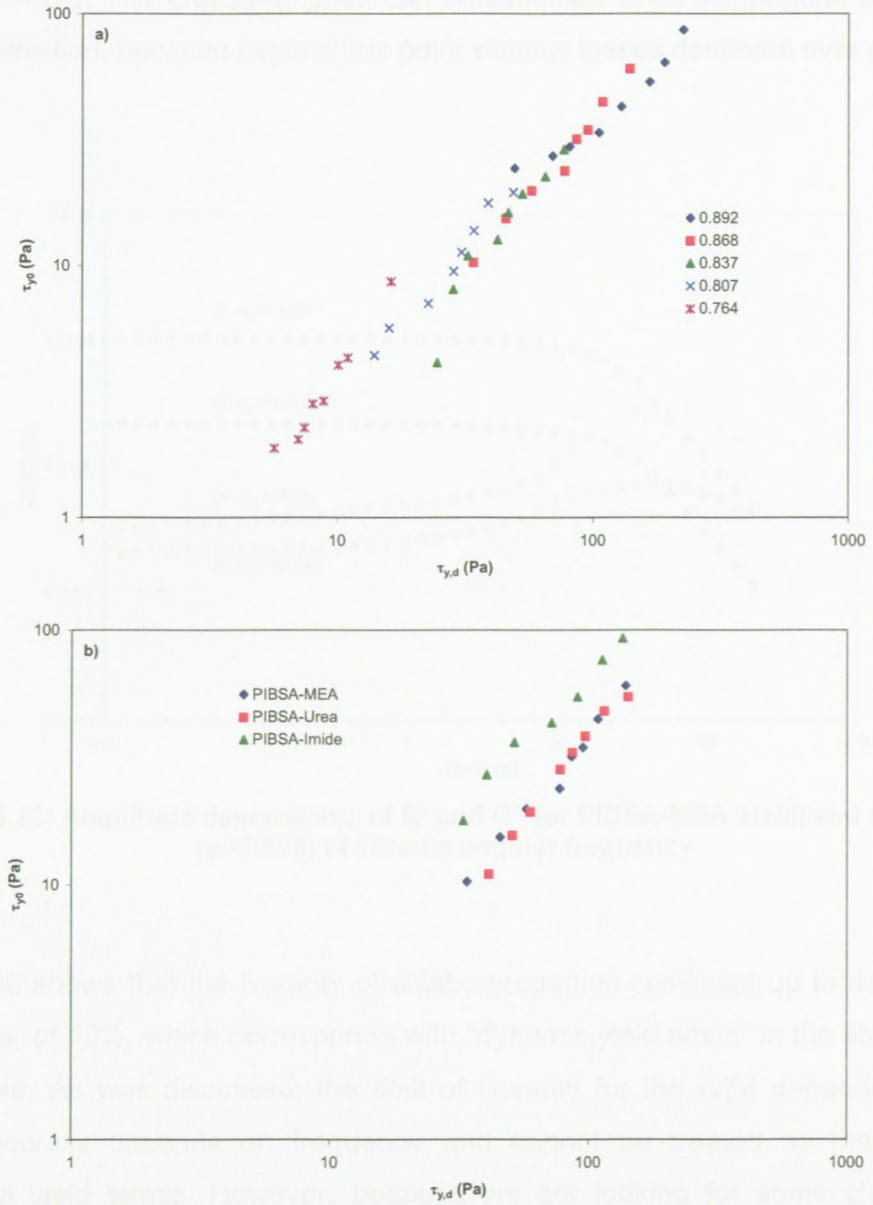

Figure 6.19: The variation of yield stresses obtained from flow curve against those obtained from strain sweep experiments of samples with different droplet sizes, for (a) PIBSA-MEA surfactant – different volume fraction, and (b) different surfactants – *φ=0.868*

The yield strain values approximated from strain sweep experiment is dependent on droplet size and volume fraction. While we showed that the yield point obtained from strain sweep experiments is frequency dependent and does not correlate with the one obtained from flow curve measurements, we will not concentrate on the variation of yield strain calculated by the Mason et al. (1996) method here.

The amplitude dependencies of the elastic (storage) modulus, G', and the loss modulus, G'', are typically shown in Figure 6.20 (see Appendix D for other emulsion samples). While the $G'(\gamma)$ dependence is a monotonous (decreasing) function, the $G''(\gamma)$ functions pass through a maximum, G''_{max}, which lies rather close to a crossover point (where $G' = G''$). This crossover point can be assumed to be the position of elastic-to-viscous transition, because beyond this point viscous losses dominate over elasticity.

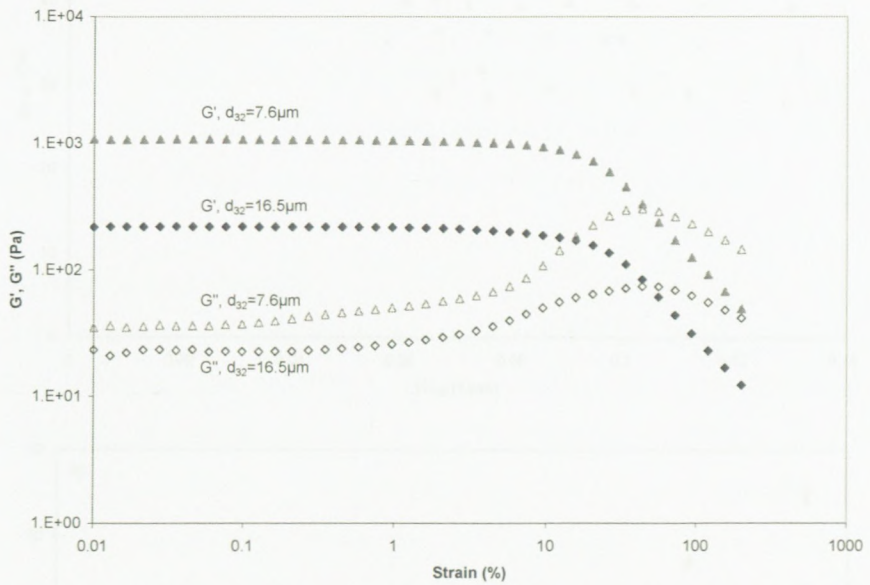

Figure 6.20: Amplitude dependence of G' and G'' for PIBSA-MEA stabilised emulsion (φ=0.868) at 10rad/s angular frequency

Figure 6.20 shows that the linearity of elastic properties continues up to deformations of the order of 10%, which corresponds with "dynamic yield strain" in the stress versus strain curve. As was discussed, the limit of linearity for the $G'(\gamma)$ dependence (yield strain) generally depends on frequency and cannot be treated as the physically meaningful yield stress. However, because we are looking for some characteristic strain, we will not concentrate on this effect here. It is worth mentioning that the stress

at the crossover point ($\tau_{cross} = G/\gamma$) is much higher than the yield stress τ_{y0} of highly concentrated emulsions. Consequently, the deformations of the elastic-to-viscous transition $\gamma_{G'=G''}$ are rather large.

As seen from Figure 6.20, the crossover points for the highest and lowest droplet size of prepared emulsions are very close. Actually, it was found that this crossover point does not depend on the droplet size in the studied range of droplet sizes (Figure 6.21a). However, a dependency on volume fraction is observed, as shown in Figure 6.21b. A slight increase in the crossover point with increasing volume fraction is observed.

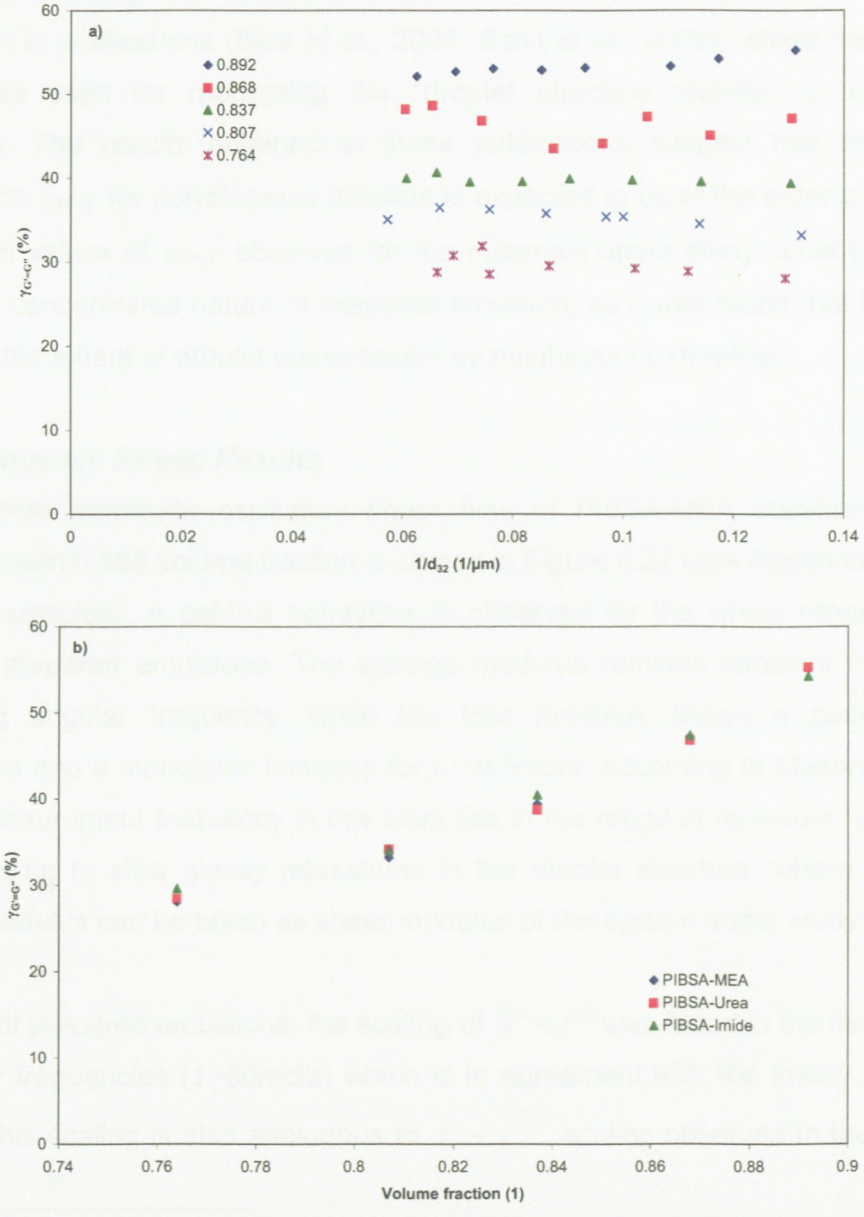

Figure 6.21: The dependency of $\gamma_{G'=G''}$ on (a) droplet size, and (b) surfactant type (d_{32}=7.5±0.1μm), for different volume fractions of prepared emulsions

It is seen that $\gamma_{G'=G''}$ strain is independent of surfactant type. While it was found that the droplet shape (state of compression) depends on the volume fraction and not droplet size, this suggest that $\gamma_{G'=G''}$ strain is controlled by the extent of droplet compression, and not by interfacial energy and interdroplet interaction. Therefore, this strain may be regarded as a geometrical elastic-to-viscous transition of confined droplets depending only on the extent of droplet compression through neighbouring droplets. Since the compressed droplet response to oscillatory shear flow probably depends on frequency, the frequency dependence of this strain is not surprising; however, as mentioned, we do not concentrate on this effect.

Such relatively large deformations of $\gamma_{G'=G''}$ are of special interest in light of the discussion in publications (Bais et al., 2005; Saiki et al., 2008), where the method of LAOS was used for monitoring the "droplet structure stability" in concentrated emulsions. The results obtained in those publications suggest that the transition deformation $\gamma_{G'=G''}$ for polydisperse droplets is expected to be of the order of 1~2%. The rather high values of $\gamma_{G'=G''}$ observed for the materials under study could be related to the highly concentrated nature of prepared emulsion, as it was found that this strain is related to the extent of droplet compression by neighbouring droplets.

6.4.3. Frequency Sweep Results

Typical small amplitude oscillatory shear flow of PIBSA-MEA stabilised explosive emulsions with 0.868 volume fraction is shown in Figure 6.22 (see Appendix E for other emulsion samples). A gel-like behaviour is observed for the whole range of droplet sizes for prepared emulsions. The storage modulus remains constant in the whole measuring angular frequency, while the loss modulus shows a plateau at low frequencies and a monotonic increase for $\omega>0.5rad/s$. According to Mason (1999), the lowest measurement frequency in this work lies in the range of minimum loss modulus corresponding to slow glassy relaxations in the droplet structure, where the plateau storage modulus can be taken as shear modulus of the system under study.

For most of prepared emulsions, the scaling of $G''\sim\omega^{1/2}$ was found in the medium range of angular frequencies (*1~50rad/s*) which is in agreement with the theory of Liu et al. (1996)*. This scaling is also analogous to $\tau_y \sim \dot{\gamma}^{1/2}$ scaling observed in the flow curve

* This scaling enhances as the value of φ-φ_c increases and d_{32} decreases.

measurements, because the loss modulus expresses the viscous contribution of viscoelastic behaviour.

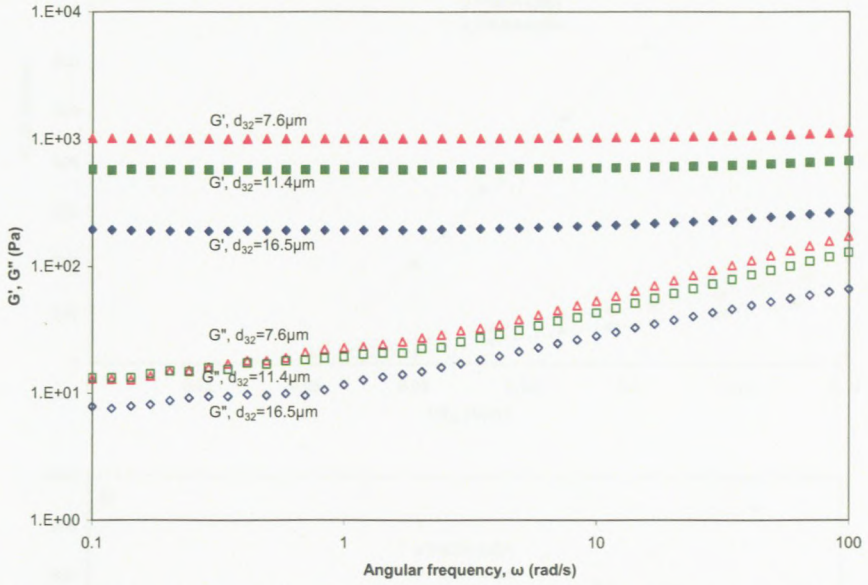

Figure 6.22: Typical variation of viscoelastic moduli against angular frequency

In the low frequency range of results, the scaling of viscoelastic moduli is in agreement with the results of Sollich's model (Sollich et al., 1997; Sollich, 1998) obtained by Mode Coupling Theory for $x \approx 1$. However, at higher frequencies, the variations of storage and loss moduli do not agree with the scaling predictions of this theory for any states (any effective noise temperature, x). This shows the need for development of the Sollich model to cover more general cases like the system under study.

As mentioned in Chapter 3, the Princen-Lacasse-Mason models predict the scaling of shear modulus with Laplace pressure. With the same analogy as the one discussed for yield stress in section 6.4.1, we should have a zero intercept for linear dependence of $G'_p - 1/d_{32}$ ($d_{32} \to \infty \Rightarrow G'_p \to 0$) based on these models. To study this, the variation of plateau storage modulus, G'_p, scaled with interfacial tension against reciprocal droplet size and reciprocal squared droplet size, is shown in Figure 6.23. In this figure, highly concentrated emulsions of $\varphi = 0.868$ stabilised with different surfactants are presented. The non-zero intercept of $G'_p/\sigma - 1/d_{32}$ dependence similar to $\tau_{y0}/\sigma - 1/d_{32}$ case and non-superimposition of results for different surfactant types, confirm the presence of interdroplet interaction for prepared highly concentrated emulsions.

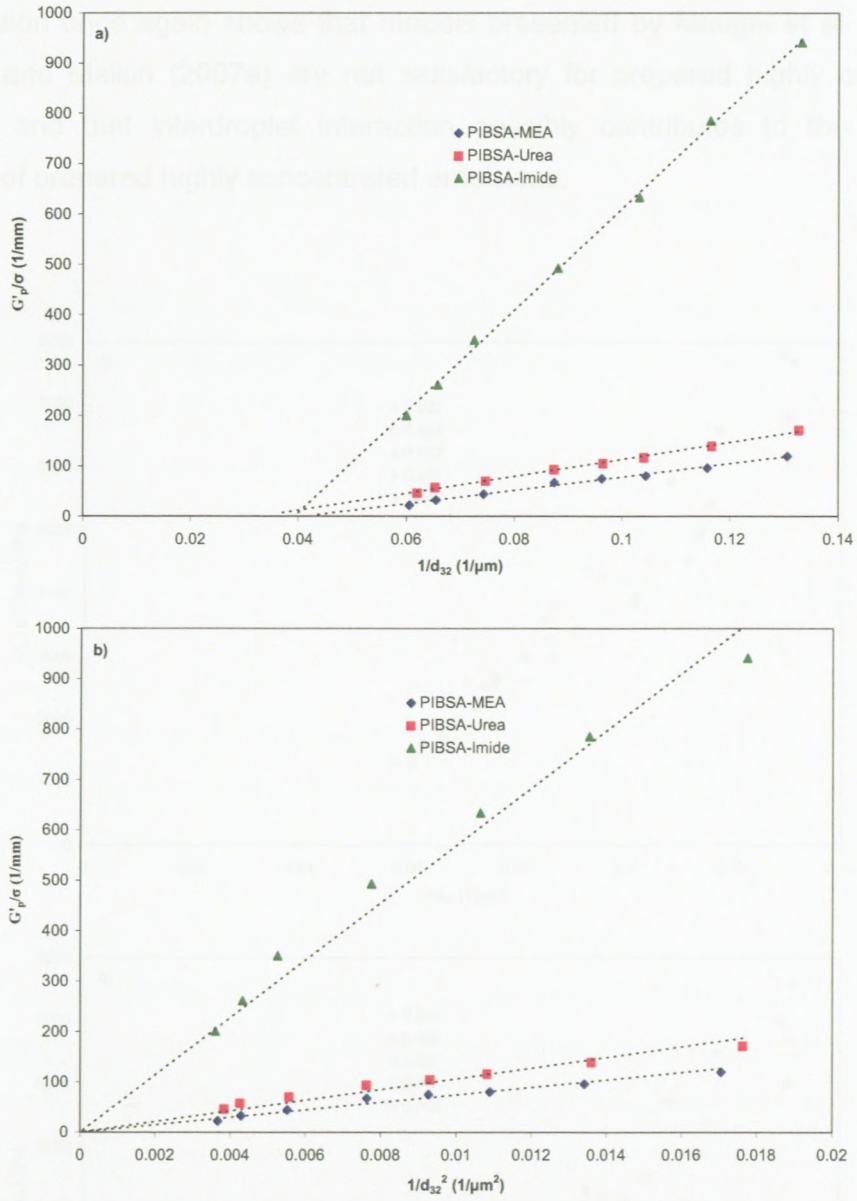

Figure 6.23: Variation of shear modulus scaled with interfacial tension against (a) $1/d_{32}$, and (b) $1/d_{32}^2$, for explosive emulsions with different surfactant types (φ=0.868)

The similar behaviour of shear modulus and yield stress is seen as expected, due to the droplet deformation-controlled mechanism of both of them. As discussed, the interfacial tension and interfacial dilatational elasticity cannot be the controlling mechanism of observed behaviour due to the non-scaling of rheological behaviour with interfacial characteristics. The detailed discussion of this unusual behaviour based on the model presented in Chapter 4, is discussed in section 6.5. It should be noticed that the scaling of shear modulus with reciprocal squared droplet size satisfies the zero intercept condition; however, the experimental results for different surfactants are not

superimposed – as with the yield stress behaviour – to assure $G'_p \sim \sigma / d_{32}{}^2$ scaling. This deviation once again shows that models presented by Mougel et al. (2006) and Masalova and Malkin (2007a) are not satisfactory for prepared highly concentrated emulsions and that interdroplet interaction possibly contributes to the rheological behaviour of prepared highly concentrated emulsions.

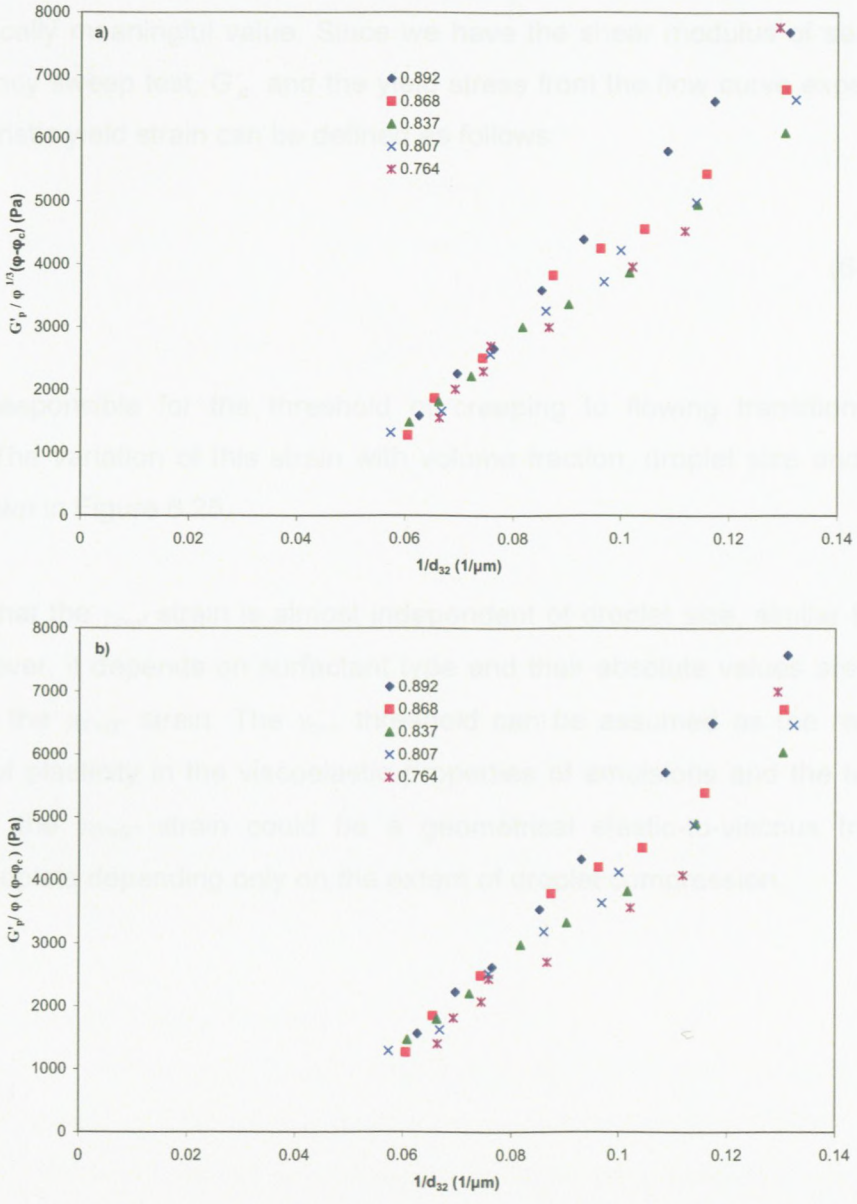

Figure 6.24: Scaling of shear modulus with (a) $\varphi^{1/3}(\varphi-\varphi_c)$, and (b) $\varphi(\varphi-\varphi_c)$

Two different scaling relations suggested by Princen and Kiss (1986), $G'_p \sim \varphi^{1/3}(\varphi-\varphi_c)$, and Mason et al. (1995) $G'_p \sim \varphi(\varphi-\varphi_c)$ were studied, as shown in

Figure 6.24. The φ_c of these scaling relationships were respectively taken as 0.712, which is suggested by Princen and Kiss (1986), and 0.695, which is found in section 6.4.1 for yield stress scaling with volume fraction. Again, it is seen that, for big droplets where the contribution of interdroplet interaction becomes negligible, a good superimposition is observed for both cases, while deviation from proposed scaling relationships in the literature becomes significant when droplet size decreases.

As discussed, the yield strain obtained from strain sweep experiment can not be used as a physically meaningful value. Since we have the shear modulus of samples from the frequency sweep test, G'_p, and the yield stress from the flow curve experiment, τ_{y0}, a characteristic yield strain can be defined as follows:

$$\gamma_{c\leftrightarrow f} = \frac{\tau_{y0}}{G'_p} \qquad (6\text{-}2)$$

which is responsible for the threshold of creeping to flowing transition in steady shearing. The variation of this strain with volume fraction, droplet size and surfactant type is shown in Figure 6.25.

It is seen that the $\gamma_{c\leftrightarrow f}$ strain is almost independent of droplet size, similar to the $\gamma_{G'=G''}$ case, however, it depends on surfactant type and their absolute values are noticeably lower than the $\gamma_{G'=G''}$ strain. The $\gamma_{c\leftrightarrow f}$ threshold can be assumed as the real physical boundary of plasticity in the viscoelastic properties of emulsions and the transition to flow, while the $\gamma_{G'=G''}$ strain could be a geometrical elastic-to-viscous transition of confined droplets depending only on the extent of droplet compression.

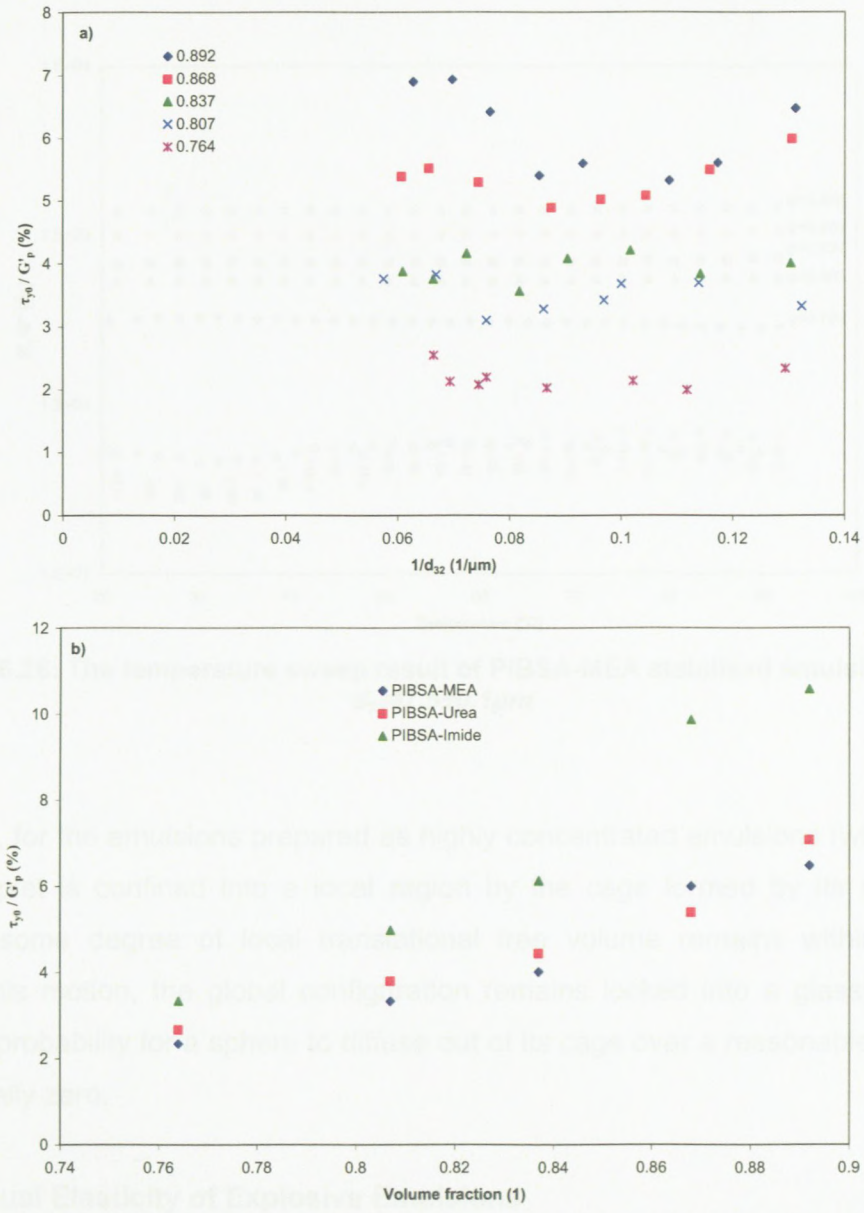

Figure 6.25: The dependency of $\gamma_{c\leftrightarrow f}$ on (a) droplet size, and (b) surfactant type (d_{32}=7.5±0.1μm), for different volume fractions of prepared emulsions

6.4.4. Temperature Sweep Results

The temperature sweep of small amplitude oscillatory flow in sufficiently low frequencies (γ=1%, ω=1rad/s) was performed, as shown typically in Figure 6.26. It is seen that the storage modulus is independent of measuring temperature in the whole volume fraction range. As it was observed in the frequency sweep experiment, the loss modulus is much lower than storage modulus and remains unchanged on increasing volume fraction. The fluctuation in the loss modulus is negligible, due to its very low values, compared to storage modulus. These results show that the volume fractions of the prepared emulsion are much higher than glass transition, $\varphi>\varphi_g$, and to neglect the kinetic energy, k_BT, in the modelling section was an appropriate assumption.

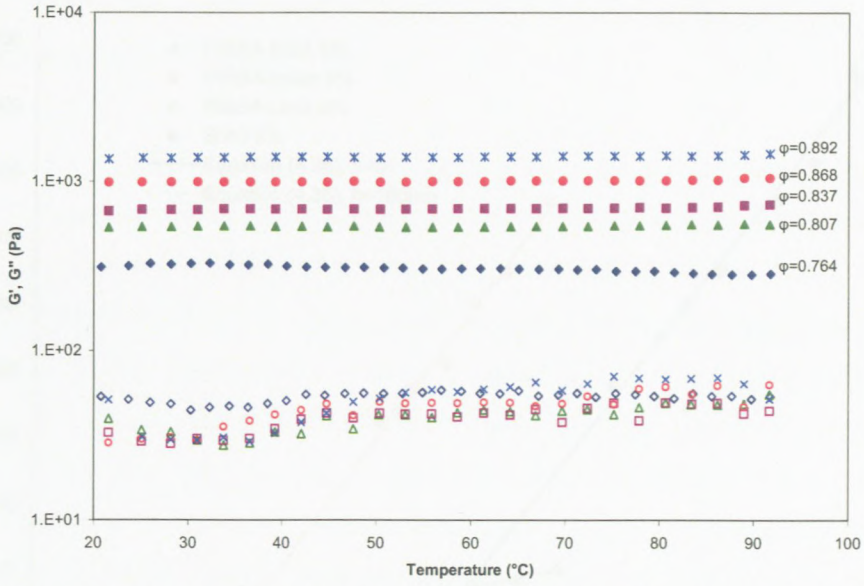

Figure 6.26: The temperature sweep result of PIBSA-MEA stabilised emulsions with d_{32}=7.5±0.1μm

Therefore, for the emulsions prepared as highly concentrated emulsions (where $\varphi>\varphi_g$), every droplet is confined into a local region by the cage formed by its neighbours; although some degree of local translational free volume remains within its cage. Despite this motion, the global configuration remains locked into a glassy structure, since the probability for a sphere to diffuse out of its cage over a reasonable time scale is essentially zero.

6.5. Unusual Elasticity of Explosive Emulsions

The droplet size distributions of samples with different surfactants were quite similar (Figure 6.4), so the increase of droplet interfacial area due to compression was the same, while the scaled shear modulus of samples at same droplet sizes appeared to be different (Figure 6.23). This principal experimental result supports the significance of the effect of interdroplet interaction on the rheological properties.

Since eq. (4-36) and the Princen-Lacasse-Mason models predict a linear dependency between G/σ and $1/d$, with intercept equal to zero, Figure 6.27 shows a deviation from this prediction for all explosive emulsions. These results support a nonlinear dependency of G/σ versus $1/d$ satisfying zero intercept, which could be a result in the presence of interdroplet interaction, eq. (4-39), through $f_{dis}(h)$ function.

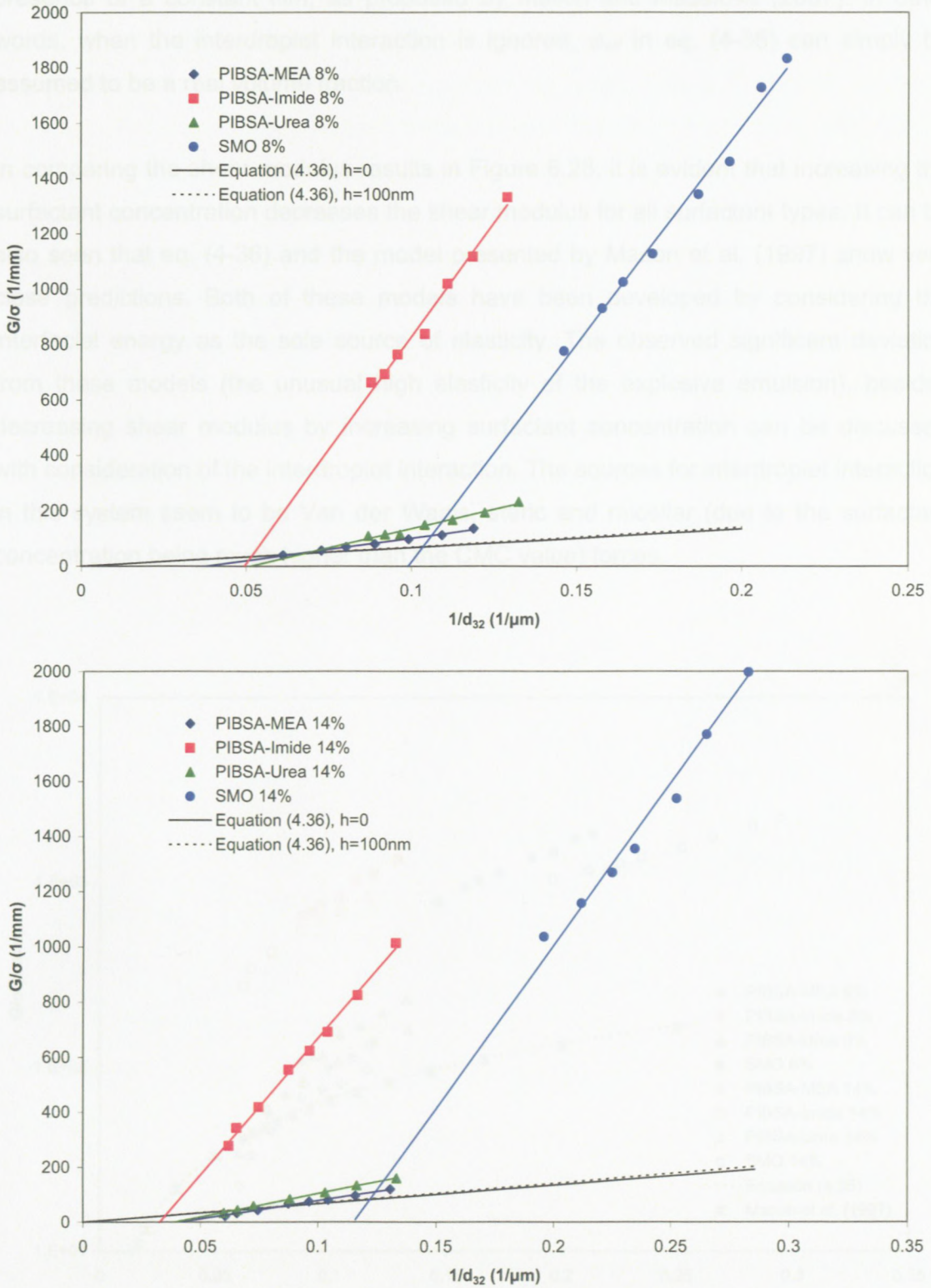

Figure 6.27: The size dependencies of shear modulus for different surfactant types and concentrations. The trend lines show the linear behaviour.

The effect of a constant film thickness (in contrast to optimised film thickness) on the shear modulus is shown in Figure 6.27. It is clear that it has a negligible effect on shear modulus. Hence, the observed high elasticity of emulsion samples is not due to the

presence of a constant film, as proposed by Malkin and Masalova (2007). In other words, when the interdroplet interaction is ignored, φ_{eff} in eq. (4-36) can simply be assumed to be a real volume fraction.

In comparing the shear modulus results in Figure 6.28, it is evident that increasing the surfactant concentration decreases the shear modulus for all surfactant types. It can be also seen that eq. (4-36) and the model presented by Mason et al. (1997) show very close predictions. Both of these models have been developed by considering the interfacial energy as the sole source of elasticity. The observed significant deviation from these models (the unusual high elasticity of the explosive emulsion), besides decreasing shear modulus by increasing surfactant concentration can be discussed with consideration of the interdroplet interaction. The sources for interdroplet interaction in this system seem to be Van der Waals, steric and micellar (due to the surfactant concentration being much higher than the CMC value) forces.

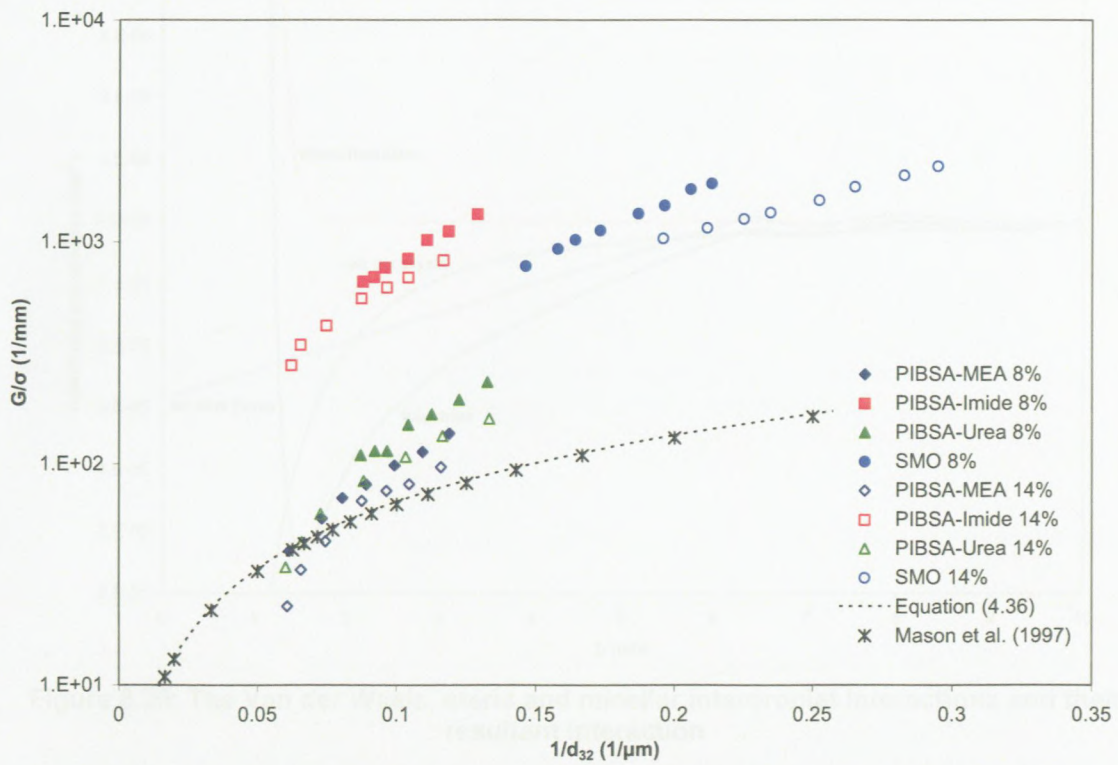

Figure 6.28: The surfactant concentration dependency of shear modulus for different surfactant types and comparison with eq. (4-36) and Mason et al. (1997) model

In order to estimate the Van der Waals interaction, the Hamaker constant, A_H, for the symmetric configuration of two identical phases interacting across a medium, can be

calculated from Lifshitz's theory (1956). Since the refractive indices of aqueous and oil phases are the same (~1.445),* the contribution of dispersion interaction in the Lifshitz theory will be zero, and the Hamaker constant can never exceed ¾*kT* (Kralchevsky et al., 2003). For estimating the steric force between polymeric surfactants adsorbed at the interface of droplets, if we assume that the oil phase is a theta solvent for a PIBSA-based surfactant, the interaction can be predicted by De Gennes's theory (1987). Finally, the semi-empirical formula suggested by Kralchevsky and Denkov (1995) can be used for the calculation of the micellar force. Reynolds et al. (2000, 2001) measured the micellar characteristics of the PIBSA-MEA surfactant in highly concentrated emulsions comprising a super-cooled aqueous solution of 80wt.% ammonium nitrate by using small-angle neutron scattering, SANS. As a typical case study, therefore, the Van der Waals, steric and micellar† interdroplet interactions for an emulsion stabilised with 14% PIBSA-MEA is shown in Figure 6.29.

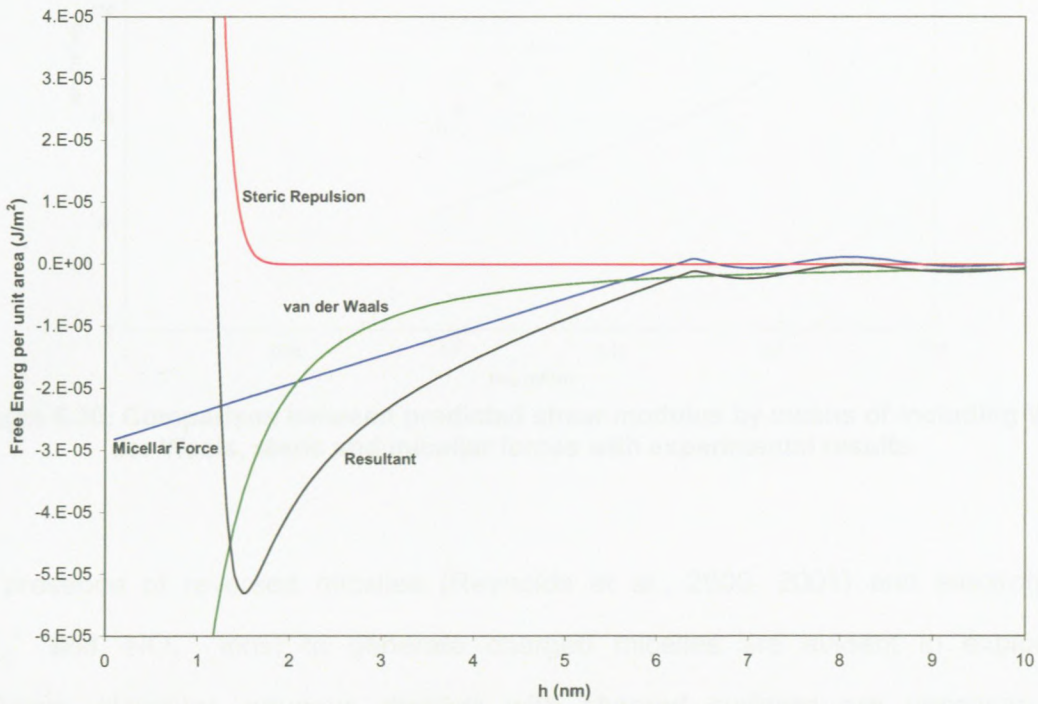

Figure 6.29: The Van der Waals, steric and micellar interdroplet interactions and their resultant interaction

* The reason why explosive emulsions are transparent

† The radius and volume fraction of micelles in an oil phase containing 14% PIBSA-MEA surfactant can be estimated respectively as 32.1Å and 0.10, by using interpolation. The aggregation number of micelles was found to be about 13.5~14.6 for different surfactant concentrations. (Reynolds et al., 2000, 2001)

The obtained resultant interaction was used to predict the shear modulus, as shown in Figure 6.30. It is clear that these assumed interactions underestimate the shear modulus of explosive emulsions. Therefore, there should be a missing interdroplet interaction, which we argue it is the electrostatic one. The electrostatic interaction for aqueous droplets in an oil phase has not been studied extensively. Recently, Hsu et al. (2005) showed experimentally that reversed micelles enhance a strong electrostatic repulsion in oil media, because, while the vast majority of uncharged reverse micelles exist in dynamic equilibrium, a very small fraction of positively and negatively charged micelles are generated by thermal fluctuations.

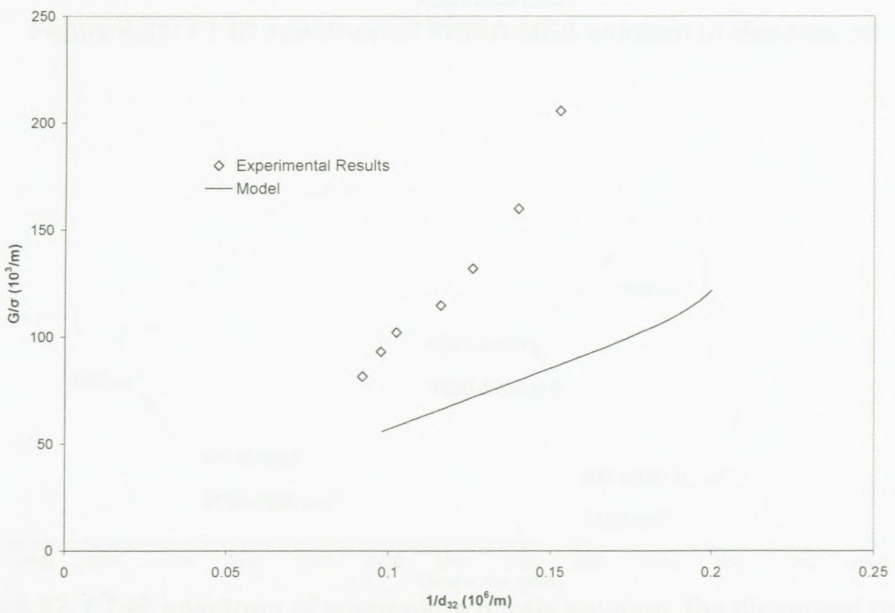

Figure 6.30: Comparison between predicted shear modulus by means of including Van der Waals, steric and micellar forces with experimental results

The presence of reversed micelles (Reynolds et al., 2000, 2001) and electrolytes (NH_4^+ and NO_3^- ions) to generate charged micelles are evident in explosive emulsions. However, aqueous droplets with charged surfaces are necessary to enhance the electrostatic repulsion (Hsu et al., 2005). Ganguly et al. (1992), by using FT-IR, found that, in the explosive emulsions, the headgroup of a surfactant forms hydrogen bonding with NH_4^+ ions of the dispersed phase, and therefore these ions concentrate close to the interface and induce a non-neutral surface charge. To prove this for PIBSA-MEA stabilised emulsions, we performed FT-IR studies for the oil phase (Figure 6.31), aqueous phase (Figure 6.32) and emulsion (Figure 6.33) by using a Spectrometer 100, Perkin Elmer, as shown.

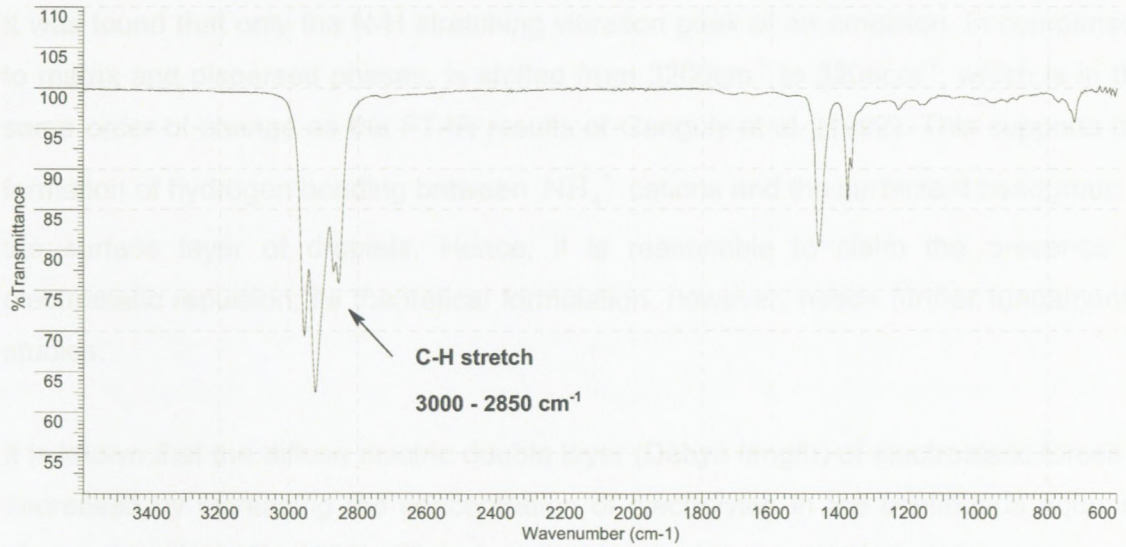

Figure 6.31: FT-IR spectrum of PIBSA-MEA solution in Mosspar oil

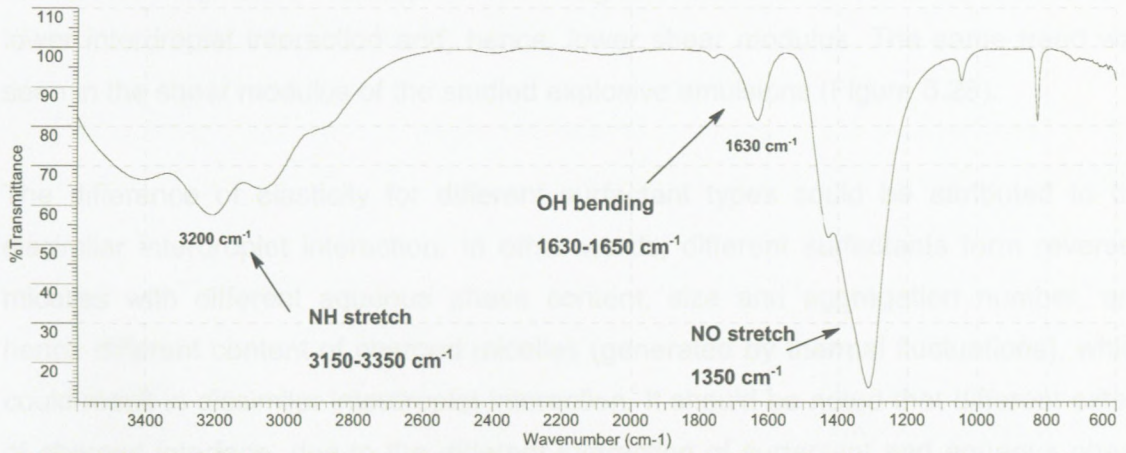

Figure 6.32: FT-IR spectrum of ammonium nitrate solution, the dispersed phase in emulsions samples

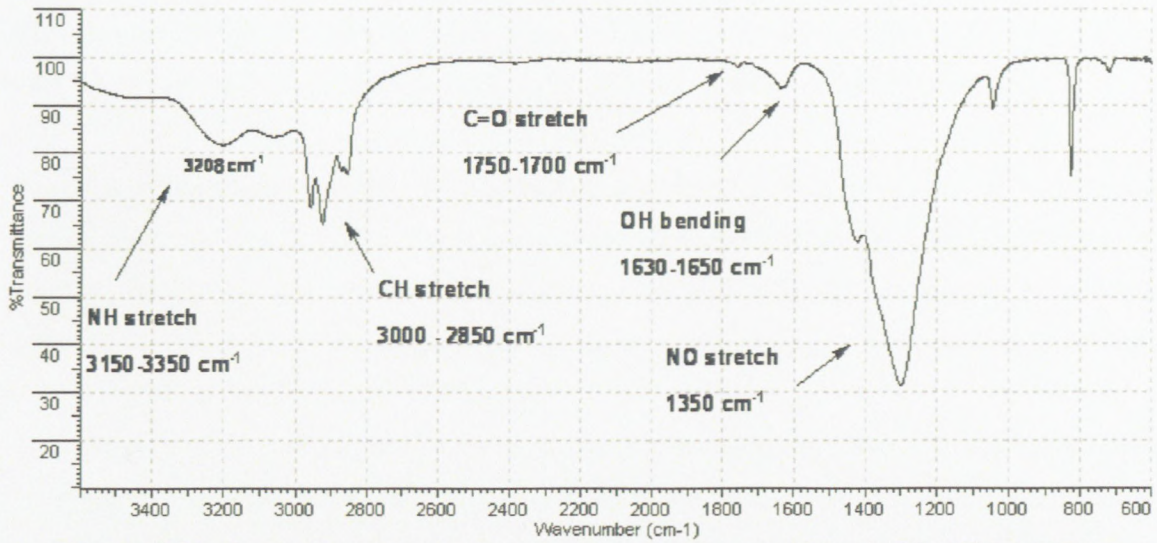

Figure 6.33: General spectrum of explosive emulsion stabilized with PIBSA-MEA

It was found that only the N-H stretching vibration peak of an emulsion, in comparison to matrix and dispersed phases, is shifted from 3200cm^{-1} to 3208cm^{-1}, which is in the same order of change as the FT-IR results of Ganguly et al. (1992). This supports the formation of hydrogen bonding between NH_4^+ cations and the surfactant headgroup in the surface layer of droplets. Hence, it is reasonable to claim the presence of electrostatic repulsion; its theoretical formulation, however, needs further fundamental studies.

It is known that the diffuse electric double layer (Debye length) of electrostatic forces is decreased by increasing the concentration of electrolytes in the continuous aqueous phase (Israelachvili, 1992). Therefore it was to be expected that increasing the reversed micelle concentration in the studied explosive emulsions will decrease the electrostatic repulsion. This implies that a higher surfactant concentration will result in lower interdroplet interaction and, hence, lower shear modulus. The same trend was seen in the shear modulus of the studied explosive emulsions (Figure 6.28).

The difference of elasticity for different surfactant types could be attributed to the dissimilar interdroplet interaction. In other words, different surfactants form reversed micelles with different aqueous phase content, size and aggregation number, and hence different content of charged micelles (generated by thermal fluctuations), which could result in dissimilar interdroplet interaction. It should be noted that different extent of charged interface, due to the different interaction of surfactant and aqueous phase ions at the interface, could also play a role in elasticity of explosive emulsions.

Chapter 7 – Summary and Conclusion

7.1. Summary

One of the most important categories of complex fluids comprises emulsions which can be seen in everyday life. An emulsion is a mixture of two immiscible substances in which one liquid (the dispersed or internal phase) is dispersed in the other (the continuous or external phase). A great deal of effort has been expended on understanding and controlling the structure and rheological properties of emulsions to ensure acceptable quality, processability and performance of final products. General concepts in emulsions science, including the emulsification process, stability and structure of emulsion after formation, and microscopic and macroscopic properties of emulsions are reviewed in Chapter 2.

The material under study in this work is explosive emulsions, which are classified as highly concentrated emulsions of an oxidiser solution in organic oil stabilised by PIBSA-based surfactants. Generally, the droplets of dispersed phase in highly concentrated emulsions are compressed by neighbouring droplet, because the volume fraction is far beyond the closest packing of spherical droplets. This closely packed configuration and the profound hydrodynamic interaction between neighbouring droplets induce mechanical interference between the droplets, thus prohibiting their free movement. Hence, while the highly concentrated emulsions consist of very low viscosity and inelastic components, they show gel-like behaviour with high elasticity and non-Newtonian flow response. As reviewed in Chapter 3, it has been suggested in the literature that this behaviour originated from interfacial energy in terms of Laplace pressure. Therefore, the scaling of rheological properties with Laplace pressure is expected, but several publications show a deviation from this scaling behaviour. It seems that the source of deviation from this scaling is interdroplet interaction, which can contribute to the rheological behaviour of highly concentrated emulsions.

The shear modulus of highly concentrated emulsions in the presence of interdroplet interaction was developed in Chapter 4. The prediction of model was verified by the data presented in the literature. It was shown that a small source of interdroplet interaction can result in deviation from scaling of shear modulus with Laplace pressure.

The material and instruments used to perform the experimental work are explored in Chapter 5. The material needed to form emulsions consisted of supersaturated oxidiser solution, hydrocarbon oil and surfactant. The droplet size of emulsions was qualitatively

measured by means of a Leica optical microscope and quantitatively measured by means of a Malvern Mastersizer 2000 instrument. The rheological properties of emulsion samples, including frequency sweep, amplitude sweep, flow curve, and temperature sweep, were obtained by using an MCR 300, Paar Physica rheometer. The Wilhelmy plate of the Kruss K100 tensiometer was used to measure the interfacial tension, CMC and surfactant concentration at the interface between the oil and the ammonium nitrate solution. These experimental methods were used to investigate highly concentrated emulsions with five different volume fractions and three different PIBSA-based surfactants with surfactant concentration of 14wt.% in an oil phase. To study the unusual elasticity of explosive emulsions, a series of emulsions with a lower surfactant concentration, 8wt.%, including a classic surfactant, SMO, were prepared. It should be noted that the proper method for measuring the yield stress and the correlation between yield stresses measured from flow curve and strain sweep experiments were also examined.

The experimental results are presented and discussed in Chapter 6. The interfacial characteristics for different surfactant types and variations of droplet size distribution for different droplet sizes, volume fractions, and surfactant types were first examined. Secondly, the proper method for estimating yield stress of prepared emulsions was investigated. Then, the rheology of samples was presented, and different scaling methods and fitting of experimental data were studied. Finally, the physics behind unusual elasticity of emulsion samples were studied by using the model that was developed, as presented in Chapter 4.

7.2. Concluding Remarks

- Two- and three-dimensional models for the shear modulus of highly concentrated emulsions were developed by including the interdroplet interaction. The new model predicts that a slight source of interdroplet interaction can result in a considerable increase in shear modulus and osmotic pressure. It was also found that the elasticity calculated in the frames of the present model is not scaled with Laplace pressure, due to the presence of the interaction term.

- Introducing interdroplet interaction resulted in deviation from the linear dependency of the Princen-Lacasse-Mason models' prediction, $G/\sigma \sim 1/d$, as a result of potential film thickness–droplet size dependency in $f_{dis}(h)$ term. However, the intercept was still zero (it still satisfies $G \rightarrow 0$, if $R \rightarrow \infty$). Increase in

droplet size also increased the film thickness, as was expected. It should be noted that the linear dependency is still present in the developed geometrical model (in the absence of interdroplet interaction).

- The employed PIBSA-based surfactants occupy almost the same area at the interface; however, they show significantly different interfacial tensions and dilatational elasticities. This suggests that the surfactant concentration at the interface for PIBSA-based surfactants may be controlled by a polymeric tail (which is the same for the PIBSA-based surfactants employed), while the interfacial elasticity may have originated from the interaction of the dispersed phase and surfactant headgroup.

- The following trend of interfacial dilatational elasticity (dynamic elasticity), as well as of the interfacial tension (static elasticity), was found: PIBSA-MEA > PIBSA-Urea > PIBSA-Imide. However, the shear modulus and yield stress of the prepared highly concentrated emulsions showed this trend: PIBSA-Imide > PIBSA-Urea ≈ PIBSA-MEA. This implied that the rheological behaviour is not controlled by the interfacial tension and/or dilatational elasticity only. In other words, the contribution of interdroplet interaction to the rheological properties of emulsion samples is significant.

- The droplet size distributions of emulsion samples were almost identical in a range of droplet sizes and volume fractions, and hence its effect on rheological behaviour could be ignored. However, this effect was somehow excluded when the area–volume mean diameter (d_{32}) was considered in studying the rheology of highly concentrated emulsions, because the rheological behaviour of highly concentrated emulsions is controlled by the interfacial area of droplets.

- The critical stress found in the oscillating tests (sometimes referred to as the "dynamic yield stress") was not constant but depended strongly on frequency. The values of the critical stress found in the oscillating experiment also did not coincide with real ("physical") yield stress estimated from flow curves. This means that the "dynamic yield stress" is in no event a physical parameter of a material, and cannot be used for comparison with any theoretical conclusion concerning yielding properties of visco-plastic materials.

- The flow curves of prepared highly concentrated emulsions showed a pronounced yield stress, but a hump in the flow curve at moderate shear rates ($\dot{\gamma} \approx 0.1-1s^{-1}$) was also seen. The Herschel-Bulkley model, eq. (2-54), with two different sets of coefficients below and above the hump, was fitted for the flow curves of all emulsion samples prepared by different surfactants, various droplet sizes and volume fractions and it was found that, in both regions, *n=0.5* resulted in a good fitting of flow curves. This was in agreement with experimental relation $\tau_y \sim Ca^{1/2}$ suggested by Princen and Kiss (1989). Therefore, it was suggested that the Windhab model be modified as: $\tau = \tau_{y0} + K\dot{\gamma}^{0.5} + (\tau_{y1} - \tau_{y0})[1-\exp(-\dot{\gamma}/\dot{\gamma}^*)]$. This new model showed excellent fitting of experimental results in the whole shear rate range of all emulsion samples.

- The Princen and Kiss (1989) theory, eq. (3-1), and Mason (1999) predict that the linear dependence of τ_{y0}/σ – $1/d_{32}$ should be superimposed for different surfactant types but depends on the volume fractions. The non-superimposition of this dependence for different surfactants shows the presence of significant interdroplet interaction. The non-zero intercept of τ_{y0}/σ – $1/d_{32}$ dependence for studied emulsions implied the existence of a non-linear dependence (resulting from interdroplet interaction) to fulfil the zero intercept requirement. Similar behaviour was observed for the G'_p/σ – $1/d_{32}$ scaling relationship.

- It was established that the zero intercept condition was fulfilled in the $\tau_{y0} \sim \sigma / d_{32}^{\ 2}$ scaling, although the experimental results for different surfactants were not superimposed. This deviation revealed that models presented by Mougel et al. (2006) and Masalova and Malkin (2007a) are not satisfactory for prepared highly concentrated emulsions. Similar behaviour was observed for the $G'_p \sim \sigma / d_{32}^{\ 2}$ scaling relationship. This could be due to the presence of a significant interdroplet interaction.

- It was found that the scaling of $\tau_y \sim \varphi^{1/3}$ resulting from the Princen and Kiss theory was not valid for prepared emulsions, while the Mason (1999) scaling relationship, $\tau_y \sim \varphi(\varphi - \varphi_c)^2$, showed sufficient superimposition with φ_c=*0.695*

for big droplet sizes – where the contribution of interdroplet interaction is less significant.

- The Capillary number of secondary yield stress (hump stress), τ_{y1}, was dependent on both volume fraction and droplet size, thus the proposed theory by Malkin and Masalova (2007) did not work in this case. This showed that the interfacial energy is not the only controlling mechanism against rolling to deformation transition, but that the interdroplet interaction may contribute to this transition.

- Finding an experimental correlation between two differently obtained yield stresses (from flow curve and strain sweep measurements) was not successful, because it depended on the surfactant type. This result confirmed again that the yield stress determined from the flow curve measurement – which is a threshold between creeping and flowing – is more realistic to report than the frequency dependent yield stress obtained from oscillation measurement.

- The strain of crossover point of G' and G'', $\gamma_{G'=G''}$, in the amplitude sweep experiment does not show any dependency on droplet size and surfactant type. However, a slight increase in the crossover point with increasing volume fraction is observed. This strain may be regarded as a geometrical elastic-to-viscous transition of confined droplets depending only on the extent of droplet compression through neighbouring droplets.

- It was found that $G''\sim\omega^{1/2}$ in the medium range of angular frequencies which is in agreement with the theory of Liu et al. (1996). This scaling is also analogous to the $\tau_v \sim \dot{\gamma}^{1/2}$ scaling observed in the flow curve measurements. In the low frequency range of results, the scaling of viscoelastic moduli is in agreement with the results of Sollich's model (Sollich et al., 1997; Sollich, 1998) obtained by Mode Coupling Theory for $x\approx1$. However, at higher frequencies, the variations of storage and loss moduli do not agree with the scaling predictions of this theory for any state.

- Two different scaling relations suggested by Princen and Kiss (1986), $G'_p \sim \varphi^{1/3}(\varphi-\varphi_c)$, and Mason et al. (1995) $G'_p \sim \varphi(\varphi-\varphi_c)$ showed a good superimposition for big droplets, while, by decreasing droplet size (and thus

increasing the interdroplet interaction significance), deviation from both scaling relationships becomes significant.

- It was seen that the ratio of yield stress to plateau storage modulus, regarded as $\gamma_{c\leftrightarrow f}$ strain, was almost independent of droplet size similar to the $\gamma_{G'=G''}$ case, but depended on surfactant type. The $\gamma_{c\leftrightarrow f}$ threshold can be assumed to be the real physical boundary of plasticity in the viscoelastic properties of emulsions and the transition to flow, while the $\gamma_{G'=G''}$ strain could be a geometrical elastic-to-viscous transition of confined droplets depending only on the extent of droplet compression.

- It was found that, in the whole volume fraction range, the storage and loss moduli are independent of measuring temperature. This was a good reason to claim that the volume fractions of prepared emulsion are much higher than glass transition, $\varphi>\varphi_g$, and neglecting the kinetic energy, k_BT, in the modelling section was an appropriate assumption.

- The effect of a constant film thickness on the shear modulus was studied. It was found that it has a negligible effect on shear modulus. Hence, the observed high elasticity of emulsion samples is not due to the presence of a constant film, as proposed by Malkin and Masalova (2007). In other words, when the interdroplet interaction is ignored, effective volume fraction, φ_{eff}, in eq. (9), can be approximated as real volume fraction.

- It was found that considering only Van der Waals, micellar and steric interactions underestimate the shear modulus of explosive emulsions. Therefore, there should be a missing interdroplet interaction, which was argued to be the electrostatic one. Reversed micelles, electrolytes and a charged interface are necessary to generate electrostatic repulsion between aqueous droplets in an oil phase (Hsu et al., 2005). The presence of reversed micelles (Reynolds et al., 2000, 2001) and electrolytes (NH_4^+ and NO_3^- ions) to generate charged micelles are evident in explosive emulsions. It was found, by using FT-IR, that the headgroup of the PIBSA-MEA surfactant forms hydrogen bonding with NH_4^+ ions of the dispersed phase, and therefore these ions concentrate close to the interface and induce a non-neutral surface charge.

- It is expected that increasing the reversed micelle concentration in the studied explosive emulsions will decrease the electrostatic repulsion. This implies that a higher surfactant concentration will result in lower interdroplet interaction and, hence, lower shear modulus. The same trend was observed in the shear modulus of the prepared explosive emulsions.

- The difference of elasticity of explosive emulsions for different surfactant types firstly could be attributed to the different structures of reversed micelles and hence different content of charged micelles, which could result in dissimilar interdroplet interaction. Secondly, different extent of charged interface, due to the different interaction of surfactant and aqueous phase ions at the interface, could play a role.

7.3. Recommendations for Future research

A number of areas have been identified as possible future research initiatives as a consequence of this study:

- Expanding the developed model to consider the effect of polydispersity of droplet size and disordered arrangement of droplets on the shear modulus of highly concentrated emulsions (in the presence of interdroplet interaction)

- Developing a theoretical framework to discuss the physics behind the observed scaling of $\tau_y \sim \dot{\gamma}^{1/2}$. This can be done by modelling the flow behaviour of highly concentrated emulsions in two different regimes of movements involving rolling and deformation

- Extending the experimental work to consider the highly concentrated emulsions with a wider rage of surfactants (e.g. different tails of PIBSA) and formulation (e.g. highly concentrated oil-in-water emulsions)

References

Abduraghimova, L.A., Rehbinder, P.A., & Serb-Serbina, N.N. 1955. Elastic-viscous properties of thixotropic structures in water suspensions of bentonite clays. *Kolloid Zh.* 17: 184-195.

Almagren, F.G., & Taylor, J.E. 1976. Geometry of soap films and soap bubbles. *Scientific American* 235: 82-93.

Alvarez-Solano, O.A. 2006. Emulsions inverses très concentrées. Influence du procédé et de la formulation sur leurs propriétés rhéologliques, Doctoral thesis, Institut National Polytechnique de Lorraine, Nancy, France.

Aronson, P.M., & Petko, M.F. 1993. Highly concentrated water-in-oil emulsions, Influence of electrolyte on their properties and stability. *J. Colloid Interface Sci.* 159: 134-147.

Aronson, P.M., & Princen, H.M. 1980. Contact angles associated with thin liquid films in emulsions. *Nature* 286: 370-372.

Asakura, S., & Oosawa, F. 1958. Interaction between particles suspended in solutions of macromolecules, *J. Polym. Sci.* 33: 183-192.

Atkins, P.W. (1994). *Physical Chemistry*, 5th ed. Oxford: Oxford University Press.

Babak, V.G., Langenfeld, A., Fa, N., & Stébé, M.J. 2001. Rheological properties of highly concentrated fluorinate water-in-oil emulsions. *Prog. Colloid Polym. Sci.* 118: 216-220.

Babak, V.G., & Stébé, M.J. 2002. Highly concentrated emulsions: physiochemical principles of formulation. *J. Dispersion Sci. Tech.* 23 (1-3): 1-22.

Bais, D., Trevisan, A., Lapasin, R., Partal, P., & Gallegos, C. 2005. Rheological characterization of polysaccharides – surfactant matrices for cosmetic O/W emulsions. *J. Colloid Interface Sci.* 290: 546-556.

Bampfield, H.A., & Cooper, J. 1985. Emulsion explosives. *Encyclopedia of Emulsion Technology*, New York: Marcel Dekker. 7: 281-306

Bancroft, W.D. 1913. Theory of emulsification. *J. Phys. Chem.* 17: 501-519.

Barnes H.A., & Walters, K. 1985. The Yield stress myth. *Rheol. Acta* 24: 323-326.

Barnes, H.A. 1995. A review of the slip (wall depletion) of polymer solutions, emulsions and particle suspensions in viscometers: its cause, character, and cure. *J. Non-Newton Fluid Mech.* 56: 221-251.

Barnes, H.A. 1999. Yield stress - a review, or "παντα ρει" - everything flows? *J. Non-Newtonian Fluid Mech.* 81: 133-178.

Barnes, H.A. 2007. The "Yield stress myth" paper – 21 year on. *Appl. Rheol.* 17: 43111(1-5).

Barry, B.W. 1975. Viscoelastic properties of concentrated emulsions. *Adv. Colloid Interface Sci.* 5: 37-75.

Becher, P. (ed.). 1983. *Encyclopaedia of Emulsion Technology*. Vol. 1 and 3, New York: Marcel Dekker.

Benali, L. 1993. Rheological and granulometrical studies of a cutting oil emulsion. I. The effect of oil concentration. *J. Colloid Interface Sci.* 156: 454-461.

Bengoechea, C., Cordobés, F., & Guerrero, A. 2006. Rheology and microstructure of gluten and soya-based o/w emulsions. *Rheol. Acta* 46, 13-21.

Bengtsson, L.A., Frostemark, F., & Holmberg, B. 1994. Speciation, Structural Characteristics and Proton Dynamics in the Systems NH_4NO_3 $1.5H_20$ and NH_4NO_3, 1.5H20- (HNO_3, NH_4F, NH_3)-H_20 at 5O°C. *J. Chem. Soc. Faraday Trans.* 90: 559-570.

Bergeron, V. 1999. Forces and structure in thin liquid soap films. *J. Phys.: Condens. Matter* 11: R215-R238.

Berthier, L., Barrat, J.L., & Kurchan, J. 2000. A two -time-scale, two-temperature scenario for nonlinear rheology. *Phys. Rev. E* 61: 5464-5472.

Bibette, J. 1992. Stability of thin film in concentrated emulsions. *Langmuir* 8: 3178-3182.

Bingham, E.C. 1922. *Fluidity and plasticity*. New York: McGraw Hill.

Bird, R.B., Armstrong, R.C., & Hassager, O. 1987. *Dynamic of Polymeric Liquids*. New York: Willey.

Bird, R.B., Dai, G.C., Yarusso, B.J. 1983. The rheology and flow of viscoplastic materials. *Rev. Chem. Eng.* 1: 1-71.

Boer, G. 2003. Composition and emulsifier. US Patent 6,630,596 B2.

Bolton, F., & Weaire, D. 1992. The effects of plateau borders in the two-dimensional soap froth. 2. General simulation and analysis of rigidity loss transition. *Phil. Mag. B* 65: 473-487.

Bonn, D., Coussot, P., Huynh, H.T., Bertrand, F., & Debregeas, G. 2002. Rheology of soft glassy materials. *Europhys. Lett.* 59: 786-792.

Bower, C., Gallegos, C., Mackley, M.R., & Madiedo, J.M. 1999. The rheological and microstructural characterization of the non-linear flow behaviour of concentrated oil-in-water emulsions. *Rheol. Acta* 38: 145-159.

Brakke, K. 1992. The surface evolver. *Exp. Math.* 1: 141-165.

Buzza, D.M.A., & Cates, M.E. 1993. Osmotic pressure of dense emulsion systems: the role of double-layer forces. *Langmuir* 9: 2264-2269.

Buzza, D.M.A., & Cates, M.E. 1994. Uniaxial elastic modulus of concentrated emulsions. *Langmuir* 10: 4503-4508

Buzza, D.M.A., Lu, C.-Y. D., & Cates, M.E. 1995. Linear shear rheology of incompressible foams. *J. Phys. France II* 5: 37-52.

Carnahan, N.F., & Starling, K.E. 1969. Equation of state for nonattracting rigid spheres. *J. Chem. Phys.* 51: 635-636.

Cates, M.E., & Sollich, P. 2004. Tensorial constitutive models for disordered foams, dense emulsions, and other soft nonergodic materials. *J. Rheol.* 48: 193-207.

Chattopadhyay, A.K. 1990. Water-in-oil emulsion explosive. US patent, 4,919,179.

Costello, B. 2008. Interfacial properties of surfactants used in explosive emulsions, Unpublished internal report to "African Explosive Limited" company.

Coussot, P., Nguyen, Q.D., Huynh, H.T., & Bonn, D. 2002. Viscosity bifurcation in thixotropic, yielding fluids. *J. Rheol.* 46: 573-589.

da Silva, G., Dlugogorski, B.Z., & Kenn, E.M. 2006. Water-in-oil emulsion foaming by thiourea nitrosation: reaction and mass transfer. *AIChE J.* 52: 1558-1565.

Danov, K.D., Petsev, D.N., Denkov, N.D., & Borwankar, R. 1993. Pair Interactions between Deformable Drops and Bubbles. *J. Chem. Phys.* 99: 7179-7189.

Davies, J.T. 1957. A quantitative kinetic theory of emulsion type. i physical chemistry of the emulsifying agent. In gas/liquid and liquid/liquid interfaces. *Proceedings of the 2nd International Congress on Surface Activity,* Vol. 1, London: Butterworths, 426-438.

de Gennes, P.G. 1987. Polymer at interface: a simplified view. *Adv. Colloid Interface Sci.* 27: 189-209.

Denkov, N.D., Petsev, D.N., &Danov, K.D. 1993. Interaction between deformable Brownian droplets. *Phys. Rev. Lett.* 71: 3226-3229.

Denkov, N.D., Petsev, D.N., & Danov, K.D. 1995. Flocculation of deformable emulsion droplets: I. droplet shape and line tension effects. *J. Colloid and Interface Sci.* 176: 189-200.

Derjaguin, B.V. 1989. *Theory of Stability of Colloids and Thin Liquid Films.* New York, Plenum Press, Consultants Bureau.

Dickinson, E. 1989. Food colloids – an overview. *Colloids Surface* 42; 191-204.

Dimitrova, T.D., & Leal-Calderon, F. 2001. Bulk elasticity of concentrated protein-stabilized emulsions, *Langmuir* 17: 3235-3244.

Dimitrova, T.D., & Leal-Calderon, F. 2004. Rheological properties of highly concentrated protein-stabilized emulsion. *Adv. Colloid Interface Sci.* 108–109: 49-61.

Dolan, A.K., & Edwards, S.F. 1975. The effect of excluded volume on polymer dispersant action, *Proc. R. Soc. London A* 343: 427-442.

Durian, D.J. 1995. Foam mechanics at the bubble scale. *Phys. Rev. Lett.* 75: 4780-4783.

Durian, D.J. 1997. Bubble scale model of foam mechanics: melting, non-linear behavior and avalanches. *Phys. Rev. E* 55: 1739-1751.

Durian, D.J. 2002. The Physics of foam. Boulder School for Condensed Matter and Materials Physics, July 1-26, 2002. www.lps.u-psud.fr/IMG/ppt/_2_structure.ppt. [Downloaded 25 September 2007].

Finkle, P., Draper, H.P., & Hildebrand, J.H. 1923. The theory of emulsification. *J. Am. Chem. Soc.* 45: 2780-2788.

Floury, J., Desrumaux, A., & Lardiéres, J. 2000. Effect of high-pressure homogenization on droplet size distribution and rheological properties of model oil-in-water emulsions, *Innovative Food Sci. Emerging Technol.* 1: 127-134.

Franco, J.M., Guerrero, A., & Gallegos, C. 1995. Rheology and processing of salad dressing emulsions. *Rheol. Acta* 34: 513-524.

Franco, J.M., Berjano, M., & Gallegos, C. 1997. Linear viscoelastisity of salad dressing emulsions. *J. Agric. Food Chem.* 45: 713-719.

Franco, J.M., Gallegos, C., & Barnes, H.A. 1998. On slip effects in steady-state flow measurements of oil-in-water food emulsions. *J. Food Eng.* 36: 89-102.

Fuchs, M., & Cates, M.E. 2002. Theory of nonlinear rheology and yielding of dense colloidal suspensions. *Phys. Rev. Lett.* 89: art. no-248304.

Gallegos, C., Berjano, M., & Choplin, L. 1992. Linear viscoelastic behavior of commercial and model mayonnaise. *J. Rheol.* 36: 465-478.

Ganguly, S., Krishna Mohan, V., Bhasu, V.C.J., Mathews, E., Adiseshaiah, K.S., & Kumar, A.S. 1992. Surfactant–electrolyte interactions in concentrated water-in-oil emulsions: FT-IR spectroscopic and low-temperature differential scanning calorimetric studies. *Colloid and Surfaces* 65: 243-256.

Gardiner, B.S., Dlugogorski, B.Z., & Jameson, G.J. 2000. The steady shear of three-dimensional wet polydisperse foams. *J. Non-Newtonian Fluid Mech.* 92: 151-166.

Gibbs, J.W. 1931. Collected Works. vol. 1, New York: Longmans, Green and Co.

Grassi, M., Lapasin, R., & Pricl, S. 1996. A study of the rheological behaviour of scleroglucan weak gel systems. *Carbohydrate Polymers* 29: 169-181.

Griffin, J. 1954. Calculation of HLB values of non-ionic surfactants, *J. Soc. Cosmet. Chem.* 5: 249-256.

Guerrero, A., Partal, P., Berjano, M., & Gallegos, C. 1996. Linear viscoelasticity of o/w sucrose palmitate emulsions. *Prog. Colloid Ploym. Sci.* 100: 246-251.

Guerrero, A., Partal, P., & Gallegos, C. 1998. Linear viscoelastic properties of sucrose ester-stabilized oil-in-water emulsions. *J. Rheol.* 42: 1375-1388.

Hales, T.C. 2001. The honeycomb conjecture. *Discrete & Computational Geometry* 25: 1-22.

Hales, R.H., Cranney, D.H., Hurley, E.K., & Preston, S.B. 2004. Emulsion phase having improved stability. US Patent 6,808,573 B2.

Hamaker, H.C. 1937. The london-van der walls attraction between spherical particles. *Physics* 4: 1058-1072.

Hébraud, P., & Lequeux, F. 1998. Mode-coupling theory for the pasty rheology of soft glassy materials. *Phys. Rev. Lett.* 81: 2934-2937.

Hemar, Y., & Horne, D.S. 2000. Dynamic rheological properties of highly concentrated protein-satbilized emulsions. *Langmuir* 16: 3050-3057.

Heymann, L., Peukert, S., Aksel, N. 2002. On the solid-liquid transition of concentrated suspensions in transient shear flow, *Rheol. Acta* 41: 307-315.

Hsu, M.F., Dufresne, E.R., & Weitz, D.A. 2005. Charge stabilization in nonpolar solvents, *Langmuir* 21: 4881-4887

Hutzler, S., Weaire, D., Bolton, F. 1995. The effects of plateau borders in the two-dimensional soap froth. 3. Further results. *Philosophical Magazine B* 71: 277-289.

Israelachvili, J. N. 1992. *Intermolecular and Surface Forces*. London, Academic Press.

Jager-Lézer, N., Tranchant, J.-F., Alard, V., Vu, C., Tchoreloff, P.C., & Grossiord, J.-L. 1998. Rheological analysis of highly concentrated w/o emulsions, *Rheol. Acta* 37: 129-138.

Khan, S.A., & Armstrong R.C. 1986. Rheology of foams .1. Theory for dry foams. *J. Non-Newton. Fluid Mech.* 22: 1-22.

Khan, S.A., & Armstrong R.C. 1987. Rheology of foams .2. Effects of polydispersity and liquid viscosity for foams having gas fraction approaching unity. *J. Non-Newton. Fluid Mech.* 25: 61-92.

Khan, S.A., Schnepper, C.A., & Armstrong R.C. 1988. Rheology of foams .3. Measurement of shear flow properties. *J. Rheol.* 32: 69-92.

Khan, S.A., & Armstrong R.C. 1989. Rheology of foams .4. Effects of gas volume fraction. *J. Rheol.* 33: 881-911.

Kharatiyan, E. 2005. *Time effects in evolution of structure and rheology of highly concentrated emulsion*. Doctoral thesis, Cape Peninsula University of Technology, Cape Town, South Africa.

Kralchevsky, P.A., & Denkov, N.D. 1995. Analytical expression for the oscillatory structural surface force, *Chem. Phys. Lett.* 240: 385-392.

Kralchevsky, P.A., Danov, K.D., & Denkov, N.D. 2003. Chemical Physics of Colloid Systems and Interfaces, in Bridi, K.S. (ed.). *Handbook of Colloid and Surface Chemistry*, 2nd Ed., CRC Press.

Kraynik, A., 1988. Foams flows. *Ann. Rev. Fluid Mech.* 20: 325-357

Kraynik, A.M., Reinlet, D.A., & Princen, H.M. 1991. The non-linear elastic behavior of polydisperse hexagonal foams and concentrated emulsions. *J. Rheol.* 35: 1235-1253.

Lacasse, M.-D., Grest, G.S., & Levine, D. 1996a. Deformation of small compressed droplets. *Phys. Rev. E* 54: 5436-5446.

Lacasse, M.-D., Grest, G.S., Levine, D., Mason, T.G., & Weitz, D. A. 1996b. Model for the elasticity of compressed emulsions. *Phys. Rev. Lett.* 76: 3448-3451.

Landau, L.D., & Lifshitz, E.M. 1986. Theory of elasticity, Oxford: Pergamon Press.

Langenfeld, A., Schmitt, V., & Stébé, M.J. 1999. Rheological behaviour of fluorinated highly concentrated reverse emulsions with temperature. *J. Colloid Interface Sci.* 218: 522-528.

Langenfeld, A., & Stébé, M.J. 2002. Effect of physico-chemical parameters on rheological properties of concentrated reverse emulsions. *Phys. Chem. Chem. Phys.* 4: 322-527.

Leal Calderon, F., Stora, T., Mondain Monval, O., Poulin, P., & Bibette, J. 1994. Direct measurement of colloidal forces. *Phys. Rev. Lett.* 72: 2959-2962.

Leal-Calderon, F., Schmitt, V., & Bibette, J. 2007. *Emulsion Science, Basic Principles*, 2nd ed., New York: Springer.

Lemaître, A. 2002. Origin of a repose angle: kinetics of rearrangement for granular materials. *Phys. Rev. Lett.* 89: art. no-064303.

Lifshitz, E.M. 1956. The theory of molecular attractive forces between solids. *Soviet Phys. JETP* (Engl. Transl.) 2: 73-83.

Lissant, K.J. 1966. The geometry of high-internal-phase-ratio emulsions. *J. Colloid Interface Sci.* 22: 462-468.

Lissant, K.J., Peace, B.W., Wu, S.H., & Mayhan, K.G. 1974. Structure of high-internal-phase-ratio emulsions. *J. Colloid Interface Sci.* 47: 416-423.

Liu, A. J., Ramaswamy, S., Mason, T. G., Gang, H., & Weitz, D. A. 1996. Anomalous viscous loss in emulsions. *Phys. Rev. Lett.* 76: 3017-3020.

Lubachevsky, B. D., & Stillinger, F.H. 1990. Geometric properties of random disk packings. *J. Stat. Phys.* 60: 561-583.

Macosko, C.W. 1994. Rheology: principles, measurements, and applications. New York: Wiley-VCH Inc.

Madiedo, J.M., & Gallegos, C. 1997. Rheological characterization of oil-in-water emulsions by means of relaxation and retardation spectra. *Recent Res. Dev. Oil Chem.* 1: 79-90.

Malkin A.Ya. 1990. Rheology of filled polymers. *Adv. Polym. Sci.* 96: 69-97.

Malkin, A.Ya., Masalova, I., Slatter, P., & Wilson, K. 2004a. Effect of droplet sizes on the rheological properties of highly concentrated w/o emulsions. *Rheol. Acta* 43: 584-591.

Malkin, A.Ya., Masalova, I., Pavlovsli, D., & Slatter, P. 2004b. Is the choice of flow curve fitting equation crucial for the estimation of pumping characteristics? *Appl. Rheol.* 14: 89-95.

Malkin, A.Ya., & Masalova, I. 2005. Rheology of super-concentrated emulsions. Luo, Y., Rao, Q. & Xu, Y. (eds.). *Advances in rheology and its applications*, Science Press USA Inc.: 5-12.

Malkin, A.Ya., & Isayev, A. 2006. *Rheology. Concepts, Methods, Applications*. Toronto: ChemTec Publication.

Malkin, A.Ya., & Masalova, I. 2007. Shear and normal stresses in flow of highly concentrated emulsions. *J Non-Newton Fluid Mech.*147: 65-68.

Manca, S., Lapasin, R., Partal, P., & Gallegos, C. 2001. Influence of surfactant addition on the rheological properties of aqueous Welan matrices. *Rheol. Acta* 40: 128-134.

Masalova, I., Malkin, A.Ya., Slatter, P., & Wilson, K. 2003. The rheological characterization and pipeline flow of high concentrated water-in-oil emulsions. *J. Non-Newt. Fluid Mech.* 112: 101-114.

Masalova, I., Taylor, M., Kharatiyan, E., & Malkin, A.Ya. 2005. Rheopexy of highly-concentrated emulsions. *J. Rheol.* 49: 839-849.

Masalova, I., Malkin, A.Ya., Kharatiya, E., Taylor, M., & Haldenwang, R. 2006a. Evolution of rheological properties of highly-concentrated emulsions in aging – emulsion-to-suspension transition. *J. Rheol.* 50: 435-451.

Masalova, I.., Malkin, A.Ya., Kharatiyan, E., & Haldenwang, R. 2006b. Scaling in pipeline flow of kaolin suspensions. *J. Non-Newton. Fluid Mech.* 136: 76-78.

Masalova, I., & Malkin, A.Ya. 2007a. Rheology of highly concentrated emulsions - concentration and droplet size dependencies. *Appl. Rheol.* 17: 42250(1-9).

Masalova, I., & Malkin, A.Ya. 2007b. Peculiarities of rheological properties and flow of highly concentrated emulsions - The role of concentration and droplet size. *Colloid J.* 69: 185-197.

Masalova, I., & Malkin, A.Ya. 2007c. A New Mechanism of Aging of Highly Concentrated Emulsions - Correlation between Crystallization and Plasticity. *Colloid J.* 69: 198-202.

Mason, T.G. 1995. *Rheology of monodisperse emulsions*. PhD dissertation, Princeton university, USA.

Mason, T.G., Bibette, J., & Weitz, D.A. 1995. Elasticity of compressed emulsions. *Phys. Rev. Lett.* 75: 2051-2054.

Mason, T.G., Bibette, J., & Weitz, D.F. 1996. Yielding and flow of monodisperse emulsions. *J. Colloid Interface Sci.* 179: 439-448.

Mason, T.G., & Bibette, J. 1996. Emulsification in viscoelastic media. *Phys. Rev. Lett.* 77: 3481-3484.

Mason, T.G., Lacasse, M.-D., Grest, G.S., Levine, D., Bibette, J., & Weitz, D. A. 1997. Osmotic pressure and viscoelastic shear moduli of compressed emulsions. *Phys. Rev. E* 56: 3150-3166.

Mason, T.G. 1999. New fundamental concepts in emulsion rheology. *Curr. Opin. Colloid Interface Sci.* 4: 231-238.

McClements, D.J. 1999. *Food Emulsion: Principles, Practice, and Techniques*. CRC Press LLC.

McGlashan, M.L. 1979. *Chemical Thermodynamics*. New York: Academic Press.

Meeker, S.P., Bonnecaze, R.T., & Cloitre, M. 2004. Slip and flow in pastes of soft particles: direct observation and rheology. *J. Rheol.* 48: 1295-1320.

Meeten, G.H. 2004. Squeeze flow of soft solids between rough surfaces. *Rheol. Acta* 43: 6-16.

Mittal, K.L. 1975. Ultracentrifugal Technique in the Study of Emulsions, *Colloidal Dispersions and Micellar Behavior*, Chapter 5: 76-96.

Moan, M., Aubry, T., & Bossard, F. 2003. Non-linear behaviour of very concentrated suspensions of platelike kaolin particles in shear flow. *J. Rheol.* 47: 1493-1504.

Morse, D.C., & Witten, T.A. 2003. Droplet elasticity in weakly compressed emulsions. *Europhys. Lett.* 22: 549-555.

Mougel, J., Alvarez, O., Baravian, C., Caton, F., Marchal, P., & Stébé, M.J. 2006. Aging of an unstable w/o emulsion with nonionic surfactant. *Rheol. Acta* 45, 555-560.

Myers, D. 2006. *Surfactant science and technology*. 3rd ed. Hoboken, New Jersey: John Wiley & Sons, Inc.

Nguyen, O.D., & Boger, D.V. 1992. Measuring the flow properties of yield stress fluids. *Ann. Rev. Fluid Mech.* 24: 47-88.

Nixon, J., & Beerbower, A. 1969. Properties of high-internal-phase emulsions: Part I, effect of emulsifier parameters. *American Chemical Society, Division of Petroleum Chemistry, Preprints* 14: 49-59.

Otsubo, Y., & Prud'homme, R.K. 1994a. Rheology of oil-in-water emulsions. *Rheol. Acta* 33: 29-37.

Otsubo, Y., & Prud'homme, R.K. 1994b. Effect of drop size on the flow behavior of oil-in-water emulsions. *Rheol. Acta* 33: 303-306.

Pal, R. 1996. Effect of droplet size on the rheology of emulsions. *AIChE J.* 42: 3181-3190.

Pal, R. 2006. Rheology of high internal phase ratio emulsions. *Food Hydrocolloids* 20: 997-1005.

Partal, P., Guerrero, A., Berjano, M., & Gallegos, C. 1997 .Influence of concentration and temperature on the flow behavior of oil-in-water emulsions stabilized by sucrose palmitate. *J. Am. Oil Chem. Soc.* 74: 1203-1212.

Perrin, P. 2000. Droplet-droplet interactions in both direct and inverse emulsions stabilized by a balanced amphiphilic polyelectrolyte. *Langmuir* 16: 881-884.

Petsev, D.N., & Bibette, J. 1995. Stability of osmotically compressed emulsions, *Langmuir* 11: 1075-1077.

Petsev, D.N., Denkov, N.D., & Kralchevsky, P.A. 1995. Flocculation of deformable emulsion droplets: Ii. Interaction energy. *J. Colloid Interface Sci.* 176: 201-213.

Petsev D.N., & Linse, P. 1997. Statistical mechanical properties of dense emulsions and microemulsions. *Phys. Rev. E* 55: 586-591.

Pickering, S.U. 1907. Emulsions. *J. Chem. Soc., Trans.* 91, 2001-2021.

Plateau, J.A.F. 1873. *Statique expérimentale et théorique des liquides soumis aux seules forces molécularies*. Paris: Gauthier-Villars.

Plucinski, S., Gupta, R.K., & Chakrabarti, S. 1998. Wall slip of mayonnaises in viscometers, *Rheol. Acta* 37: 256-269.

Pons, R., Solans, C., Stébé, M.J., Erra, P., & Ravey, J.C. 1992. Stability and rheological properties of gel emulsions. *Prog. Colloid Polym. Sci.* 89: 110-113.

Pons, R., Solans, C., & Tadros, Th.F. 1995. Rheological behaviour of highly concentrated oil-in-water (o/w) emulsions. *Langmuir* 11: 1966-1971.

Ponton, A., Clement, P., & Grossiord, J.L. 2001. Collaboration of Princen's theory to cosmetic concentrated water-in-oil emulsions. *J. Rheol.* 45: 521-526.

Princen, H.M. 1979. Highly concentrated emulsions .1. Cylindrical systems. *J. Colloid Interface Sci.* 71: 55-66.

Princen, H.M., Aronson, M.P., & Moser, J.C. 1980. Highly concentrated emulsions .2. Real systems: the effect of film thickness and contact angle on the volume fraction in creamed emulsions. *J. Colloid Interface Sci.* 75: 246-270.

Princen, H.M. 1983. Rheology of foams and highly concentrated emulsions .1. Elastic properties and yield stress of a cylindrical model system. *J. Colloid Interface Sci.* 91: 160-171.

Princen, H.M. 1985. Rheology of foams and highly concentrated emulsions .2. Experimental study of the yield stress and wall effects for concentrated oil-in-water emulsions. *J. Colloid Interface Sci.* 105: 150-171.

Princen, H.M., & Kiss, A.D. 1986. Rheology of foams and highly concentrated emulsions .3. Static shear modulus. *J. Colloid Interface Sci.* 112: 427-437.

Princen, H.M. 1986. Osmotic pressure of foams and highly concentrated emulsions.1. Theoretical consideration. *Langmuir* 2: 519-524.

Princen, H.M., & Kiss, A.D. 1987. Osmotic pressure of foams and highly concentrated emulsions .2. Determination from the variation in volume fraction with height in an equilibrated column. *Langmuir* 3: 36-41.

Princen, H.M., & Kiss, A.D. 1989. Rheology of foams and highly concentrated emulsions .4. An experimental study of the shear viscosity and yield stress of concentrated emulsions. *J. Colloid Interface Sci.* 128: 176-187.

Reinelt, D.A., & Kraynik, A.M. 1990. On the shearing flow of foams and concentrated emulsions. *J. Fluid Mech.* 215: 431-455.

Reinlet, D., & Kraynik, A. 1996. Simple shearing flow of a dry Kelvin soap film. *J. Fluid Mech.* 311: 327-343.

Reiner, M. 1958. in *Handbuch Der Physik*. Vol. 6. Elastizität und Plastizität, Berlin: Springer.

Reynolds, P.A., Gilbert, E.P., & White, J.W. 2000. High internal phase water-in-oil emulsions studied by small-angle neutron scattering. *J. Phys. Chem. B* 104: 7012-7022.

Reynolds, P.A., Gilbert, E.P., & White, J.W. 2001. High internal phase water-in-oil emulsions and related microemulsions studied by small angle neutron scattering. 2. The Distribution of Surfactant. *J. Phys. Chem. B* 105: 6925-6932.

Reynolds, P.A., McGillivray, D.J., Gilbert, E.P., Holt, S.A., Henderson, M.J., & White, J.W. 2003. Neutron and X-ray reflectivity from polyisobutylene-based amphiphiles at the air-water interface. *Langmuir* 19: 752-761.

Rocca, S., & Stébé, M.J. 2000. Mixed concentrated water/oil emulsions (fluorinated/hydrogenated): Formulation, properties, and structural studies. *J. Phys. Chem. B* 104: 10490-10497.

Romero, A., Cordobés, F., Puppo, M.C., Guerrero, A., & Bengoechea, C. 2008. Rheology and droplet size distribution of emulsions stabilized by crayfish flour. *Food Hydrocolloids* 22: 1033-1043.

Russel, W.B., Saville, D.A., & Schowalter, W.R. 1989. *Colloidal Dispersions,* Cambridge: Cambridge University Press.

Saiki, Y., Horn, R.G., & Prestidge, C.A. 2008. Droplet structure instability in concentrated emulsions. *J. Colloid Interface Sci.* 320: 569-574.

Schlaepfer, A.U.M. 1918. Water-in-oil emulsions. *J. Chem. Soc.* 113: 522-526.

Seth, J.R., Cloitre, M., & Bonnecaze, R.T. 2006. Elastic properties of soft particle pastes. *J. Rheol.* 50: 353-376.

Sherman, P. (ed.). 1968. *Emulsion Science*. London: Academic Press.

Shinoda, K., & Friberg, S. 1986. *Emulsion and Solubilization*, New York: Wiley.

Sollich, P., Lequeux, F., Hebraud, P., & Cates, M. E. 1997. Rheology of soft glassy materials. *Phys. Rev. Lett.* 78: 2020-2023.

Sollich, P. 1998. Rheological constitutive equation for a model of soft glassy materials. *Phys. Rev. E* 58: 738-759.

Stokes, J.R., Telford, J.H., Williamson, A.-M. 2005. The flowability of ice suspensions, *J. Rheol.* 49: 139-148.

Tadros, Th.F. 1994. Fundamental principles of emulsion rheology and their applications. *Colloids Surf. A* 91: 38-55.

Tadros, Th.F. 2005. *Applied Surfactants: Principles and Applications*. Weinheim: WILEY-VCH Verlag GmbH & Co. KGaA.

Taylor, J.E. 1976. Structure of singularities in soap-bubble-like and soap-film-like minimal surfaces. *Ann. Math.* 103: 489-539.

Tewari, S., Schiemann, D., Durain, D.J, Knobler, C.M., Langer, S.A., & Liu, A.J. 1999. Statistics of shear-induced rearrangement in a two-dimensional model foam. *Phys. Rev. E* 60: 4385-4396.

Venter, P.N., & Kruger, F. 1996. Emulsifier, European Patent 0 718 033 A2.

Vinogradow, G.W., Pawlow, W.P. 1961. Elastische Strukturfestigkeit in plastisch-dispersen Systemen, *Rheol. Acta* 1: 455-470.

Walstra, P. 2003. *Physical chemistry of foods*. New York: Marcel Dekker.

Weaire, D., Fu, T.L., & Kermode J.P. 1986. On the shear elastic-constant of a 2-dimensional foam forth. *Philosophical Magazine B* 54: L39-L43.

Webber, R. M. 1999. Relation between Laplace pressure and the rheology of high internal phase emulsions, *Presented at the Spring Meeting AIChE*, Houston, TX: 228-232.

Windhab, E. 1993. Bericht: IV. Tagung Lebensmittel rheologie detmold.

Appendix A: Droplet Size Distribution Results

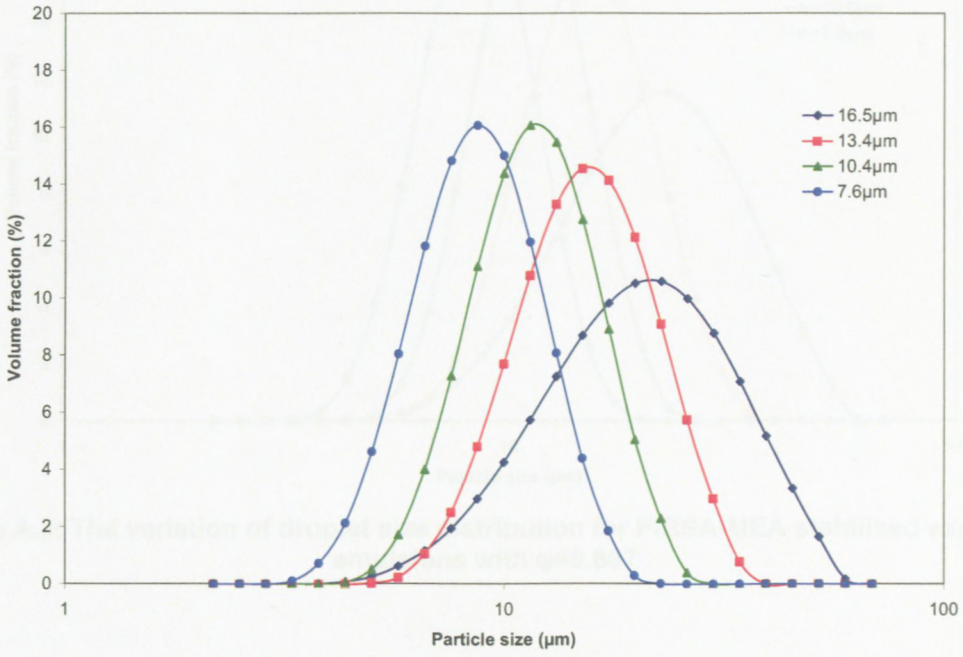

Figure A.1: The variation of droplet size distribution for PIBSA-MEA stabilised explosive emulsions with φ=0.868

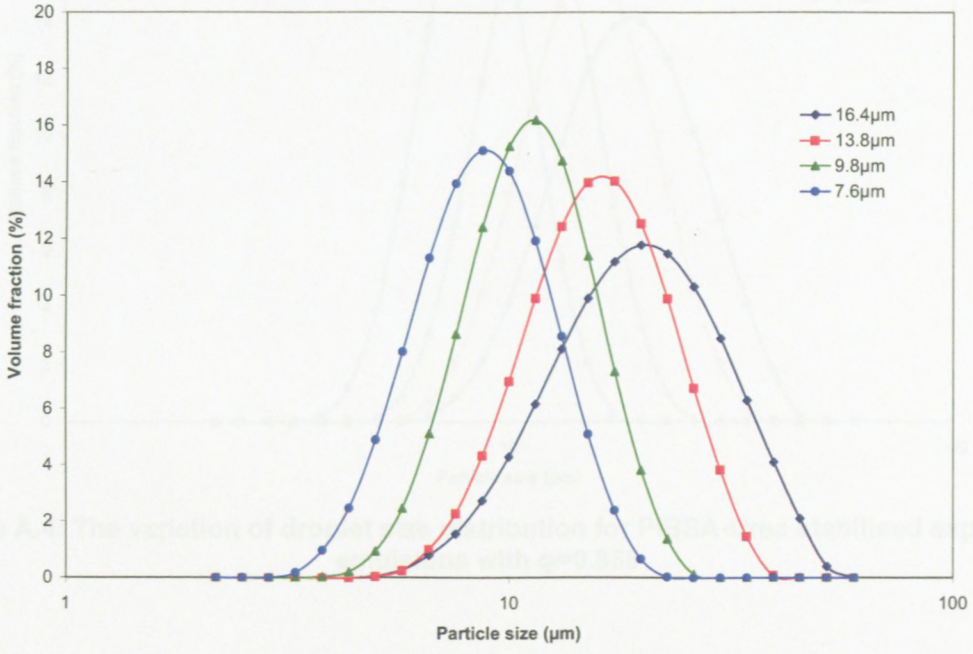

Figure A.2: The variation of droplet size distribution for PIBSA-MEA stabilised explosive emulsions with φ=0.837

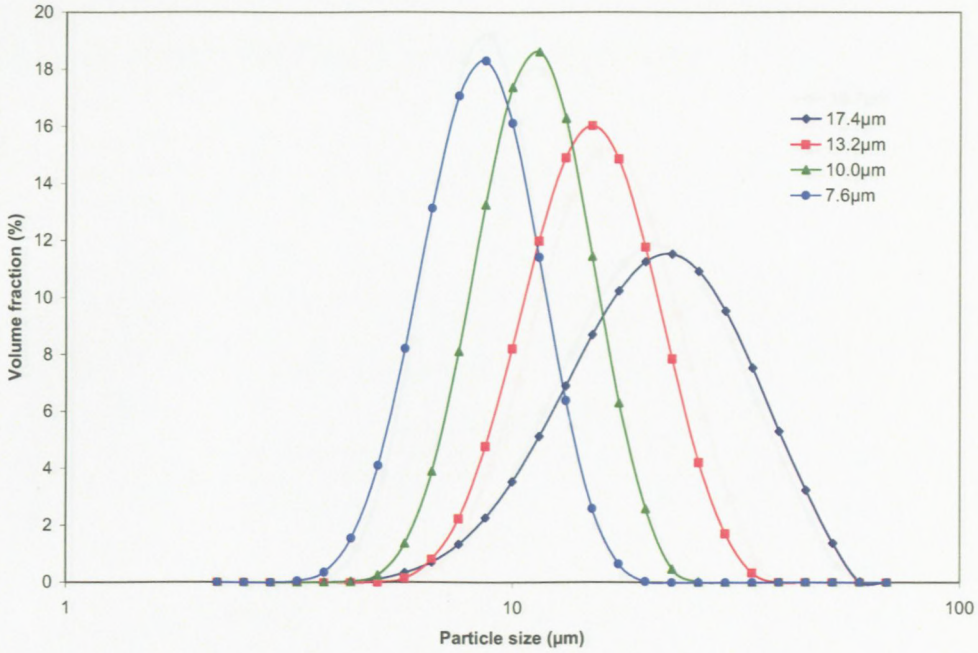

Figure A.3: The variation of droplet size distribution for PIBSA-MEA stabilised explosive emulsions with φ=0.807

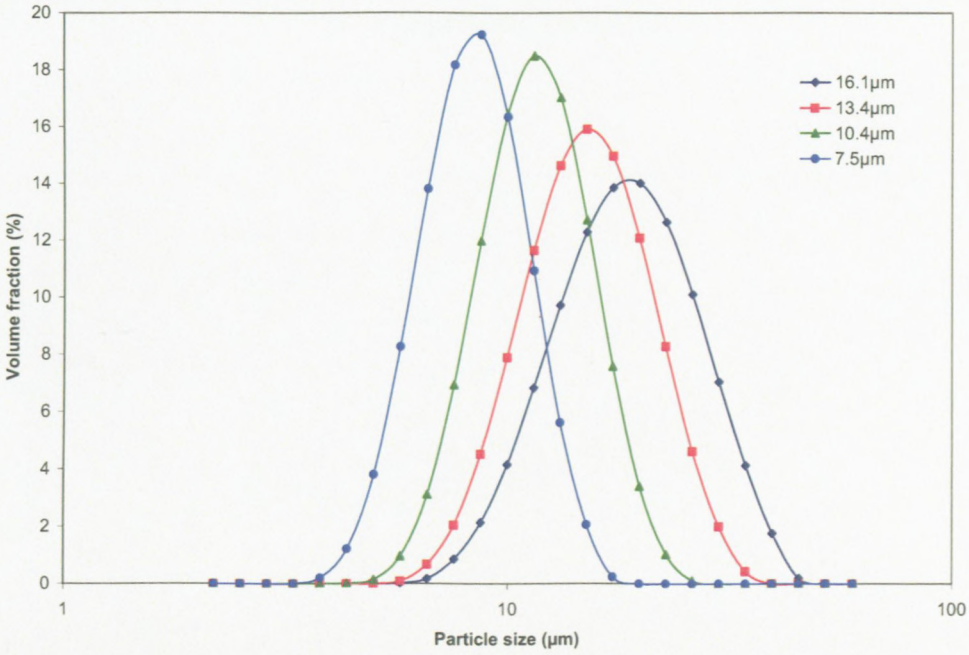

Figure A.4: The variation of droplet size distribution for PIBSA-Urea stabilised explosive emulsions with φ=0.868

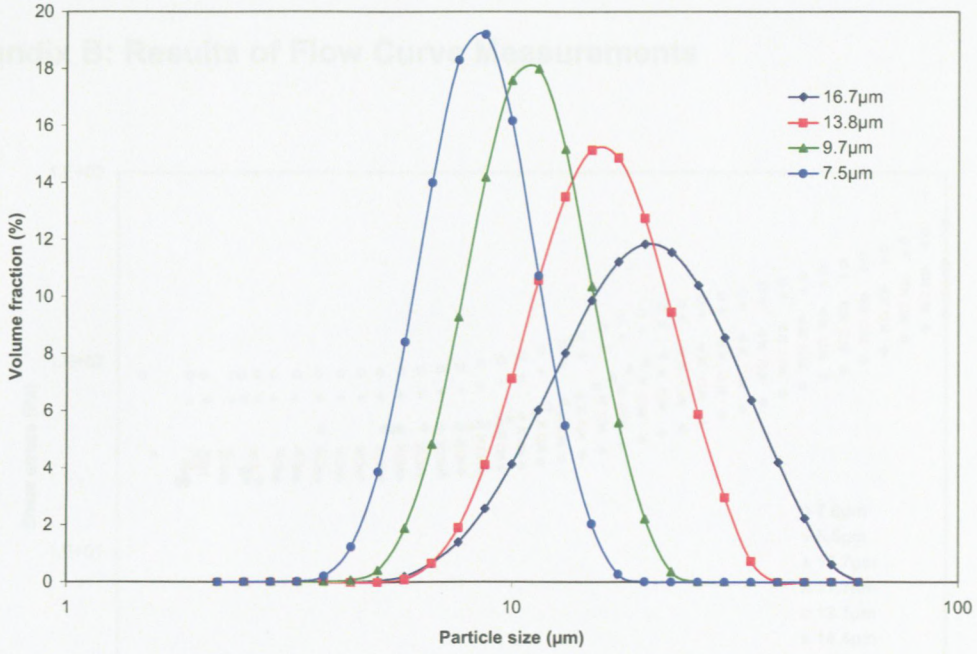

Figure A.5: The variation of droplet size distribution for PIBSA-imide stabilised explosive emulsions with φ=0.868

Appendix B: Results of Flow Curve Measurements

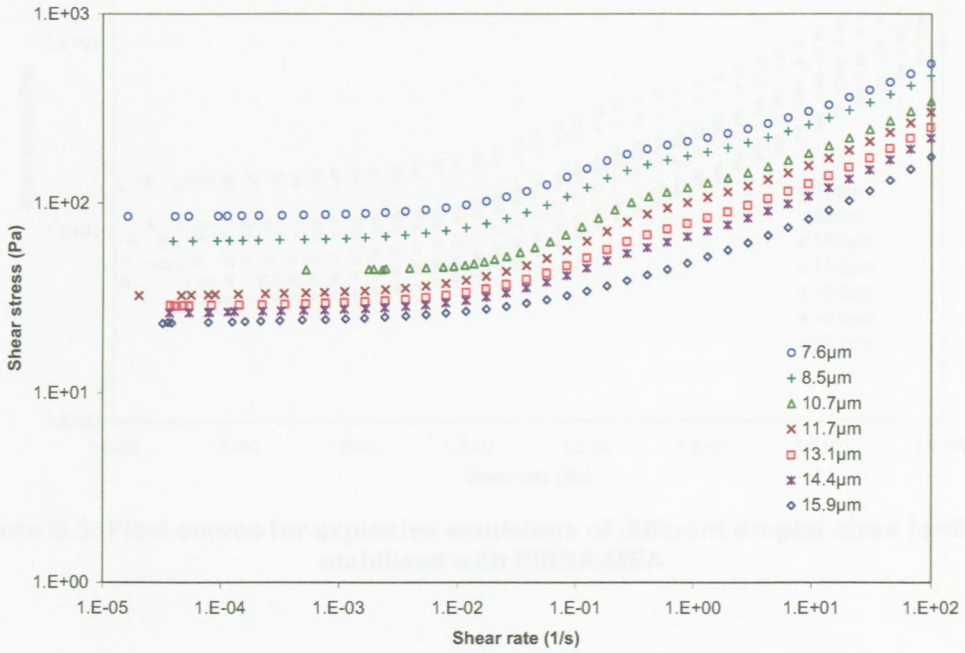

Figure B.1: Flow curves for explosive emulsions of different droplet sizes (φ=0.892) stabilised with PIBSA-MEA

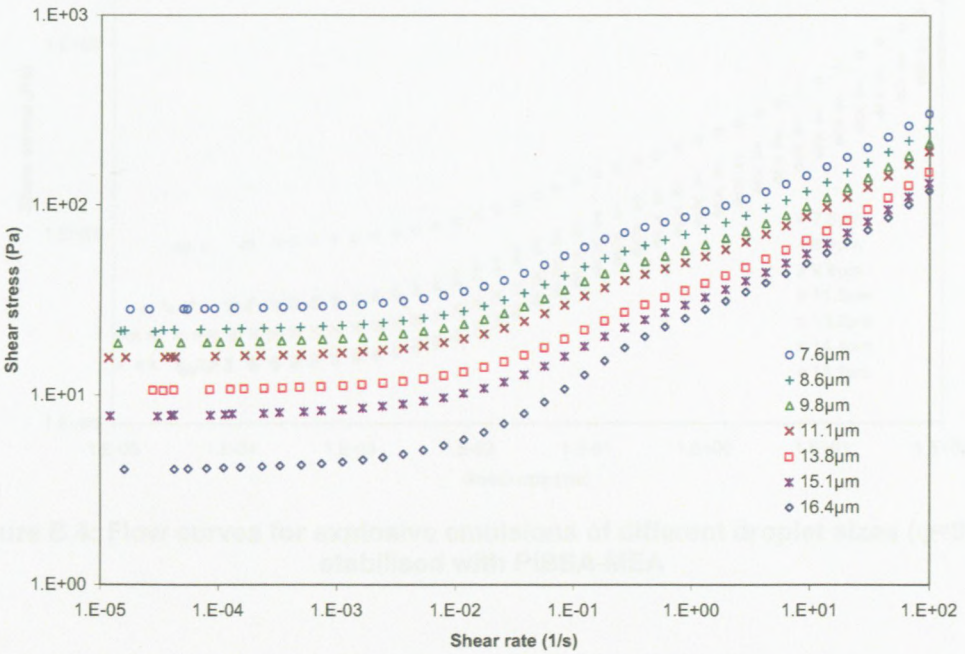

Figure B.2: Flow curves for explosive emulsions of different droplet sizes (φ=0.837) stabilised with PIBSA-MEA

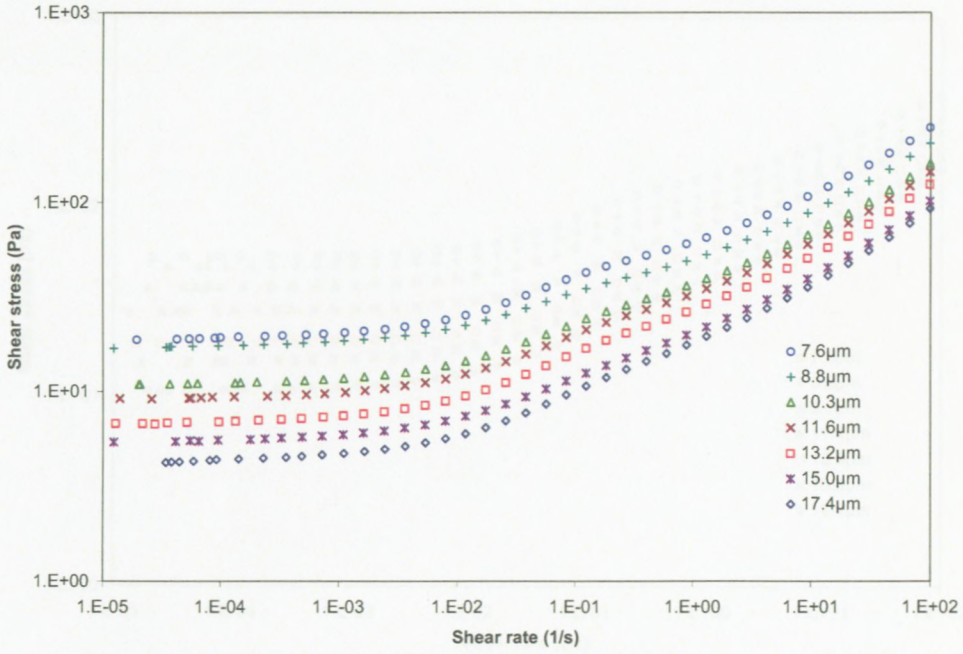

Figure B.3: Flow curves for explosive emulsions of different droplet sizes (φ=0.807) stabilised with PIBSA-MEA

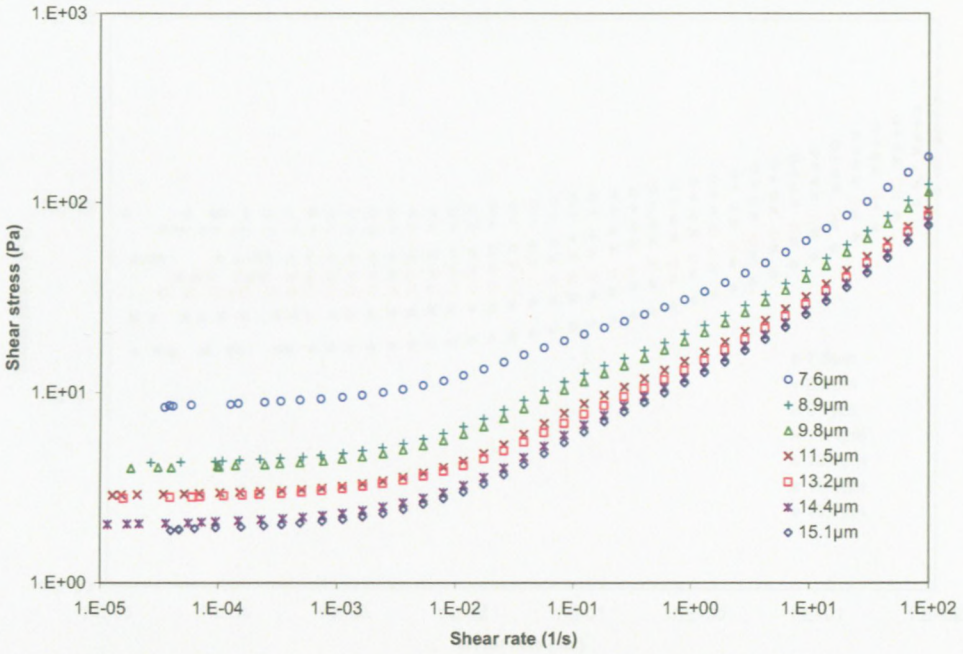

Figure B.4: Flow curves for explosive emulsions of different droplet sizes (φ=0.764) stabilised with PIBSA-MEA

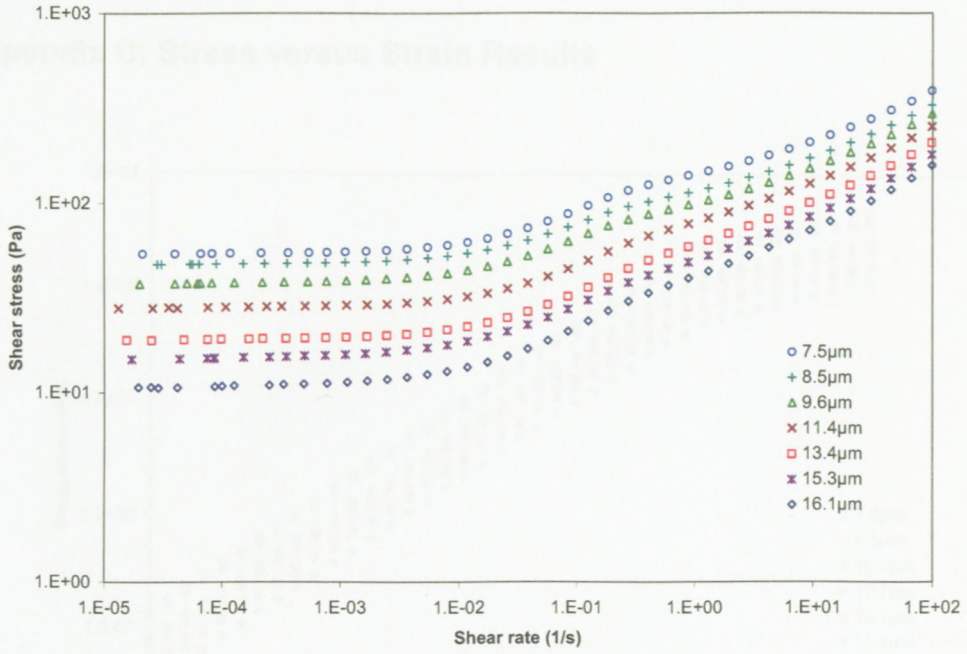

Figure B.5: Flow curves for explosive emulsions of different droplet sizes (φ=0.868) stabilised with PIBSA-Urea

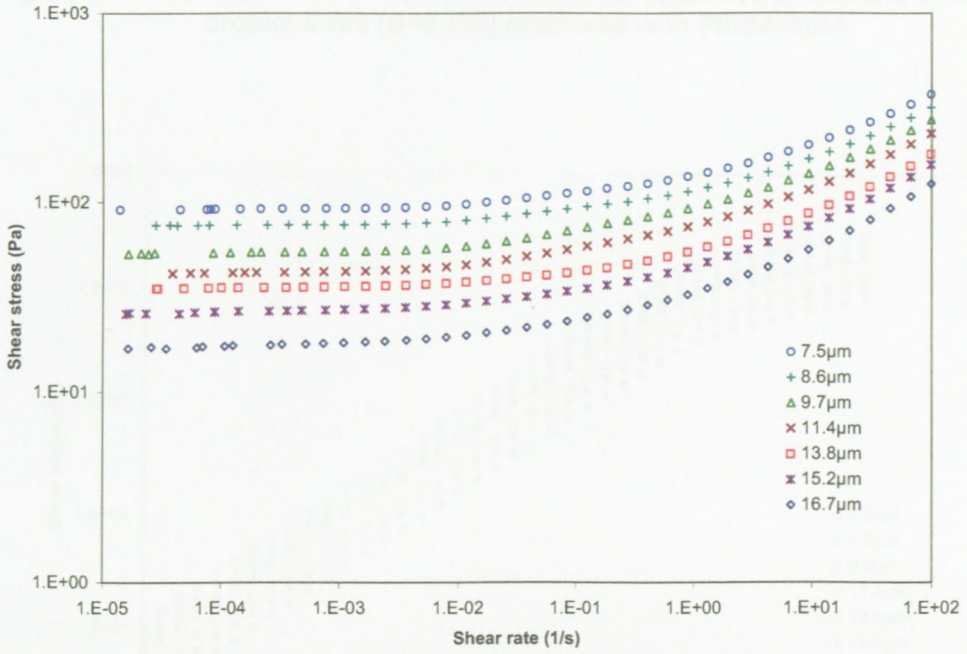

Figure B.6: Flow curves for explosive emulsions of different droplet sizes (φ=0.868) stabilised with PIBSA-Imide

Appendix C: Stress versus Strain Results

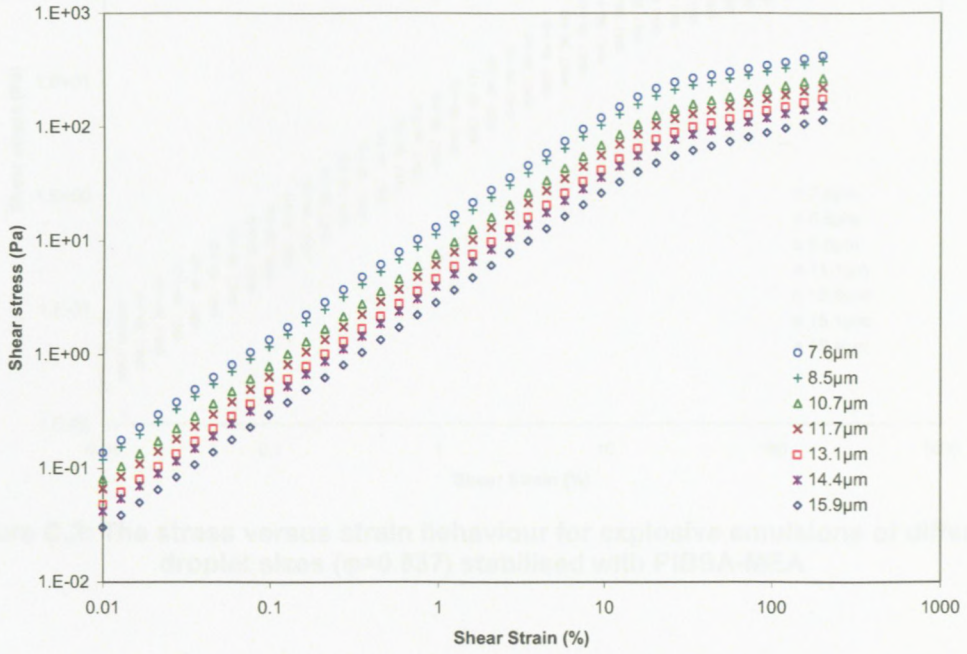

Figure C.1: The stress versus strain behaviour for explosive emulsions of different droplet sizes (φ=0.892) stabilised with PIBSA-MEA

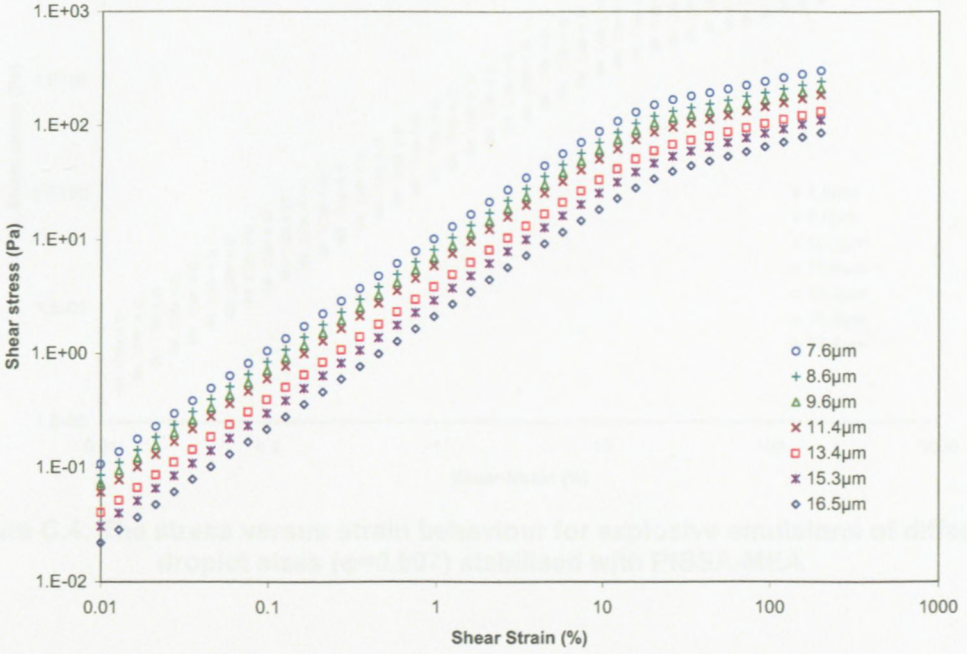

Figure C.2: The stress versus strain behaviour for explosive emulsions of different droplet sizes (φ=0.868) stabilised with PIBSA-MEA

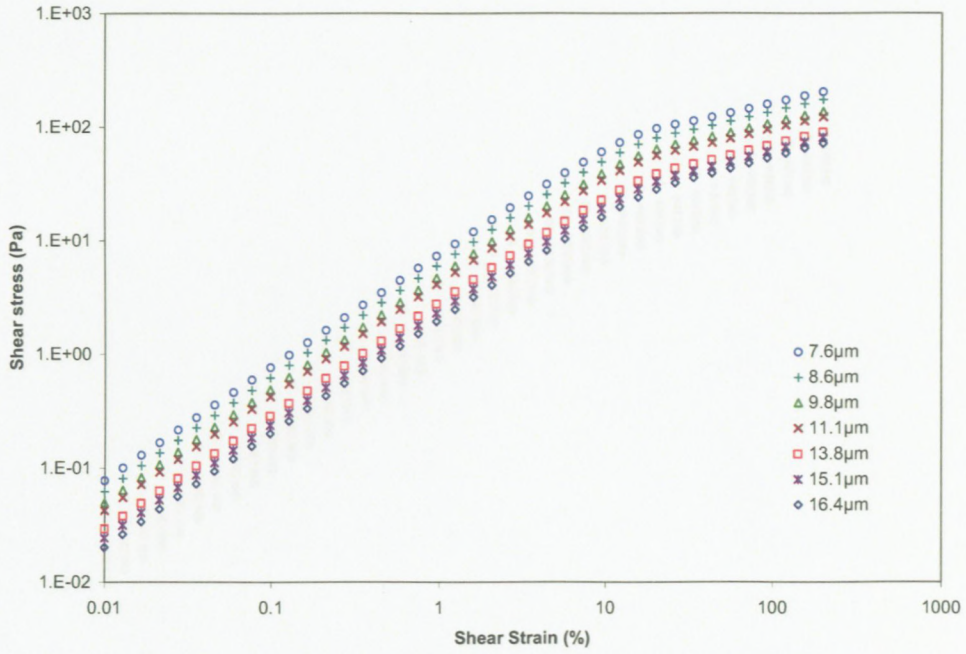

Figure C.3: The stress versus strain behaviour for explosive emulsions of different droplet sizes (φ=0.837) stabilised with PIBSA-MEA

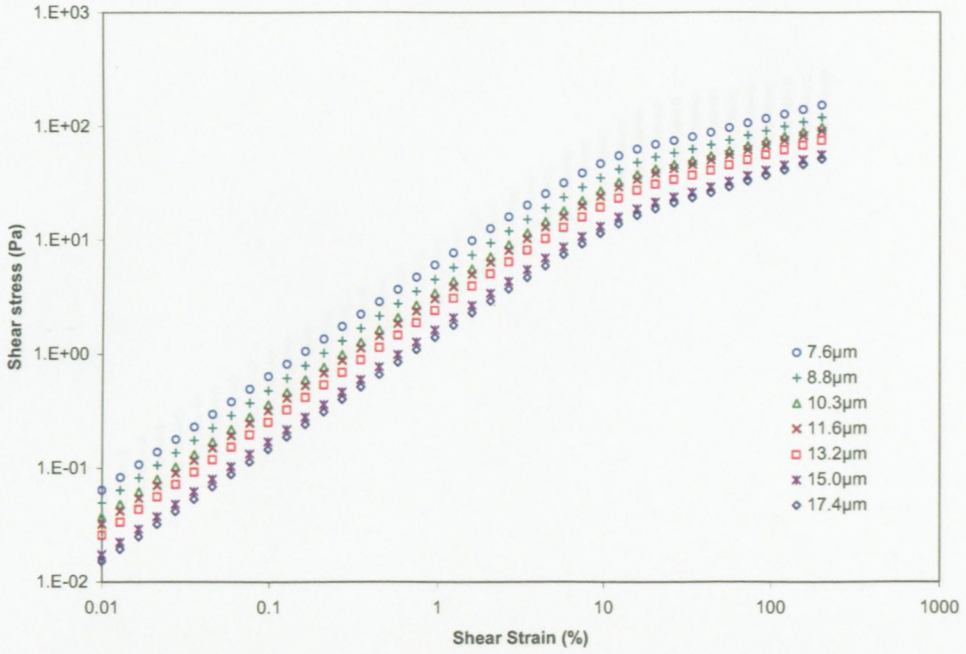

Figure C.4: The stress versus strain behaviour for explosive emulsions of different droplet sizes (φ=0.807) stabilised with PIBSA-MEA

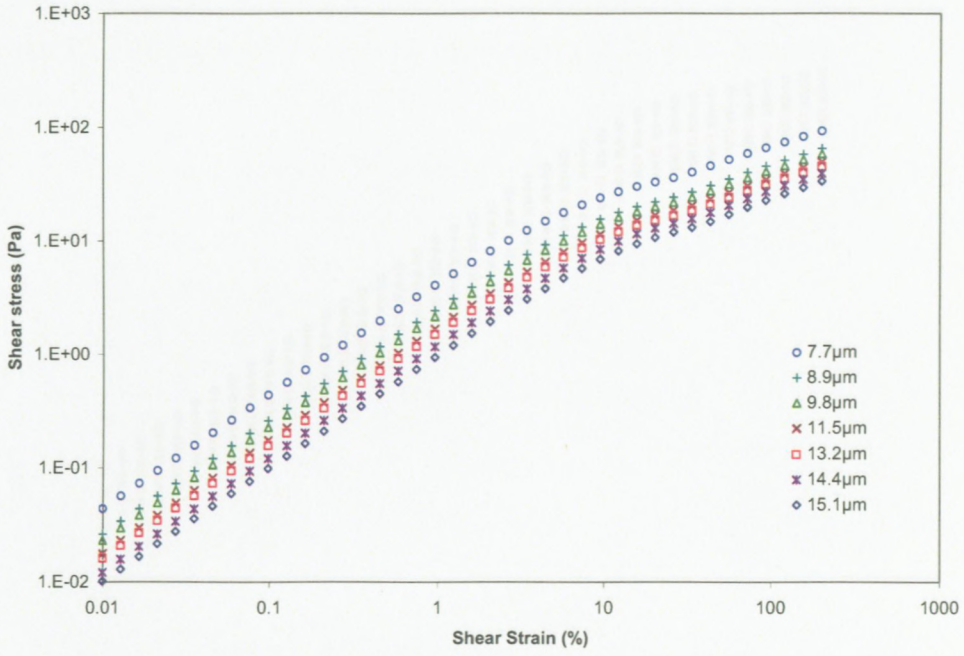

Figure C.5: The stress versus strain behaviour for explosive emulsions of different droplet sizes (φ=0.764) stabilised with PIBSA-MEA

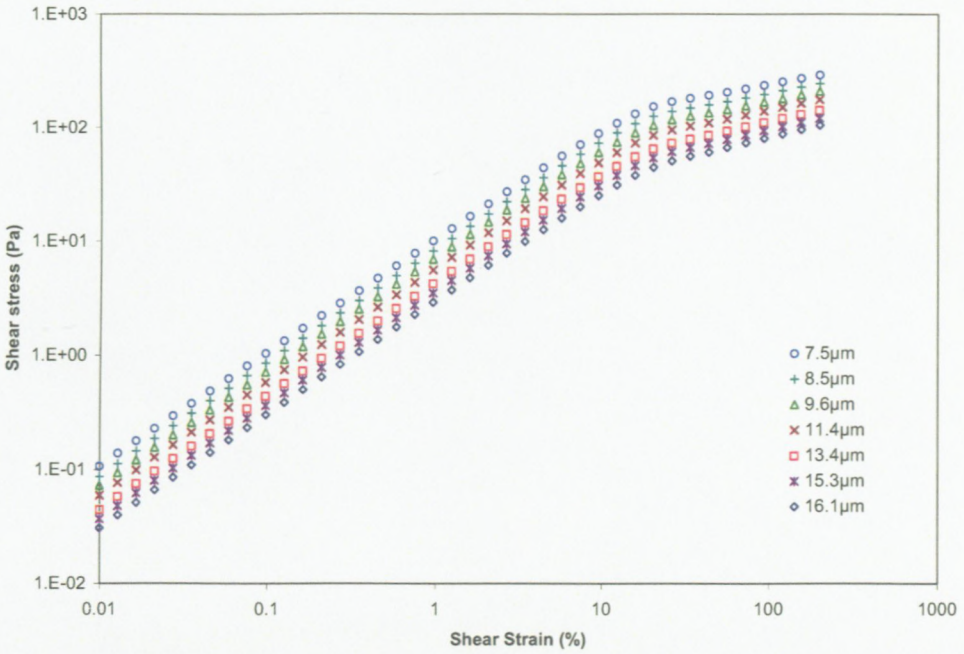

Figure C.6: The stress versus strain behaviour for explosive emulsions of different droplet sizes (φ=0.868) stabilised with PIBSA-Urea

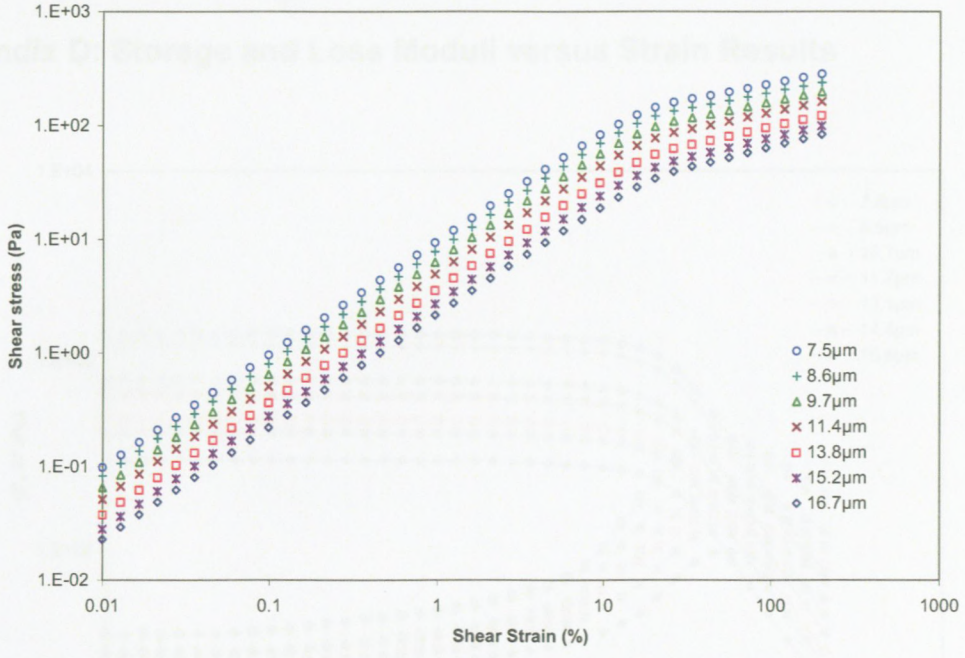

Figure C.7: The stress versus strain behaviour for explosive emulsions of different droplet sizes (φ=0.868) stabilised with PIBSA-Imide

Appendix D: Storage and Loss Moduli versus Strain Results

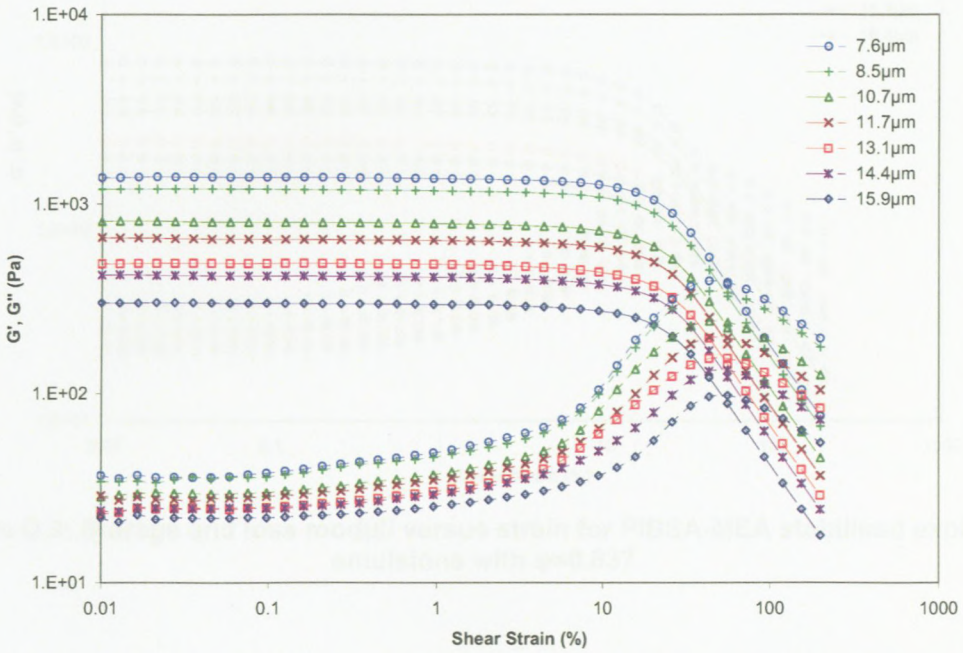

Figure D.1: Storage and loss moduli versus strain for PIBSA-MEA stabilised explosive emulsions with φ=0.892

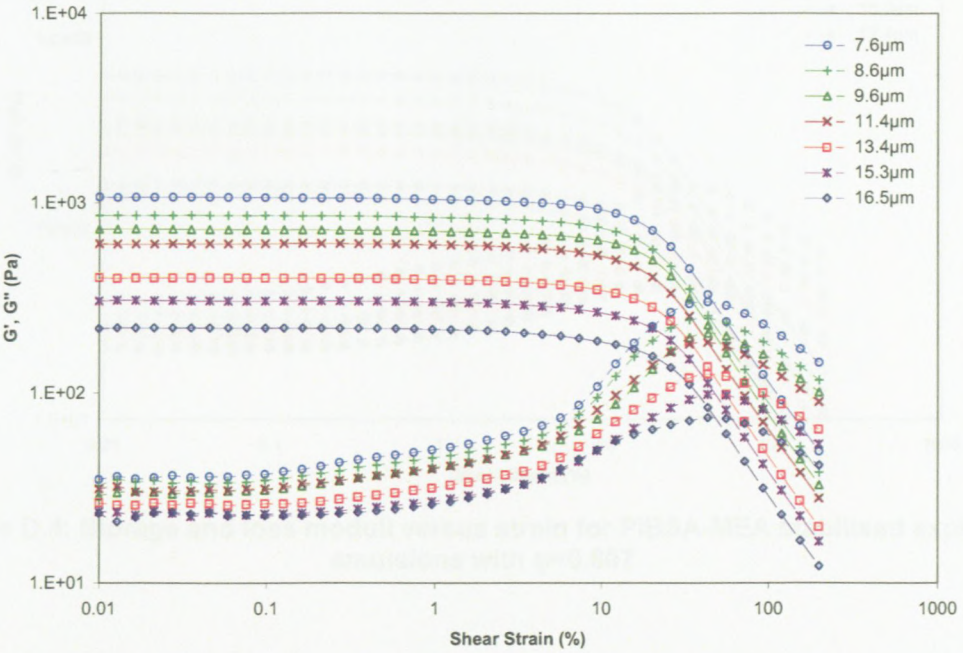

Figure D.2: Storage and loss moduli versus strain for PIBSA-MEA stabilised explosive emulsions with φ=0.868

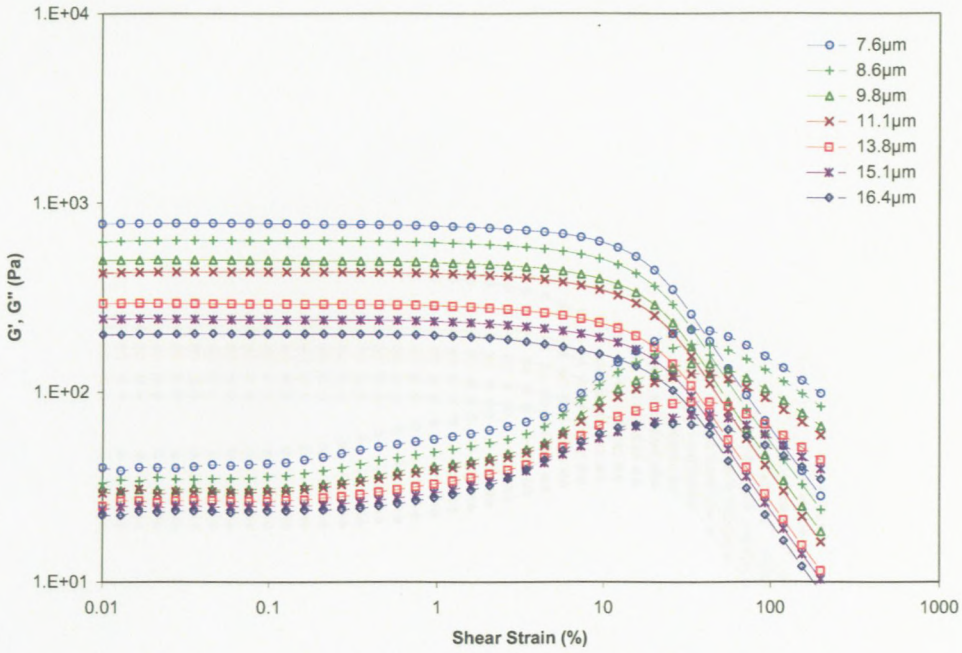

Figure D.3: Storage and loss moduli versus strain for PIBSA-MEA stabilised explosive emulsions with φ=0.837

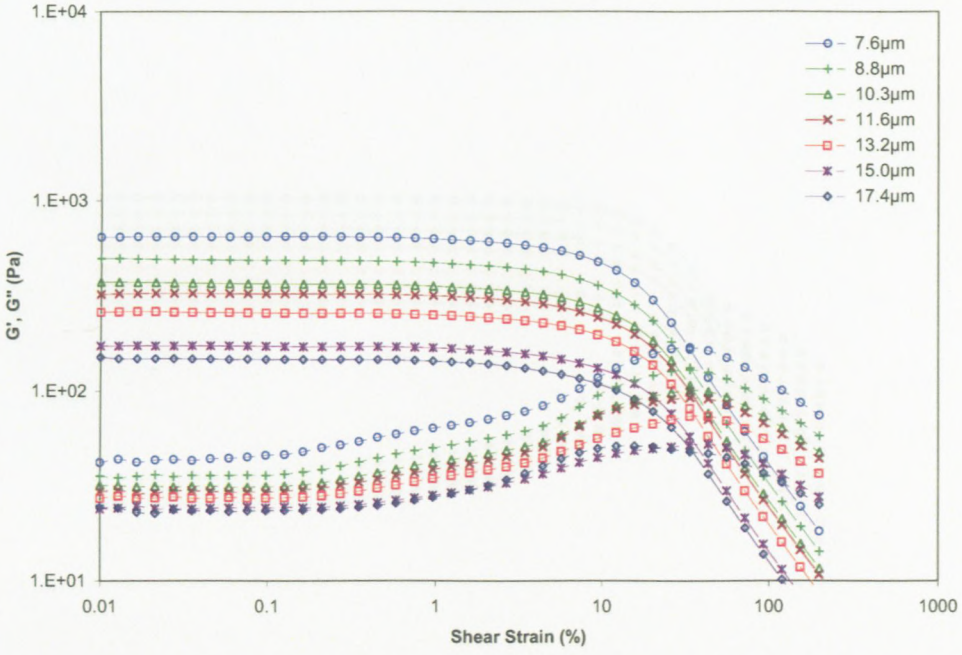

Figure D.4: Storage and loss moduli versus strain for PIBSA-MEA stabilised explosive emulsions with φ=0.807

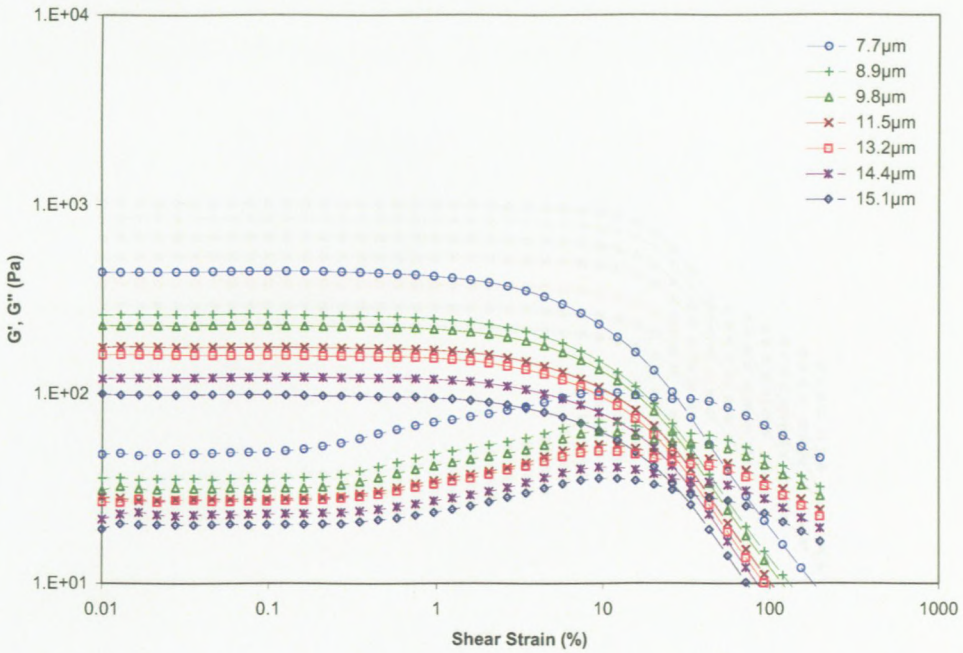

Figure D.5: Storage and loss moduli versus strain for PIBSA-MEA stabilised explosive emulsions with φ=0.764

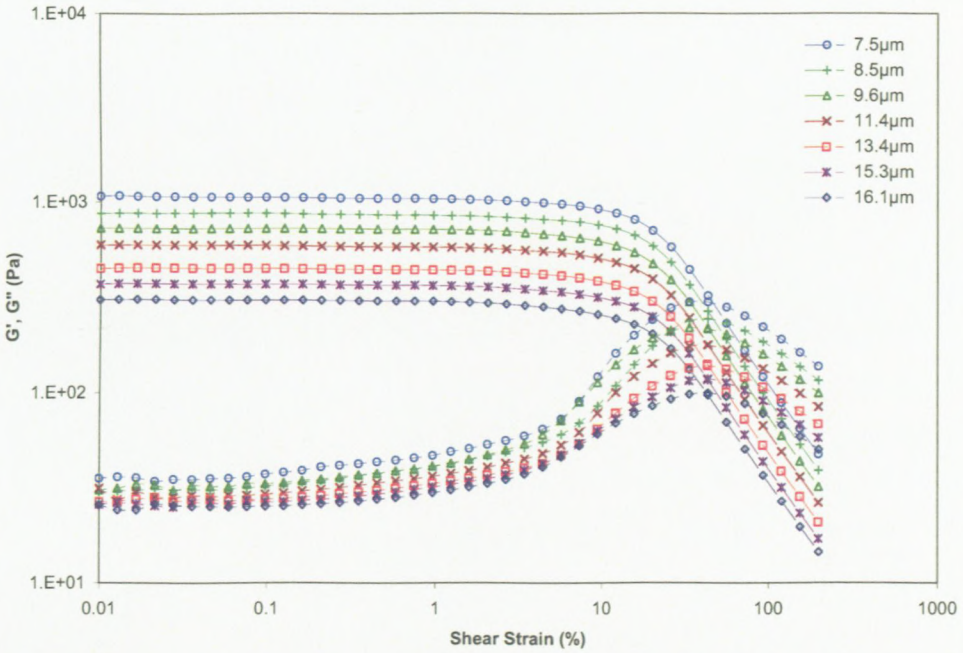

Figure D.6: Storage and loss moduli versus strain for PIBSA-Urea stabilised explosive emulsions with φ=0.868

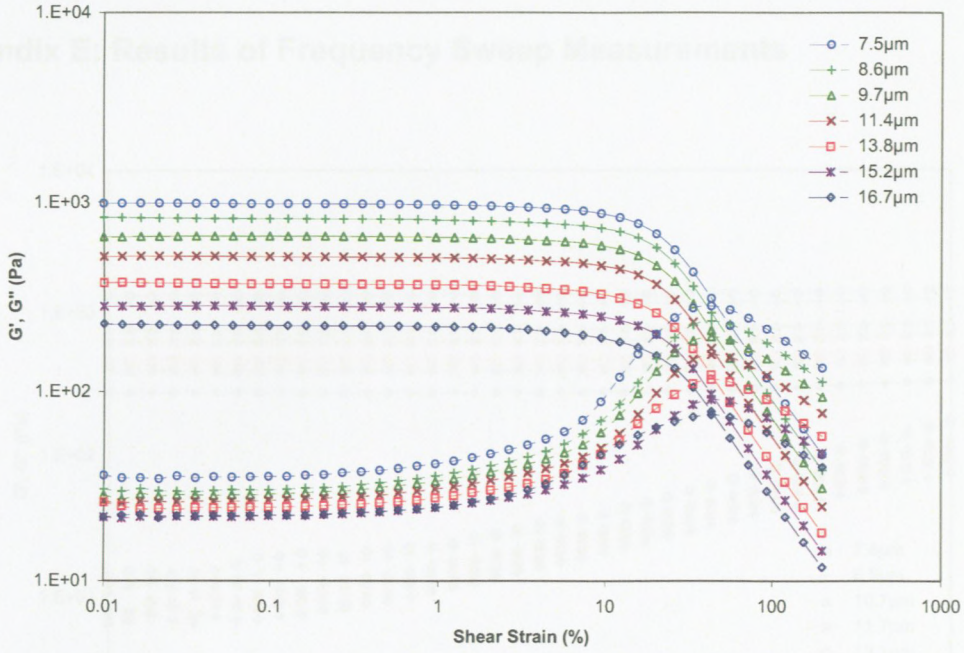

Figure D.7: Storage and loss moduli versus strain for PIBSA-Imide stabilised explosive emulsions with φ=0.868

Appendix E: Results of Frequency Sweep Measurements

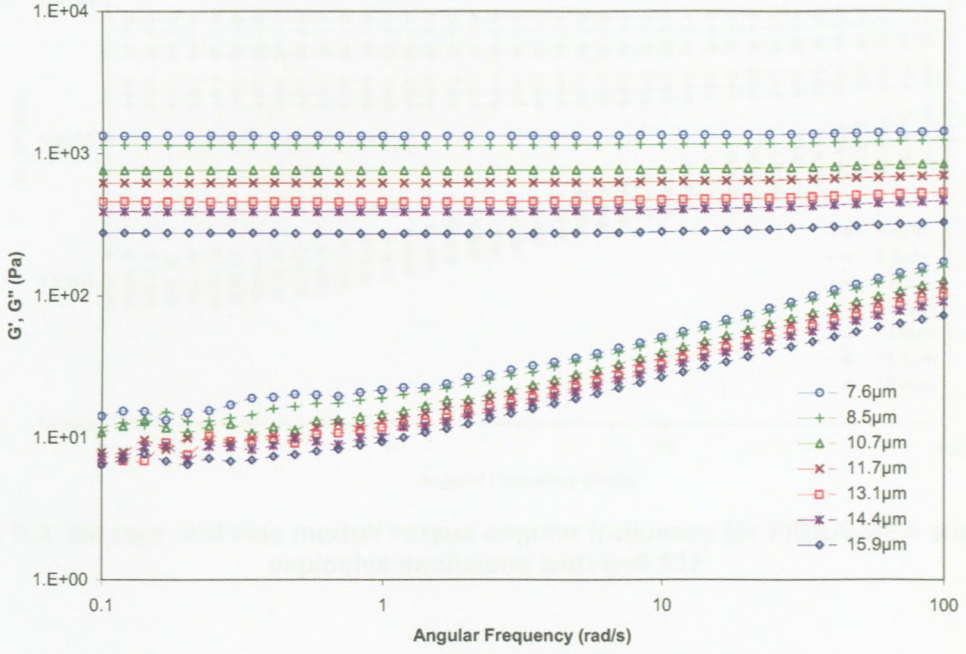

Figure E.1: Storage and loss moduli versus angular frequency for PIBSA-MEA stabilised explosive emulsions with φ=0.892

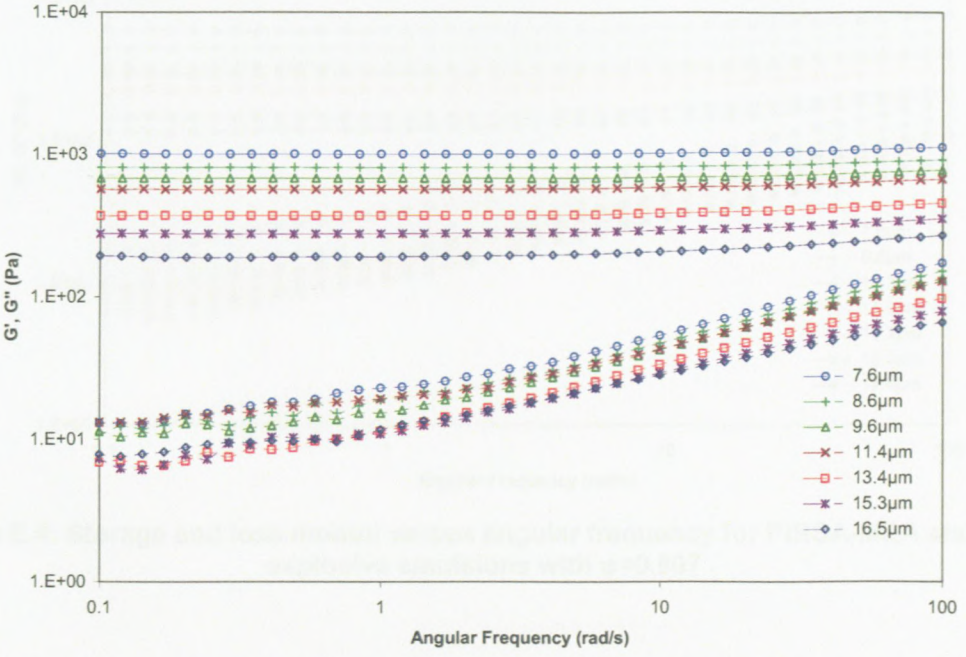

Figure E.2: Storage and loss moduli versus angular frequency for PIBSA-MEA stabilised explosive emulsions with φ=0.868

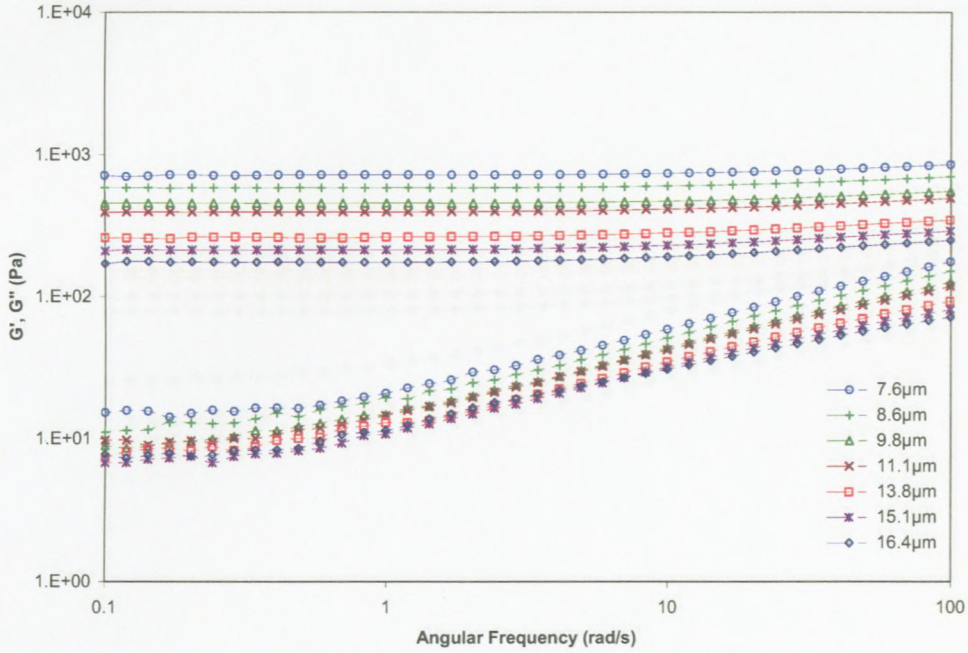

Figure E.3: Storage and loss moduli versus angular frequency for PIBSA-MEA stabilised explosive emulsions with φ=0.837

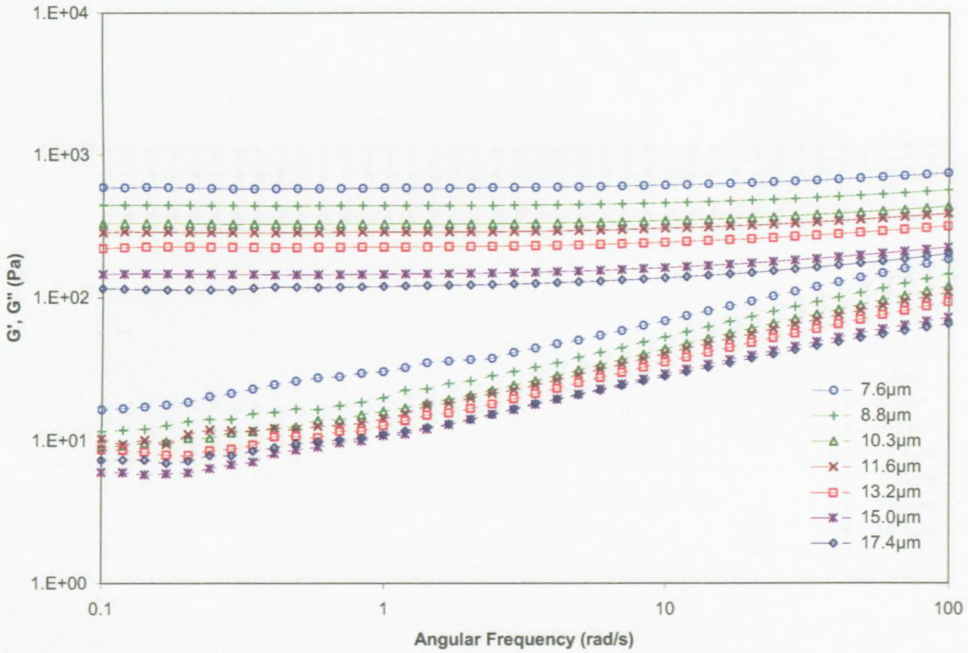

Figure E.4: Storage and loss moduli versus angular frequency for PIBSA-MEA stabilised explosive emulsions with φ=0.807

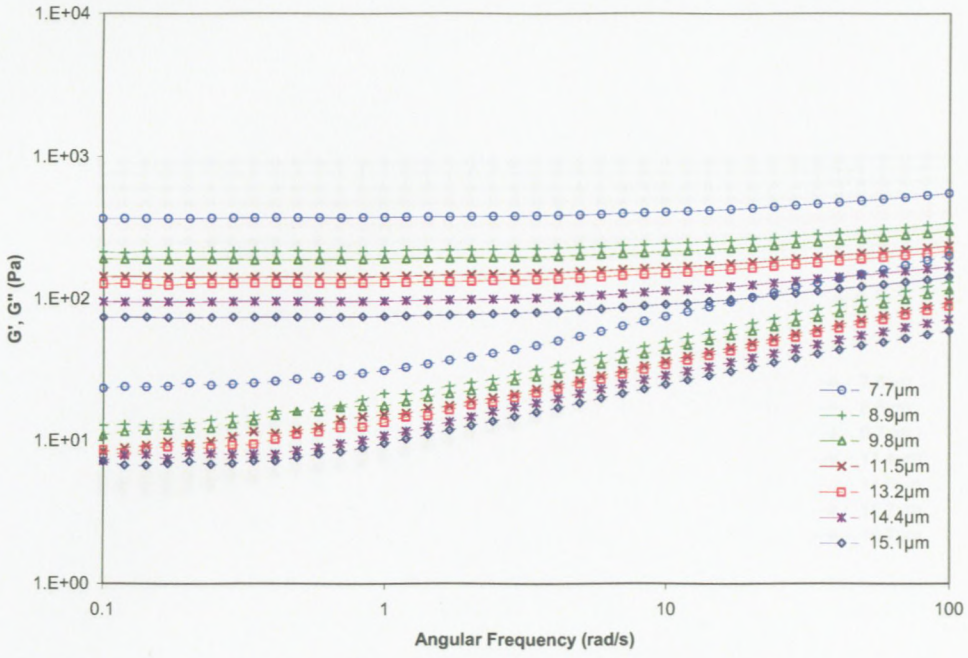

Figure E.5: Storage and loss moduli versus angular frequency for PIBSA-MEA stabilised explosive emulsions with φ=0.764

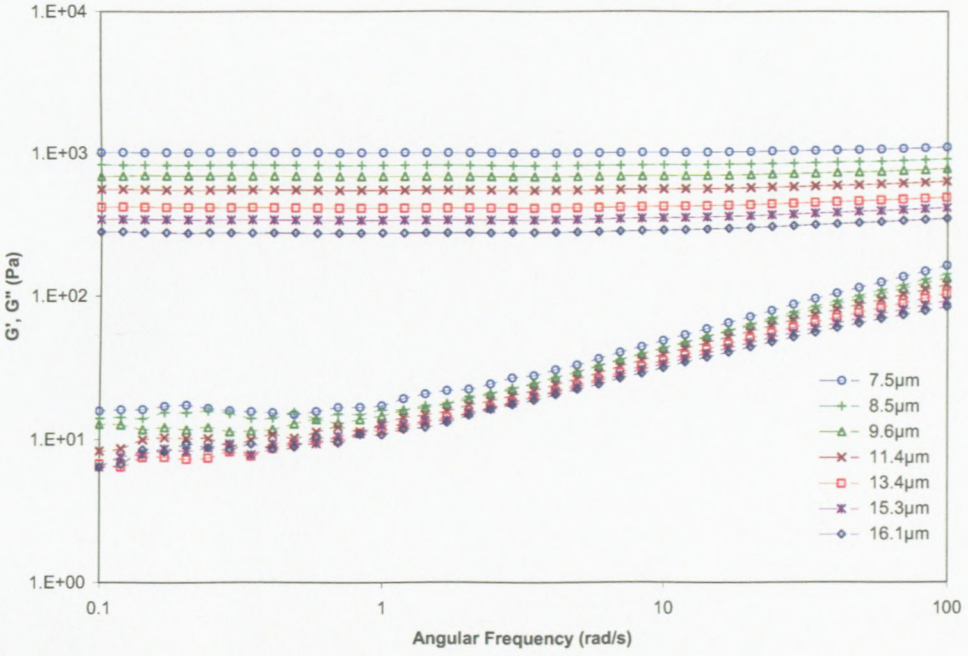

Figure E.6: Storage and loss moduli versus angular frequency for PIBSA-Urea stabilised explosive emulsions with φ=0.868

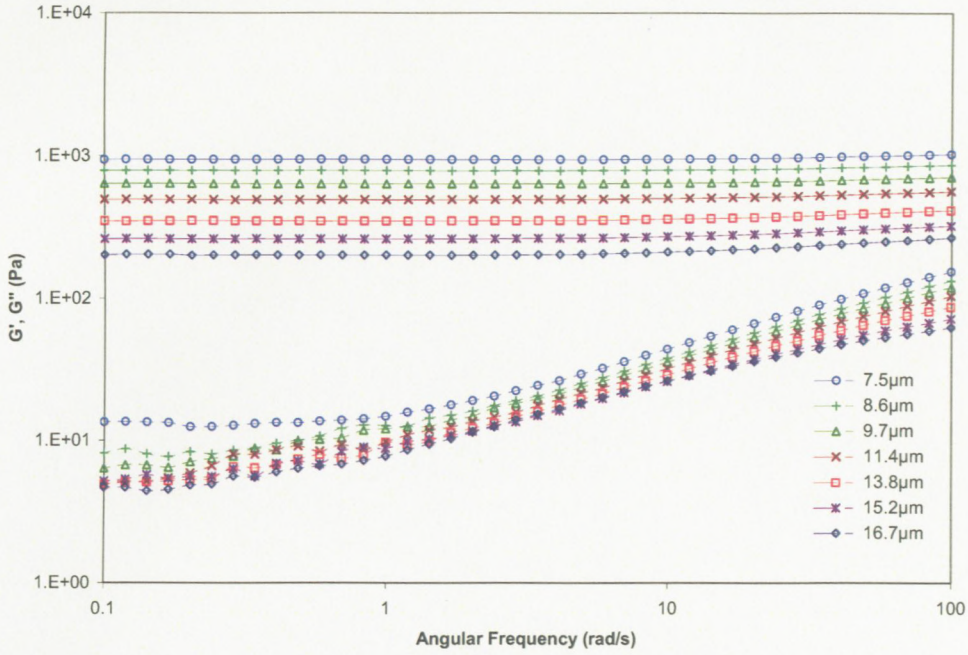

Figure E.7: Storage and loss moduli versus angular frequency for PIBSA-Imide stabilised explosive emulsions with φ=0.868